

**From plastids to peroxisomes:  
Function of the JA precursor, 12-oxo-phytodienoic  
acid (OPDA), in *Arabidopsis thaliana***

Dissertation  
zur Erlangung des  
Doktorgrades der Naturwissenschaften (Dr. rer. nat.)  
der  
Naturwissenschaftlichen Fakultät I – Biowissenschaften  
der Martin-Luther-Universität  
Halle-Wittenberg,  
vorgelegt  
von Frau Khansa Mekkaoui

Gutachter:

- 1: Prof. Dr. Bettina Hause
- 2: Prof. Dr. Ingo Heilmann
- 3: Prof. Dr. Andreas Schaller

Verteidigungsdatum: 29.01.2024



## Table of contents

|  |      |
|--|------|
| Table of contents.....   | III  |
| Abbreviations .....  | VI   |
| List of figures.....   | VIII |
| List of tables .....   | XI   |
| 1 Introduction .....   | 1    |
| 1.1 Jasmonic acid .....  | 1    |
| 1.1.1 The functions of JA in defense .....   | 1    |
| 1.1.2 The functions of JA in development.....  | 2    |
| 1.1.3 JA signaling.....  | 2    |
| 1.2 The biosynthesis of JA .....   | 3    |
| 1.2.1 The regulation of JA biosynthesis.....   | 5    |
| 1.2.2 Allene oxide synthase (AOS).....   | 5    |
| 1.2.3 Allene oxide cyclase (AOC).....  | 5    |
| 1.2.4 OPDA reductase (OPR) .....   | 6    |
| 1.3 OPDA - only a JA precursor or a distinct signaling compound?.....  | 6    |
| 1.3.1 The function of OPDA from an evolutionary point of view.....   | 7    |
| 1.3.2 The <i>opr3</i> single mutant as a genetic resource for studying OPDA signaling. ....                                      | 7    |
| 1.3.3 The functions of OPDA in vegetative processes.....   | 8    |
| 1.3.4 OPDA triggers different transcriptional responses from JA. ....  | 8    |
| 1.3.5 OPDA signaling as a reactive electrophilic species. ....   | 9    |
| 1.4 OPDA transport.....  | 10   |
| 1.5 Aims and objectives .....  | 11   |
| 2 Results.....   | 14   |
| 2.1 Determination of OPDA signaling using a transcriptional approach. ....   | 14   |
| 2.1.1 The JA-biosynthesis mutants have altered AOC proteins levels and OPDA content. 14  |      |
| 2.1.2 Restitution of the JA-positive feedback loop in the <i>opr2/3</i> mutant to make its OPDA levels comparable to Col-0 ..... | 15   |
| 2.1.3 Dissection of the wound-induced transcriptional response to identify OPDA signaling. ....                                  | 17   |
| 2.1.4 Replication of the same transcriptional approach with adult leaves shows similar results as seedlings.....                 | 26   |
| 2.1.5 The endogenous rise of OPDA compared to the exogenous application of the compound. ....                                    | 27   |
| 2.2 The subcellular distribution of OPDA can indicate putative signaling function.....   | 30   |
| 2.2.1 Targeting of OPR3 to different cell compartments. ....   | 31   |
| 2.2.2 Complementation of the <i>opr2/3</i> double mutant with different organelle targeted OPR3                                  | 35   |

---

|       |   |    |
|-------|---|----|
| 2.2.3 | The effect of the targeting of OPR3 to other organelles on JA biosynthesis ....   | 38 |
| 2.2.4 | Testing the cytosolic occurrence of OPR3 when targeted to other organelles.   | 40 |
| 2.2.5 | Tissue-specific expression of <i>OPR2</i> and <i>OPR3</i> and its relation to the fertility of the <i>opr3</i> single mutant. ....  | 44 |
| 2.3   | Towards the identification of a plastid located OPDA transporter. ....  | 45 |
| 2.3.1 | A pipeline to identify a putative plastid located OPDA transporter. ....  | 46 |
| 2.3.2 | Characterization of the selected transporter candidates .....   | 50 |
| 3     | Discussion.....   | 59 |
| 3.1   | Does OPDA exert an independent signaling function in addition to being a JA precursor in Arabidopsis? .....   | 59 |
| 3.1.1 | The supply of JA during development mimics the JA positive feedback loop...59   |    |
| 3.1.2 | Wounding results in a major transcriptional change which is independent from JA-pathway. ....   | 60 |
| 3.1.3 | JA-Ile mediates a distinct transcriptional change showing its clear function in wounding.....   | 61 |
| 3.1.4 | OPDA does not mediate a transcriptional response in wounding.....   | 62 |
| 3.1.5 | The exogenous OPDA treatment differs from the endogenous rise of the compound. ....   | 63 |
| 3.2   | Can OPDA as a signaling molecule translocate to other cell compartments? .....  | 66 |
| 3.2.1 | Incorporation of targeting signals to the primary sequence of OPR3 defines its subcellular destination. ....  | 66 |
| 3.2.2 | Nucleus, cytosol, chloroplast, and mitochondria located OPR3 can reconstitute JA biosynthesis in the <i>opr2/3</i> double mutant. ....  | 67 |
| 3.2.3 | Is the substrate of OPR3 translocating to different organelles or the OPR3 directed to various organelles might occur also within the cytosol? .....                                | 68 |
| 3.2.4 | The fertility of the <i>opr2/3</i> double mutant can be restored by cytosolic OPR3, whereas native cytosolic OPR2 is insufficient for the fertility of the <i>opr3</i> mutant. .... | 69 |
| 3.3   | The export of OPDA from the chloroplast inner envelope. ....  | 70 |
| 3.4   | Summary and conclusion .....  | 73 |
| 4     | The flower-specific transcription factors MYB21 and MYB24 are wound-responsive. ....  | 75 |
| 4.1   | Introduction .....  | 75 |
| 4.1.1 | Flower development in Arabidopsis.....  | 75 |
| 4.1.2 | JA regulation of flowering. ....  | 76 |
| 4.1.3 | The role of MYB21/MYB24 in Arabidopsis flower development. ....   | 77 |
| 4.1.4 | Aims and objectives .....   | 78 |
| 4.2   | Results.....  | 79 |
| 4.2.1 | <i>MYB21</i> and <i>MYB24</i> are wound-inducible in a JA-dependent manner.....   | 79 |
| 4.2.2 | Analysis of developmental phenotypes of <i>myb21</i> and <i>myb24</i> mutant plants. ..   | 83 |
| 4.2.3 | Seedlings etiolation in the <i>myb21</i> and <i>myb24</i> mutants.....  | 85 |
| 4.2.4 | Seed development in the <i>myb21</i> and <i>myb24</i> mutants .....   | 87 |



---

|       |  |     |
|-------|--|-----|
| 4.3   | Discussion.....  | 88  |
| 4.3.1 | MYB21 and MYB24 are wound-responsive in vegetative tissue.....   | 88  |
| 4.3.2 | Are MYB21 and MYB24 not regulating the JA-pathway in wounded leaves, or their effect is not detected due to the experimental design? ..... | 90  |
| 4.4   | Summary and conclusion .....   | 92  |
| 5     | General summary.....   | 93  |
| 6     | Material and methods.....  | 95  |
| 6.1   | Plant material and growth conditions.....  | 95  |
| 6.2   | Plant treatments .....   | 96  |
| 6.3   | Molecular biology methods.....   | 97  |
| 6.4   | Biochemical methods .....  | 106 |
| 6.5   | Plant phenotyping .....  | 110 |
| 6.6   | Microscopy.....  | 111 |
| 6.7   | Figures and statistical analysis.....  | 111 |
|       | References.....  | 112 |
|       | Appendix .....   | 128 |
|       | Acknowledgments .....  | 173 |
|       | Curriculum vitae .....   | 175 |
|       | Erklärung.....   | 177 |

## Abbreviations

|                 |  |
|-----------------|--|
| 13-HPOT         | Hydroperoxylinolenic acid                |
| 4,5-ddh JA      | 4,5-didehydro jasmonic acid              |
| AOC             | Allene Oxide Cyclase                     |
| AOS             | Allene Oxide Synthase                    |
| BiFC            | Bimolecular fluorescence complementation |
| <i>CaMV 35S</i> | Cauliflower Mosaic virus                 |
| cDNA            | Complementary DNA                        |
| CDS             | Coding sequence                          |
| CLH             | Chlorophyllase                           |
| COI1            | Coronatine insensitive1                  |
| CTS             | Comatose                                 |
| CYP20-3         | Cyclophilin20-3                          |
| DEGs            | Differentially expressed genes           |
| dn-OPDA         | 12-dinor-oxo- phytodienoic acid          |
| ER              | Endoplasmic Reticulum                    |
| Fig             | Figure                                   |
| Fig S           | Supplementary figure                     |
| FPKM            | Fragments per kilobase per million       |
| GO              | Gene Ontology                            |
| GLVs            | Green leaf volatiles                     |
| GRX480          | Glutaredoxin 480                         |
| GSH             | Glutathione                              |
| GUS             | $\beta$ -glucuronidase                   |
| HPL             | Hydroperoxide lyase                      |
| Ile             | Isoleucine                               |
| JA              | Jasmonic acid                            |
| JA-Ile          | (+)-Jasmonic Acid-Isoleucin              |
| JAR1            | Jasmonate resistant 1                    |
| JAs             | Jasmonates                               |
| JAZ             | Jasmonate ZIM Domain                     |
| lncRNA          | Long non-coding RNA                      |
| LOX2            | Lipoxygenase 2                           |
| MeJA            | Methyl jasmonate                         |
| MYB             | MYB domain protein                       |

|               |   |
|---------------|---|
| NATA1         | N-acetyltransferase activity1                         |
| OPC-6:0       | 3-oxo-2-(20(Z)-pentenyl)-cyclopentane-1-hexanoic acid |
| OPC-8:0       | 3-oxo-2-(20(Z)-pentenyl)-cyclopentane-1-octanoic acid |
| OPDA          | cis-12-oxo-phytodienoic acid                          |
| OPR3          | OPDA Reductase 3                                      |
| OYE           | Old yellow enzyme                                     |
| PCA           | Principle component analysis                          |
| qPCR          | Quantitative polymerase chain reaction                |
| RES           | Reactive electrophilic species                        |
| Table S       | Supplementary table                                   |
| TFs           | Transcription factors                                 |
| ZAT10         | Salt tolerance zinc finger 10                         |
| $\alpha$ -LeA | Alpha linolenic acid                                  |
| YFP           | Yellow fluorescent protein                            |

## List of figures

|   |    |
|---|----|
| <b>Fig. 1.1</b> Simplified model of JA-Ile perception and signaling.....  | 3  |
| <b>Fig. 1.2</b> The biosynthesis of JA/JA-Ile. ....   | 4  |
| <b>Fig. 1.3</b> The concept of the trans-organellar complementation of the <i>opr2/3</i> double mutant. 12  |    |
| <b>Fig. 2.1</b> Ten-days seedlings of <i>opr2/3</i> and <i>aos</i> mutants have altered AOC proteins levels and produce lower amounts of OPDA than Col-0. ....  | 14 |
| <b>Fig. 2.2</b> MeJA pretreatment restitutes AOC proteins levels in the mutants and the production of OPDA in response to wounding in the <i>opr2/3</i> double mutant. ....                             | 16 |
| <b>Fig. 2.3</b> The seedlings pretreatment and wounding experimental setup and the different comparisons of the transcriptome between each of the genotypes/conditions. ....                            | 18 |
| <b>Fig. 2.4</b> Hierarchical clustering and principal component analysis (PCA) from mRNA-seq data illustrating the transcriptional change induced 1 hour post wounding.....                             | 19 |
| <b>Fig. 2.5</b> The JA/OPDA-independent wounding response .....   | 21 |
| <b>Fig. 2.6</b> The JA-dependent wounding response .....  | 23 |
| <b>Fig. 2.7</b> Wound-induction of JA-dependent, wound responsive genes. ....   | 24 |
| <b>Fig. 2.8</b> The OPDA-mediated transcriptional change .....  | 25 |
| <b>Fig. 2.9</b> Exogenous OPDA treatment of the <i>opr2/3</i> mutant results in the induction of sulfur metabolism in addition to JA-signaling unlike its endogenous rise upon wounding. ....           | 29 |
| <b>Fig. 2.10</b> The removal of the SRL signal results in the alteration of OPR3 import to peroxisomes .....  | 31 |
| <b>Fig. 2.11</b> OPR3 targeted to the ER, cytosol, nucleus, and chloroplasts colocalizes with the corresponding organelle marker in <i>N. benthamiana</i> protoplasts. ....                             | 33 |
| <b>Fig. 2.12</b> OPR3 shows the expected subcellular localizations in stable transformed <i>opr2/3</i> double mutants.....  | 36 |
| <b>Fig. 2.13</b> The restitution of the <i>opr2/3</i> mutant’s fertility by OPR3 targeted to different organelles .....   | 37 |
| <b>Fig. 2.14</b> The <i>opr2/3</i> +ER-OPR3 complementation lines show low restitution of the JA pathway in wounded leaves and flower buds.....   | 38 |
| <b>Fig. 2.15</b> <i>cis</i> -OPDA, JA and JA-Ile levels in wounded leaves of the <i>opr2/3</i> +NI-OPR3 and <i>opr2/3</i> +Cy-OPR3 T1 generation.....   | 40 |
| <b>Fig. 2.16</b> A BiFC system to test the cytosolic occurrence of OPR3 when targeted to another organelle. ....  | 41 |
| <b>Fig. 2.17</b> The OPR3 BiFC transient system in <i>N. benthamiana</i> leaves indicates possible “cytosolic occurrence of OPR3” in the targeting system.....  | 42 |
| <b>Fig. 2.18</b> Change of the tissue-specific expression of <i>OPR2</i> using the <i>OPR3</i> and <i>35S</i> promoters results in the restitution of fertility of the <i>opr2/3</i> double mutant..... | 44 |
| <b>Fig. 2.19</b> The pipeline used to select putative OPDA transporters from the RNAseq datasets obtained from wounded plants.....  | 46 |
| <b>Fig. 2.20</b> Half of the candidates co-expressed with JA-biosynthetic and/or signaling genes but only six showed predictions for plastid localization. ....   | 47 |
| <b>Fig. 2.21</b> Subcellular localization of DTX37 in <i>N. benthamiana</i> leaves and its expression upon wounding in <i>A. thaliana</i> . ....  | 50 |
| <b>Fig. 2.22</b> Isolation of <i>dtx37</i> T-DNA insertion line and determination of its OPDA/JA/JA-Ile levels.....   | 51 |
| <b>Fig. 2.23</b> STR1 subcellular localization in <i>N. benthamiana</i> leaves and its expression upon wounding in <i>A. thaliana</i> . ....  | 53 |
| <b>Fig. 2.24</b> Isolation of <i>str1</i> T-DNA insertion line and determination of its OPDA/JA/JA-Ile levels .....   | 54 |
| <b>Fig. 2.25</b> PEC1 is wound-inducible only in the presence of JA. ....   | 55 |

|   |     |
|---|-----|
| <b>Fig. 2.26</b> Isolation of <i>pec1.3</i> T-DNA insertion line and determination of its OPDA/JA/JA-Ile levels.....  | 56  |
| <b>Fig. 2.27</b> The <i>PD1</i> and <i>PD2</i> double mutants have altered OPDA levels following wounding and priming and accumulate lower AOC proteins levels.....                                     | 58  |
| <b>Fig. 3.1</b> Model summarizing the transcriptional response by endogenous OPDA formation versus exogenous OPDA treatment .....   | 65  |
| <b>Fig. 4.1</b> Schematic representation of the developmental stages of Arabidopsis flowers. ....   | 76  |
| <b>Fig. 4.2</b> The regulatory network for stamen development in Arabidopsis.....   | 77  |
| <b>Fig. 4.3</b> MYB21 and MYB24 are wound-inducible in leaf and seedlings in a JA-dependent manner.....   | 80  |
| <b>Fig. 4.4</b> Expression of <i>MYB21(7kb)pro::GUS</i> reporter gene in 4-week-old rosette leaf at control and after wounding.....   | 81  |
| <b>Fig. 4.5</b> The dynamics of the JA pathway upon wounding do not show remarkable differences between the mutants <i>myb21</i> and <i>myb24</i> and Col-0.....  | 82  |
| <b>Fig. 4.6</b> The <i>myb21</i> mutant plants have bigger rosettes, higher trichome number per leaf and longer roots than Col-0.....   | 84  |
| <b>Fig. 4.7</b> MeJA-mediated root growth inhibition of Col-0 and the <i>myb21</i> and the <i>myb24</i> mutants .....   | 85  |
| <b>Fig. 4.8</b> Etiolated seedlings of the <i>myb21</i> mutant have longer hypocotyl than Col-0 and <i>myb24</i> seeds can germinate in the dark.....   | 86  |
| <b>Fig. 4.9</b> Seeds of <i>myb21</i> and <i>myb24</i> mutants germinate faster than Col-0.....   | 87  |
| <b>Fig. 6.1</b> Ten-day-old seedlings grown in liquid media .....   | 95  |
| <b>Fig. 6.2</b> Golden Gate cloning strategy for the targeting of OPR3 fused to YFP to different cell compartments.....   | 102 |
| <b>Fig. 6.3</b> The BiFC constructs design for organelle targeting of OPR3 with YFP halves. ....  | 106 |
| <b>Fig. 6.4</b> Determination of the anti-AOC immunoblot detection range. ....  | 109 |
| <b>Fig. S1</b> Anti-AOC immunoblots with four biological replicates.....  | 128 |
| <b>Fig. S2</b> AOC protein levels restitution in the mutants is MeJA-dose-dependent. ....   | 128 |
| <b>Fig. S3</b> The MeJA pretreatment experimental setup to mimic the JA-positive feedback loop during development.....  | 128 |
| <b>Fig. S5</b> Time-course of OPDA, JA and JA-Ile accumulation upon wounding in seedlings of Col-0 and <i>opr2/3</i> .....  | 129 |
| <b>Fig. S4</b> Anti-AOC proteins immunoblots with three biological replicates. ....   | 129 |
| <b>Fig. S6</b> PCA projection of the seedlings' transcriptome of Col-0, <i>opr2/3</i> and <i>aos</i> following MeJA and water pretreatment. ....  | 133 |
| <b>Fig. S7</b> Clustering of the transcriptional wounding response in Col-0, <i>opr2/3</i> and <i>aos</i> seedlings pretreated with MeJA during development.....  | 134 |
| <b>Fig. S8</b> Mimicking of the JA feedback loop during development restitutes AOC proteins levels and OPDA in the <i>opr2/3</i> double mutant. ....  | 144 |
| <b>Fig. S9</b> Hierarchical clustering and PCA of the wound-induced transcriptional change in adult leaves of Col-0, the JA-deficient <i>opr2/3</i> and <i>aos</i> mutants.....                         | 145 |
| <b>Fig. S10</b> The OPDA-mediated transcriptional change in adult leaves.....   | 146 |
| <b>Fig. S11</b> Clustering of the transcriptional response in <i>opr2/3</i> after treatment with OPDA with the wounding transcriptional response in Col-0, <i>opr2/3</i> and <i>aos</i> seedlings ..... | 147 |
| <b>Fig. S12</b> OPR3 $\Delta$ SRL colocalizes with mCherry and shows a cytosolic localization.....  | 148 |
| <b>Fig. S13</b> Targeting of OPR3 to the ER, cytosol, nucleus, chloroplast, and mitochondria showed successful subcellular localization when transiently expressed in <i>N. benthamiana</i> leaves..    | 149 |
| <b>Fig. S14</b> Detection of the organelles-targeted OPR3-YFP fusion proteins in <i>N. benthamiana</i> transient assays. ....   | 151 |
| <b>Fig. S15</b> Genotyping and anti-YFP immunoblotting of the <i>opr2/3</i> complementation lines confirm that their phenotypes are due to the function of the organelle targeted OPR3.....             | 151 |
| <b>Fig. S16</b> Complementation of the <i>opr3-1</i> single mutant with ER and Px-OPR3.....   | 152 |

---

|  |     |
|--|-----|
| <b>Fig. S17</b> Phenotyping of the stem length and fertility-related parameters of the <i>opr2/3</i> +ER-OPR3 lines shows partial fertility. ....                                  | 153 |
| <b>Fig. S18</b> In vitro pollen germination assay shows restitution of the pollen germination in the <i>opr2/3</i> +Px-OPR3 and <i>opr2/3</i> +ER-OPR3 complementation lines. .... | 154 |
| <b>Fig. S19</b> The BiFC positive and negative controls. ....  | 155 |
| <b>Fig. S20</b> Quantification of the YFP signal indicates higher cytosolic “leakage” of OPR3 when targeted to the mitochondria. ....  | 156 |
| <b>Fig. S21</b> The <i>opr3-1</i> single mutant is not fertile, even when grown until senescence. ....   | 157 |
| <b>Fig. S22</b> The OPR3pro::YFP shows induction of expression in response to MeJA in <i>N. benthamiana</i> leaves. ....   | 157 |
| <b>Fig. S23</b> Detection of the transporter-GFP fusion proteins after transient expression in <i>N. benthamiana</i> leaves. ....  | 164 |
| <b>Fig. S24</b> Subcellular localization of DTX9, DTX28 and DTX36. ....  | 164 |
| <b>Fig. S25</b> MYB21 and MYB24 are MeJA-responsive in leaves. ....  | 165 |
| <b>Fig. S26</b> GUS reporter assay shows no expression with 2 kb MYB21 and MYB24 promoters. ....   | 165 |
| <b>Fig. S27</b> Anthocyanins accumulation in the 6th leaf following its detachment from the rosette. ....  | 166 |
| <b>Fig. S28</b> MeJA-mediated root growth inhibition. ....   | 166 |
| <b>Fig. S29</b> <i>myb21</i> and <i>myb24</i> reach bolting time later than Col-0. ....  | 166 |
| <b>Fig. S30</b> OPR3 promoter sequence (2299 bp) ....  | 171 |

## List of tables

|                  |   |     |
|------------------|---|-----|
| <b>Table 1.1</b> | List of the organelles used for the complementation assay and their objectives. ..  | 13  |
| <b>Table 2.1</b> | DEGs in the opr2/3 mutant compared to aos in seedlings and adult leaves.....  | 27  |
| <b>Table 2.2</b> | Overview of the selected putative OPDA transporter candidates, and their corresponding T-DNA insertion lines. ....                            | 49  |
| <b>Table 6.1</b> | Targeting sequences used for OPR3 and their corresponding cell compartments. ....   | 101 |
| <b>Table 6.2</b> | List of the constructs used for subcellular localization in <i>N. benthamiana</i> leaves. ....  | 104 |
| <b>Table 6.3</b> | List of the organelle markers used for co-localization studies of OPR3 targeting. ....  | 105 |
| <b>Table S1</b>  | List of differentially expressed genes upon MeJA pretreatment during development.....   | 130 |
| <b>Table S2</b>  | List of wound-responsive genes which are independent from JA/OPDA pathway and classified under the GO term: cellular response to stress. .... | 135 |
| <b>Table S3</b>  | List of wound-responsive genes which are JA-dependent.....  | 141 |
| <b>Table S4</b>  | List of transporters candidates .....   | 158 |
| <b>Table S5</b>  | Arabidopsis mutant and transgenic lines and their corresponding genotyping primers .....  | 167 |
| <b>Table S6</b>  | Arabidopsis mutant and transgenic lines and their corresponding genotyping primers. ....  | 167 |
| <b>Table S7</b>  | List of cloning primers .....   | 169 |
| <b>Table S8</b>  | List of constructs used for Arabidopsis stable transformation.....  | 172 |
| <b>Table S9</b>  | List of constructs used for <i>N. benthamiana</i> transient assays.....   | 172 |

# 1 Introduction

## 1.1 Jasmonic acid

Jasmonic acid (JA), a well-known phytohormone, is one of the most extensively studied compounds within the oxylipin family. The latter is a diverse group of signaling molecules derived from the oxidation of polyunsaturated fatty acids (PUFAs) in plants and other organisms (Wasternack and Feussner, 2018). They serve as important mediators in various physiological and developmental processes, as well as in responses to biotic and abiotic stresses (Creelman and Mulpuri, 2002; Wasternack and Feussner, 2018). JA, JA amino acid conjugates and methyl jasmonate (MeJA), collectively called JAs, function primarily as signaling molecules coordinating plant defenses, growth, and responses to stress, and play a major role in defense when plants are exposed to stressors such as insect attacks, mechanical wounding, or pathogen infections (Antico et al., 2012; Schaller and Stintzi, 2008; Vijayan et al., 1998). JAs also influence plant growth and development, including seed germination, root growth, and flowering (Staswick et al., 1992; Dave et al., 2011; Park et al., 2013; Wasternack et al., 2013; Browse and Wallis, 2019).

### 1.1.1 The functions of JA in defense

JA plays a central role in plants defense in response to mechanical wounding, herbivory attack and necrotrophic and biotrophic fungal pathogens, and this role has been extensively studied. When a plant undergoes mechanical damage, herbivory or fungal attack, JA-Ile acts as a signaling molecule, rapidly accumulating at the site of injury and triggering a cascade of defense responses to protect the plant from potential pathogens and to aid in wound healing (Antico et al., 2012; Howe and Jander, 2008; Wasternack and Hause, 2013). JA-Ile induces the expression of genes related to plant defense, such as those encoding defensive proteins and enzymes that produce toxic compounds (Howe et al., 2004; Reymond et al., 2000). JA stimulates the synthesis of defensive compounds, which act as toxins or repellents, deterring herbivores from feeding on the plant or inhibiting their growth and development such as proteinase inhibitors and secondary metabolites like alkaloids, phenolics, terpenoids, and glucosinolates (Howe and Jander, 2008; Wasternack and Hause, 2013). Additionally, JA induces the emission of volatiles by the plant which can attract natural enemies of the herbivores, providing indirect defense (i.e., attracting predators or parasitoids to control herbivore populations) (Engelberth et al., 2004; Howe and Jander, 2008; Wasternack and Hause, 2013).

JA is also required for the systemic response; the local burst of JA in response to pathogens or herbivory attack is thought to mediate the activation of defense-related genes in the undamaged parts of the plant leading to an enhanced resistance (Browse and Howe, 2008; Li et al., 2002; Truman et al., 2007). Whether JAs or their precursors are the mobile compounds



responsible for the systemic response in plants, it is still unclear. While in tomato it was shown that the systemic accumulation of JA in undamaged sites did not occur as a result of JA or JA-Ile transport from the damaged site but rather through de novo synthesis (Koo et al., 2009), a recent study in Arabidopsis has identified OPDA as the mobile signal translocating from damaged shoots to intact roots and subsequently initiating systemic JA signaling (Schulze et al., 2019).

### **1.1.2 The functions of JA in development.**

In addition to defense, JA plays a crucial role in various aspects of plant development, including root growth, seeds and reproductive organs development, and ultimately, plant senescence. JA influences root growth and architecture. It can inhibit primary root growth (Chen et al., 2011) and promote lateral root development (Cai et al., 2014), helping plants to explore the soil for nutrients and water. JA also inhibits seed germination in rice with cooperation with abscisic acid (Wang et al., 2020), whereas JA induces the release of seed dormancy in Arabidopsis and wheat (Singh et al., 2017; Nguyen et al., 2022). Male sterility is recognized as one of the typical characteristics of JA-deficiency and -insensitivity and is observed in JA-biosynthesis and signaling mutants (Chehab et al., 2011; Feys et al., 1994; Park et al., 2002; Stintzi and Browse, 2000; Xie et al., 2017). JA therefore coordinates stamen filament elongation, anther dehiscence, and pollen viability and was shown to regulate petal and stamen growth through the actions of the transcription factors MYB21 and MYB24 (Cheng et al., 2009; Huang et al., 2020; Reeves et al., 2012).

### **1.1.3 JA signaling**

JA signaling is a complex process involving a series of molecular events triggered by the presence of the bioactive conjugate of JA, JA-Ile. In the absence of JA-Ile, jasmonate ZIM-domain (JAZ) proteins act as repressors of JA-responsive genes. Upon JA-Ile accumulation, the signaling process begins with the perception of JA-Ile by the F-box protein, coronatine insensitive 1 (COI1), and the formation of the receptor complex consisting of the Skp1/Cullin/F-box (SCF)-JAZ which leads to the ubiquitination and degradation of JAZ proteins, hence removing the repression on the basic-helix-loop-helix (bHLH) transcription factor MYC2 and releasing the expression of JA-responsive genes (Chini et al., 2009; Devoto et al., 2002; Sheard et al., 2010; Xie et al., 2017; Xu et al., 2002).

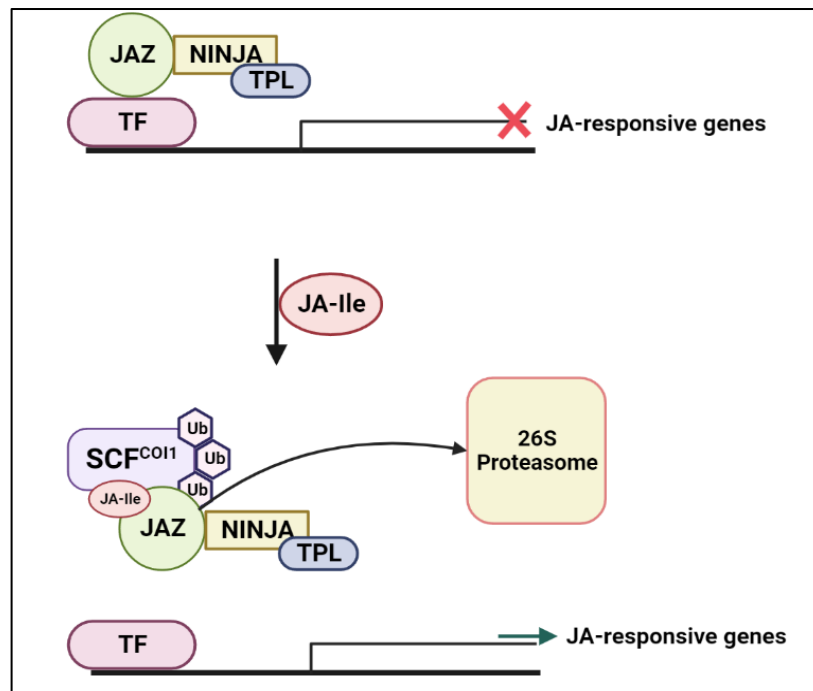


**Fig. 1.1 Simplified model of JA-Ile perception and signaling.**

Skp1, Cullin and F-box proteins; COI1: coronatine insensitive1; JAZ: jasmonate ZIM-domain protein; TF: transcription factor; TPL: TOPLESS protein; NINJA: NOVEL INTERACTOR OF JAZ; Ub: ubiquitin.

## 1.2 The biosynthesis of JA

The biosynthesis of JAs initiates from galactolipids-derived fatty acids that are present in the chloroplast membranes; the C18:3 alpha linolenic acid ( $\alpha$ -LeA) and the C16:3 hexadecatrienoic acid (Wasternack, 2007; Wasternack and Hause, 2013a). The release of  $\alpha$ -LeA is activated by stresses, such as herbivory attack or mechanical damage, and is catalyzed by lipase activity (Wasternack, 2007). The released  $\alpha$ -LeA and hexadecatrienoic acid are oxygenated by incorporation of a molecular oxygen in the C-13 position of their carbon chains by the action of plastid-located LIPOXYGENASES (LOXs) corresponding to four 13-LOXs in *Arabidopsis*; LOX2, LOX3, LOX4 and LOX6 (Bannenberget al., 2009). The formed (S)-configured fatty acid hydroperoxides, 13- hydroperoxylinolenic acid (13-HPOT) and 11-hydroperoxyhexadecatrienoic acid (11-HPHT), are converted by the subsequent action of ALLENE OXIDE SYNTHASE (AOS) and ALLENE OXIDE CYCLASE (AOC) resulting in the formation of *cis*-12-oxo-phytodienoic acid (OPDA) and 12-dinor-oxo-phytodienoic acid (*dn*-OPDA), respectively (Bannenberget al., 2009). While AOS is encoded by a single-copy gene in *A. thaliana* (Park et al., 2002), the AOC family comprises four genes (Stenzel et al., 2003). The AOS and AOC reactions are suggested to be coupled due to the instability of the produced allene oxides (Schaller and Stintzi, 2009).

OPDA and *dn*-OPDA are the final products of the plastid-located part of JA biosynthesis, as it continues in the peroxisome, where reduction of the cyclopentenone ring of OPDA and *dn*-OPDA is catalyzed by a peroxisomal OPDA REDUCTASE (OPR3) resulting in the formation of 3-oxo-2-(20(Z)-pentenyl)-cyclopentane-1-octanoic (OPC-8:0) and hexanoic (OPC-6:0)

acids, respectively (Schaller et al., 2000). Comes after, two to three rounds of  $\beta$ -oxidation where shortening of the hexanoic and octanoic acid side chains of OPC-8:0 and OPC-6:0 occurs yielding jasmonic acid (Schaller and Stintzi, 2009). The cytosol-released JA is conjugated to Isoleucine (Ile) by the enzyme JASMONATE RESISTANT 1 (JAR1) resulting in the formation of the biologically active JA-Ile (Suza and Staswick, 2008).

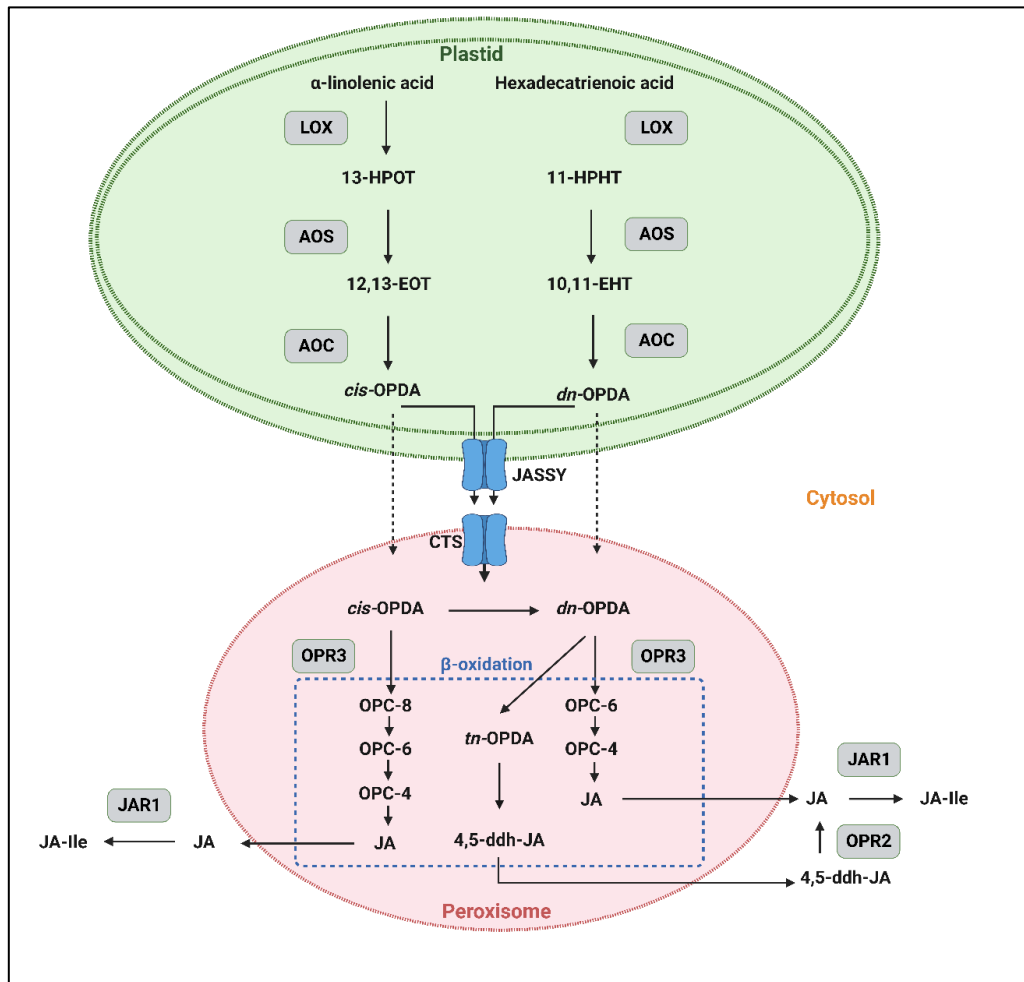


**Fig. 1.2 The biosynthesis of JA/JA-Ile.**

Biosynthesis starts with the release of  $\alpha$ -linolenic acid and hexadecatrienoic acid from chloroplast-membrane galactolipids. Abbreviations for compounds: 13-HPOT, (13S)-hydroperoxyoctadecatrienoic acid; 11-HPHT, 11(S)-hydroperoxy-hexadecatrienoic acid; 12, 13-EOT, 12,13(S)-epoxyoctadecatrienoic acid; 10, 11-EHT, 10,11-(S)-epoxy hexadecatrienoic acid; *cis*-(+)-OPDA, *cis*-(+)-12-oxophytodienoic acid; *dn*-OPDA, dinor-12-oxo phytodienoic acid; OPC-8, 3-oxo-2-(2-pentenyl)-cyclopentane-1-octanoic acid; OPC-6, 3-oxo-2-(2-pentenyl)-cyclopentane-1-hexanoic acid; OPC-4, 3-oxo-2-(2-(Z)-pentenyl)-cyclopentane-1-butanoic acid; *tn*-OPDA, tetranor-OPDA; 4,5-ddh-JA, 4,5-didehydrojasmonic acid; JA, jasmonic acid; JA-Ile, jasmonyl isoleucine. Abbreviations for enzymes/proteins: LOX, lipoxygenase; AOS, allene oxide synthase; AOC, allene oxide cyclase; OPR3, 12-oxophytodienoate-10,11-reductase 3; OPR2, 12-oxophytodienoate-10,11-reductase 2; JAR1, jasmonoyl-isoleucine synthetase; JASSY, OPDA transporter; CTS, comatose. Dashed arrows represent ion trapping mechanism of import into peroxisome proposed by (Theodoulou et al., 2005)

An alternative path for the formation of JA occurs when the peroxisomal *cis*-OPDA/*dn*-OPDA directly undergo three/two rounds of  $\beta$ -oxidation yielding 4,5-didehydro-JA (4,5-ddh-JA), which is released to the cytosol and then reduced to JA by OPR2 (Chini et al., 2018)

JA can form conjugates with various amino acids, such as leucine, valine, and alanine. For example, jasmonoyl-leucine (JA-Leu), jasmonoyl-valine (JA-Val) and jasmonoyl-alanine (JA-Ala) are some of the known conjugates, their relevance is however still unknown (Yan et al., 2016). JA is also methylated by the JA CARBOXYL METHYLTRANSFERASE (JMT) to form JA methyl ester (MeJA), the latter is considered to be the volatile form of JA and serves as a signaling molecule involved in plant defense and stress responses (Farmer and Ryan, 1990).

### 1.2.1 The regulation of JA biosynthesis

JA biosynthesis is subject to feedback regulation since upon the perception of JA signals, specific genes encoding proteins involved in JA biosynthesis and signaling can be induced. For instance, the expression of genes encoding enzymes such as LOXs, AOS and AOCs can be upregulated by JA itself and this positive feedback loop ensures an increased production of JA and promotes the amplification of JA signaling (Reymond et al., 2004). The development of leaves from young stages to the fully developed stage is accompanied by an increase of the protein levels of JA-biosynthetic enzymes LOX, AOS and AOC and this positive feedback loop during development is thought to induce expression of undetectable levels of mRNAs of these enzymes while leading to their accumulation at the protein levels (Stenzel et al., 2003).

### 1.2.2 Allene oxide synthase (AOS)

AOS belongs to a family of cytochrome P450, the CYP74 enzymes (Hughes et al., 2009), and is a key enzyme in the biosynthesis of JA since it catalyzes the entrance reaction in the biosynthesis of the most important intermediate in JA biosynthesis, *cis*-OPDA. AOS acts on 13-HPOT as its substrate and competes with the hydroperoxide lyase (HPL) branch, which is responsible for the production of Green leaf volatiles (GLVs) (Farmer and Goossens, 2019; Vincenti et al., 2019). AOS is located in the chloroplast and tomato AOS was shown to associate to the inner envelope of chloroplasts (Blée and Joyard, 1996; Froehlich et al., 2001). The disruption of the AOS gene results in the disruption of OPDA formation and consequently JA biosynthesis (Park et al., 2002; Von Malek et al., 2002). The *aos* (or *dde2-2*) mutant exhibits a severe male sterility phenotype consisting of defects in anther dehiscence, filament elongation and pollen development and all three processes can be rescued by application of JA (Park et al., 2002; Von Malek et al., 2002).

### 1.2.3 Allene oxide cyclase (AOC)

AOC is a single gene in *Solanum lycopersicum* while in *Arabidopsis thaliana*, four genes encode for functional AOC: AOC1, AOC2, AOC3, and AOC4. The *aoc1*, *aoc3* and *aoc4* single and double mutants do not show JA-deficiency related phenotypes indicating functional redundancy, and no *aoc2* mutant was characterized in *Arabidopsis* (Stenzel et al., 2012). The trimeric structure of AOC was first identified in *Arabidopsis thaliana*. The crystal structure of *Arabidopsis* AOC revealed that three AOC monomers form a stable trimeric assembly and that

the trimeric form of AOC is thought to be functionally important for its enzymatic activity (Hofmann et al., 2006; Otto et al., 2016).

#### 1.2.4 OPDA reductase (OPR)

The OPRs are a group of enzymes that are part of the Old Yellow Enzyme (OYE) family. OPRs are flavin mononucleotide (FMN)-dependent oxidoreductases found in plants (Williams and Bruce, 2002). In *A. thaliana*, the OPR gene family includes three members and is divided into two groups based on their substrate specificity. AtOPR1 and AtOPR2, preferentially catalyze the reduction of (9*R*,13*R*)-12-oxophytodienoic acid which is not directly involved in the biosynthesis of JA, while AtOPR3 is capable of converting 9*S*,13*S*-OPDA to OPC-8:0 which is subsequently converted to JA (Schaller et al., 1998). The crystal structure of OPR3 was observed in studies conducted on *A. thaliana* and tomato enzymes. SIOPR3 forms homodimers, where the binding pocket for the substrate is obstructed by loop L6 from the adjacent protomer and this dimerization is suggested to regulate its enzymatic activity by self-inhibition (Breithaupt et al., 2006). In contrast, the crystal structures of AtOPR3 revealed that the protein exists as a monomer (Han et al., 2011).

The *opr3* mutant in Arabidopsis is male sterile due to impairments in JA production and its sterility, like the *aos* mutant, translates in defects of the floral organs involving anther dehiscence, stamen elongation and pollen development (Stintzi and Browse, 2000; Von Malek et al., 2002). Compared to the *aos* mutant, *opr3* exhibited increased resistance against necrotrophic fungus; a defense response that was initially attributed to OPDA. However, it transpired that this mutant accumulated significant levels of JAs upon fungal infection (Chehab et al., 2011). Further characterization of the *opr3* single mutant by (Chini et al., 2018), identified a secondary route of JA production in the absence of OPR3 through OPR2, and made available the *opr2opr3* (*opr2/3*) double mutant. In this pathway, OPDA undergoes direct peroxisomal  $\beta$ -oxidation, leading to the formation of *dn*-OPDA, *tn*-OPDA, and 4,5-ddh-JA (see Fig.1.1). Upon exiting the peroxisome, 4,5-ddh-JA is subsequently reduced to JA in the cytosol by the action of OPR2 (Chini et al., 2018). OPR1, however, did not show involvement in JA biosynthesis apart from showing activity towards 9*R*,13*R*-OPDA and 9*S*,13*S*-OPDA, but the latter with low efficiency (Schaller et al., 2000).

### 1.3 OPDA - only a JA precursor or a distinct signaling compound?

OPDA has been known to be not only the precursor of JA but also a signaling molecule with distinct roles from JA-Ile. Substantial efforts were made to uncouple the function of OPDA as a signaling molecule with a distinct role from JA/JA-Ile in different plant species. The Arabidopsis *opr3* single mutant which accumulates OPDA but not JA/JA-Ile, was used as a genetic resource to study the signaling of OPDA (Stintzi and Browse, 2000; Stintzi et al., 2001). However, the ability of this mutant to produce the bioactive JA-Ile under specific conditions

was demonstrated recently and uncovered the OPR2 mediated pathway for JA production (Chini et al., 2018). Hence, uncoupling OPDA from JA productions is still experimentally limited in *A. thaliana*. Although the signaling ability of OPDA has been suggested in *A. thaliana*, the mechanism of its signaling and the components mediating the signaling response are so far unknown.

### 1.3.1 The function of OPDA from an evolutionary point of view

This distinct function of OPDA partially derives from the evolutionary history of OPDA/JA biosynthesis/signaling in the plant lineage, area that remains a matter of ongoing research. While JA and its derivatives are conserved in seed plants (Lyons et al., 2013; Pedranzani et al., 2007), they were not detected in several lower plants like green algae, mosses and liverworts (Han, 2017) and emerged within lycophytes (Chini et al., 2023). Recent work on *Marchantia polymorpha* has identified *dn*-OPDA and *dn-iso*-OPDA as the signaling compounds binding to the MpCOI1 receptor and inducing similar defense- and growth inhibition-related transcriptional reprogramming as JA-Ile in *A. thaliana* (Monte et al., 2018, 2020). The evolution of JA pathway was traced to three main events resulting in the modification of hormone perception in vascular plants. These events include a mutation of the COI1 receptor switching its ligand specificity from *dn*-OPDA/*dn-iso*-OPDA to the more polar compound JA-Ile, and the adaptation of activities of two key enzymes OPR3, evolving from cytosolic OPRs, helped *cis*-OPDA/*dn*-OPDA entry to  $\beta$ -oxidation and JAR1 mediated JA conjugation to Ile (Monte et al., 2018). A more recent work, suggests that in lycophytes and bryophyte, *dn-iso*-OPDA is the bioactive hormone perceived by the COI1-JAZ complex, thus analogous to JA-Ile in other vascular plants (Chini et al., 2023). Since *dn*-OPDA but not *dn-iso*-OPDA accumulates in Arabidopsis this suggested that it might have a signaling function in vascular plants, however *dn*-OPDA did not induce the AtCOI1-JAZ complex formation in Arabidopsis and indicated that its function does not transcend being a JA precursor (Monte et al., 2022).

### 1.3.2 The *opr3* single mutant as a genetic resource for studying OPDA signaling.

Several studies relied on the *opr3* mutant to characterize OPDA signaling, since this mutant can produce OPDA but not JA (Stintzi and Browse, 2000). The mutant showed resistance to insect and fungal attack and wound induction of JA-dependent genes suggesting an overlapping role of OPDA with JA (Stintzi et al., 2001). Later on, this mutant was shown to accumulate JA levels which explains its resistance to necrotrophic fungus (Chehab et al., 2011). Indeed, recent work corroborated the fact that this single mutant accumulates significant amounts of the JA-Ile through the cytosolic OPR2 and by using the *opr3opr2* double mutant which is JA-deficient but produces OPDA, they demonstrated that the *opr3* resistance against fungal pathogens is due to JA and not OPDA (Chini et al., 2018). Hence, all previous work



utilizing the *opr3* single mutant to infer distinct OPDA signaling and function is compromised by the presence of JA/JA-Ile in this mutant (Ribot et al., 2008; Stintzi and Browse, 2000; Taki et al., 2005).

### 1.3.3 The functions of OPDA in vegetative processes

It is known that OPDA rather than JA is responsible for the initiation of tendril coiling (Stelmach et al., 1998). This study, however, relied mainly on quantifying OPDA and used exogenous application of OPDA without determining its conversion rate to JA-Ile. More recent work on tendril coiling in grapevine addressed the formation of JA and JA-Ile in addition to OPDA (Malabarba et al., 2019). JA regulates different developmental processes including seed germination, in which JA has an inhibitory effect and this effect is in synergy with abscisic acid (ABA) (Ellis and Turner, 2002; Singh et al., 2017; Varshney and Majee, 2021). In *Arabidopsis* the inhibitory effect of JA on seed germination was attributed to OPDA by several studies. A study on COMATOSE, an ABC transporter involved in peroxisomal import of substrates for  $\beta$ -oxidation, showed that the *cts* loss-of-function mutant exhibits severe block in seed germination and accumulated elevated levels of JA and OPDA. Its crossing with the *aos* mutant, unlike with *opr3*, rescued the seed germination. These results implied that OPDA rather than JA is the inhibitory compound of seed germination (Barros-Galvão et al., 2019; Dave et al., 2011). Taking into account that *opr3* unlike *aos* accumulated some JA levels questions, however, these results. OPDA is also thought to be involved in the regulation stomatal opening, in the same way as for seed germination, JA was shown to induce stomatal closure (Förster et al., 2019; Geng et al., 2016; Munemasa et al., 2011) but further research work favored OPDA as the regulator of stomatal opening using double mutant analysis including the *aos* and *opr3* mutants (Chang et al., 2023; Simeoni et al., 2022). Hence, whether JA and/or OPDA are regulating these processes is still unclear since in most of the above-cited work the experimental limitation of OPDA production being non uncoupled from that of JA/JA-Ile, is remaining.

### 1.3.4 OPDA triggers different transcriptional responses from JA.

In the scope of characterizing the putative signaling function of OPDA in angiosperms, comparative analyses of plant responses to OPDA and JA feedings experiments were performed in *Arabidopsis* and rice and identified distinct responses to both compounds, thus attributing these responses to distinct functions of each of the compounds (Taki et al., 2005). A set of genes were identified as OPDA-specific response genes which were induced by exogenous OPDA but not by exogenous JA or MeJA, and a subset of these genes was characterized as wound- and OPDA-responsive in a COI1-independent manner. These genes encompassed mainly stress-responsive genes, e.g. *ZAT10*, *FAD-OXR*, *ERF5*, *DREB2A* (Taki et al., 2005). Another OPDA-regulated gene in response to drought but in a COI1-dependent

manner was *PHO1;H10* (Ribot et al., 2008). In rice, overexpression of AOC but not OPR3 significantly increased rice resistance to the brown planthopper, *Nilaparvata lugens*, and enabled the identification of a set of OPDA-responsive genes (Guo et al., 2014). The limitations in the use of exogenous OPDA or overproducing it to deduce OPDA-responsive genes in these studies is that exogenous OPDA as a JA precursor gets converted into JA/JA-Ile and determinations of *de novo* synthesized JA/JA-Ile and other oxylipins were not considered. Thus, in these experimental conditions OPDA production is not fully uncoupled from that of JA/JA-Ile. A comparative transcriptional analysis of exogenous OPDA and phytoprostanes PPA<sub>1</sub>, which are oxidized lipids and like OPDA contain  $\alpha,\beta$ -unsaturated carbonyl structure, commonly induced the transcription of genes related to general detoxification and stress responses, and activated mechanisms of a broad-spectrum detoxification to reduce oxidative stress (Mueller et al., 2008). Additionally, GSH adducts of OPDA and PPA<sub>1</sub> were observed, indicating that both being reactive electrophilic species (Mueller et al., 2008). Their conjugation might be a mechanism to render them inactive.

### 1.3.5 OPDA signaling as a reactive electrophilic species.

Several lipid oxidation products contain  $\alpha$ ,  $\beta$ -unsaturated carbonyl groups and are termed as reactive electrophilic species (RES) because they have a strong tendency to react with nucleophilic molecules by Michael addition, and oxylipins like OPDA and the green leaf volatile E-2-hexenal, are oxylipins RES (Améras et al., 2003; Farmer and Davoine, 2007). This electrophilic property is thought to convey biological activities including signaling to OPDA by protein-binding and protein-modifying capacity (Améras et al., 2003; Maynard et al., 2021; Müller et al., 2017; Park et al., 2013). *In vitro* assays showed interaction of OPDA with members of the thioredoxin family, including a plastidial TRX-f1 which activity got impaired by covalently binding to OPDA (Maynard et al., 2021). Binding of OPDA to cytosolic thioredoxins and glutaredoxins (GRX) from *A. thaliana* was also demonstrated *in vitro* and was termed as OPDAylation, however, *in vivo* evidence of the biological relevance of OPDA binding to these proteins is missing (Knieper et al., 2022). OPDA binding to the CYCLOPHILIN20-3 (CYP20-3) triggered the formation of the cysteine synthase complex activating sulfur assimilation (Park et al., 2013). This process was suggested as a signaling mechanism of OPDA to regulate cysteine biosynthesis leading to increased GSH production and regulation of the cellular redox homeostasis (Müller et al., 2017; Park et al., 2013). GSH adducts of OPDA were also detected in several *in vivo* studies, and was shown to be targeted to the vacuole for degradation (Mueller et al., 2008; Ohkama-Ohtsu et al., 2011). OPDA exerted cytotoxicity when infiltrated in leaves or sprayed on seedlings resulting in damaging of the photosystem II (Améras et al., 2003; Mueller et al., 2008). This might be attributed to the electrophilic nature of OPDA possibly leading to a general detoxification process.



## 1.4 OPDA transport

JA biosynthesis occurs in different cell compartments, starting with the chloroplast moving to peroxisome and cytosol, and its signaling would manifest following the import of JA-Ile to the nucleus. Intracellular distribution of JA, its derivatives and precursors would therefore be subjected to transport from and in the above-mentioned cell compartments and to a modulation of their intracellular distributions in response to internal and external cues. The intracellular transport of JA was partially elucidated, when the dually localized ATP binding cassette (ABCG) AtJAT1, residing in the nuclear envelope and the plasma membrane, was shown to mediate both the cellular efflux of JA and the nuclear influx of JA-Ile but its loss of function do not alter the plants fertility (Li et al., 2017). Additionally, the glucosinolate transporter, GTR1, from *Arabidopsis* exhibited JA-Ile transport ability in *Xenopus oocytes* and its loss of function resulted in altered transport of JA and JA-Ile from wounded to distal leaves in addition to reduced male fertility (Saito et al., 2015). Unlike JA, the intracellular transport of OPDA was not uncovered until recently.

### OPDA export from the chloroplast

The JA precursor, OPDA, is synthesized in the chloroplast and is then reduced by OPR3 in the peroxisome. Therefore, its transport from plastids to peroxisomes is required. No plastid-located transporter for OPDA has been characterized until JASSY was identified by Guan et al. (2019). JASSY is a plastid outer envelope protein possessing a lipid-binding START-like domain, and was shown to exhibit channel-like properties facilitating the export of OPDA from the chloroplast (Guan et al., 2019). The loss of JASSY resulted in decreased tolerance to cold stress and increased susceptibility to pathogen attack but not the male sterility phenotype characteristic of JA-deficiency (Guan et al., 2019). Since OPDA is synthesized in the plastid stroma, its transport through the inner envelope of the chloroplast is expected. OPDAT1, an ortholog of AtFAX3 in poplar trees (*Populus trichocarpa*), was recently described as a plastid inner envelope transporter involved in exporting OPDA from plastids (Zhao et al., 2021). In *Arabidopsis*, however, the transport of OPDA from the inner envelope through the aqueous intermembrane space, is still unknown. Nevertheless its import into the peroxisome to be further metabolized into JA, was described to be partially carried out by the peroxisomal ATP binding cassette (ABC) transporter COMATOSE (CTS), in addition to another passive mechanism of import suggesting that OPDA-free acid (OPDA-H<sup>+</sup>) is membrane permeable and can enter the peroxisome without the need for a transport protein (Theodoulou et al., 2005). Like *jassy*, CTS loss of function do not show the male sterility phenotype, hence further clarification on OPDA transport is still awaiting.

## 1.5 Aims and objectives

Following the identification of the cytosolic formation of JA from 4,5-dhhJA by OPR2 (Chini et al., 2018), the major work effort achieved to elucidate OPDA signaling and distinct function from JA/JA-Ile was put under questioning since the *opr3* single mutant was shown not to be the appropriate genetic background to uncouple OPDA from JA functions. Through this work we re-address OPDA (*cis*-OPDA or *dn*-OPDA) signaling hypothesis in *A. thaliana* and specifically its mediation of gene expression using the appropriate JA-deficient mutant, the *opr2opr3* (*opr2/3*) double mutant (Chini et al., 2018). We hypothesize that if OPDA has a signaling capacity, it would mediate transcriptional changes, either through direct mediation of transcription in the nucleus or indirectly through the characterized CYP20-3 complex module. Thus, it is expected to identify at the transcriptional level an OPDA-specific response and specifically a set of “OPDA-specific response genes”. We also hypothesize that OPDA (*cis*-OPDA or *dn*-OPDA) as a signaling molecule mediating gene expression as reported previously (Dave and Graham, 2012; Park et al., 2013; Ribot et al., 2008; Taki et al., 2005), would need to translocate primarily to the nucleus or eventually to other cell compartments in order to exert its signaling capacity. Finally, since it is still not known how OPDA is exported from the chloroplast inner envelope, we hypothesize that as a signaling molecule OPDA would regulate its own transport in the same fashion as JA does. In other words, we hypothesize that a chloroplast inner envelope-located transporter for OPDA would be transcriptionally regulated by OPDA thus would belong to the set “OPDA-specific response genes”. The following three hypotheses were addressed in this thesis work:

### **(I) OPDA, as a signaling molecule, mediates gene expression.**

To investigate the signaling capacity of OPDA in *A. thaliana* and knowing that mechanical wounding is a major cue for JA and OPDA accumulation and signaling, a comparative transcriptional approach was set to dissect the wounding response in the presence of JA/JA-Ile (Col-0), presence of OPDA only (*opr2/3* double mutant) and the absence of both (*aos*). In this comparative approach, the use of the *opr2/3* mutant would uncouple the OPDA-dependent events from those of JA and additionally, and of equal importance, the use of the *aos* mutant would uncouple the OPDA-dependent events from those that are wound dependent but independent from JA and OPDA. Hence, by analyzing JA signaling and its effects on the transcriptome and by isolating the wound events that are independent from OPDA and JA in the *aos* mutant, we would be able to identify the transcriptional change solely mediated by OPDA in the *opr2/3* double mutant. Additionally, comparisons between the transcriptional change induced by the endogenous rise of OPDA and treatment with OPDA would better clarify its innate function in addition to being a JA precursor.

**(II) OPDA, as a signaling molecule, translocates to the nucleus and eventually to other cell compartments.**

The suggested model for OPDA signaling either through a COI-dependent or independent path (summarized in Dave and Graham, 2012), would necessitate the import of *cis*-OPDA or *dn*-OPDA to the nucleus in order to mediate transcriptional change. To address this question, an organellar complementation approach was developed to identify the hypothetical translocation of OPDA to the nucleus or eventually to other cell compartments. The approach consists of complementing the *opr2/3* double mutant with OPR3 targeted to a different organelle than the peroxisome where it occurs naturally. Only if the substrate of OPR3, OPDA, is available in the tested compartment, OPC-8/OPC-6 can be produced and eventually the JA production can resume (Fig. 1.3).

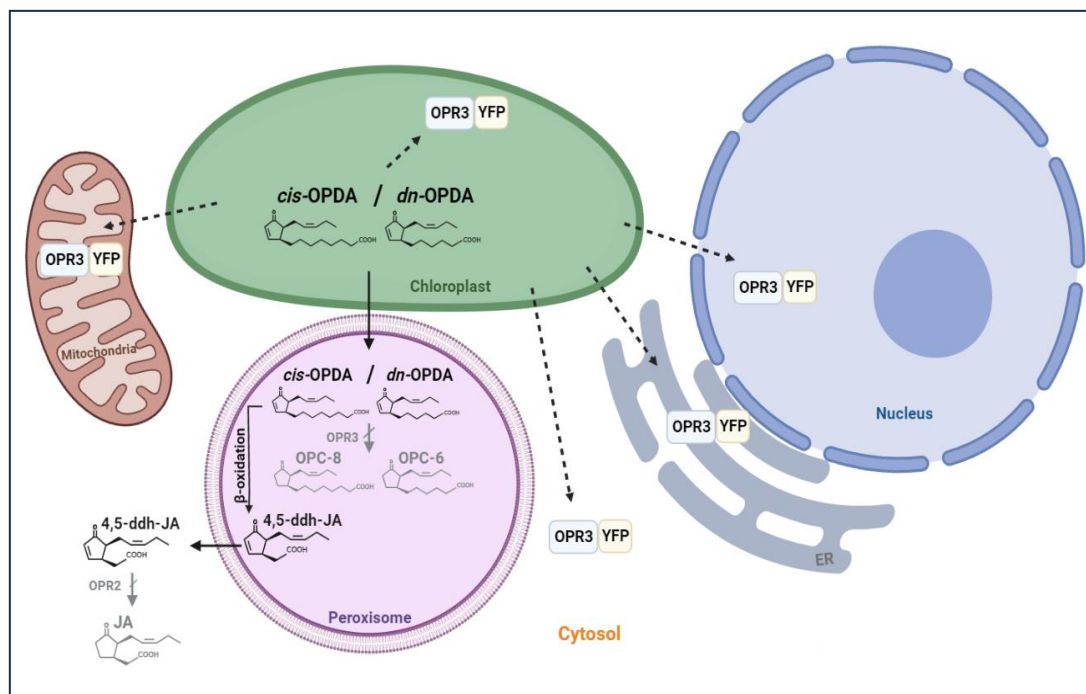


**Fig. 1.3 The concept of the trans-organelle complementation of the *opr2/3* double mutant.**

The *opr2/3* mutant is complemented with OPR3 fused to YFP and targeted to a different organelle than peroxisomes.

Dashed arrows show hypothetical translocation of OPDA to the different cell compartments. Pathways in grey are those blocked in the *opr2/3* double mutant background. The loss of function of OPR3 and OPR2 stops the formation of OPC-8/OPC-6 from *cis*-OPDA/*dn*-OPDA and JA from 4,5-ddh-JA, respectively. Abbreviations: OPR3, 12-oxophytodienoate-10,11-reductase 3; OPR2, 12-oxophytodienoate-10,11-reductase 2; *cis*-(+)-OPDA, *cis*-(+)-12-oxophytodienoic acid; *dn*-OPDA, dinor-12-oxophytodienoic acid; 4,5-ddh-JA, 4,5-didehydrjasmonic acid; OPC-8, 3-oxo-2-(2-pentenyl)-cyclopentane-1-octanoic acid; OPC-6, 3-oxo-2-(2-pentenyl)-cyclopentane-1-hexanoic acid; JA, jasmonic acid

In addition to the nucleus and to consolidate our approach, OPR3 should be targeted to the plastid stroma expecting it to be able to access the OPDA pool synthesized there. In accordance with literature, a biochemical continuity exists between the chloroplast and the ER, and substrates produced in the chloroplasts could be available in the ER (Mehrshahi et al.,

2013; Mehrshahi et al., 2014). Therefore, the ER lumen was also chosen to test this hypothesis for OPDA. The two last compartments to be tested were the cytosol and the mitochondria, where OPDA is not expected to be present and would serve as negative controls. By complementing the JA-deficient mutant with OPR3 in the above-mentioned cell compartments (Table 1.1), we aim to identify the putative translocation of OPDA to the nucleus and additionally to get an insight on the intracellular distribution of OPDA.

**Table 1.1 List of the organelles used for the complementation assay and their objectives.**

| <b>Cell compartment</b> | <b>Objective</b>   |
|-------------------------|--|
| Peroxisome              | Technical positive control for the complementation assay       |
| Chloroplast             | Test the access to the pool of OPDA in the chloroplast         |
| ER                      | Test the biochemical continuity between ER and the chloroplast |
| Nucleus                 | Test the presence of OPDA as a signaling molecule              |
| Cytosol                 | Negative control where OPDA is not expected to be available    |
| Mitochondria            | Negative control where OPDA is not expected to be available    |

### **(III) A chloroplast-located transporter of OPDA is transcriptionally regulated by OPDA.**

Although we aim to elucidate the transcriptional changes caused by OPDA in the first place, we also hypothesize that OPDA as a precursor for JA production and/or as a signaling molecule would regulate its own transport. Therefore, the generated transcriptional dataset from the first objective will be analyzed for the identification of a putative transporter that would localize to the chloroplast inner envelope and would be transcriptionally OPDA-responsive. The analysis and selection of the putative transporters would rely mainly on predictions and general parameters defined from the data collected from available databases. Additionally, characterization of mutants for the corresponding selected candidates would indicate whether they have a putative function, initially, related to JA biosynthesis and then to OPDA transport.

## 2 Results

### 2.1 Determination of OPDA signaling using a transcriptional approach.

To elucidate putative OPDA signaling, a transcriptional profiling of Col-0 and of the JA-deficient mutants, *opr2opr3* (*opr2/3*) and *aos*, was designed.

#### 2.1.1 The JA-biosynthesis mutants have altered AOC proteins levels and OPDA content.

A JA-mediated positive feedback loop leading to the accumulation of the JA-biosynthetic enzymes LOX2, AOS and AOC proteins (AOC1, AOC2, AOC3 and AOC4) during plant development, was characterized and its absence in the JA-deficient mutant *opr3* resulted in lower tissue levels of these proteins (Stenzel et al., 2003). To quantify the effect of the deficiency of the *opr2opr3* (*opr2/3*) double mutant in the JA-feedback loop in terms of accumulation of the JA biosynthetic enzyme levels, the AOC proteins from total protein extracts of seedlings were determined by immunoblotting using an anti-AOCs polyclonal antibody detecting all four Arabidopsis AOC proteins. Normalization of the immunoblotting using this antibody showed linear detection range of the AOC proteins amounts (see Material and methods, section 6.4.3).

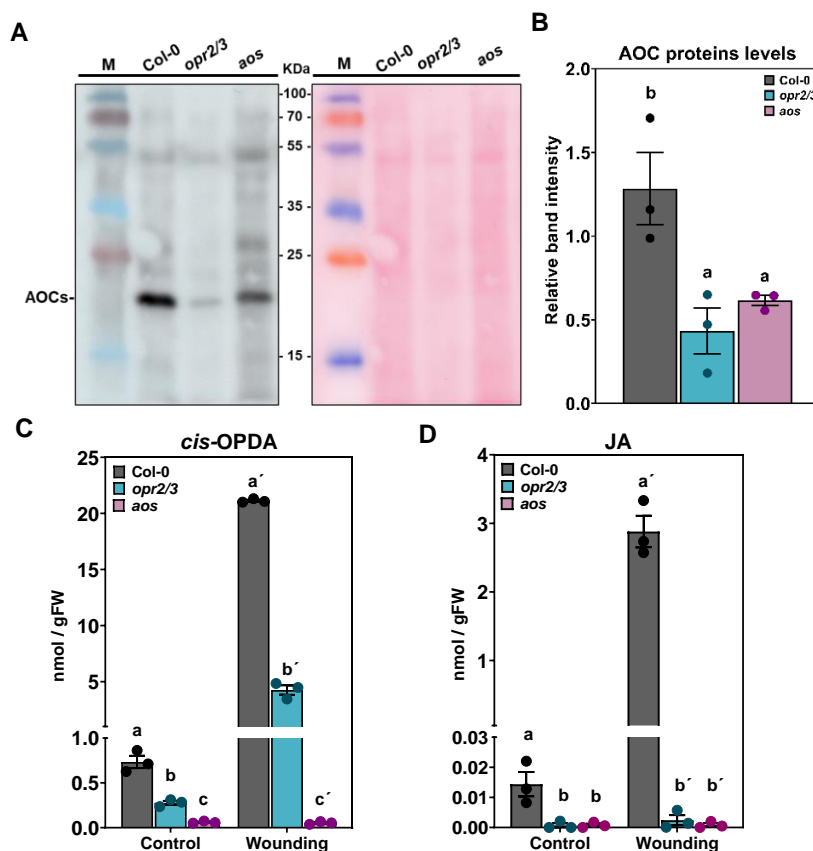


**Fig. 2.1** Ten-days seedlings of *opr2/3* and *aos* mutants have altered AOC proteins levels and produce lower amounts of OPDA than Col-0.

**A:** Anti-AOC immunoblot. 7  $\mu$ g of total protein extract was loaded per lane. Protein staining with Ponceau S. was used as internal control. M= protein marker.

**B:** Quantification of AOC proteins levels from the immunoblot in (A). Relative AOCs' band intensity was calculated in relation to the Ponceau S. control (immunoblot replicates are shown in Appendix, Fig. S1). **C, D:** *cis*-OPDA (C) and JA (D) levels determined by LC/MS in 10-day-old seedlings of Col-0, *opr2/3* and *aos* under control conditions and 1 hour post wounding. In (B), (C) and (D) bars represent means of

three biological replicates (single dots) with 30 seedlings each ( $\pm$ SEM). Different letters denote statistically significant differences among genotypes (within treatments) as determined by One-Way ANOVA followed by Tukey HSD ( $p < 0.05$ ).

The AOC proteins bands in the immunoblots showed lower intensity in the JA-biosynthesis deficient mutants *opr2/3* and *aos* than in Col-0 (Fig. 2.1A), and quantification of these proteins levels by densitometry showed statistically significant reduction of the proteins in the mutants in comparison to Col-0 (Fig. 2.1B). The JA-feedback loop was thought to confer the tissue ability to accumulate a sufficient amount of JA-biosynthesis enzymes to produce jasmonates during developmental processes (Stenzel et al., 2003). In this context, the JA and OPDA contents in ten-day-old seedlings were determined by LC/MS and quantified in nmol per gram fresh weight in relation to internal standards (Fig. 2.1C, D). At control condition, a pool of around 0.7 nmol OPDA was already detected in Col-0. This pool was reduced by half in the *opr2/3* double mutant and was not detected in the *aos* mutant. Upon wounding, OPDA levels increased to 18 nmol g<sup>-1</sup> in Col-0 while the *opr2/3* mutant accumulated one third of this amount. *aos* is OPDA-deficient and did not accumulate OPDA upon wounding. Only Col-0 was able to accumulate JA upon wounding, the mutants had almost undetectable levels of JA, not exceeding the range of 0.002 nmol, at both conditions, validating their JA deficiency.

### **2.1.2 Restitution of the JA-positive feedback loop in the *opr2/3* mutant to make its OPDA levels comparable to Col-0**

Since the *opr2/3* double mutant produced significantly lower OPDA levels than Col-0 upon wounding, studying OPDA signaling in this mutant necessitated firstly the restitution of its OPDA levels to Col-0's levels. To do so, mimicking of the JA-mediated positive feedback loop during development was performed by adding 1 µM of jasmonic acid methyl ester (MeJA) to the seedlings' growth media at different time points and with different frequencies. Pretreatment with MeJA two times or more during development increased the AOC proteins in the mutants the closest to the levels of Col-0 (Fig. S2). Consequently, the experimental design was set to three MeJA-pretreatments scheduled on the 4<sup>th</sup>, 5<sup>th</sup> and 6<sup>th</sup> days of seedling development, whereas water was added as mock-pretreatment of seedlings serving as control (Fig. S3).

Detection of the AOC proteins levels in mock-pretreated and MeJA-pretreated seedlings by immunoblotting showed that the MeJA pretreatment restituted their levels in the mutants to Col-0's levels unlike the mock pretreatment with water (Fig. 2.2A-B). This indicated that the increased basal transcript levels of these biosynthetic enzymes due to the JA-feedback loop is accompanied by the increase of their protein levels. To verify whether the restitution of the biosynthetic enzymes levels enhances the ability of the seedlings to produce jasmonates, *cis*-OPDA, *dn*-OPDA, JA and JA-Ile levels were determined in Col-0, *opr2/3* and *aos* at control condition (-wounding) and 1 hour post wounding (+wounding) (Fig. 2.2C).



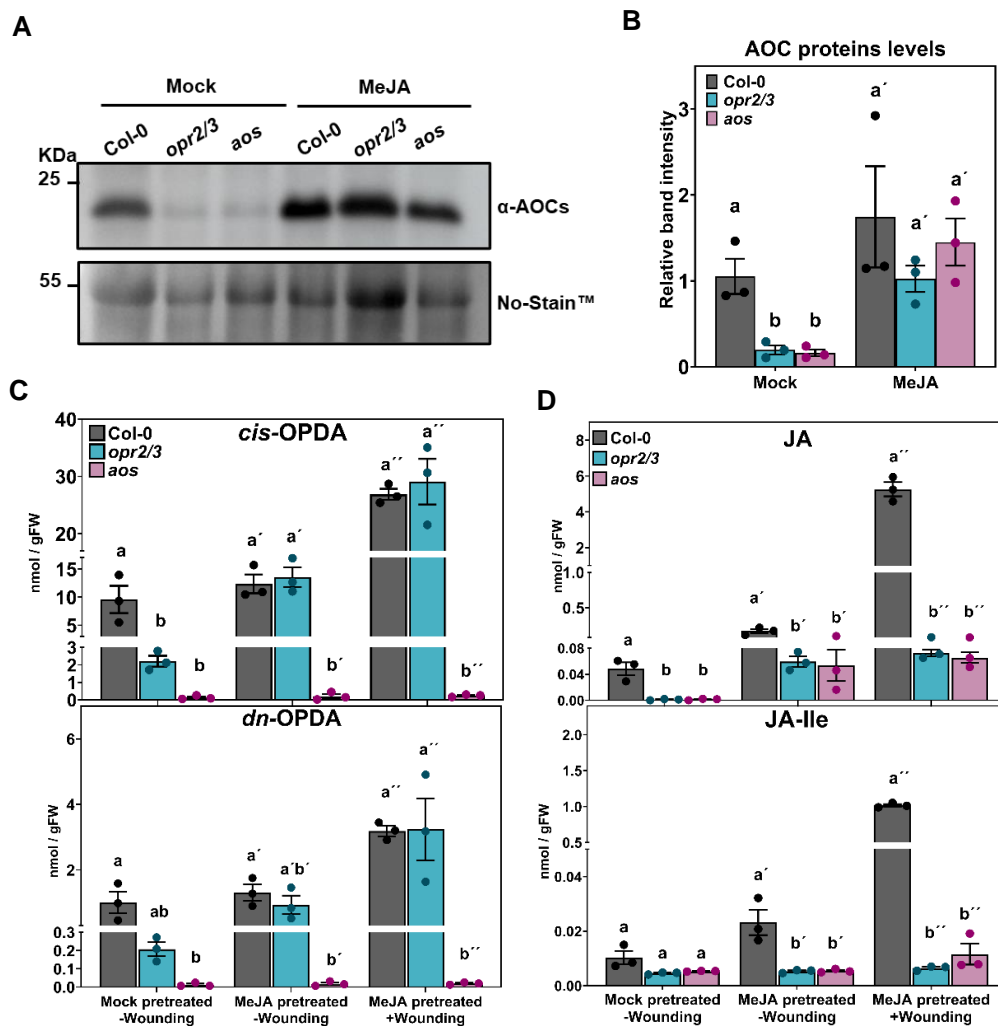


**Fig. 2.2 MeJA pretreatment restitutes AOC proteins levels in the mutants and the production of OPDA in response to wounding in the *opr2/3* double mutant.**

Ten-day-old seedlings from Col-0, *opr2/3* and *aos* were pretreated with MeJA during development (MeJA) or with water (Mock).

**A:** AOC proteins levels determination in seedlings of Col-0, *opr2/3* and *aos* by immunoblotting from 7  $\mu$ g total protein extract using anti-AOCs primary antibody. Total protein staining with NoStain™ was used as internal control. M= protein marker.

**B:** Quantification of AOC proteins levels from the immunoblot in (A) using Image J (immunoblot replicates are shown in Appendix, Fig. S4). Relative AOC proteins bands intensity was calculated in relation to the total protein intensity of the NoStain™ control.

**C, D:** *cis*-OPDA, *dn*-OPDA, JA and JA-Ile levels were determined by LC/MS in seedlings of Col-0, *opr2/3* and *aos* at control (-wounding) and 1 hour post wounding (+wounding). 10-day-old seedlings were pretreated with MeJA or water (Mock) during development. In (B) and (C) bars represent means of three biological replicates (single dots) with 120 seedlings each ( $\pm$ SEM). Different letters denote statistically significant differences among genotypes (within treatments) as determined by One-Way ANOVA followed by Tukey HSD ( $p < 0.05$ ).

In the absence of MeJA pretreatment, seedlings of Col-0 accumulated statistically higher levels of *cis*-OPDA than those of the *opr2/3* double mutant and the MeJA pretreatment in the absence of wounding resulted in the compensation of these altered *cis*-OPDA levels in *opr2/3*. Wounding of Col-0 and *opr2/3* seedlings pretreated with MeJA resulted in the accumulation of equal levels of *cis*-OPDA in both genotypes. With lower overall levels than *cis*-OPDA, *dn*-

OPDA showed accumulation with statistically similar levels between *opr2/3* and Col-0. The induction of OPDA by wounding in the *opr2/3* mutant was restituted to the OPDA levels in Col-0 also at earlier time-points of wounding (Fig. S5). The bioactive hormone, JA-Ile and its precursor, JA, accumulated upon wounding only in Col-0 as expected since *opr2/3* is JA-deficient (Fig. 2.2D). Being both JA and OPDA deficient, seedlings of the *aos* mutant did not accumulate any of the measured compounds and served as a negative control to validate the experimental design (Fig. 2.2C-D).

### 2.1.3 Dissection of the wound-induced transcriptional response to identify OPDA signaling.

To determine the putative signaling of OPDA through mediation of gene regulation in plant defense responses, and specifically wounding, mRNA sequencing was performed for detection of gene transcriptional change, since the biosynthesis of JA and its precursor OPDA, is induced by wounding (Glauser et al., 2008; Hoo et al., 2008; Koo et al., 2009) and OPDA's ability to orchestrate the expression of genes independently from JA was previously described for *Arabidopsis* (Taki et al., 2005). To properly dissect the wound-induced transcriptional response, a comparative approach included genetic backgrounds where JA/OPDA are present (Col-0), only OPDA is present (*opr2/3*), and both JA and OPDA are absent (*aos*). Such setup enables the uncoupling of the presumed OPDA signaling from the JA/OPDA-independent signaling responses upon wounding (Fig 2.3A). Hence several comparisons between samples were performed and mainly the transcriptional change specific to Col-0, *opr2/3* and *aos* would characterize JA signaling, OPDA signaling and the JA/OPDA-independent signaling, respectively (Fig. 2.3B).

By pretreating the seedlings with MeJA it was expected to induce some transcriptional changes and specifically changes in the basal expression levels of some genes due to the residual effect of MeJA four days after the pretreatment. To determine this residual effect a comparison between the MeJA-pretreated and the mock-pretreated (water) seedlings for all the genotypes was performed (Fig. 2.3B). For each of the genotypes, more or less twenty genes were differentially expressed in a specific manner due to the pretreatment and 20 genes were commonly differentially expressed in all the genotypes (Fig. 2.3C). These DEGs included mainly JA-responsive genes related to biosynthesis, defense and signaling (Table S1).

For instance, transcript levels of different JA-biosynthesis enzymes like *LOX2*, *AOC2* and *AOS* were up-regulated in the JA-deficient mutants compared to Col-0 since their basal levels were lower in these mutant genotypes due to the JA deficiency (Table S1). To get an overview on the effect of MeJA pretreatment, a principal component analysis of the whole transcriptome of Col-0, *opr2/3* and *aos* was performed (Fig. S6) and showed conservation of the variances between genotypes when MeJA and mock pretreatment conditions were compared. Hence the



MeJA pretreatment did not induce major changes in the transcriptome and rather induced the deficient transcripts of JA-responsive genes in the mutants and enhanced their levels in Col-0. Consequently, MeJA pretreated samples were used for the determination of JA, OPDA signaling in the wound response for the following experiments.

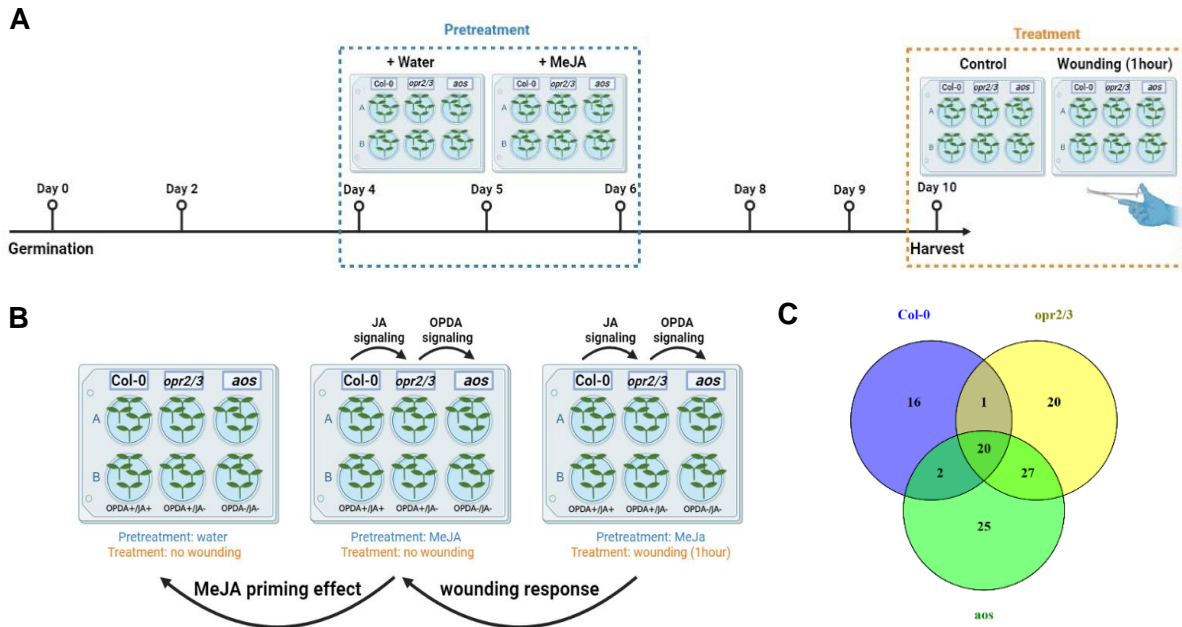


**Fig. 2.3 The seedlings pretreatment and wounding experimental setup and the different comparisons of the transcriptome between each of the genotypes/conditions.**

Ten-day-old seedlings of Col-0, *opr2/3* and *aos* were grown in liquid  $\frac{1}{2}$  MS medium and experiments were performed in triplicates with 120 seedlings per biological replicate.

**A:** Schedule of the seedling's growth, the MeJA pretreatment during development and the wounding as a final treatment on the 10<sup>th</sup> day of development. Wounding was performed using forceps and wounded samples were harvested 1h post-wounding while the controls were kept unwounded. Samples were sent for mRNA sequencing to Novogene.

**B:** The transcriptome comparisons between genotypes/conditions, shown in black arrows, indicate the signaling process/molecule to be characterized.

**C:** Venn diagram showing the differentially expressed genes (DEGs) due to the pretreatment with MeJA (priming) during development on the transcriptome of each genotype, with 20 DEGs being common to all genotypes. DEGs were determined with fold change (FC) and false discovery rate (FDR) cutoffs of  $\pm 2$  and 0.05, respectively.

### 2.1.3.1 The wound-induced overall change in the transcriptome.

The transcriptomic data showed an overall big change in gene expression due to wounding with mostly a similar pattern of change of the transcriptome of the three genotypes when we consider the 2000 most variable genes in the data set (Fig. 2.4A). Only Col-0 showed a subset of genes with a distinct pattern of transcription different than *opr2/3* and *aos* at control condition and upon wounding (regions marked with brackets in Fig. 2.4A). The transcriptional profile of *opr2/3* and *aos*, however, showed a high similarity at both conditions. PCA of the RNA-seq data consolidated these results and indicated that Col-0 shows the most different transcriptional profile in comparison to *opr2/3* and *aos* at control and wounding conditions (Fig. 2.4B). While Col-0 showed the highest variance in comparison to both mutants at control condition, its variance increased upon wounding, which could be attributed to the activation of

a JA signaling that is absent in the mutants. And when comparing *opr2/3* and *aos*, the PCA plot showed a very high overlap between both genotypes despite the presence of OPDA in *opr2/3* at control condition and its induction upon wounding in comparison to *aos*.

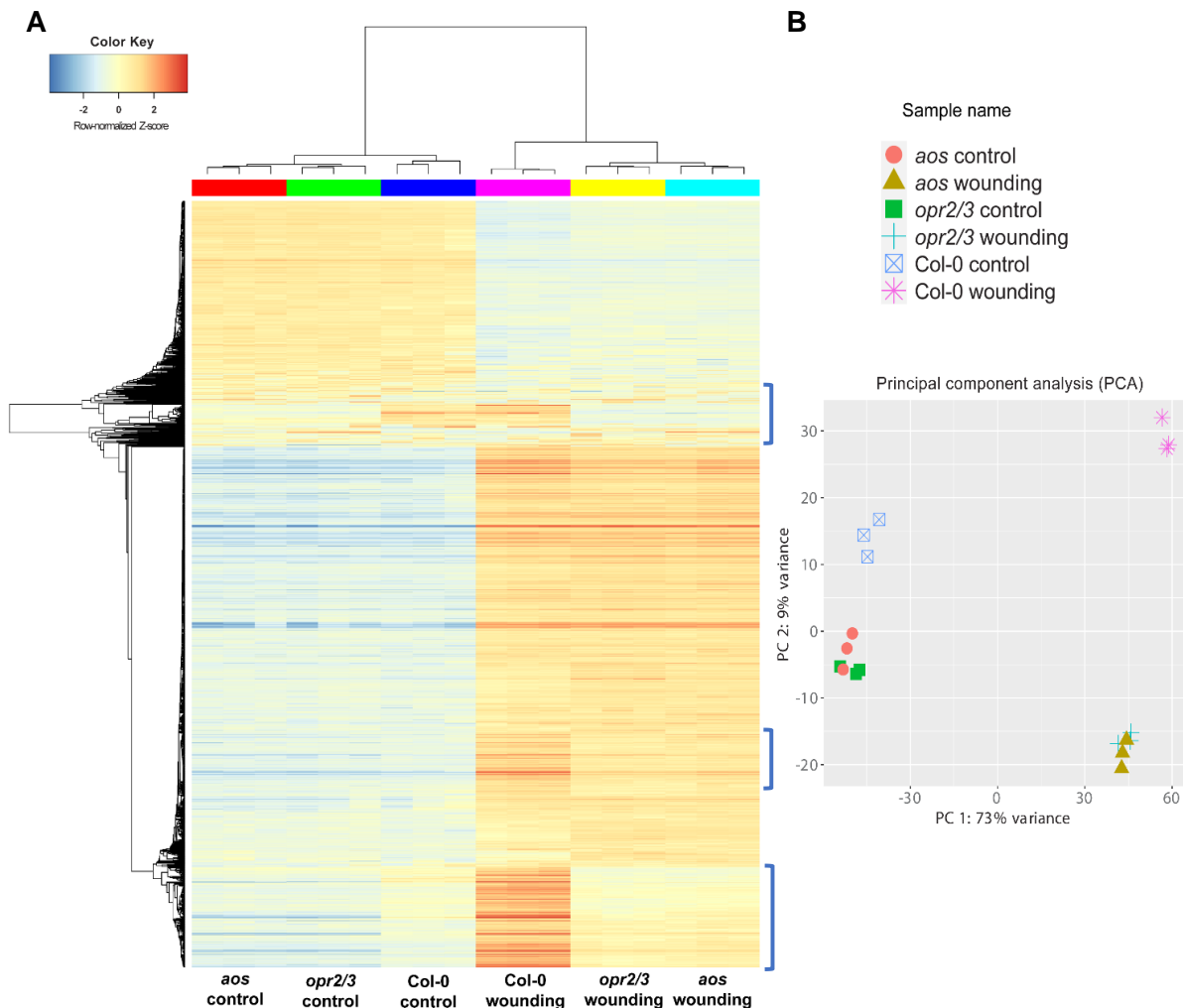


**Fig. 2.4 Hierarchical clustering and principal component analysis (PCA) from mRNA-seq data illustrating the transcriptional change induced 1 hour post wounding.**

Ten-day-old seedlings from Col-0, *opr2/3* and *aos* were pretreated with MeJA during development and were either unwounded (control) or harvested 1h post wounding with forceps (wounding).

**A:** Hierarchical clustering with heatmap of the 2000 most variable genes based on RNAseq FPKM values transformed into Row normalized Z-score with a threshold of  $\pm 4$ . The data is centered by subtracting the average expression level for each gene. The distance matrix is  $1 - r$ , where  $r$  is Pearson's correlation coefficient. The average linkage is used (Bottom 25% of genes regarding expression level are excluded). Regions marked with blue brackets show a different expression pattern between the genotypes.

**B:** PCA projection in two-dimensional space of the RNAseq data with PC1 showing variation in the dataset due to wounding while PC2 showing the variation due to the genotypes.

The overview on the wound-induced transcriptional response indicated that the JA pathway mediates only a part of the wound-induced transcriptional response, since Col-0 showed few subclusters of DEGs in comparison to the mutants (shown in blue brackets in Fig. 2.4A). To further characterize the wounding response in each of the genotypes, the 2000 most variable genes were clustered according to their expression pattern across all the samples using the

K-means clustering with gene ontology enrichment analysis performed on the clusters (Fig. S7). The clustering resulted in six subgroups, two of which (cluster 6 and 2) showed a distinct transcriptional profile in Col-0 in comparison to *opr2/3* and *aos*. Both clusters showed enrichment in wound, immune and JA-mediated responses indicating a JA-mediated defense response absent in the biosynthetic mutants. The other subgroups resulting from the clustering were mainly enriched in stress responses and this response was similar in all the genotypes independently from the JA pathway.

### **2.1.3.2 A general transcriptional stress response, JA/OPDA-independent, occurs upon wounding.**

Being deficient in both JA and OPDA productions, the *aos* mutant served as a negative control for uncoupling the actual OPDA-mediated signaling from wound-induced signaling processes which are independent from the JA/OPDA pathway, and which could be attributed to OPDA signaling. Hence, all genes that are similarly differentially expressed in Col-0, *opr2/3* and *aos* would constitute a JA/OPDA-independent wounding response. 1460 genes were commonly differentially expressed in response to wounding in Col-0, *opr2/3* and *aos* with an FDR of 0.05 and a fold-change threshold of  $\pm 2$  (Fig. 2.5A). Gene ontology (GO) analysis of this set of genes showed enrichment in processes like cellular response to stress, response to chemical and to oxygen levels (Fig. 2.5B). To further dissect the transcriptional response to wounding in the three genotypes in terms of expression levels and not only in terms of fold change, the ratios of FPKM for Col-0/*opr2/3* and Col-0/*aos* were calculated. Only DEGs which expression levels were not at least twice as high or low in Col-0 than *opr2/3* or *aos* were considered wound-inducible in a JA/OPDA-independent manner. 1332 out of the 1460 DEGs fitted this criterion and within this list, a subset of 211 genes were enriched in GO term cellular response to stress (Table S2). Also known stress-responsive genes, like *OPR1*, *ZAT6*, *ZAT8*, *ZAT12* (Beynon et al., 2009; Davletova et al., 2005; Shi et al., 2014), were included in this subcluster (Fig. 2.5C). Interestingly, 22 out of these 211 genes were identified previously as OPDA-responsive by exogenous treatment of Arabidopsis seedlings (Taki et al., 2005). Similarly, despite the absence of OPDA in the *aos* mutant two main OPDA-responsive genes, *DREB2A* and *FAD-OXR*, were induced to the same extent as in Col-0 and *opr2/3*.

Technical validation of the expression of these genes by qRT-PCR confirmed that they were induced in an OPDA-independent manner (Fig. 2.5D). *ZAT10*, another main OPDA-responsive gene (Taki et al., 2005) and known to be involved in abiotic stress responses (Mittler et al., 2006), was also up-regulated by wounding in all genotypes. *ZAT10* did not belong to the DEGs commonly induced in all the genotypes, because it was induced in *aos* to a lesser extent than

in *opr2/3* and Col-0 (FC lower than 2). Its induction in *aos* by wounding was, however, independent of OPDA (Fig. 2.5D).

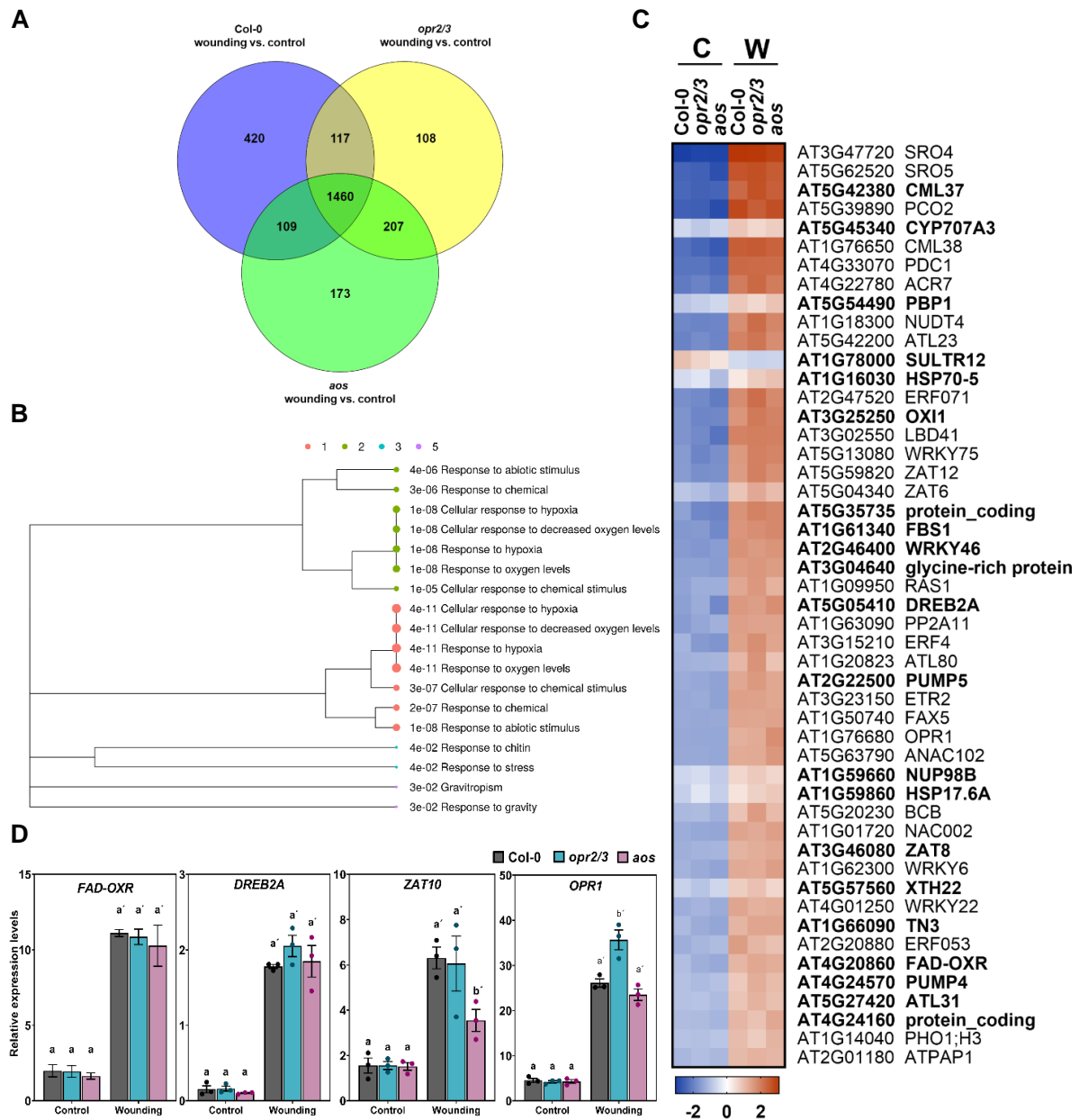


**Fig. 2.5 The JA/OPDA-independent wounding response**

Ten-day-old seedlings from Col-0, *opr2/3* and *aos* were pretreated with MeJA during development and were either unwounded (Control) or harvested 1h post wounding with forceps (Wounding).

**A:** Venn diagram representing differentially expressed genes by wounding in Col-0 in comparison to *opr2/3* and *aos*. 1640 DEGs were common to all genotypes and were identified by using FDR and FC cutoffs of 0.05 and 2, respectively.

**B:** Hierarchical clustering tree summarizing significant pathways enriched in the 1460 genes common to all genotypes from (A). Gene ontology analysis is based on the category “biological process”.

**C:** Heatmap illustrating 50 out of 211 DEGs enriched in GO term response to stress from (B), with C: control and W: wounding. Average FPKM values of three independent biological replicates were transformed into row normalized Z-Score. Genes in bold were identified as OPDA-responsive DEGs in previous work (Taki *et al.*, 2005).

**D:** qRT-PCR validation of known OPDA-responsive genes. *FAD-OXR*, *DREB2A*, *ZAT10* and *OPR1* expression in Col-0, *opr2/3* and *aos* mutants at control and wounding conditions. Transcript levels were normalized to those of *PP2A*. Bars represent means of three biological replicates (single dots;  $\pm$ SEM).

Different letters denote statistically significant differences among genotypes (within treatments) as determined by One-Way ANOVA followed by Tukey HSD ( $p < 0.05$ ).

### 2.1.3.3 A JA-mediated response is distinct in the transcriptional wounding response.

To identify the JA-mediated wounding response, the transcriptome of Col-0 was compared to those of the JA-deficient mutants *opr2/3* and *aos* at control condition and upon wounding. The comparisons, depicted in the Venn diagram in Fig. 2.6A, showed that 58 genes were differentially expressed in Col-0 independently of the condition and that wounding resulted in 231 novel genes differentially expressed in Col-0 in comparison to the mutants. The 58 DEGs that showed JA-dependent differential expression in Col-0 at control and wounding conditions were enriched in JA-signaling components, mainly JAZ transcriptional repressors and JA-responsive genes involving genes encoding JA biosynthesis enzymes (*AOC2*, *JOX2* and *JRG21*) and defense proteins (*VSPs* and *PDFs*) (Fig. 2.6B-C). The expression levels of selected JA-responsive genes from this list were determined by qRT-PCR (Fig. 2.6D). The JA-signaling genes *JAZ1*, *JAZ7*, *JAZ10*, the biosynthesis gene *AOC2* and the JA-responsive gene *CLH1* showed differential expression in Col-0 in comparison to the mutants already at basal levels in control condition. Wounding led to a higher induction of these transcripts in Col-0 in comparison to the mutants confirming the JA-dependent basal expression and up-regulation upon wounding.

Wounding resulted in the increase of the number of DEGs in Col-0 in comparison to the JA-deficient mutants *opr2/3* and *aos* (Fig. 2.6A), since wounding resulted in 231 DEGs specific to Col-0. This set of DEGs showed enrichment in JA and wounding response processes as (Table S3). For instance, the JA-signaling transcriptional repressors *JAZ2*, *JAZ6*, *JAZ8*, *JAZ9* and *JAZ13* were up-regulated upon wounding and showed significantly higher expression levels in the Col-0 background in comparison to *opr2/3* and *aos* (Fig. 2.7). Other JA-responsive genes like *GRX480* and *LOX2* showed JA-dependent differential expression in Col-0 mainly upon wounding. Note that the biosynthetic enzyme *LOX2* had similar basal transcripts in Col-0 and the mutants due to the MeJA pretreatment during development (Table S1) and was not induced in the mutants upon wounding rather its transcripts decreased, indicating that the induction of its transcripts is JA-dependent (Fig. 2.7).

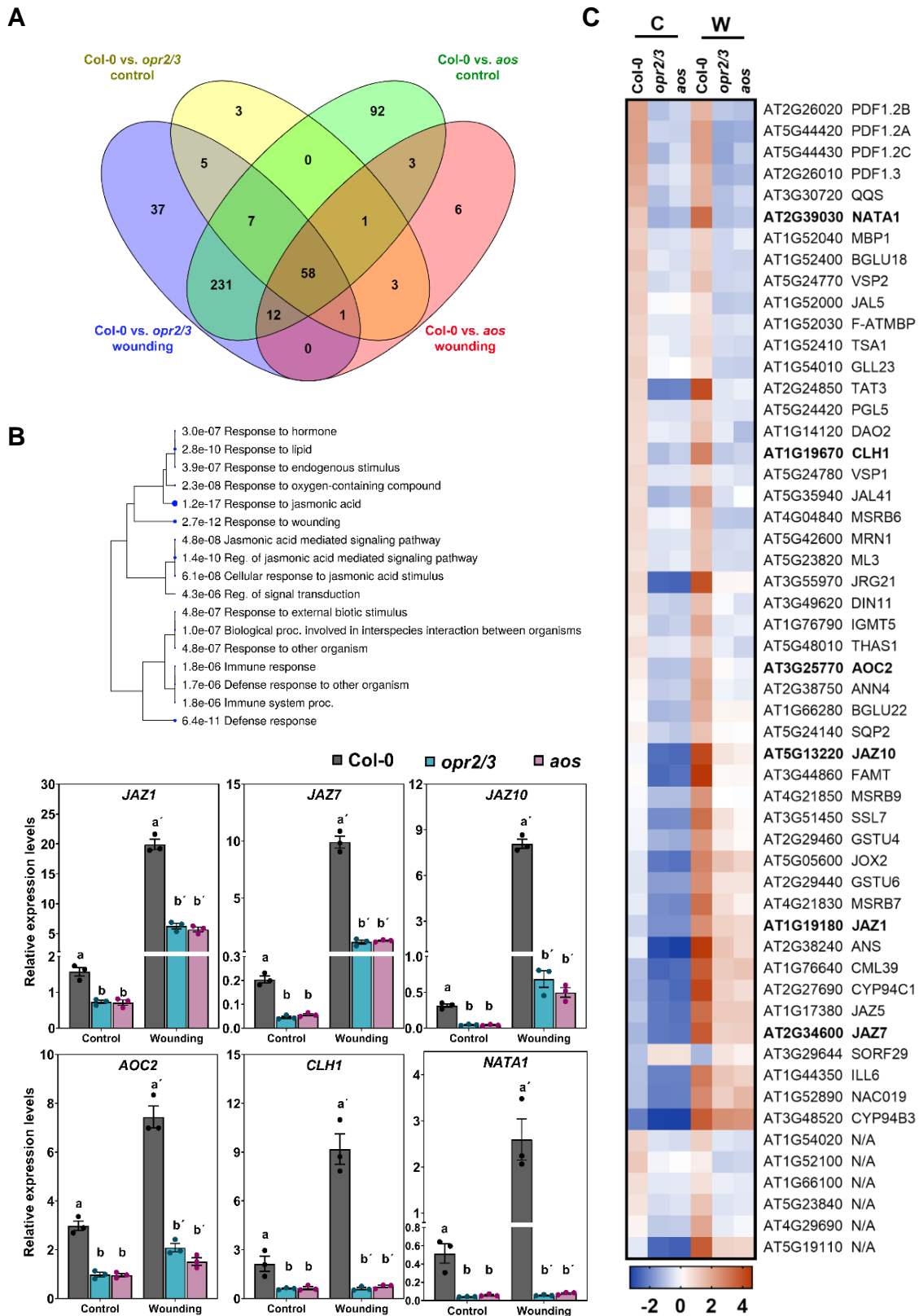


**Fig. 2.6 The JA-dependent wounding response**

Ten-day-old seedlings from Col-0, *opr2/3* and *aos* were pretreated with MeJA during development and were either unwounded (Control) or harvested 1h post wounding with forceps (Wounding).

**A:** Venn diagram representing 231 differentially expressed genes identified by RNAseq in Col-0 in comparison to *opr2/3* and *aos* upon wounding and 58 differentially expressed genes in Col-0 independently of the condition (FDR cutoff: 0.05, FC cutoff:  $\pm 2$ ).



**B:** Hierarchical clustering tree summarizing significant pathways enriched in the 58 genes from (B). Gene ontology analysis performed based on biological process.

**C:** Heatmap illustrating the 58 JA-dependent differentially expressed genes common to all comparisons in (A) with C: control condition and W: wounding. Average FPKM values of three independent biological replicates were transformed into row normalized Z-Score. Genes in bold were validated by qRT-PCR in (D). N/A: not annotated.

**D:** qRT-PCR validation of selected genes from (C). Relative transcript levels of *JAZ1*, *JAZ7*, *JAZ10*, *AOC2*, *CLH1* and *NATA1* in Col-0, *opr2/3* and *aos* mutants at control and wounding conditions. Transcript levels were normalized to those of *PP2A*. Bars represent means of three biological replicates (single dots;  $\pm$ SEM). Different letters denote statistically significant differences among genotypes (within treatments) as determined by One-Way ANOVA followed by Tukey HSD ( $p < 0.05$ ).

The signaling function of the JA pathway manifested in the transcriptomic data in three modes of action; first its presence at basal levels at control condition maintained the transcripts of certain genes at higher or lower levels (Fig. 2.6C). Second, the induction of JA/JA-Ile biosynthesis upon wounding resulted in an induction of a set of genes exclusively in the presence of JA-Ile, with no induction occurring in the absence of JA/JA-Ile. Within this set of genes are *CLH1*, *NATA1*, *LOX2*, *JAZ6* and *JAZ13* (Fig. 2.6D, Fig. 2.7). The third mode of action is that the induction of JA/JA-Ile levels upon wounding resulted in a significantly higher amplification of the transcripts of a set of JA-responsive genes which were induced but to very low extents in the biosynthesis mutants, such as *JAZ1*, *JAZ7* and *JAZ10* (Fig. 2.6A).

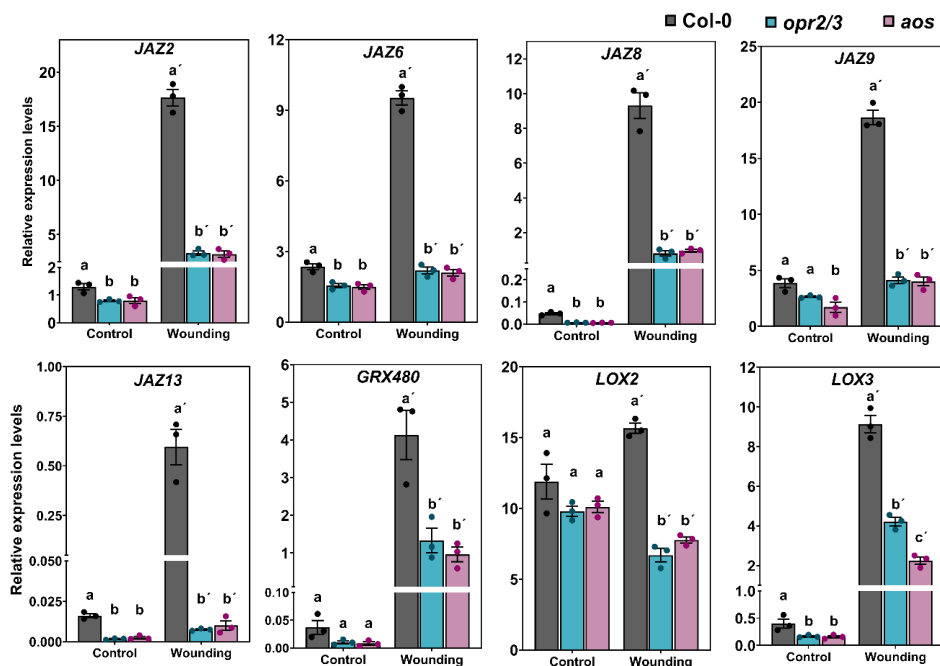


**Fig. 2.7 Wound-induction of JA-dependent, wound responsive genes.**

Ten-day-old seedlings from Col-0, *opr2/3* and *aos* were pretreated with MeJA during development and were either unwounded (Control) or harvested 1h post wounding with forceps (wounding).

Expression levels of JAZ signaling components were determined by qRT-PCR at control and wounding conditions and were normalized to those of *PP2A*. Bars represent means of three biological replicates (single dots;  $\pm$ SEM). Different letters denote statistically significant differences among genotypes (within treatments) as determined by One-Way ANOVA followed by Tukey HSD ( $p < 0.05$ ).

### 2.1.3.4 The OPDA-mediated transcriptional change is rather minor or absent.

The comparison of the transcriptome of Col-0, *opr2/3* and *aos* at control and wounding conditions did not show any particular response in *opr2/3* different than in *aos* which, if present, would have indicated a signaling role of OPDA during wounding (as previously shown in Fig. 2.4). To further investigate the possibility of a subtle OPDA-mediated transcriptional responses, Col-0 was omitted from the transcriptome comparisons to allow distinction of small differences between the *opr2/3* and *aos* genotypes.

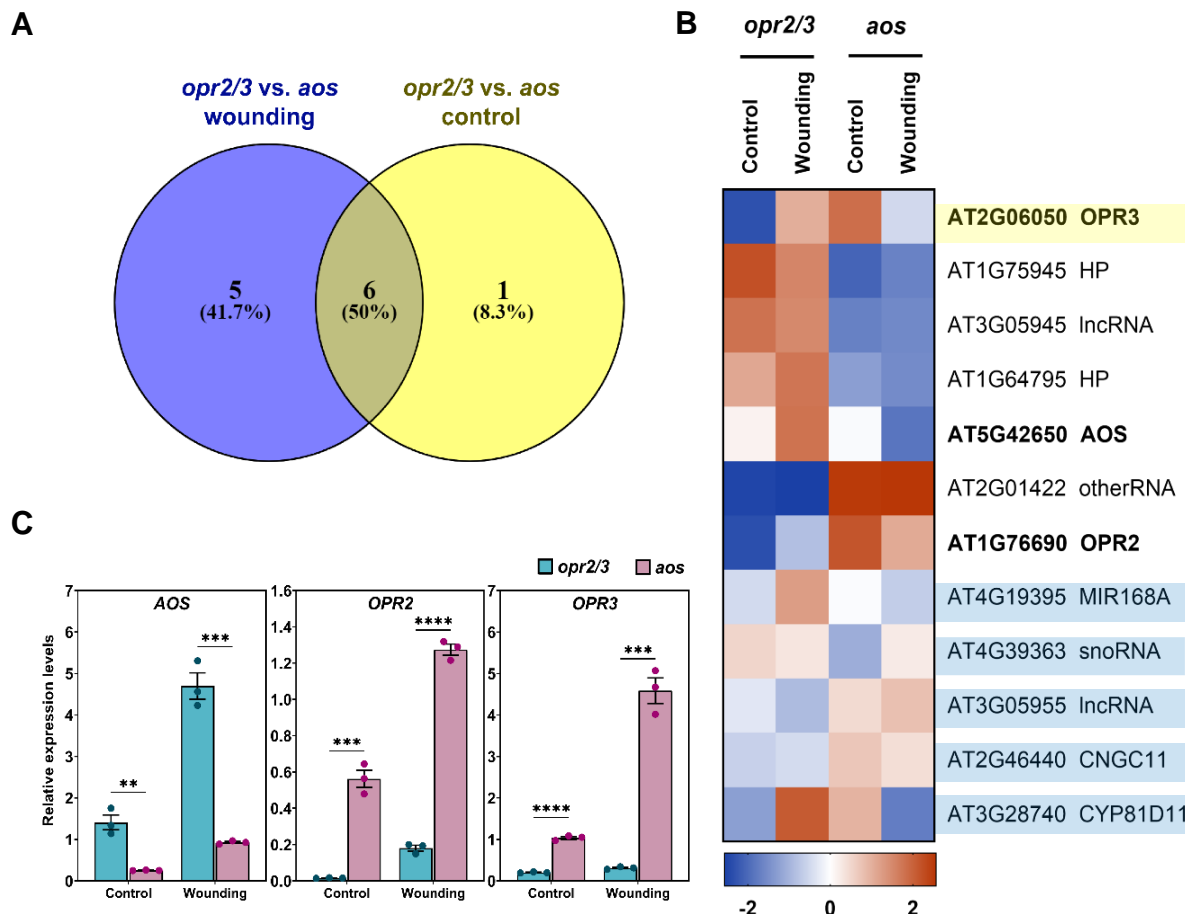


**Fig. 2.8 The OPDA-mediated transcriptional change**

Ten-day-old seedlings from Col-0, *opr2/3* and *aos* were pretreated with MeJA during development and were either unwounded (Control) or harvested 1h post wounding with forceps (wounding).

**A:** Venn diagram representing the 12 differentially expressed genes in *opr2/3* when compared to *aos* with 6 out of the 12 being common to control and wounding conditions (FDR cutoff: 0.05, FC cutoff:  $\pm 2$ ).

**B:** Heatmap illustrating the expression levels of the eleven differentially expressed genes in *opr2/3* in comparison to *aos* from (A). The Average FPKM values of three independent biological replicates were transformed into row-normalized Z-Score. Genes highlighted in yellow and blue correspond to the groups from the Venn diagram in (A) and non-highlighted genes are in the intersection. Genes in bold were validated by qRT-PCR in (C). HP: hypothetical protein.

**C:** qRT-PCR of selected genes from (B). AOS, OPR2, and OPR3 expression in *opr2/3* and *aos* mutants at control and wounding conditions. Transcript levels were normalized to those of *PP2A*. Bars represent means of three biological replicates (single dots;  $\pm$ SEM). Asterisks denote statistically significant differences among genotypes (within treatments) as determined by student t-test (\*  $p < 0.05$ , \*\*  $p < 0.01$ , \*\*\*  $p < 0.001$ , \*\*\*\*  $p < 0.0001$ ).



The comparison of *opr2/3* transcriptome to that of *aos* under control and wounding conditions resulted in 11 DEGs with an FDR of 0.05 and a minimum FC of  $\pm 2$  as cutoffs (Fig. 2.8A). Both genotypes differ only with seven genes at control condition and 11 genes upon wounding, six of which were common between both conditions. Within these DEGs, three genes representing fundamental differences between the genotypes were *AOS*, *OPR2* and *OPR3* (Fig. 2.8B). *OPR2* and *OPR3* were down-regulated in the *opr2/3* double mutant and *AOS* down-regulated in the *aos* mutant, which is in accordance with the mutations of the corresponding genotypes (Fig. 2.8C). The genotypes differed upon wounding by a cyclic nucleotide-gated ion channel (*CNGC11*), which was down-regulated in *opr2/3* in comparison to *aos* and a cytochrome P450 (*CYP81D11*) which was up-regulated in the *opr2/3*. Interestingly, *CYP81D11* was shown to induce a set of volatiles, including a volatile oxylipin 1-octen-3-ol (Bruce et al., 2008; Chen et al., 2019). The other DEGs between *opr2/3* and *aos* were five uncharacterized RNA species including two long non-coding RNAs (lncRNA), which could be involved in the regulation of the *AOS*, *OPR2* and *OPR3* genes and therefore their levels were affected in the mutants' backgrounds differently. These results indicated a very narrow difference between *opr2/3* and the *aos* mutants in addition to OPDA not showing any of the modes of action of the signaling molecule JA-Ile implying that both the presence of OPDA at basal levels and its endogenous rise during wounding did not mediate a transcriptional response.

#### **2.1.4 Replication of the same transcriptional approach with adult leaves shows similar results as seedlings.**

The same experimental design was reproduced using adult *A. thaliana* rosettes grown on soil, with adjusting the MeJA pretreatment to be applied by spraying the rosette instead of being added to the media as done for the seedlings (Fig. S8). mRNA sequencing of the samples showed similar transcriptomic change as observed in seedlings, with a JA-induced response characteristic of the Col-0 genotype in the contrary to the *opr2/3* and *aos* mutants which showed similar transcriptional changes at control and wounding conditions and their transcriptomes overlapped when analyzed by PCA (Fig. S9A, B). A common transcriptional response between the three genotypes was enriched in stress-responsive genes and included genes previously attributed as OPDA-responsive genes (Taki et al., 2005), which is in accordance with the results found in seedlings (Fig. S9C, D). And the comparisons between the *opr2/3* and *aos* genotypes to assess the effect of presence/absence of OPDA resulted in a low number of DEGs (22), 13 out of these DEGs were mainly up regulated in the absence of OPDA, in the *aos* mutant, at basal condition in comparison to the *opr2/3* (Fig. S10A-C). Nine DEGs were also found in the same comparison between *opr2/3* and *aos* done in seedlings and within these DEGs *CYP81D11* and the RNA species. The RNAseq data from adult leaves showed higher variability between biological replicates which could be noticed from the heatmap and the PCA plot (Fig. S10A-B), and this is due to the application of MeJA

pretreatment by spraying in contrast to seedlings where the pretreatment was added to the media and showed higher homogeneity between biological replicates. Hence, *opr2/3* and *aos* adult leaves transcriptomes were compared at control and wounding conditions in the absence of MeJA pretreatment (water was sprayed instead of MeJA during development), and despite *opr2/3* accumulating significant levels of OPDA in comparison to *aos*, only eleven genes showed differential expression like in seedlings. (Fig. S10C). When the results from seedlings and adult leaves are crossed, the resulting main differences between *opr2/3* and *aos* independently from the developmental stage are only eight genes (Table 2.1). *OPR2*, *OPR3* and *AOS* constituting the fundamental differences between the mutant backgrounds are excluded, thus only two hypothetical proteins and three RNA species with unknown function are the main differences between the presence of OPDA and its absence at control and under wounding conditions.

**Table 2.1 DEGs in the *opr2/3* mutant compared to *aos* in seedlings and adult leaves.**

| Gene ID   | Gene name/description |
|---|-----------------------|
| <b>Genes up regulated in the <i>opr2/3</i> background</b>   |                       |
| AT5G42650   | AOS                   |
| AT1G75945   | Hypothetical protein  |
| AT1G64795   | Hypothetical protein  |
| AT3G05945   | lncRNA                |
| <b>Genes down regulated in the <i>opr2/3</i> background</b> |                       |
| AT1G76690   | <i>OPR2</i>           |
| AT2G06050   | <i>OPR3</i>           |
| AT3G05955   | lncRNA                |
| AT2G01422   | other RNA             |

### 2.1.5 The endogenous rise of OPDA compared to the exogenous application of the compound.

The transcriptomic results described above indicated that the endogenous OPDA was unable to mediate a transcriptional change in *A. thaliana*, neither at basal levels nor upon its rise after wounding. Additionally, several genes previously shown as OPDA-inducible (Taki et al., 2005), were induced in the absence of OPDA in the wounded *aos* mutant. Previous work on OPDA signaling, however, adopted a different approach either using the *opr3* single mutant or exogenously applying OPDA to seedlings or leaves of JA-deficient mutants (Taki et al., 2005). Therefore, seedlings of the *opr2/3* double mutant treated with 25  $\mu$ M OPDA for 30 min were included in the RNAseq experiment. To characterize the response of the *opr2/3* mutant to the endogenous rise or exogenous application of OPDA, the transcriptomes of *opr2/3* after wounding and after application of OPDA were compared. Data from wounded Col-0 were added to this comparison as a reference for JA-mediated transcription, whereas data from wounded *aos* served as a negative control for transcriptional changes mediated by other

signaling molecules in the absence of OPDA and JA. All seedlings including those exogenously fed with OPDA were pretreated with MeJA during development to restore the JA-biosynthetic protein levels in the mutants.

K-means clustering of the wounding response in all the genotypes with the *opr2/3* exogenously fed with 25  $\mu$ M OPDA, showed that within the 1000 variable genes a cluster was up-regulated mainly in the exogenous OPDA feeding condition and was enriched in genes involved in sulfate reduction and assimilation processes (Fig. S11). The pathway of sulfur assimilation comprised APS reductases like *APR1*, *APR2* and *APR3* and an ATP-sulfurylase, *APS1*, which were up-regulated in *opr2/3* by exogenous OPDA and did not respond to endogenous OPDA (Fig. 2.9A). And most interestingly, the sulfate-deficiency induced gene *SDI1* (Howarth et al., 2009). Validation of these transcriptional changes by qRT-PCR showed significant induction of *SDI1*, *APS1* and *APR1* in *opr2/3* by OPDA treatment in comparison to the endogenous accumulation of OPDA upon wounding in the same mutant background (Fig. 2.9B). Stress-responsive transcription factor *ERF094* also showed a specific induction to only exogenous OPDA (Fig. 2.9B). In regard to that, it was found that OPDA-GSH adducts are formed and get degraded in the vacuole as a mean of cell detoxification (Ohkama-Ohtsu et al., 2011), consequently the induction of the sulfur metabolism by exogenous application of OPDA to the *opr2/3* mutant indicates a process of cell detoxification leading to the activation of sulfur metabolism. The clustering of the transcriptome also showed an interesting subset of genes up-regulated by exogenous OPDA which were also induced only in Col-0 by wounding, meaning that they are JA-regulated (Fig. S11). This gene cluster was indeed enriched in JA-signaling and JA-mediated wounding response and encompassed several *JAZ* transcriptional repressors (Fig. 2.9A).

One reason for the induction of JA-signaling might be the conversion of the exogenous OPDA to JA when fed to the *opr2/3* double mutant. To verify this hypothesis, OPDA, JA and JA-Ile levels were quantified in *opr2/3* seedlings exogenously fed with 25 $\mu$ M OPDA and compared to the wounded seedlings endogenously accumulating OPDA (Fig 2.9C). Levels of JA-Ile were significantly enhanced in the *opr2/3* double mutant by exogenous OPDA treatment, while no statistically significant difference was found at wounding in comparison to the controls. Expression levels of JA-signaling components confirmed this observation and showed significant increase in *JAZ7*, *JAZ6*, *JAZ9*, *JAZ10* and *JAZ13* transcripts in the *opr2/3* double mutant by OPDA treatment in comparison to the rise of endogenous OPDA during wounding (Fig 2.9D).

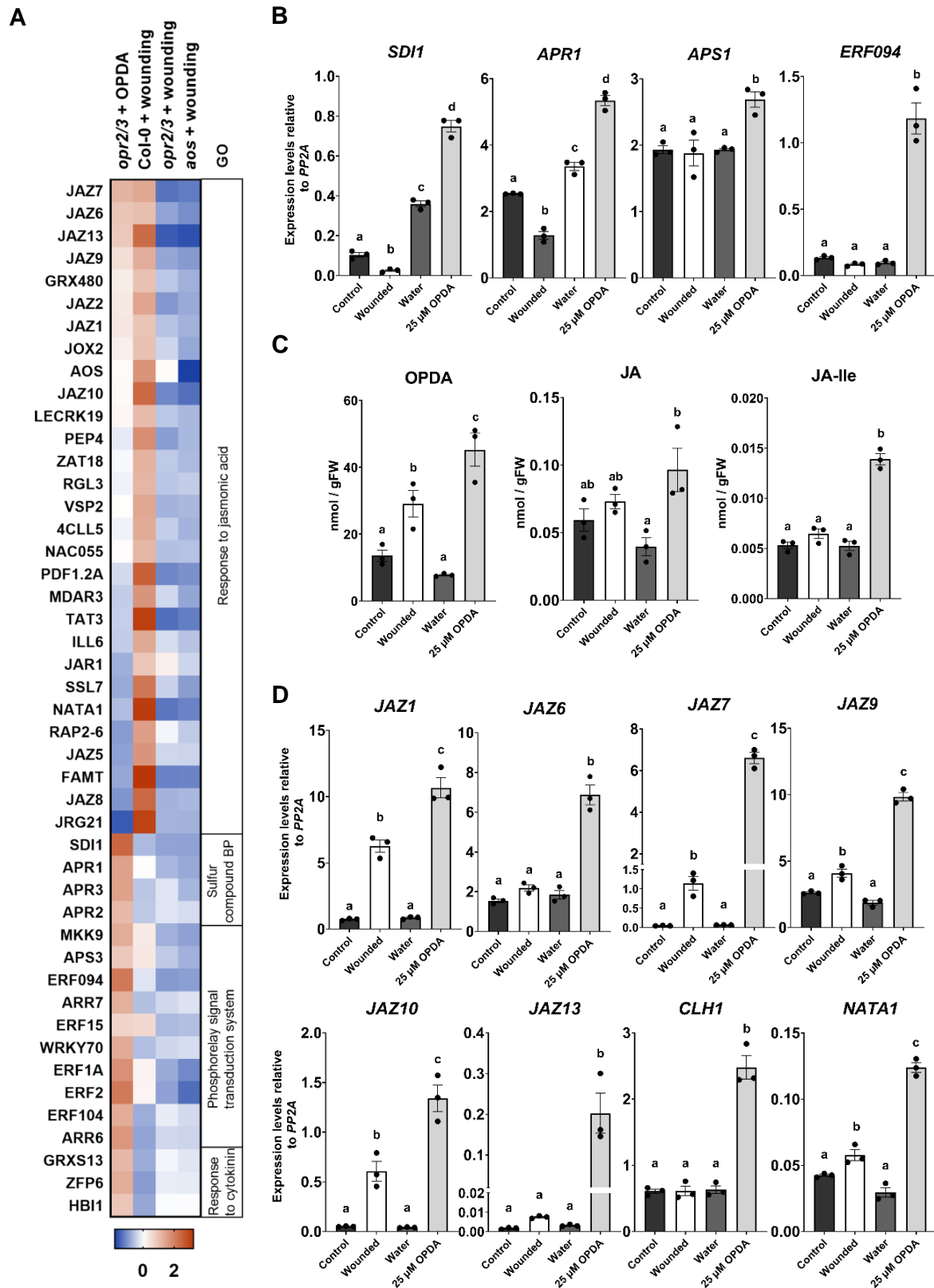


**Fig. 2.9 Exogenous OPDA treatment of the *opr2/3* mutant results in the induction of sulfur metabolism in addition to JA-signaling unlike its endogenous rise upon wounding.**

Ten-day old Seedlings from Col-0, *opr2/3* and *aos* were pretreated with MeJA during development and were harvested 1h post wounding with forceps (+wounding) or treated with 25  $\mu$ M OPDA (+ OPDA).

**A:** Heatmap illustrating the DEGs which showed specific transcriptional change upon treatment of *opr2/3* with 25  $\mu$ M OPDA in comparison to wounded *opr2/3*. Genes were organized according to their Gene ontology functional classes (GO). The Average FPKM values of three independent biological replicates were transformed into row-normalized Z-Score.

**B, C and D:** Validation of the specific response of the *opr2/3* mutant to exogenous OPDA with expression levels of stress-responsive genes (**B**), OPDA, JA and JA-Ile levels (**C**), and expression levels of JA-signaling components (**D**). Seedlings of *opr2/3* were treated with 25  $\mu$ M OPDA for 30 min or wounded (1 hour post wounding) and their respective controls water-treated (water) and non-wounded (control). Bars represent the means of three biological replicates (single dots) with 120 seedlings each. Different letters denote statistically significant differences among samples as determined by One-Way ANOVA followed by Tukey's HSD test ( $p < 0.05$ ).

Interestingly, several genes identified as JA-specific (see section 2.1.3.3) due to their specific induction in Col-0 upon wounding, were also induced upon OPDA treatment of the *opr2/3* mutant. For instance, *CLH1*, *JAZ6* and *JAZ13* transcripts were upregulated in a significant and specific manner in the *opr2/3* upon OPDA treatment in comparison to wounded and non-treated seedlings (Fig 2.9D). While other JA-responsive genes such as *JAZ1*, *JAZ7*, *JAZ9*, and *JAZ10* displayed slight induction upon wounding in *opr2/3*, they exhibited significantly higher induction upon OPDA treatment of *opr2/3* (Fig 2.9D). Both determinations of hormone and JA-markers transcript levels indicated that the exogenous application of OPDA led to partial amounts getting converted to JA and JA-Ile. These low JA-Ile levels induced significant differential expression of several JA-responsive genes at the transcriptional level. In contrast, although wounded *opr2/3* seedlings accumulated OPDA, no significant amounts of JA-Ile were formed.

## **2.2 The subcellular distribution of OPDA can indicate putative signaling function.**

The results from the transcriptional approach showed different responses triggered by OPDA accumulation when exogenously applied compared to its endogenous rise, suggesting a compartmentalization of OPDA upon its production.

A second approach to investigate whether OPDA could still act as a signaling molecule was to investigate the subcellular distribution of OPDA. Whether OPDA as a JA-precursor is compartmentalized upon its production as suggested by the transcriptional approach or it can translocate to other cell compartments was the question to be investigated. In the case of OPDA mediating regulation of gene expression, its translocation to the nucleus would be expected. To investigate this hypothesis, we chose to perform a trans-organellar complementation of the *opr2/3* double mutant and it consisted of complementing this double mutant with OPR3 targeted to a different organelle than peroxisomes, where it normally occurs, to verify where its substrate, OPDA, could be present. Such approach was performed in the case of tocopherols to investigate the biochemical continuity between chloroplasts and ER, and showed that substrates present in the chloroplast could be accessible to their corresponding enzymes from the ER (Mehrshahi et al., 2013).



### 2.2.1 Targeting of OPR3 to different cell compartments.

OPR3 is a peroxisomal protein that is imported to the peroxisomal matrix through the peroxisomal targeting signal 1 (PTS1) which consists of a tripeptide at the extreme carboxy tail of the protein (Gould et al., 1989). OPR3 contains a variation of the -SKL (serine-lysine-leucine) prototypic PTS1 signal corresponding to an -SRL (serine-arginine-leucine). This tripeptide was first removed to enable the targeting of OPR3 to other organelles and C- and N-terminal fusions of OPR3 $\Delta$ SRL with YFP were transiently expressed in *N. benthamiana* leaves and compared to OPR3-YFP fusions (Fig. 2.10).

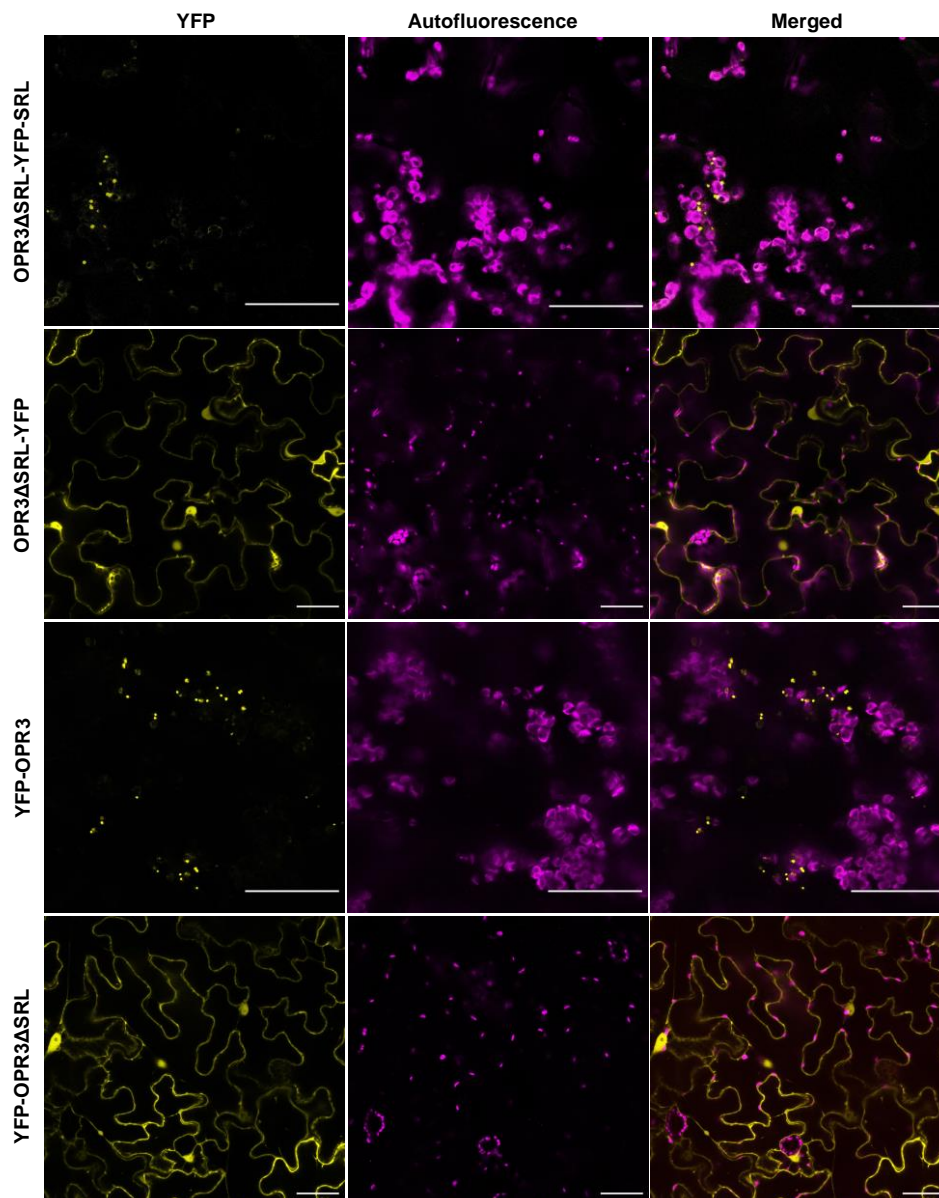


**Fig. 2.10 The removal of the SRL signal results in the alteration of OPR3 import to peroxisomes**

OPR3 $\Delta$ SRL either fused C- or N-terminally to YFP was transiently expressed in *N. benthamiana* leaves using the *CaMV* 35S promoter and imaged 48-72h post infiltration. OPR3 $\Delta$ SRL-YFP-SRL and YFP-OPR3 were used as controls where the SRL peroxisomal targeting is present. The yellow and magenta signals correspond to YFP and to chlorophyll autofluorescence, respectively. Scale bars: 50  $\mu$ m.

In the presence of the SRL carboxy-signal, OPR3-YFP formed a punctuate signal that is typical of peroxisome-targeted proteins. Transient expression of OPR3 $\Delta$ SRL together with free triple mCherry in *N. benthamiana* leaves confirmed colocalization of both signals to the cytosol (Fig. S12). The removal of this signal indeed resulted in a cytosolic localization of OPR3 indicating that the SRL tripeptide is solely responsible for the targeting of OPR3 to peroxisomes (Fig. 2.10).

Since the oxidoreductase domain of OPR3 is situated in the middle of the protein sequence, it was not clear whether its fusion to YFP at the C- or N- terminus would affect its activity. Thus, the targeting of OPR3 to different organelles was designed with YFP fusions at both termini.

### 2.2.1.1 ER targeting of OPR3

The import of soluble proteins to the ER/secretory apparatus relies on an N-terminal signal peptide (SIP) which is theoretically cleaved off following import (Kunze and Berger, 2015). The signal peptide permits co-translational entrance of the protein to the ER and its traveling along the secretory pathway, therefore to retain the protein within the ER a H/KDEL C-terminal tag is needed (De Meyer and Depicker, 2014). To test the ER targeting of OPR3 $\Delta$ SRL-YFP, transient expression assays were initially performed in *N. benthamiana* leaves (Fig. S13A, B). Both ER-targeted OPR3-YFP and YFP-OPR3, expressed under the 35S promoter, showed a clear net-like structure in the epidermal cells in addition to signal surrounding the nuclei corresponding to an ER localization. Detection of the fusion protein from the transient assays showed the expected molecular weight of 72 kDa (Fig. S14A). To validate the ER localization of OPR3, colocalization with an mCherry ER marker was performed in *N. benthamiana* protoplasts and showed superposition of the YFP and mCherry signals in a network-like structure within the cell and surrounding the nucleus (Fig. 2.11A, B).

### 2.2.1.2 Cytosolic targeting of OPR3

OPR3 $\Delta$ SRL-YFP showed cytosolic localization, however its localization extended also to the cell nuclei as the YFP signal was clearly visible there (Fig. 2.10). To make the targeting of OPR3 exclusively to the cytosol, a nuclear export signal (NES) was added to the carboxy-end of the OPR3-YFP fusions. The NES consists of 12-leucine-rich amino acids derived from the HIV1 REV protein (Kosugi et al., 2008). The inclusion of an NES signal permitted indeed to keep OPR3 within the cytosol as the transient assays showed in *N. benthamiana* leaves (Fig. S13C, D), and the 71 kDa expressed fusion protein was detected from the infiltrated leaves (Fig. S14B). While the mScarlett cytosolic marker showed both nuclear and cytosolic localizations, the use of the NES resulted in a YFP signal surrounding the nuclei validating an exclusive cytosolic localization of OPR3 (Fig. 2.11C, D).



### 2.2.1.3 Nuclear targeting of OPR3

The nuclear localization signal (NLS) from simian virus 40 (SV40), consisting of seven Lysine-rich amino acids, was used to target OPR3 to the nucleus (Lu et al., 2021; Raikhel, 1992). The detection of the nuclear OPR3-YFP protein of 71 kDa was successfully done by anti-YFP immunoblotting (Fig. S14B).

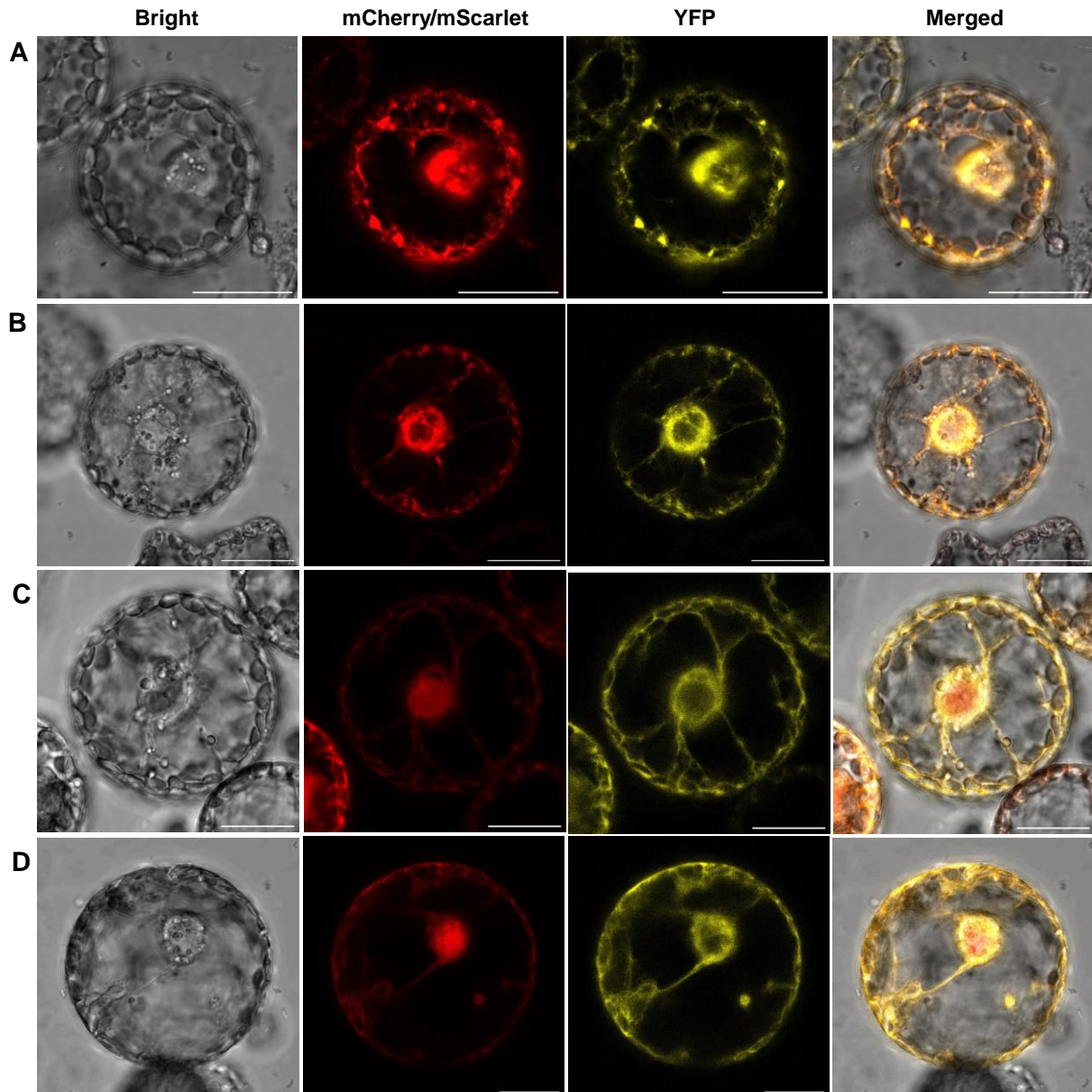


**Fig. 2.11 OPR3 targeted to the ER, cytosol, nucleus, and chloroplasts colocalizes with the corresponding organelle marker in *N. benthamiana* protoplasts.**

The protoplasts were transiently co-transformed with each construct and its corresponding organelle marker, and imaged 12 h post transformation. The yellow signal corresponds to YFP, the red to the mCherry organelle marker, and the gray to the bright field. Scale bars: 20  $\mu$ m.

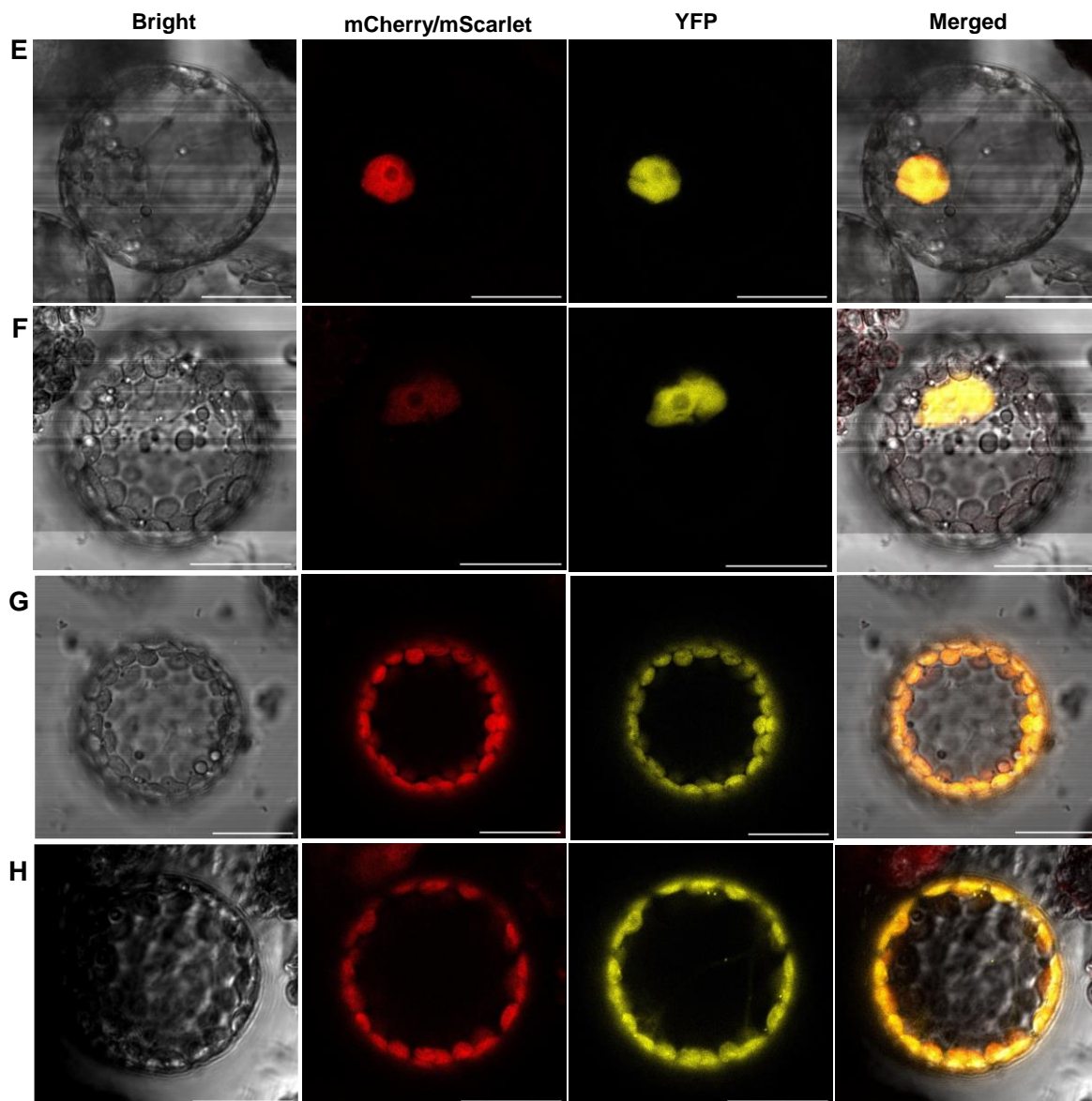
**A, B:** ER-targeted OPR3 colocalizes with the WAK-mCherry-KDEL marker. The YFP fusions being SIP-OPR3 $\Delta$ SRL-YFP-HDEL (**A**) and SIP-YFP-OPR3 $\Delta$ SRL-HDEL (**B**).

**C, D:** Cytosol-targeted OPR3 colocalizes with the mScarlet marker in the cytosol but not inside the nucleus. The YFP fusions being OPR3 $\Delta$ SRL-YFP-NES (**C**) and YFP-OPR3 $\Delta$ SRL-NES (**D**).

**E, F:** Nucleus-targeted OPR3 colocalizes with the HTA6-mCherry marker. The YFP fusions being NLS-OPR3 $\Delta$ SRL-YFP (**E**) and NLS-YFP-OPR3 $\Delta$ SRL (**F**).

**G, H:** Plastid stroma-targeted OPR3 colocalizes with the RubisCO-mCherry marker. The YFP fusions being cTP-OPR3 $\Delta$ SRL-YFP (**G**) and cTP-YFP-OPR3 $\Delta$ SRL (**H**).

Fig. 2.11 (continued)



Transient expression assays in *N. benthamiana* leaves confirmed OPR3 localization to the nucleus when fused to the SV40 NLS (Fig. S13E, F). Validation of this localization by colocalization with an mCherry nuclear marker in protoplasts showed superposition of the YFP and mCherry signals (in a single round/oval shape per cell) corresponding to the nucleus (Fig. 2.11E, F).

#### 2.2.1.4 Plastid stroma-targeting of OPR3

To allow the import of OPR3 to the chloroplasts, a chloroplast target peptide (cTP) was added to the N-terminal region of OPR3-YFP fusions. The initial 51 to 65 amino acids from the chloroplastic protein AtRECA1 (AT1G79050) were used as a cTP for OPR3 (Eseverri et al., 2020; Rowan et al., 2010). OPR3-YFP fusions colocalized with the chlorophyll autofluorescence in *N. benthamiana* epidermal cells showing successful import to the

chloroplasts (Fig. S13G, H). The presence of the YFP signal within the stromules of plastids, which are stroma-filled tubular extensions from the chloroplasts (Brunkard et al., 2015), confirmed stroma-localization of OPR3 (Fig. S13H).

#### 2.2.1.5 Mitochondrial targeting of OPR3

The targeting to the mitochondria like the chloroplast, relies on an N-terminal located transit peptide (mTP). The mTP from the mitochondrial heat shock protein AtHSP60 (AT3G23990), which is a mitochondria molecular chaperone, consists of 31 amino acids (Komiya et al., 1994; Lister et al., 2004). OPR3 showed mitochondrial localization when it was fused to this mTP and transiently expressed in *N. benthamiana* leaves. The YFP signal formed small dots forming cloud-like structures surrounding the nucleus and scattered in the cell (Fig. S13I, J). Immunodetection of YFP from the infiltrated leaves confirmed the presence of the OPR3-YFP fusions corresponding to around 73 kDa (Fig. S14C). Transient expression in *N. benthamiana* protoplasts however did not show mitochondrial targeting (data not shown), nevertheless the results from the leaf infiltration were considered as successful targeting.

#### 2.2.2 Complementation of the *opr2/3* double mutant with different organelle targeted OPR3

The *opr2/3* mutant lines complemented with organelle-targeted OPR3 corresponding to ER (*opr2/3*+ER-OPR3), cytosol (*opr2/3*+Cy-OPR3), nucleus (*opr2/3*+NI-OPR3), chloroplast (*opr2/3*+Cp-OPR3), and mitochondria (*opr2/3*+Mt-OPR3) were transformed using constructs containing either OPR3-YFP or YFP-OPR3 driven by the *p35S* promoter and *tOCS* terminator unless mentioned differently (see material and methods, section 6.3.7.1). Additional *opr2/3* lines complemented with peroxisome-targeted OPR3-YFP (*opr2/3*+Px-OPR3) and with an empty vector (*opr2/3*+EV) were used as positive and negative controls, respectively. A second positive control was Col-0 transformed with the empty vector (Col-0+EV).

To validate that the designed organellar-targeting of OPR3, previously tested transiently in *N. benthamiana* leaves and protoplasts, is also functional in *A. thaliana* system, subcellular localization of OPR3 in the generated stable transgenic lines was checked by fluorescence microscopy (Fig. 2.12). Visualization of the YFP signal in the leaves of the *opr2/3* complementation lines showed clear localization of OPR3 in each of the tested compartments -peroxisomes, ER, cytosol, nucleus, chloroplast, and mitochondria (Fig. 2.12A-F). Despite the unsuccessful colocalization of mitochondria targeted OPR3 in *N. benthamiana* protoplasts, clear mitochondrial localization was observed in *A. thaliana* leaves (Fig. 2.12F).



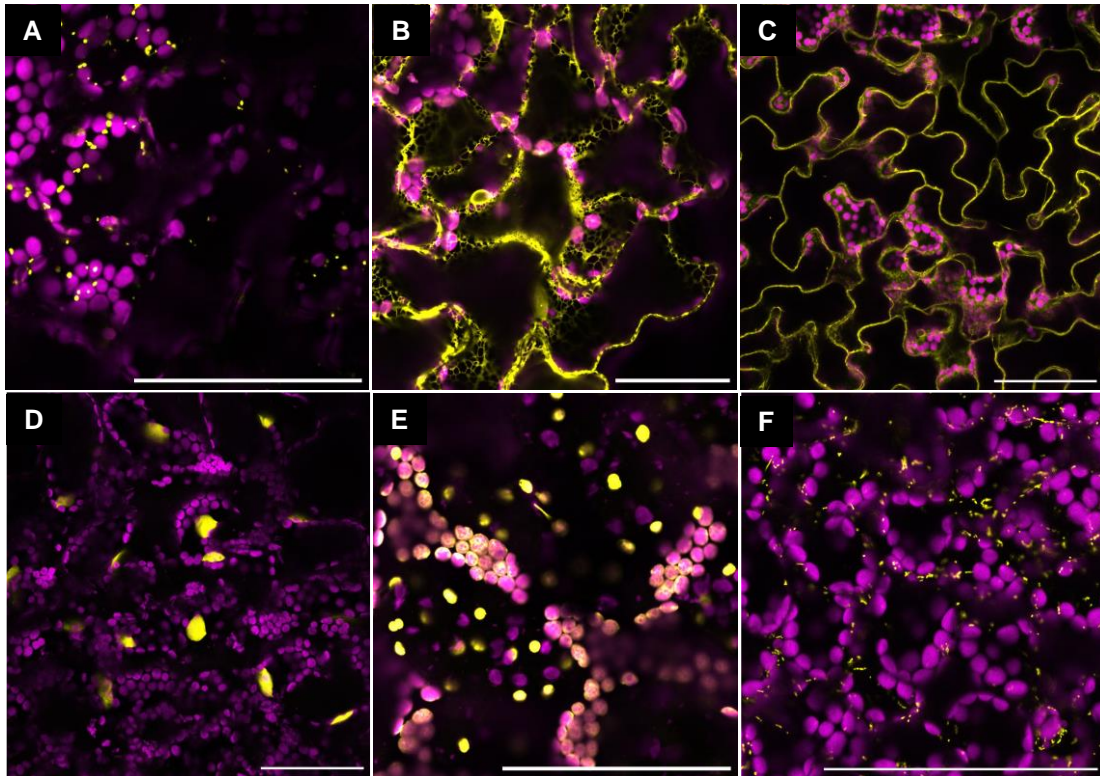


**Fig. 2.12 OPR3 shows the expected subcellular localizations in stable transformed *opr2/3* double mutants.**

Imaging was performed on leaf tissue of stable transgenic lines of T1 generation with *opr2/3*+Px-OPR3 (A), *opr2/3*+ER-OPR3 (B), *opr2/3*+Cy-OPR3 (C), *opr2/3*+NL-OPR3 (D), *opr2/3*+Cp-OPR3 (E), *opr2/3*+Mt-OPR3 (F). The yellow signal corresponds to YFP, and the magenta is chlorophyll autofluorescence. Cp: chloroplast, Cy: cytosol, ER: endoplasmic reticulum, Mt: mitochondria, NL: nucleus, Px: peroxisome. Scale bars: 100  $\mu$ m.

One aspect of JA-deficiency in *Arabidopsis* mutants is male sterility which is characteristic of JA-signaling and JA-biosynthetic mutants including the *aos* and *opr2/3* mutants where the biosynthesis pathway is interrupted in the chloroplast and peroxisome, respectively. At the open flower stage of *A. thaliana*, the stamen elongates to the stigma and anthers release pollen to enable pollination (Smyth et al., 1990). JA-deficiency, for instance in the *opr3* single mutant, translates in impediments in the anther filament elongation, anther dehiscence and pollen germination (Stintzi and Browse, 2000).

Dissection of the open flower bud from Col-0+EV showed elongated stamens and released pollen as expected at this stage unlike the *opr2/3*+EV which had shorter stamens and its anthers were not dehiscing (Fig. 2.13A). Peroxisome-targeted OPR3 was used as a positive control for assessing the success of the complementation the *opr2/3* double mutant, and indeed it complemented the male sterility phenotype as the open flower buds were like those of Col-0 (Fig. 2.13A). Surprisingly, each of the organelle targeted OPR3 resulted also in the complementation of the male sterility of the *opr2/3* double mutant. The ER lines, however, showed lower dehiscence of the anthers and less pollen release in comparison to the other complementation lines (Fig. 2.13A). During further development, the *opr2/3* double mutant was

not able to form siliques, unlike Col-0, and it also showed slightly different architecture in terms of height, branching and flower number (Fig. 2.13B). In line with the phenotype of the open flower buds, the complemented *opr2/3* lines recovered their ability to make siliques and only the *opr2/3*+ER-OPR3 line showed later silique formation as the initial flowers on the stem did not form siliques (Fig. 2.13B).



**Fig. 2.13 The restitution of the *opr2/3* mutant's fertility by OPR3 targeted to different organelles**  
 Displayed are the open flower buds at stage 14 (A) and plants inflorescence following silique formation (B) of Col-0+EV, *opr2/3*+EV and the *opr2/3* complemented lines. EV: Empty vector; Cp: chloroplast, Cy: cytosol, ER: endoplasmic reticulum, Mt: mitochondria, NI: nucleus, Px: peroxisome.

**A:** Open flower buds showing pollen release by anthers. The flower buds are from T3 generation single insertion homozygous lines for all lines except for the *opr2/3*+Mt-OPR3 which were T2 single insertion. Note the non-dehiscent anthers in (B) and reduced dehiscence of anthers in (D). Scale bars: 0.5 mm.

**B:** Plant inflorescences showing silique production. Plants were photographed after fruit set at days 50-60 post germination. Note the developed siliques marked by asterisks.

### 2.2.3 The effect of the targeting of OPR3 to other organelles on JA biosynthesis

To confirm that the complementation of the sterility phenotype of the *opr2/3* double mutant by each of the organelle-targeted OPR3 is due to complementation of the JA biosynthesis pathway, *cis*-OPDA, JA and JA-Ile levels were determined in leaves and flower buds of the complementation lines. The first two complementation lines that were characterized for JA biosynthesis restitution were the *opr2/3*+ER-OPR3 and *opr2/3*+Px-OPR3 lines (Fig. 2.14).

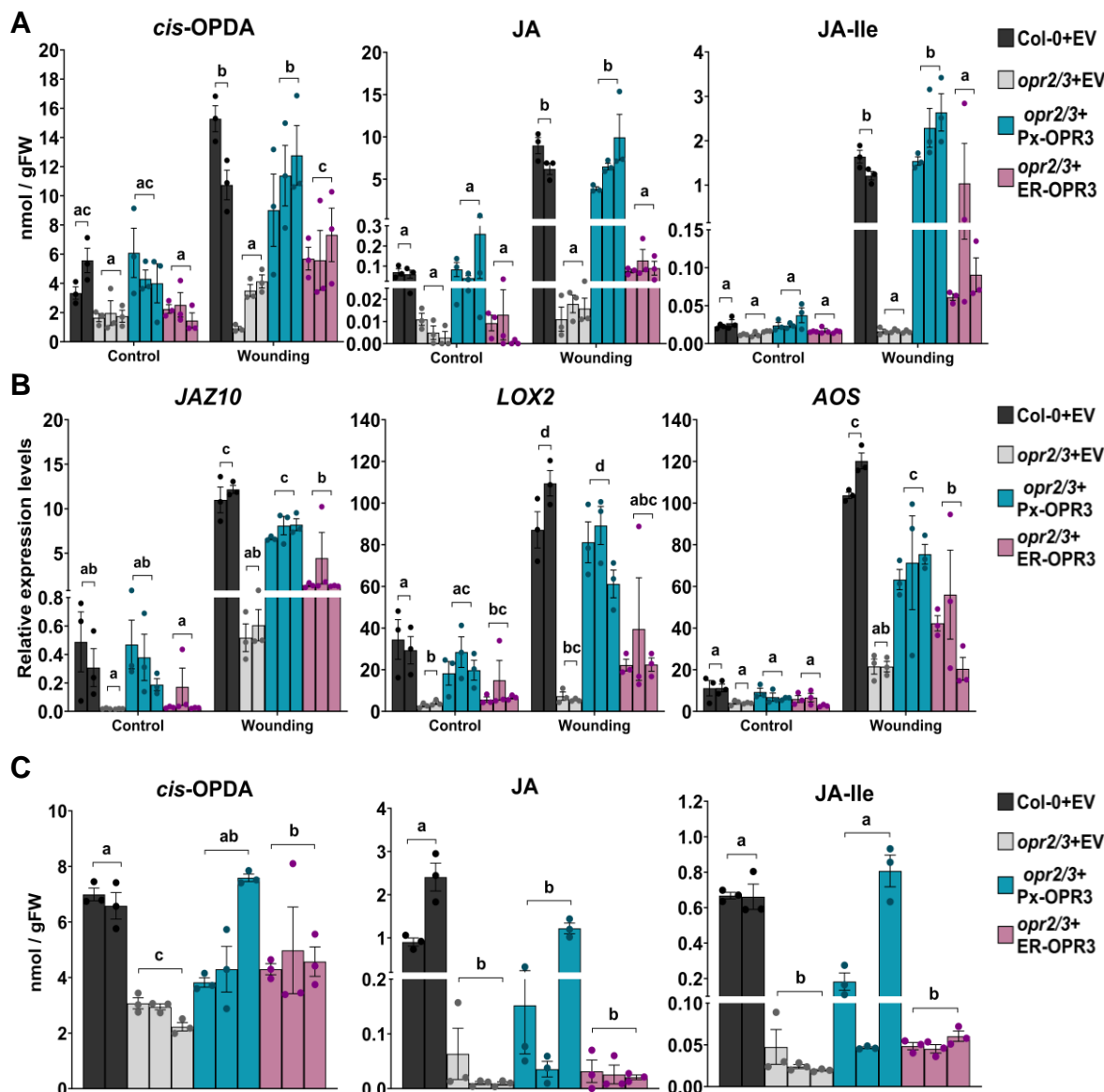


**Fig. 2.14** The *opr2/3*+ER-OPR3 complementation lines show low restitution of the JA pathway in wounded leaves and flower buds.

Col+EV and *opr2/3*+EV complementation lines were used as positive and negative controls, respectively. Data was collected from homozygous single-insertion lines of the T3 generation. For each of the genotypes three independent transgenic lines with three biological replicates were used (except for the Col-0+EV, which had two independent lines). Bars represent means of each independent line with three biological replicates (single dots;  $\pm$ SEM).

**A:** *cis*-OPDA, JA and JA-Ile levels were determined in 4-week-old rosette leaves which were wounded with forceps and harvested 1h following wounding or unwounded as controls.

**B:** Expression levels of *JAZ10*, *LOX2* and *AOS* were determined in relation to *PP2A* from the wounding experiment in (A) with 3 biological replicates per independent line.



**C:** Hormone levels were determined from flower buds at the developmental stage 12 with around 40-50 mg weight of flower buds per sample. Different letters denote statistically significant differences among means of the genotypes (independent lines were pooled per genotype) determined by Two-way ANOVA (**A**, **B**), and One-way ANOVA (**C**) followed by Tukey HSD ( $p < 0.05$ ).

A wounding experiment of 4-week-old rosettes was performed and showed that the leaves of *opr2/3+EV* accumulated lower OPDA levels than Col-0+EV at control as well as 1 h after wounding in addition to JA/JA-Ile deficiency as expected (Fig. 2.14A). Full restitution of the biosynthesis pathway by OPR3 was observed in the *opr2/3+Px-OPR3* complemented line since OPDA, JA and JA-Ile levels were statistically similar to those of Col-0+EV (Fig. 2.14A). ER-localized OPR3, however, restituted JA biosynthesis only slightly in the *opr2/3* double mutant, with a slight induction of OPDA in comparison to the *opr2/3+EV* in addition to slightly but not statistically significant higher JA and JA-Ile levels in leaves (Fig. 2.14A). Expression levels of the JA-responsive genes *JAZ10*, *LOX2* and *AOS*, showed the same pattern of induction of JA-signaling as the JA-Ile hormone production in these lines (Fig. 2.14B).

Since the male sterility phenotype of the *opr2/3+EV* is due to JA-deficiency in the flower buds, hormone profiling was also performed in this tissue. The developmental stage 12 of flower buds was characterized as the main stage where JA plays a role in male fertility (Browse and Wallis, 2019; Stintzi and Browse, 2000). While *opr2/3+EV* was deficient in JA and JA-Ile, the *opr2/3+Px-OPR3* lines were able to accumulate Col-0-equivalent levels of the bioactive form and the ER complementation resulted in a slight but not statistically significant induction of JA-Ile (Fig. 2.14C). In line with their partial fertility phenotype, the *opr2/3+ER-OPR3* lines showed partial restitution of JA biosynthesis and signaling. Validation that the JA restitution phenotype is solely due to the subcellular localization of OPR3 was performed by genotyping of the lines and determination of the accumulation of the transgene at the protein level (Fig. S15). The ER-complementation lines accumulated similar OPR3 levels compared the peroxisome lines indicating that the JA restitution phenotype is rather related to the subcellular localization of OPR3. Additionally, the *opr3* single mutant showed the same phenotypes when complemented with ER and peroxisome targeted OPR3, excluding any contribution of OPR2 to these phenotypes (Fig. S16). Further characterization of the fertility phenotypes in the *opr2/3+ER-OPR3* and *opr2/3+Px-OPR3* lines, in terms of flower and silique formation and pollen germination consolidated the partial fertile phenotype of the ER complementation lines (Fig. S17 and S18). Most importantly, this result indicated that JA-Ile functions in a dose-dependent manner and that OPR3 localized to the ER could have access to low amounts of its substrate, OPDA, therefore JA biosynthesis could take place partially.

The other tested organelles showed a full restitution of fertility phenotype indicating a full restitution of JA biosynthesis. A preliminary wounding experiment was performed to characterize the first generation of the *opr2/3*-complementation lines with the nuclear and



cytosolic-OPR3. 4-week-old rosettes were harvested 1h following wounding and with biological replicates pooled together. Hormone levels in the wounded leaves of the *opr2/3*+NI-OPR3 and the *opr2/3*+Cy-OPR3 T1 lines showed accumulation of high JA and JA-Ile levels at 1h following wounding (Fig. 2.15). Knowing that Col-0+EV lines could accumulate around 5-10 nmol/g FW JA upon wounding from previous experiments (Fig. 2.14A), these preliminary results point toward a full restitution of JA/JA-Ile biosynthesis when OPR3 is targeted to the nucleus and the cytosol, and putatively in the plastids and mitochondria, indicating possible presence of OPR3's substrate in these organelles.

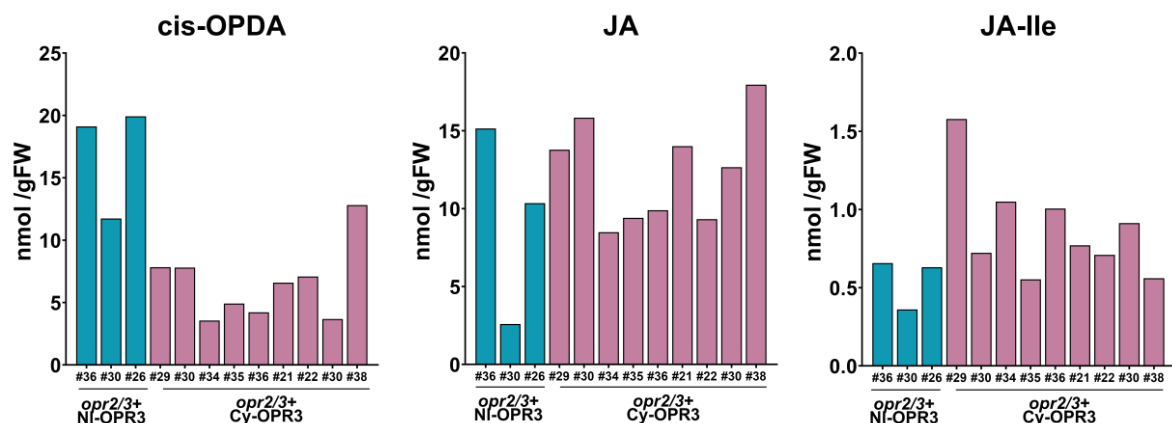


**Fig. 2.15 cis-OPDA, JA and JA-Ile levels in wounded leaves of the *opr2/3*+NI-OPR3 and *opr2/3*+Cy-OPR3 T1 generation.**

Leaves were harvested 1 h following wounding and tissue from five replicates was pooled together.

#### 2.2.4 Testing the cytosolic occurrence of OPR3 when targeted to other organelles.

The import of proteins to the ER is known to be co-translational while to all other tested organelles, cytosol, nucleus, chloroplast, and mitochondria the synthesis of the pre-protein occurs first in the cytosol prior to its import to the organelle. Interestingly, only the ER-targeted OPR3 led to a partial restitution of JA pathway while all other tested organelles showed full restitution at least of the flower phenotype. One common compartment, where OPR3 is synthesized before import to any of the tested compartments is the cytosol, therefore the restitution of JA biosynthesis in the *opr2/3* complementation lines might be due to the presence of newly synthesized OPR3-YFP in the cytosol before its import into the respective organelles. Despite the absence of any cytosolic YFP “leaking” signal in the *opr2/3* complemented lines by the YFP tagged OPR3, the possible presence of an amount of a functional OPR3 in the cytosol that is undetectable by the fluorescence microscopy prior to its import to the corresponding organelle, was hypothesized and was named “cytosolic occurrence of OPR3”. Testing of this hypothesis was carried out by transient BiFC assays in *N. benthamiana* leaves and was performed by Fiona Smith (B.Sc.). The concept was to find out whether an organelle-

targeted OPR3 fused to one half of YFP could meet a cytosolic-OPR3 fused to the other half of YFP (Fig. 2.16).

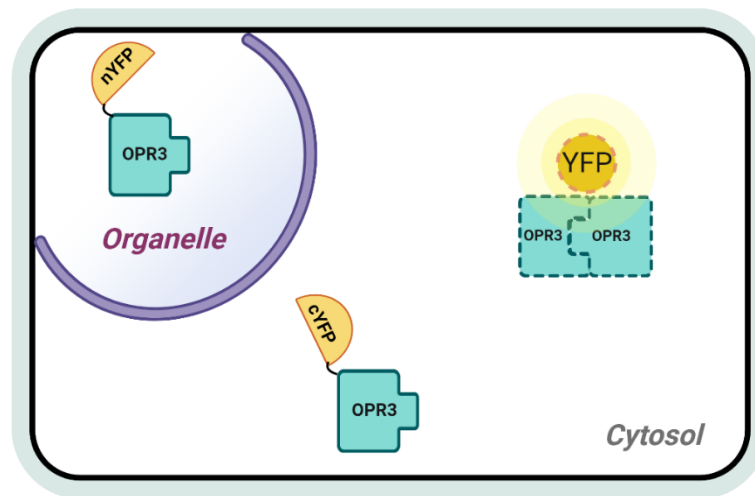


**Fig. 2.16 A BiFC system to test the cytosolic occurrence of OPR3 when targeted to another organelle.**

An organelle targeted OPR3 fused to a non-fluorescent half of YFP (n/cYFP) would emit a YFP signal upon only if it is able to dimerize with the cytosolic OPR3 fused to the other half of YFP. Hence the reconstitution of a cytosolic YFP signal would indicate the “cytosolic occurrence of OPR3” when targeted to another organelle.

The “cytosolic occurrence of OPR3” hypothesis was tested for three compartments (ER, peroxisomes and mitochondria) using constructs, in which both half YFP cassettes were present (*35Spro::OPR3-organelle1-nYFP* and *35Spro::OPR3-organelle2-cYFP*) in addition to an infiltration control (*NOSpro::NLS-mCherry*). Initial testing of the functioning of the BiFC system was performed by targeting the OPR3-fused to the YFP halves to the same organelle expecting the reconstitution of the YFP signal in the corresponding organelle (Fig. S19A). Peroxisome, ER, cytosol and mitochondria showed organelle specific YFP signal, and single YFP halves showed no YFP signal validating our BiFC system (Fig. S19A, B). For each of the tested organelles, two combinations with the YFP halves were used to ensure that the results are not affected by the position of the nYFP and cYFP halves. An important organelle to test was the peroxisome where OPR3 resides naturally, and there the YFP signal was reconstituted not only in the cytosol but also in the peroxisomes, indicating that the cytosolic OPR3-n/cYFP was able to be co-imported there by the peroxisomal OPR3-n/cYFP (Fig. 2.17A-B). These results nicely illustrated the previously reported piggybacking import mechanism of peroxisomes (Thoms *et al.*, 2015; Incarbone *et al.*, 2018). Another important control that was used to verify the specificity of the BiFC system, was the inclusion of the monomeric variant of OPR3, OPR3<sup>E292K</sup>, which has lower dimerization ability (Sperling N., 2012). By utilizing OPR3<sup>E292K</sup> we could determine whether the reconstitution of the YFP signal depended on the dimerization of OPR3 itself or the YFP halves. Peroxisomal targeting of OPR3<sup>E292K</sup> with both n/cYFP halves did not generate a YFP signal indicating that the reconstitution of the YFP relied

mainly on the dimerization of OPR3 (Fig. 2.17C). This result is however contradictory since OPR3<sup>E292K</sup> was expected to be still able to dimerize and generate a YFP signal, albeit with lower intensity compared to OPR3 (Sperling N., 2012).

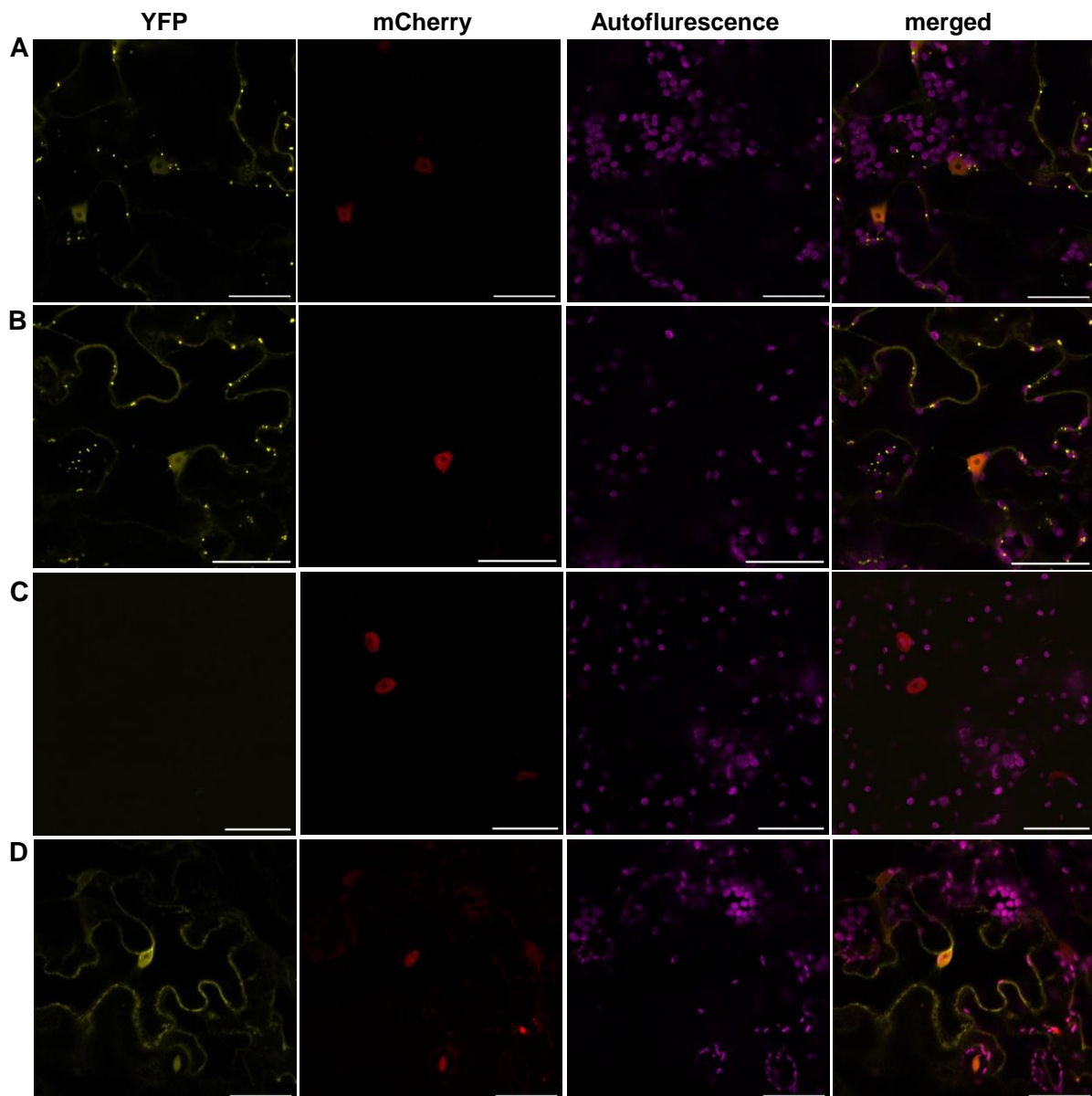


**Fig. 2.17 The OPR3 BiFC transient system in *N. benthamiana* leaves indicates possible “cytosolic occurrence of OPR3” in the targeting system.**

*N. benthamiana* leaves were imaged 48 h post-infiltration. The yellow signal corresponds to YFP, red to mCherry and magenta to chlorophyll autofluorescence. Scale bars: 50  $\mu$ m.

**A, B:** Peroxisome and cytosolic OPR3 split-YFP results in a low cytosolic YFP signal with Px-OPR3-nYFP/Cy-OPR3-cYFP (**A**) and Px-OPR3-cYFP/Cy-OPR3-nYFP (**B**).

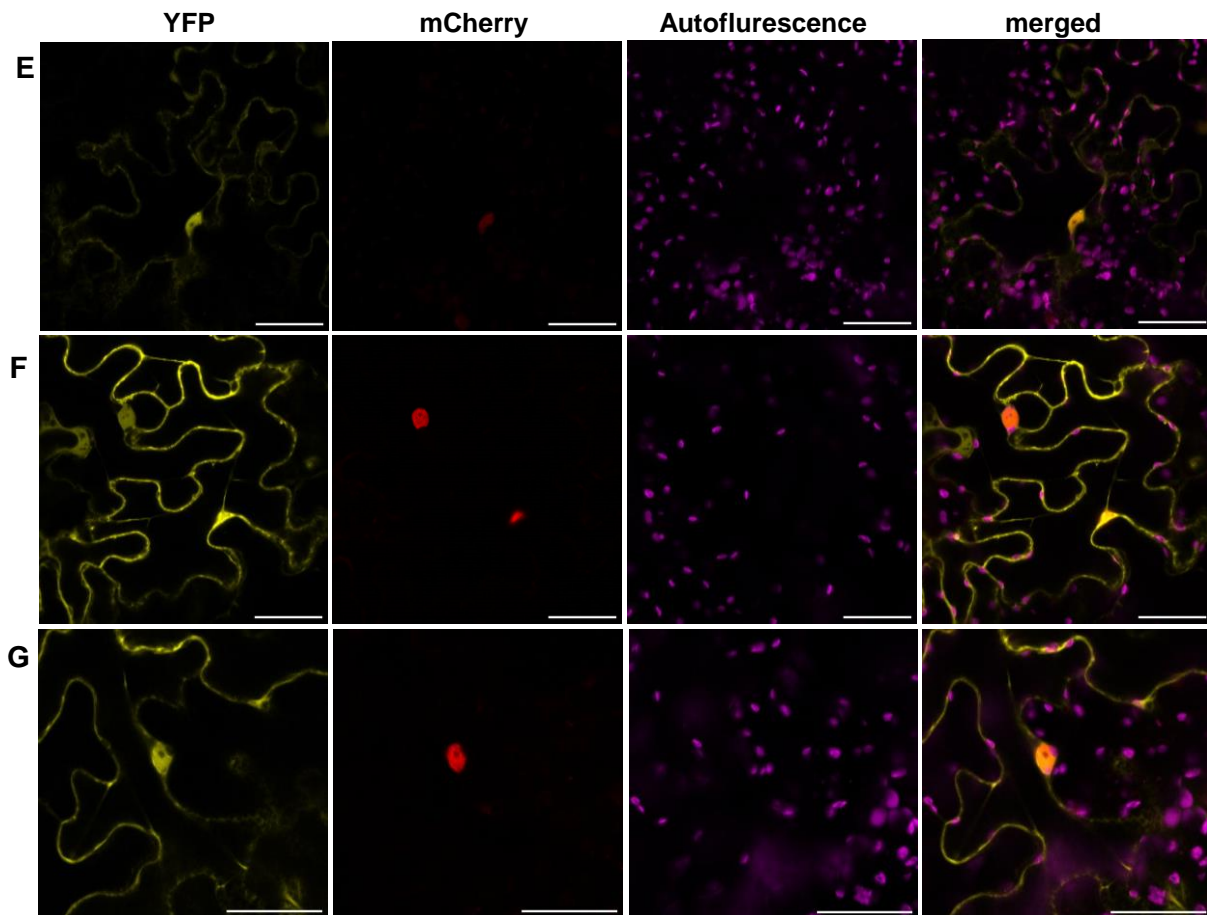
**C:** Peroxisome targeting of the monomeric variant of OPR3 (E292K) does not show reconstitution of YFP the signal with Px-E292K-nYFP/Px-E292K-cYFP.

**D, E:** ER and cytosolic OPR3 split YFP result in a low cytosolic YFP signal with ER-OPR3-nYFP/Cy-OPR3-cYFP (**C**) and ER-OPR3-cYFP/Cy-OPR3-nYFP (**D**).

**F, G:** Mitochondria and cytosolic OPR3 split YFP result in a strong cytosolic YFP signal with Mt-OPR3-nYFP/Cy-OPR3-cYFP (**E**) and Mt-OPR3-cYFP/Cy-OPR3-nYFP (**F**).

Cy: cytosol, ER: endoplasmic reticulum, Mt: mitochondria, Px: peroxisome.

Fig. 2.17 (continued)



Combination of cytosolic OPR3-n/cYFP with the ER-targeted OPR3-n/cYFP resulted in the reconstitution of the YFP signal in the cytosol with a low signal intensity (Fig. 2.17C, D). Mitochondria also showed a cytosolic YFP signal but with higher intensity than the one of the ER/cytosol (Fig. 2.17E-F). Quantification of the cytosolic YFP signal in relation to the mCherry infiltration control corroborated this observation by showing statistically higher cytosolic YFP signal in the mitochondria/cytosol pair in comparison to ER/cytosol pair (Fig. S20A, B). These results hint towards a “cytosolic occurrence of OPR3” in our targeting system that could be the reason for the partial and full complementation of JA-deficiency of the *opr2/3* double mutant. Hence, the restitution of JA pathway might have occurred due to the presence of OPR3 in the cytosol before import and its substrate OPDA. The subcellular localization of OPR3 in the complemented lines, however, does not show any cytosolic occurrence. Collectively, the BiFC results hint towards a cytosolic occurrence of OPR3 when targeted to other organelles, however, considering the possibility that the self-assembly of the YFP halves could be also the reason for the formation of cytosolic signal, these results are not conclusive.



## 2.2.5 Tissue-specific expression of *OPR2* and *OPR3* and its relation to the fertility of the *opr3* single mutant.

As shown previously, the relatively low cytosolic occurrence of OPR3 in the ER-OPR3 complemented *opr2/3* lines could reconstitute partially JA biosynthesis and its fertility and the cytosol targeted OPR3 showed initial results of full JA biosynthesis restitution (Fig. 2.13, Fig. 2.14). OPR2, which is a cytosolic enzyme involved in the OPR3 bypass pathway, can convert 4,5-ddh-JA to JA and thus in the *opr3* single mutant low amounts of JA are formed through OPR2 (Chini et al., 2018). These amounts, however, are not able to confer any fertility to the *opr3* single mutant (Stintzi and Browse, 2000).

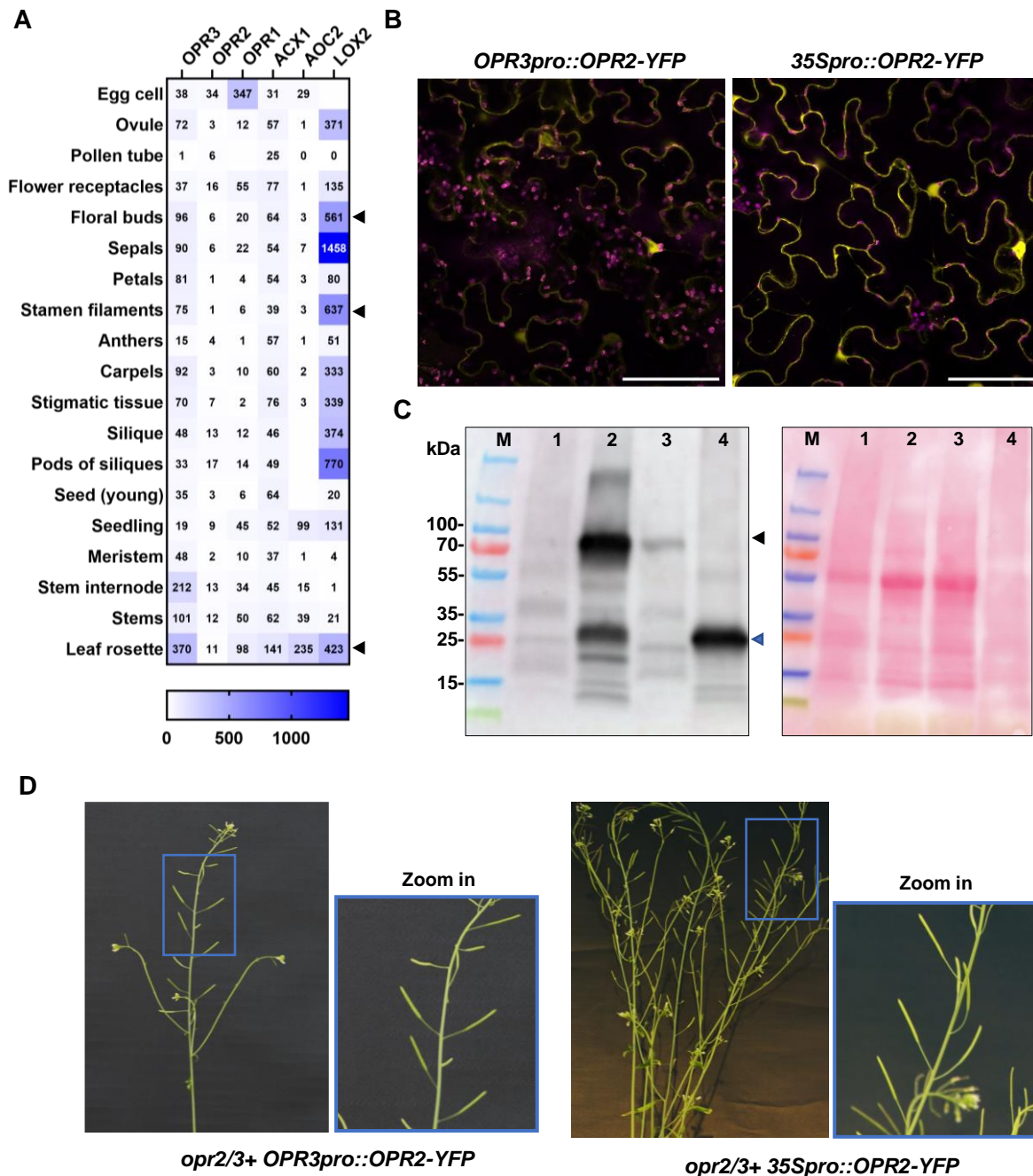


**Fig. 2.18** Change of the tissue-specific expression of *OPR2* using the *OPR3* and *35S* promoters results in the restitution of fertility of the *opr2/3* double mutant.

**A:** Tissue-specific expression of *OPR2* and *OPR3* indicates main differences in the flower buds, stamens, and rosette leaves (black arrows). Raw expression data was retrieved from CoNeKt database.

**B:** *OPR2*-YFP is cytosolic as shown by transient expression in *N. benthamiana* leaves using the 35S and the *OPR3* promoters. *N. benthamiana* leaves were imaged 48 h after infiltration and pretreated with MeJA prior to imaging for the *OPR3pro::OPR2-YFP* construct. The yellow signal corresponds to YFP and magenta to chlorophyll autofluorescence. Scale bars: 100  $\mu$ m.

**C:** anti-YFP immunoblot from total protein extracts from the transient assays in (B). Lane 1: non infiltrated leaves, lane 2: *35Spro::OPR2-YFP*, lane 3: *OPR3pro::OPR2-YFP* and lane 4: *35Spro::YFP* control. Black arrow points to *OPR2*-YFP (70 kDa) and blue arrow points to YFP (27 kDa). M: protein marker.

**D:** Plant inflorescences showing silique production in the T1 generation of the *opr2/3+* *OPR3pro::OPR2-YFP* and *opr2/3+* *35spro::OPR2-YFP*.

Validation of the full sterility of the *opr3* single mutant was concluded from phenotyping of *opr3-1* mutants that were grown until senescence and did not form siliques (Fig. S21). A question that arose from these observations was, how the cytosolic presence of *OPR3* could reconstitute JA biosynthesis even partially, while the cytosolic *OPR2* was not able to? To answer this question, tissue-specific expressions of *OPR2* and *OPR3* were investigated from the database in addition to the *LOX2* and other JA-biosynthetic enzymes (Fig. 2.18).

Interestingly, the expression levels of *OPR2* were lower than those of *OPR3* and *LOX2* in the flower buds and specifically in the stamen filaments in addition to the leaf rosette. Such low expression of *OPR2* in these tissues could be the reason for the very low JA formation through 4,5-ddh-JA and for the *opr3* single mutant being still sterile despite the presence of these low JA/JA-Ile contents. To test this hypothesis, *OPR2* was fused to YFP and expressed under the *CaMV 35S* and the *OPR3* promoters then used to complement the *opr2/3* double mutant. Both constructs showed cytosolic localization of *OPR2* in transient assays in *N. benthamiana* leaves (Fig. 2.18B-C). The *OPR3pro::OPR2-YFP* construct showed responsiveness to MeJA in *N. benthamiana* leaves by accumulating higher levels of *OPR3*-YFP in the MeJA treated leaves (Fig. S22).

The expression of the *35Spro::OPR2-YFP* and *OPR3pro::OPR2-YFP* in the *opr2/3* double mutant resulted in the restitution of *opr2/3* fertility which manifested by silique formation in the first generation of transgenic lines (Fig. 2.18D). Therefore, it is to conclude that *OPR2* can replace *OPR3* function in JA formation within *opr3* mutants, but its natural levels are too low due to its tissue-specific expression.

### 2.3 Towards the identification of a plastid located OPDA transporter.

The formation of JA occurs in the peroxisome and involves the conversion of its precursor, OPDA, to OPC:8 by *OPR3* followed by three rounds of  $\beta$ -oxidation (C. Wasternack, 2007). The formation of OPDA, however, takes place in the plastids from the  $\alpha$ -linolenic acid pathway, OPDA is therefore moving out of the plastids to be imported to the peroxisomes (Theodoulou et al., 2005). JASSY was identified as a plastid outer membrane transporter of OPDA (Guan

et al., 2019), yet it is known that the inner envelope of the plastid constitutes the actual barrier between the plastid stroma and the cytosol (Facchinelli and Weber, 2011). An OPDA transporter is therefore expected to be present in the chloroplast inner envelope.

This work initially hypothesized that OPDA, as a signaling molecule, would transcriptionally regulate its own transport out of the plastid and that a plastid located transporter would be found in the list of OPDA-responsive genes. Since as demonstrated in section 2.1, OPDA did not show ability to mediate gene expression upon its accumulation at basal levels or upon wounding, it became evident that the transport of OPDA, as a JA precursor, is likely transcriptionally regulated by JA. This hypothesis is line with the ability of JA to mediate the transcription of its biosynthetic enzymes through a positive feed-back loop upon its biosynthesis (Stenzel et al., 2003). It is therefore speculated that not only JA biosynthetic enzymes but also the components responsible for JA and its precursors transport would also be transcriptionally regulated by JA.

### 2.3.1 A pipeline to identify a putative plastid located OPDA transporter.

To identify an OPDA transporter within our RNAseq datasets obtained from wounded plants, a pipeline was set where only up regulated genes by wounding in a JA-dependent manner were selected without a specific fold change cutoff (Fig. 2.19). DEGs uniquely induced in Col-0 or commonly induced in Col-0 but to a lesser extent in the mutants *opr2/3* and *aos* were considered putatively induced by JA. The obtained genes were filtered according to their functional annotation by *Mercator4 V2* and those with a predicted transport function were retained. Several genes showed a non-assigned function, and within these only genes having a StaR-related lipid transfer (START)-lipid domain were considered. The obtained candidate transporters from seedlings and adult leaf RNAseq datasets were crossed and only common genes to both datasets, which are independent from the plant developmental stage, were retained (Table S4). As we are searching for a chloroplast located transporter, subcellular localization prediction of the candidates was performed using *ChloroP* and *SUBA5* databases.

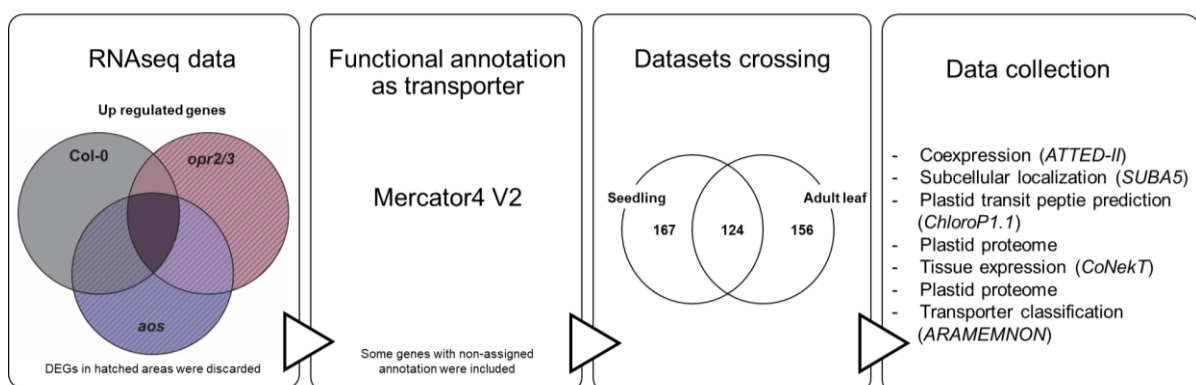


**Fig. 2.19** The pipeline used to select putative OPDA transporters from the RNAseq datasets obtained from wounded plants.



Up-regulated genes by wounding were selected without a fold change cutoff, then were annotated with *Mercator4 V2* and those with transporter as functional annotation were retained. Few genes with non-assigned function were also retained. Only transporters that were common between seedlings and adult leaf datasets were retained. For the 124 common candidates, data was collected from different databases to predict possible relation to OPDA transport in terms of subcellular localization, co-expression with JA-related genes, tissue expression and transport classification.

Considering that an OPDA transporters would be involved in JA-biosynthesis, its co-expression with at least one of the JA-biosynthetic enzymes (*LOXs*, *AOS*, *AOCs* and *OPRs*) and/or JA-signaling transcription factors (*JAZs*) was expected (Fig. 2.19). Additionally, leaf tissue expression levels were retrieved from *CoNeKt* database and candidates with leaf expression value close to zero were discarded. To evaluate a putative OPDA transport function for the 124 candidates, those meeting most of the pipeline filters were selected as putative OPDA transporters candidates (Table S4).

Within the list of 124 candidates almost half of the genes co-expressed with JA-related genes, however only six showed plastid subcellular localization prediction by *SUBA5* database (Fig. 2.20A-B). Four out of the six plastid-predicted transporters also showed a prediction for a chloroplast transit peptide sequence and a cleavage site by *ChloroP 1.1* server (At1g04570, At5g01500, At1g80300 and At5g02940). At5g01500 is a characterized thylakoid ATP/ADP carrier belonging to the Mitochondrial carrier transporters (MC) group (Thuswaldner et al., 2007) and At1g80300 was also characterized as an inner membrane plastid ADP/ATP carrier, *NTT1* (Deniaud et al., 2012). From the remaining two candidates, At1g04570 belongs to the folate biopterin transporter (FBT) family which is part of the Major facilitator superfamily of transporters (MFS), but lacked folate transport activity (Eudes et al., 2010). It had no data regarding co-expression with JA-related genes and showed a low leaf expression raw value therefore was discarded (Table S4). The last candidate out of these four transporters predicted to be in the chloroplast was At5g02940, known as *PEC1*, was interestingly identified as a protein of unknown function present the proteome of the chloroplast mixed inner and outer envelopes (Simm et al., 2013).

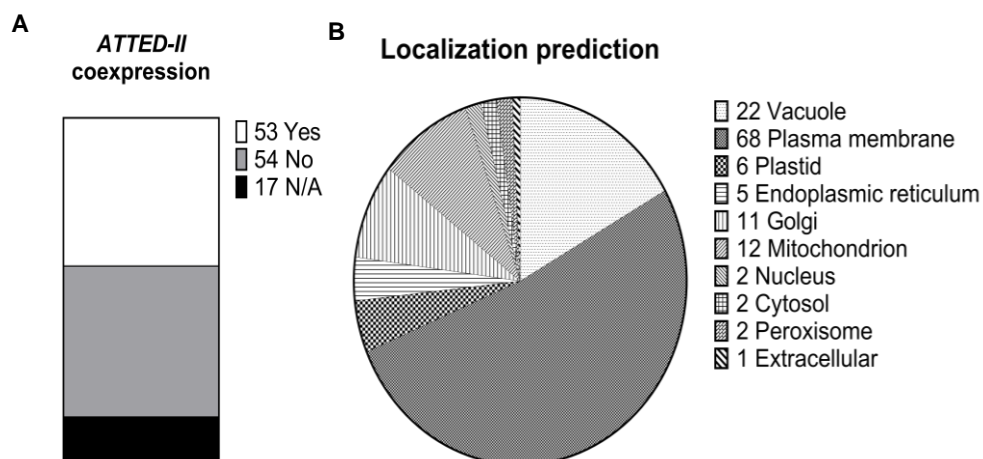


**Fig. 2.20** Half of the candidates co-expressed with JA-biosynthetic and/or signaling genes but only six showed predictions for plastid localization.

**A:** Number of candidate genes co-expressing with JA-related genes in *ATTED-II* database. When the transporter candidate co-expressed with at least one of the JA-biosynthetic enzymes (biosynthetic steps from *LOXs* to *OPRs*) or a *JAZ* signaling repressor, it was counted as co-expressing (Yes), else (No) and not assigned when data was not available (N/A).

**B:** Pie chart showing the predicted subcellular localization of the 124 candidate transporters by *SUBA5*. Most of the transporters had one attributed localization, only seven were predicted for more than one compartment.

It belongs to the Pollux/Castor-type voltage-gated ion channel and was not characterized yet when it was selected as a putative transporter candidate in this work. Due to tight co-expression with JA-biosynthetic genes, specifically those related to OPDA biosynthesis (*LOX2*, *AOS* and *AOC2*) and its leaf expression value around 33.5, it was retained as a putative OPDA transporter candidate (Table 2.2, Table S4).

Since only one plastid-predicted candidate showed possibility of involvement in OPDA transport out of chloroplasts, other candidates which did not have a plastid localization prediction by *SUBA5*, were chosen. *At5g54170* was an interesting candidate since it had a prediction for a chloroplast transit peptide by *ChloroP1.1* and it co-expressed with JA biosynthetic and signaling genes (Table S4). This gene encodes for a putative membrane protein of an unknown function containing the START-type lipid-binding domain, thus we named it *STR1*.

Other interesting transporters were those belonging to the family of Multidrug efflux transporters (*MATE*), from which eight members showed response to wounding and co-expression with JA biosynthetic and signaling genes but no prediction for plastid localization (Table S4). *At1g61890*, known as *DTX37*, was selected since it showed tight co-expression with JA biosynthesis genes and high leaf expression levels in addition to the highest induction in response to wounding in comparison to the other gene family members (Table 2.2, Table S4). Summarizing this selection, in total three putative transporters were chosen for further studies as listed in Table 2.2.

Table 2.2 Overview of the selected putative OPDA transporter candidates, and their corresponding T-DNA insertion lines.

| AGI   | Gene name    | LogFC <sup>A</sup> |               |            | Adjusted p-value <sup>B</sup> |               |            | Plastid proteome <sup>C</sup> | cTP <sup>D</sup> | SUBA plastid <sup>E</sup> | Coexpressed JA-related genes <sup>F</sup>                    | Predicted TMD <sup>G</sup> | T-DNA line <sup>H</sup>     |
|---|--------------|--------------------|---------------|------------|-------------------------------|---------------|------------|-------------------------------|------------------|---------------------------|--|----------------------------|-----------------------------|
|   |              | Col-0              | <i>opr2/3</i> | <i>aos</i> | Col-0                         | <i>opr2/3</i> | <i>aos</i> |                               |                  |                           |  |                            |                             |
| <b>DTX-type metabolite transporter family</b>                               |              |                    |               |            |                               |               |            |                               |                  |                           |  |                            |                             |
| AT1G61890   | <i>DTX37</i> | 3.11               | 1.97          | 1.80       | 1.00E-12                      | 1.53E-10      | 3.58E-10   | No                            | No               | No                        | <i>LOX3, LOX4, AOC3, OPR3, JAZ1, JAZ10, JAZ5, JAZ7, JAZ8</i> | 12                         | GABI_497E04<br>SALK_151525C |
| <b>Polyketide cyclase/dehydrase and lipid transport superfamily protein</b> |              |                    |               |            |                               |               |            |                               |                  |                           |  |                            |                             |
| AT5G54170   | <i>STR1*</i> | 2.13               | 1.17          | 0.91       | 1.57E-11                      | 1.27E-08      | 1.99E-07   | No                            | Yes              | No                        | <i>LOX3, OPR3, JAZ1, JAZ10, JAZ6, JAZ7, JAZ8</i>             | 2                          | SALK_143476C                |
| <b>Pollux/Castor-type voltage-gated ion channel</b>                         |              |                    |               |            |                               |               |            |                               |                  |                           |  |                            |                             |
| AT5G02940   | <i>PEC1</i>  | 1.19               | -0.08         | 0.04       | 2.56E-09                      | 4.24E-01      | 7.43E-01   | Yes                           | Yes              | Yes                       | <i>LOX2, AOS, AOC2, AOC1, OPR3, JAZ6</i>                     | 3                          | SALK_013399                 |

<sup>A</sup> LogFC (fold change) values are from seedlings of Col-0, *opr2/3* and *aos* 1 hour after wounding relative to control. All genotypes were pretreated with MeJA during development.

<sup>B</sup> False discovery rate corrected p-value.

<sup>C</sup> Belonging or not to the defined proteome of the chloroplast envelopes (Simm et al., 2013).

<sup>D</sup> Chloroplast transit peptide (cTP) prediction using ChloroP 1.1 prediction server.

<sup>E</sup> Subcellular localization prediction to the plastid using SUBA5 database.

<sup>F</sup> Co-expression data by ATTED-II database.

<sup>G</sup> Transmembrane spans prediction by AramTmMultiCon on Aramemnon database.

<sup>H</sup> T-DNA line from NASC database.

\* Gene name attributed in this work.

## 2.3.2 Characterization of the selected transporter candidates

### 2.3.2.1 The DTX/MATE candidate: DTX37

The MATE family counts 58 members in *Arabidopsis*, from which only five were characterized based on mutant phenotype and found to transport a range of substrates including flavonoids, citrate, alkaloids, antibiotics and putatively salicylic acid (Shoji et al., 2009). The DTX family members form five clusters, and are predicted to play different functions due to diversity of their sequences (Legong et al., 2002). Eight of the DTX members responded to wounding in our experiment and they all contained eight to twelve predicted transmembrane spans. DTX37 was selected as a putative OPDA transporter candidate because it showed the highest up-regulation upon wounding in comparison to the other gene family members (Table 2.2, Table S1).

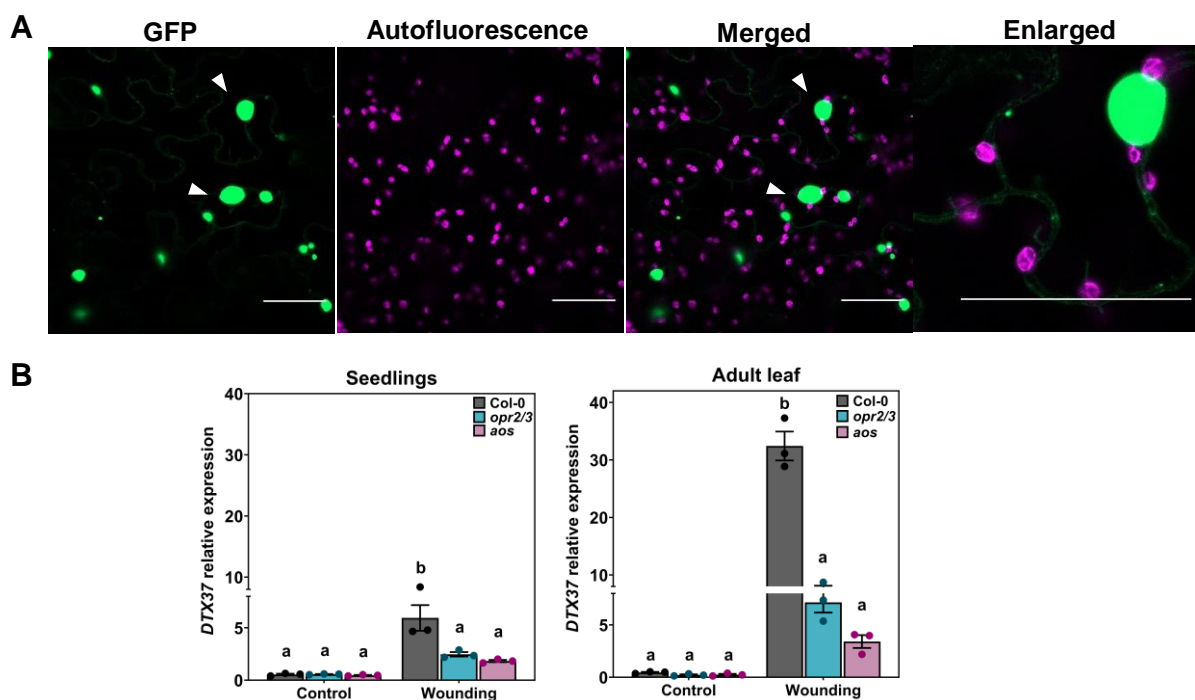


**Fig. 2.21 Subcellular localization of DTX37 in *N. benthamiana* leaves and its expression upon wounding in *A. thaliana*.**

**A:** Subcellular localization of DTX37-GFP expressed transiently in *N. benthamiana* leaves. The green signal corresponds to GFP and the magenta to chlorophyll autofluorescence. Scale bars: 20  $\mu$ m.

**B:** DTX37 transcript accumulation in seedlings and adult leaves samples from technical validation of the mRNAseq experiment. Relative expression was determined by qRT-PCR and normalized to *PP2A*. Bars represent means of three biological replicates (single dots;  $\pm$ SEM). Different letters denote statistically significant differences among genotypes/conditions as determined by Two-way ANOVA followed by Tukey HSD test ( $p < 0.05$ ).

The subcellular localization of DTX37 did not yield a conclusive result since it formed GFP aggregates, which did not correspond to any of the cell organelles (Fig. 2.21A). Detection of the DTX37-GFP fusion protein showed a smear of higher molecular weights confirming the formation of protein aggregates (Fig. S23). Additionally subcellular localization of other family

members, DTX9, DTX28 and DTX36, showed similar results indicating that the C-terminal fusion to GFP was not suitable for this protein family (Fig. S24).

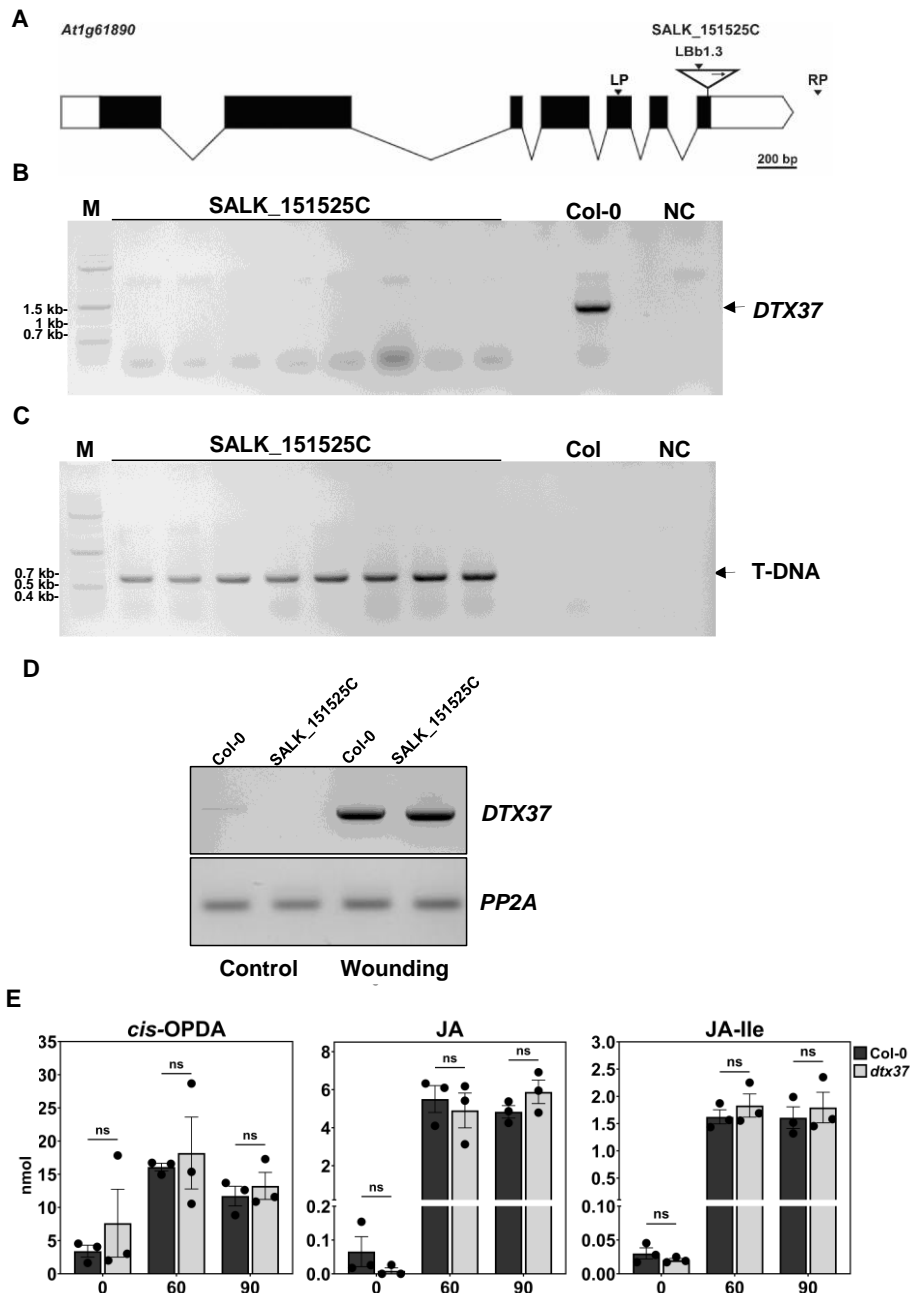


**Fig. 2.22 Isolation of *dtx37* T-DNA insertion line and determination of its OPDA/JA/JA-Ile levels.**

**A:** Shown are the gene structure of *DTX37*, the position and orientation of the T-DNA insertion in the SALK\_151525C line and the genotyping primers sites (LP, left primer; RP, right primer; LBB1.3, T-DNA border primer). Black box, lines, and white box represent exons, introns, and untranslated regions, respectively with a scale of 200 bp.

**B, C:** Genotyping of two-week-old *Arabidopsis* plants by PCR amplification of the wild type allele band (1246 bp) using LP and RP primers (**B**), and of the T-DNA band (563-863 bp) using LBB1.3 and RP primers (**C**). Homozygous individuals for the T-DNA insertion are those showing no amplification in (**B**) and the expected band in (**C**). The 1kb plus DNA ladder (Thermofisher Scientific) was used as a molecular weight marker (M) and a PCR with water instead of genomic DNA was used as negative control (NC).

**D:** *DTX37* expression determined by RT-PCR (1105 bp fragment) using RNA extracted from 4-week-rosette leaf of the mutant line and Col-0 under control and 1h post wounding. *PP2A* (126 bp) was used as control.

**E:** *cis*-OPDA, JA and JA-Ile levels at 0-, 60- and 90-minutes post wounding of leaf number eight in 4-week-adult plants of Col-0 and the *dtx37* mutant. Bars represent means of three biological replicates (single dots;  $\pm$ SEM). Asterisks denote statistically significant differences between the mutant and Col-0 within treatment as determined by Student's t-test ( $p < 0.05$ ).

*DTX37* showed a JA-dependent transcript accumulation at 1 h after wounding, since its induction was higher in Col-0 in comparison to the JA-biosynthetic mutants *opr2/3* and *aos*, in addition to an overall higher transcript level in adult leaves in comparison to seedlings (Fig. 2.21B), indicating the accumulation of the gene's transcripts during development.

An initial T-DNA-insertion line was selected for *DTX37*, The GABI\_497E04, which did not show homozygosity for the insertion however few individuals were male sterile (no pollen release), and their fertility was not rescued by MeJA treatment of the flower buds (data not shown). Further analysis of this line was not possible due to the low seed stock.

A second mutant line was therefore selected, SALK\_151525C, where the T-DNA insertion was predicted to be located at the last exon of the gene (Fig. 2.22A). While it was possible to isolate mutant individuals showing homozygosity for the T-DNA insertion, *DTX37* transcripts were detectable in these individuals (Fig. 2.22B-D). Interestingly, the mutant line showed no transcript accumulation at control condition suggesting a knockout of the gene; however, in response to wounding it accumulated similar transcript levels to Col-0 (Fig. 2.22D). Despite the T-DNA insertion being predicted to be within the last exon of *DTX37*, the detection of *DTX37* transcripts upon wounding suggests a splicing-out of the T-DNA insertion. Thus, the actual T-DNA insertion line is not suitable to study the function of *DTX37* since it is not a loss-of-function mutant line. Nevertheless, a wounding experiment was performed with the SALK\_151525C line and indicated no differences between the mutant and Col-0 in terms of OPDA, JA and JA-Ile levels upon wounding (Fig. 2.22E).

### 2.3.2.2 The START-lipid domain containing candidate: STR1 (At5g54170)

The START domain is implicated in the binding of lipid/sterol in mammals, and the plant proteins with the same domain are predicted to play a role in lipid binding, transport and signaling (Schrick et al., 2004). *A. thaliana* contains 35 START proteins, of which STR1 might function in lipid transport in or out of a membrane since it contains two putative transmembrane domains (Schrick et al., 2004).

STR1 fusion with GFP showed colocalization to the ER and the chloroplasts when transiently expressed in *N. benthamiana* leaves (Fig. 2.23A-B). While the net-like structure indicated an ER localization, plastidial GFP signal was also detected with ring-like structures surrounding the chloroplasts where the GFP signal intensified. Immunoblotting using an anti-GFP antibody validated the presence of the GFP fusion protein in the transient assays (Fig. S23). To validate this dual organelle localization, ER and plastid outer envelope markers were transiently expressed in *N. benthamiana* leaves and showed colocalization of STR1-GFP to ER and



chloroplasts (Fig. 2.23B). *STR1* was wound-responsive in a JA-dependent manner since its transcript levels were induced upon wounding in seedlings and adult leaves with a significantly higher up-regulation in Col-0 in comparison to the *opr2/3* and *aos* mutants (Fig. 2.23C).

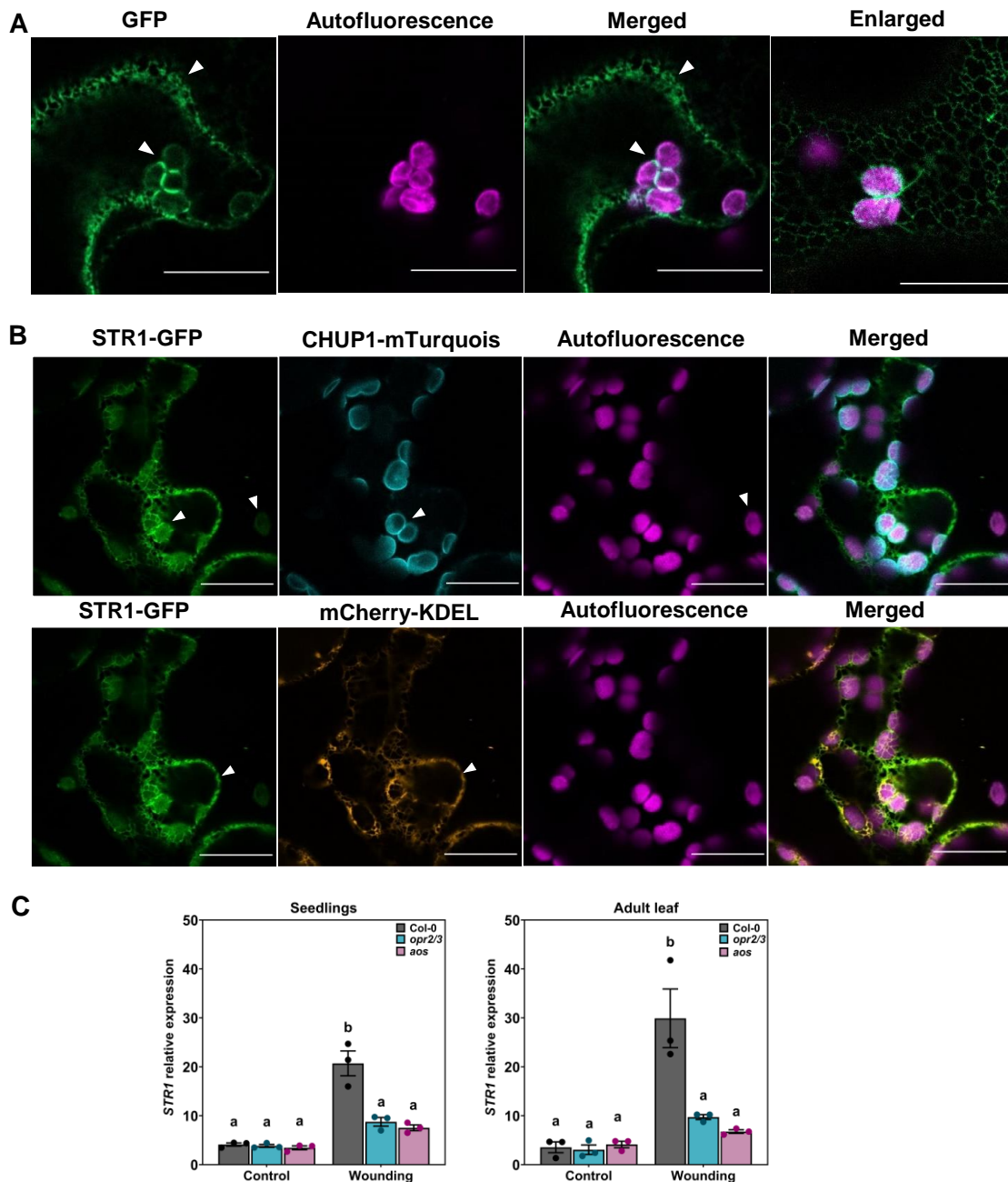


**Fig. 2.23** *STR1* subcellular localization in *N. benthamiana* leaves and its expression upon wounding in *A. thaliana*.

**A, B:** Subcellular localization (**A**) and colocalization with ER and plastid outer envelope markers (**B**) of *STR1*-GFP expressed transiently in *N. benthamiana* leaves. The green signal corresponds to *STR1*-GFP and the magenta to chlorophyll autofluorescence. The blue signal corresponds to plastid outer-envelope marker CHUP1-mTurquoise and the orange signal corresponds to ER marker WAK2-mCherry-KDEL. Scale bars: 20  $\mu$ m.

**C:** *STR1* transcript accumulation in seedlings and adult leaves samples from technical validation of the mRNAseq experiment. Relative expression was determined by qRT-PCR and normalized to *PP2A*. Bars represent means of three biological replicates (single dots;  $\pm$ SEM). Different letters denote statistically significant differences among genotypes/conditions determined by Two-Way ANOVA followed by Tukey HSD test ( $p < 0.05$ ).



To investigate the putative involvement of *STR1* in OPDA transport, a homozygous T-DNA insertion line was isolated, SALK\_143476C (Fig. 2.24A-C). This mutant line, however, showed accumulation of low levels of *STR1* transcripts at control and wounding conditions, indicating that *STR1* might be knocked down rather than knocked-out in this mutant background (Fig. 2.24D). Nevertheless, OPDA, JA and JA-Ile levels were determined in the leaf number eight of *str1* at the stage of 4-week-old and the results showed no differences in the local accumulation of OPDA, JA and JA-Ile between the mutant and Col-0 at control and 1 h after wounding (Fig. 2.24E).

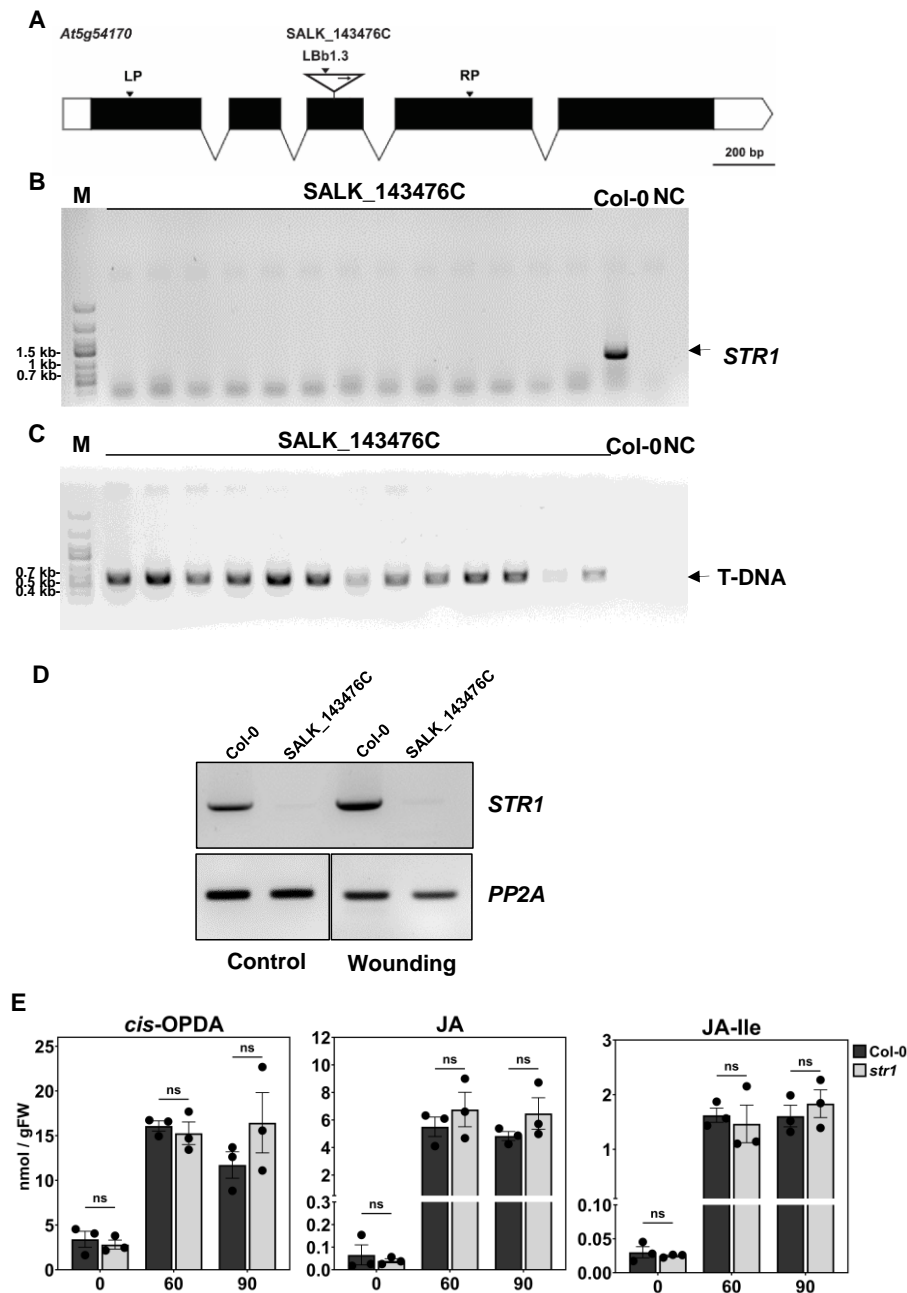


**Fig. 2.24 Isolation of *str1* T-DNA insertion line and determination of its OPDA/JA/JA-Ile levels**

**A:** Shown are the gene structure of *STR1*, the position and orientation of the T-DNA insertion in the SALK\_143476C line and the genotyping primers sites (LP, left primer; RP, right primer; LBb1.3, T-DNA

border primer). Black box, lines, and white box represent exons, introns, and untranslated regions, respectively with a scale of 200 bp.

**B, C:** Genotyping of two-week-old *Arabidopsis* plants by PCR amplification of the wild type allele band (1084 bp) using LP and RP primers (**B**), and of the T-DNA band (489-789 bp) using LBb1.3 and RP primers (**C**). Homozygous individuals for the T-DNA insertion are those showing no amplification in (**B**) and the expected band in (**C**). The 1kb plus DNA ladder (Thermofisher Scientific) was used as a molecular weight marker (M) and a PCR with water instead of genomic DNA was used as negative control (NC).

**D:** *STR1* expression determined by RT-PCR (632 bp fragment) using RNA extracted from 4-week-rosette leaf of the mutant line and Col-0 under control and 1h post wounding. *PP2A* (126 bp) was used as control.

**E:** *cis*-OPDA, JA and JA-Ile levels at 0-, 60- and 90-minutes post wounding of leaf number eight in 4-week-adult plants of Col-0 and the *str1* mutant. Bars represent means of three biological replicates ( $\pm$ SEM). Asterisks denote statistically significant differences between the mutant and Col-0 within treatment as determined by Student's t-test ( $p < 0.05$ )

### 2.3.2.3 The pollux/castor candidate: PEC1

The Pollux/Castor-type voltage-gated ion channel domain is implicated in modulating the nuclear membrane envelope potential (Charpentier et al., 2008). *PEC1* (At5g02940) contained in addition to that domain a domain of unknown function (DUF1012), which was identified in 2021 as regulator of  $K^+$  conductance (RCK) (Volkner et al., 2021). *PEC1* was shown to localize to the plastid inner-envelope and to function as ion channel and shown to be a potassium ion channel with putative permeability to calcium (Volkner et al., 2021). *PEC1* was transcriptionally induced by wounding only in the presence of JA/JA-Ile since its transcript levels were upregulated only in Col-0 background and not in the JA-biosynthetic mutants *opr2/3* and *aos* (Fig. 2.25).

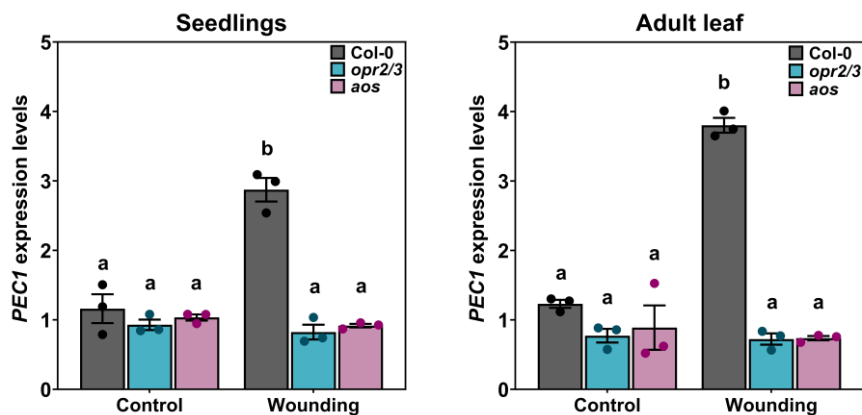


**Fig. 2.25** *PEC1* is wound-inducible only in the presence of JA.

*PEC1* transcript accumulation in seedlings and adult leaves samples from technical validation of the mRNAseq experiment. Relative expression was determined by qRT-PCR and normalized to *PP2A*. Bars represent means of three biological replicates (single dots;  $\pm$ SEM). Different letters denote statistically significant differences among genotypes/conditions determined by Two-Way ANOVA followed by Tukey HSD test ( $p < 0.05$ ).

The SALK\_013399 T-DNA line was isolated and characterized as a knock-out for *PEC1* gene (Fig. 2.26A-D), and validation of no *PEC1* transcript accumulation of this line was performed by RT-PCR at control and wounding conditions (Fig. 2.26E). The wounding of this mutant

showed statistically lower levels of OPDA than Col-0 accumulating in leaf number eight only at 60 minutes after wounding (Fig. 2.26F). JA levels, but not JA-Ile, were slightly but not significantly lower also at 60 min after wounding. These results hint towards putative involvement of PEC1 in the accumulation of OPDA upon wounding.

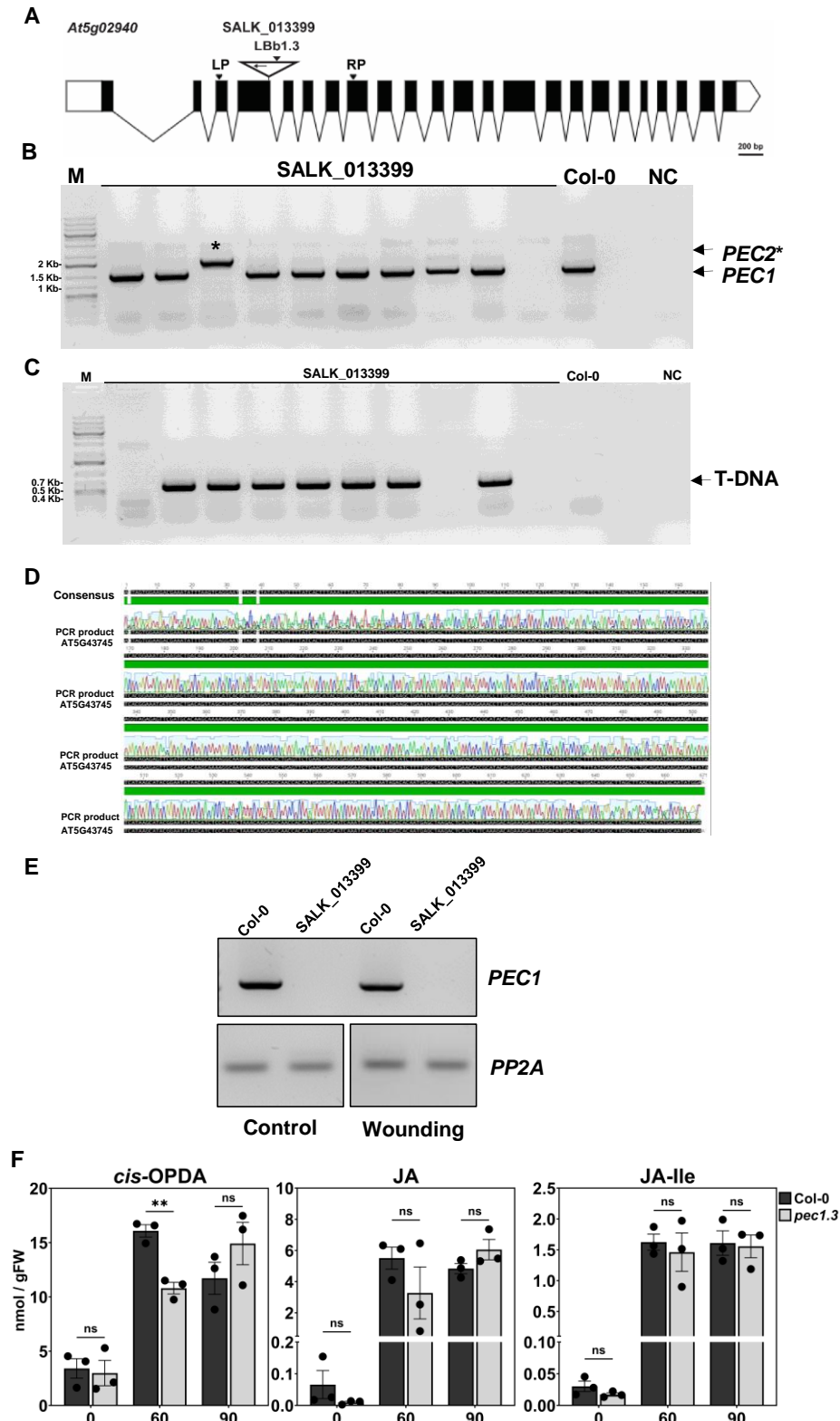


**Fig. 2.26 Isolation of *pec1.3* T-DNA insertion line and determination of its OPDA/JA/JA-Ile levels**  
**A:** Shown are the gene structure of *PEC1*, the position and orientation of the T-DNA insertion in the SALK\_013399 line and the genotyping primers sites (LP, left primer; RP, right primer; Lb1.3, T-DNA

border primer). Black box, lines, and white box represent exons, introns, and untranslated regions, respectively with a scale of 200 bp.

**B, C:** Genotyping of two-week-old *Arabidopsis* plants by PCR amplification of the wild type allele band (1059 bp) using LP and RP primers (**B**), and of the T-DNA band (509-809 bp) using LBb1.3 and RP primers (**C**). Only one homozygous individual for the T-DNA insertion was isolated showing amplification of *PEC2* gene in (**B**) and the expected band in (**C**). The 1kb plus DNA ladder (Thermofisher Scientific) was used as a molecular weight marker (M) and a PCR with water instead of genomic DNA was used as negative control (NC).

**D:** Sequencing and alignment of the PCR product (marked with \* in **B**) showed that the amplicon corresponds to the *PEC2* gene sequence (At5g43745).

**E:** *PEC1* expression determined by RT-PCR (587 bp) from RNA extracted from 4-week-rosette leaf of the mutant line and Col-0 under control and 1h post wounding. PP2A (126 bp) was used as control.

**F:** *cis*-OPDA, JA and JA-Ile levels at 0-, 60- and 90-minutes post wounding of leaf number eight in 4-week-adult plants of Col-0 and the *pec1.3* mutant. Bars represent means of three biological replicates (single dots;  $\pm$ SEM). Asterisks denote statistically significant differences between the mutant and Col-0 within each treatment as determined by Student's t-test (\*  $p < 0.05$ , \*\*  $p < 0.01$ ).

Further experiments to characterize the function of this candidate in relation to JA biosynthesis were performed in collaboration with Prof. Hans-Henning Kunz, LMU-München using the *pec1pec2* double mutants, *PD1* and *PD2*, kindly provided by the group. Unpublished work has revealed that *PEC1* protein levels increased in response to wounding and MeJA treatment. Additionally, these levels were reduced in the JA-mutant backgrounds of *jar1* and *coi1* indicating a JA-dependent accumulation of *PEC1* (H.-H. Kunz, pers. commun.). To investigate the potential function of *PEC1* in relation to JA/OPDA pathway, wounding experiments using the double mutants *PD1* and *PD2* were performed using 5-week-old *A. thaliana* plants. Here, leaf number eight was wounded and local levels of OPDA, JA and JA-Ile in the wounded leaf were measured (Fig. 2.27A). The *PD1* and *PD2* double mutants showed lower OPDA levels at 1 h after wounding in comparison to Col-0. JA and JA-Ile levels, however, did not differ between the mutants and Col-0 both at control and wounding conditions. Further experiments to test the response of the mutants to priming by wounding or MeJA treatment during development were performed in sterile conditions using two-week-old seedlings. Priming resulted in an increase of OPDA levels in all genotypes both by wounding and treatment with 5  $\mu$ M MeJA, yet *PD1* and *PD2* mutants accumulated significantly less OPDA than Col-0 indicating a putative role of *PEC1* and *PEC2* in OPDA accumulation in response also to priming (Fig. 2.27B). These lower OPDA levels did not affect JA and JA-Ile in the mutants. To determine whether these lower OPDA levels were due to alterations in the levels of JA biosynthesis enzymes, AOC protein levels were determined by immunoblotting (Fig. 2.27C). The JA-overproducer mutant *fou2*, which is a gain-of-function mutant of the vacuolar cation channel TPC1, was used as a control for an upregulation of the JA-pathway (Beyhl et al., 2009). AOC proteins levels were higher in the *fou2* than Col-0 indicating their up-regulation due to JA upregulation while *PD1* and *PD2* mutants showed lower contents of AOC proteins in comparison to Col-0 (Fig. 2.27C-

D). These results are, however, from one biological replicate, but indicate putative involvement of PEC1 in the accumulation/biosynthesis of OPDA.

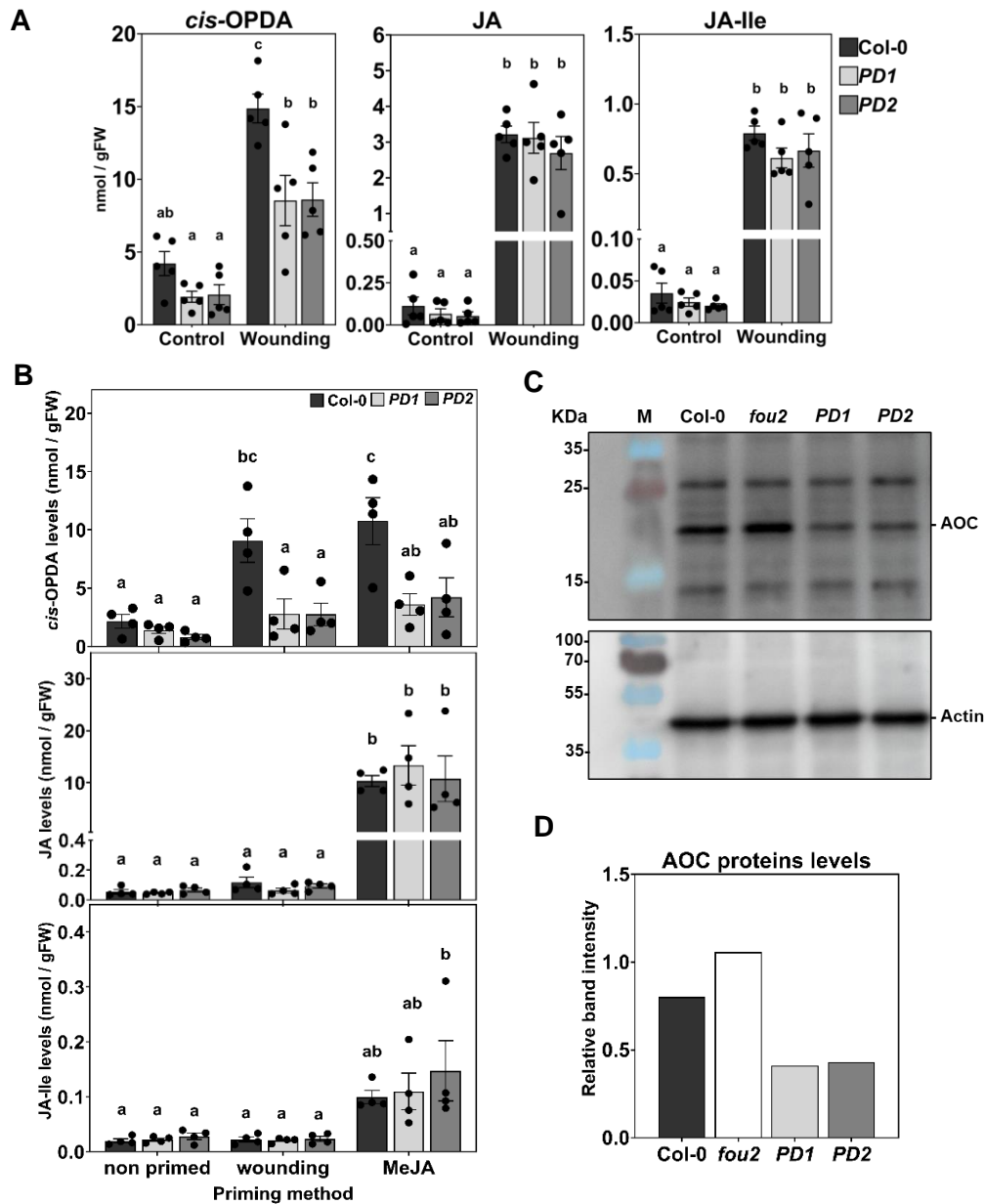


**Fig. 2.27** The *PD1* and *PD2* double mutants have altered OPDA levels following wounding and priming and accumulate lower AOC proteins levels.

**A:** *cis*-OPDA, JA and JA-Ile levels in 5-week-old adult leaves of Col-0 and the *PD1* and *PD2* mutants at control and 1h after wounding. Leaf number eight was wounded with forceps. Bars represent means of four biological replicates (single dots;  $\pm$ SEM).

**B:** *cis*-OPDA, JA and JA-Ile levels in two-week-old seedlings of Col-0 and the *PD1* and *PD2* mutants primed twice during development by wounding with forceps or by treatment with 5  $\mu$ M MeJA. Bars represent means of four biological replicates with 30 seedlings each (single dots;  $\pm$ SEM).

**C:** Determination of AOC protein levels in Col-0, *fou2*, *PD1* and *PD2* by immunoblotting from adult leaves using total protein extracts and anti-AOCs primary antibody.  $\beta$ -actin was used as loading control. M= protein size marker.

**D:** Quantification of AOC proteins levels from the immunoblot in (C) using Image J. Relative AOCs' band intensity was calculated in relation to  $\beta$ -actin bands with one biological replicate.

Different letters in (A) and (B) denote statistically significant differences among genotypes (within treatment) as determined by Two-Way ANOVA followed by Tukey HSD test ( $p < 0.05$ ).

### 3 Discussion

#### 3.1 Does OPDA exert an independent signaling function in addition to being a JA precursor in *Arabidopsis*?

Jasmonate is a major defense hormone and the role of the signaling molecule JA-Ile in defense and its mechanism of signaling were characterized in response to pathogens, herbivory attacks and mechanical wounding (Wasternack and Hause, 2013; Wasternack et al., 1998). Wounding of plants results in a local burst of jasmonic acid production including of its precursor OPDA and consequently in a cascade of JA-Ile signaling and transcriptional change leading to local and systemic defense responses (Howe et al., 2004). Hence mechanical wounding is a suitable context to study also the signaling of OPDA. To be able to dissect the wounding response and uncouple the role of OPDA from JA, a comparative analysis of the transcriptome was developed to investigate putative OPDA signaling in the wounding response of *Arabidopsis thaliana* and relied on characterizing differences in the transcriptional changes induced in the presence/absence of JA and OPDA. The signaling capacity of OPDA in *Arabidopsis* was previously reported (Park et al., 2013; Ribot et al., 2008; Taki et al., 2005), but the specific mechanism of its action as a signaling molecule has not been characterized in Angiosperms. The recent identification of an OPR3-independent pathway of JA production in the *opr3* mutant (Chini et al., 2018), a major genetic background previously used to characterize OPDA signaling, is now challenging the validity of the functions that were attributed OPDA based on this genotype. Here, we re-addressed the question about OPDA signaling using the *opr2/3* JA-deficient genetic background and investigated the putative signaling of the endogenous bulk formation of OPDA upon wounding.

##### 3.1.1 The supply of JA during development mimics the JA positive feedback loop.

One limitation in the use of the *opr2/3* double mutant is that due to its JA-deficiency and the absence of the JA positive feedback loop responsible of the tissue accumulation of the biosynthetic enzymes (Stenzel et al., 2003b), the mutant accumulates lower levels of OPDA than the wild-type (Col-0). Since we aim to characterize OPDA signaling and mediation of transcriptional change, it was important to even out the levels of OPDA production between the mutant and Col-0. Considering that the basal presence of JA is the trigger for the increasing levels of the JA biosynthetic enzymes in the developing tissue (Stenzel et al., 2003a), the experimental design included supplying the media or the plants with low levels of MeJA (1  $\mu$ M) at few time points of the development. This pretreatment was designed to be terminated few days before the tissue/plant harvest time to circumvent the effect of the immediate transcriptional response to exogenous JA supply on the plant's transcriptome, thereby only the residual effect of this pretreatment would manifest on the transcriptome. JA pretreatment during development restituted AOC proteins levels in the *opr2/3* and the *aos* mutants, and



consequently restituted the ability of *opr2/3* to produce wildtype amounts of OPDA at basal levels and also upon triggering its production by mechanical wounding. In line with the histochemical analysis showing LOX2, AOS and AOC enzymes' accumulation in leaf tissue during development and their alteration in the *opr3* single mutant due to the disruption of the JA positive feedback loop during development (Stenzel et al., 2003b), our results validate the role of this positive feedback loop in the regulation of the basal levels of the biosynthetic enzymes and consequently in setting the tissue ability to produce OPDA/JA in response to stresses. As mimicking of the JA feedback loop during development restored the ability of the *opr2/3* double mutant to reach wild-type levels of OPDA production, no differences could be seen in Col-0 in terms of OPDA or JA-Ile accumulations. Furthermore, the pretreatment resulted in a higher up-regulation of JA biosynthesis enzymes, like AOS, AOC2 and LOX2 in the JA-mutants than Col-0, suggesting a lower effect of the JA-feedback loop in the presence of JA in Col-0. This goes with previous data arguing against the effect of the positive feedback loop in JA formation in Col-0 (Scholz et al., 2015). Despite the reconstitution of the JA-positive feedback loop in the JA-deficient mutants, the *aos* and the *opr2/3* mutants remained incapable of producing JA and JA-Ile since only Col-0 was able to metabolize OPDA into JA at basal levels and upon wounding according to the hormone measurements.

### **3.1.2 Wounding results in a major transcriptional change which is independent from JA-pathway.**

To be able to dissect the wounding response and uncouple the role of OPDA from JA, a comparative analysis of the transcriptome was carried out using MeJA pretreated Col-0, *opr2/3* and *aos* genotypes which were wounded for 1 hour and sent for mRNA sequencing. Col-0 accumulating both JA and OPDA is the background for determining JA-related responses; the *opr2/3* double mutant would indicate only OPDA-specific responses due to its JA-deficiency and ability to produce OPDA (these OPDA-responses could be partially shared by Col-0), and the *aos* mutant would enable the identification of JA/OPDA-independent wounding responses, which could be inadvertently attributed to OPDA if the comparison does not include this mutant.

Despite being deficient in both JA and OPDA production, the *aos* mutant showed a major transcriptional change upon wounding that was also common to Col-0 and *opr2/3*, and this transcriptional response comprised mainly induction of general stress response pathways, with genes related to oxidative stress, and regulation of transcription. This indicates that other signaling processes occur in response to mechanical wounding leading to the regulation of transcription in seedlings and adult leaves. Similar observations were already reported, highlighting the occurrence of water stress upon wounding (Reymond et al., 2000), and the contribution of electric signals, in addition to ethylene and ABA response factors in the local wound transcriptional response (Delessert et al., 2004). The general stress response, equally

induced in all the genotypes independently from OPDA, comprised genes that were previously categorized as OPDA-specific response genes like *FAD-OXR*, *DREB2A* and *ZAT10* (Taki et al., 2005), which in our comparative analysis were induced by wounding independently from OPDA and JA. These genes are stress-inducible and were reported to be responsive to several abiotic stresses (Davletova et al., 2005; Mittler et al., 2006; Mizoi et al., 2019; Sakuma et al., 2006). Although the contribution of this general stress response to the plant defense is either low or not yet well elucidated, it is established that JA-deficiency results in higher susceptibility and alteration of plant defense against herbivore attacks and necrotrophic pathogens. JA-deficient and JA-signaling mutants get more damaged when attacked (Goodspeed et al., 2012; Guo et al., 2018; Verhage et al., 2011). Additionally, JA-Ile was found to account for 30% of plants defense against insects in nature (Schuman et al., 2018). Oxidative stress is a main component not only of the wounding response, but also of several biotic and abiotic stresses, and reactive oxygen species (ROS) accumulation upon leaf injury was reported, (Prasad et al., 2020), however their role in wounding is yet to be characterized.

### **3.1.3 JA-Ile mediates a distinct transcriptional change showing its clear function in wounding.**

By comparing the transcriptome of Col-0 to those of the JA deficient mutants *opr2/3* and *aos*, it was possible to associate a specific transcriptional signature to the bioactive signaling of JA-Ile not only at 1 hour following wounding but also at control condition. A general look at the transcriptome using principal component analysis, indicated that the transcriptome of Col-0 had the highest variance in comparison to the mutants in the absence of wounding and this variance increased upon wounding, validating a specific signaling role of JA-Ile in the wound response. By closely looking at the differences between the genotypes independently from the condition, Col-0 showed enrichment in JA pathway, wounding, and immune responses. At control condition, and despite the MeJA pretreatment during development, transcripts of several JA-responsive genes like *JAZ1*, *JAZ2*, *JAZ10*, *JAZ13*, *AOC2* were higher in Col-0 due to basal JA levels. Similar pattern was observed in other known JA-responsive and defense genes including several plant defensin genes *PDFs* (Brown et al., 2003; Chang et al., 1994), the chlorophyllase *CLH1* which is involved in damage control (Kariola et al., 2005) and N-acetyltransferase activity1, *NATA1*, which is responsible in the production of N-acetylputrescine (Adio et al., 2011; Lou et al., 2016). Upon wounding several JA-responsive genes showed induction only in the presence of JA, like *CLH1*, *NATA1*, *JAZ13*, *LOX2* and other JA-responsive genes showed significantly higher levels of accumulation of their transcripts in the presence of JA and very low induction in the absence of JA. A low induction of some of the *JAZ* transcription factors in the absence of JA-Ile signaling was previously reported (Hoo et al., 2008). Overall, JA/JA-Ile showed a signature in the modulation of the plant transcriptome translating into three aspects: (i) maintaining differential expression of a set of

genes by its presence at basal levels; (ii) inducing a JA-specific transcriptional change upon its accumulation by wounding; and (iii) affecting the magnitude of change of a specific set of genes under wounding condition. These results are in accordance with the established function of JA/JA-Ile in the local wound response in Arabidopsis and other plant species (Hoo et al., 2008; Howe, 2004; Koo and Howe, 2009; Wasternack et al., 2006).

### 3.1.4 OPDA does not mediate a transcriptional response in wounding.

As mentioned before, several of the stress responsive genes that were previously classified as OPDA-specific response genes due to their induction upon exogenous OPDA treatment and their response to wounding (Taki et al., 2005), were induced independently from OPDA's absence in seedlings and adult leaves of the *aos* mutant. Thus, these genes would be rather categorized as wounding responsive and might have a role in the stress response since they are known to be responsive to other stresses as previously reported. The analysis of the effect of the presence of OPDA in comparison to its absence on the transcriptome of seedlings, by comparing the transcriptomes of *opr2/3* and *aos*, showed differential expression of only nine genes. Result which is in accordance with the PCA analysis of the transcriptome of both genotypes which showed regrouping indicating no or very low differences. The nine DEGs include the *OPR2*, *OPR3* and *AOS* which transcripts are expected to differ between the two mutants due to their loss-of-function in *opr2/3* and *aos*, respectively. Among the nine DEGs, five were RNA species with unknown functions (long noncoding RNA, micro-RNA, and other RNA) being likely regulatory RNAs. Their transcript levels could be altered due to the loss-of-function genetic backgrounds. Only the micro-RNA, *MIR168A*, was previously characterized and shown to be stress and ABA responsive (W. Li et al., 2012). The remaining up-regulated gene encodes a cytochrome P450 enzyme, *CYP81D11*, and was characterized as *cis*-jasmonate inducible (Bruce et al., 2008; Matthes et al., 2011; Matthes et al., 2010). *Cis*-jasmonate (CJ), a volatile emitted following herbivory damage as an indirect defense to attract parasitoids (Birkett et al., 2000), is related to JA and was thought to be the volatile product from JA catabolism (Koch et al., 1997). More recent work has, however, identified *cis*-OPDA and *iso*-MeOPDA as precursors for the formation of CJ in Arabidopsis leaves and other plant species (Dabrowska and Boland, 2007). Thus, the induction of *CYP81D11* only in the *opr2/3* background hints towards further metabolization of *cis*-OPDA into CJ. In summary, these results suggest not only that the expected OPDA-inducible transcriptional change do not occur in our experiments with seedlings but also that previously characterized OPDA-response genes are generally responsive to wounding independently from OPDA.

In addition to the nine DEGs between *opr2/3* and *aos* found in seedlings, sixteen novel genes showed differential expression in adult leaves in comparison to seedlings when the transcriptomes of *opr2/3* and *aos* were compared. Whether these are OPDA-responsive genes

only in adult leaves is less likely if we take into consideration that the experimental setup using adult leaves resulted in higher variation between biological replicates. In the absence of the MeJA pretreatment and despite *opr2/3* accumulating significant levels of OPDA in comparison to *aos*, the putative OPDA transcriptional change consisted of two genes encoding hypothetical proteins, and three RNA species with unknown function. Whether these are actual genes responsive to OPDA or indirectly de-regulated due to the loss-of-function of *OPR2* and *OPR3* versus *AOS* is yet to be uncovered. The regulatory function of such RNA species, and specifically long non coding RNA (Statello et al., 2021), suggests their putative function in the regulation of the JA pathway. Nevertheless, having only five transcriptionally modulated genes questions the reported putative OPDA signaling capacity. Additionally, the overall JA signature in modulating gene expression by inducing a specific set of genes and amplifying transcription of other set of genes, is not found when OPDA signaling was investigated in the transcriptomic data. These results are contrasting with the previous research work reporting direct signaling of OPDA by inducing transcriptional change (Ribot et al., 2008; Taki et al., 2005) and indirect regulation of gene expression of several stress responsive genes through the binding to the CYP20-3 (Park et al., 2013).

### **3.1.5 The exogenous OPDA treatment differs from the endogenous rise of the compound.**

Most of the reported signaling effect of OPDA derives from experiments where exogenous OPDA was supplied to the plants (Park et al., 2013; Ribot et al., 2008; Taki et al., 2005), while this work relied on the endogenous rise of OPDA and showed only few deregulated genes. To investigate the differences between both approaches, a comparison of the transcriptional change induced by exogeneous OPDA treatment and the one induced by the endogenous rise of OPDA was performed. Interestingly, despite the *OPR3* and *OPR2* loss of function, the *opr2/3* double mutant fed with exogenous OPDA was able to partially convert it into low levels of JA and JA-Ile and these levels were enough to induce a significant JA-dependent transcriptional change in the *opr2/3* mutant. The JA response resulting from the application of OPDA to the *opr2/3* double mutant included genes, which were found in our approach to be JA-specific, since they were not induced in the absence of JA, like *NATA1* and *CLH1*. The formation of JA-Ile by exogenous OPDA in the *opr2/3* background is likely to occur through *OPR1* due to the reported low activity of *OPR1* towards *cis*-OPDA (Schaller et al., 2000). Exogenously supplied OPDA might flood the cytosol, thus is available to the cytosolic *OPR1*, whereas the endogenously produced OPDA might stay in the plastid stroma due to its sequestration in the chloroplasts by its biosynthetic enzymes (Pollmann et al., 2019). Such a compartmentalization of the endogenously produced OPDA could be one explanation for the differences in the outcomes between the endogenous rise of OPDA and its exogenous application. It is tempting to speculate that *cis*-OPDA homeostasis is highly regulated, since several *cis*-OPDA amino

acid conjugates from Arabidopsis were recently identified (Brunoni, 2023). Alternatively, another explanation would be that higher amounts of OPDA were metabolized to JA/JA-Ile in the cytosol when exogenously supplied than when endogenously produced. JA-Ile formation through OPR1 in the *opr2/3* double mutant upon OPDA application would necessitate the use of a triple mutant background *opr1opr2opr3*, which could not be obtained by crossing (Chini et al., 2018). Our results highlight the importance of the cytosolic pathway of JA formation through cytosolic OPR2 and OPR1. They are in accordance with the ubiquitous presence of this pathway in plant species and its independent function in addition to the major OPR3-mediated route of JA formation (Chini et al., 2023, 2018).

A second response that was induced by exogenous OPDA treatment but not by the endogenous rise of OPDA upon wounding, was the sulfur metabolism pathway. The induction of this pathway is in line with the described OPDA and wound-dependent up regulation of sulfur assimilation through its binding to CYP20-3 (Müller et al., 2017; Park et al., 2013). However, the induction of the transcription of components of sulfur metabolism only by exogenous OPDA supply but not by its endogenous bulk formation indicates that this transcriptional response is specific to the exogenous OPDA treatment rather than an innate signaling function of OPDA (Fig. 4.1). OPDA as an electrophilic species (RES), was shown to disturb redox homeostasis (Mueller and Berger, 2009) and to inhibit photosynthesis as shown by a decrease of the photosystem II fluorescence (Améras et al., 2003; Mueller et al., 2008). In parallel, the *in planta* conjugation of OPDA to GSH, which is an important antioxidant substance, and its degradation in the vacuole were also demonstrated (Ohkama-Ohtsu et al., 2011). This hints towards a detoxification of OPDA when exogenously supplied to plants resulting in the induction of sulfur starvation and the up regulation of sulfur assimilation pathway rather than a direct signaling function of OPDA. Such response was previously reported under cadmium stress in Arabidopsis where the induction of sulfur assimilation pathway transcriptionally correlates with greater supply of GSH (Harada, et al., 2002). This claim could be further substantiated by determining OPDA-GSH adducts formation and monitoring the cell redox state in wounded and OPDA treated samples.

The fact that only the exogenous OPDA led to the alternative cytosolic JA formation and putative detoxification process with both inducing transcriptional change, suggested that the perceived transcriptional change by OPDA application is mainly induced by JA-Ile and by processes, which are not intrinsically activated by endogenous OPDA formation (Fig. 4.1). Possible compartmentalization of the major portion of the endogenously produced OPDA by wounding could be an explanation for these different responses, however, this statement should be further consolidated by determination of *cis*-OPDA levels in chloroplast fractions.

Taken together, the transcriptomic data indicates that OPDA does not mediate a transcriptional change as a signaling molecule in *Arabidopsis* seedlings or adult leaf tissue at basal levels or

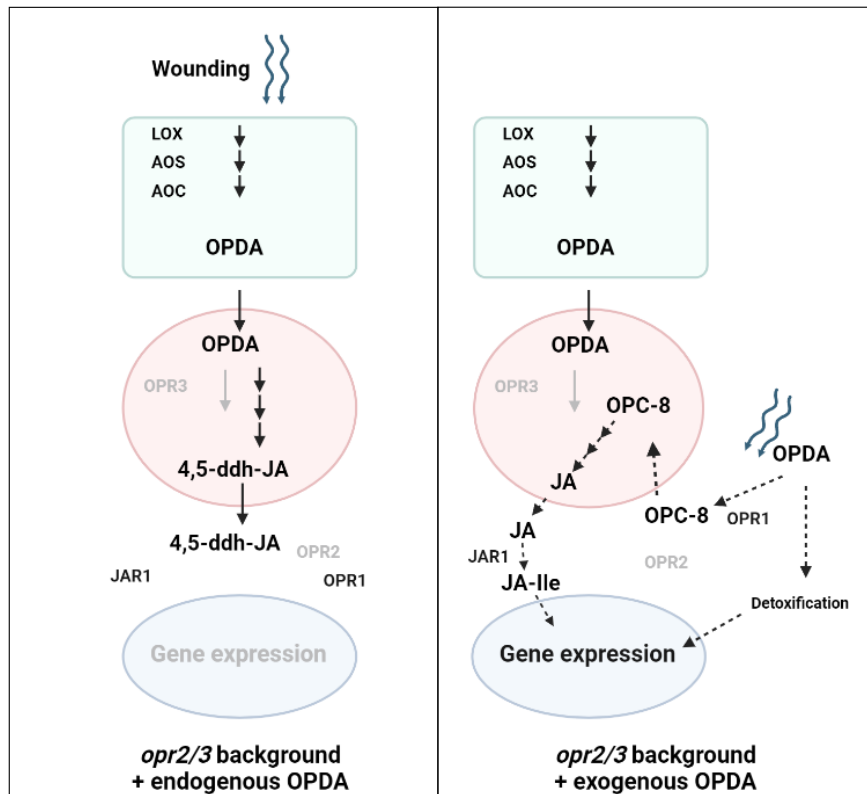


**Fig. 3.1 Model summarizing the transcriptional response by endogenous OPDA formation versus exogenous OPDA treatment**

upon its bulk formation by wounding. These results are in accordance with the recent findings suggesting that *dn*-OPDA perception by the CO11 receptor does not occur in *Arabidopsis thaliana* and that *dn-iso*-OPDA rather than *dn*-OPDA is the bioactive molecule in mosses and it does not occur in *Arabidopsis* (Chini et al., 2023; Monte et al., 2022).

Left panel shows the wound-induced bulk OPDA formation in the *opr2/3* mutant which does not induce gene expression. The right panel shows the alternative formation of JA when OPDA is supplied to the *opr2/3* mutant and flooding the cytosol, leading to the induction of JA-Ile signaling and OPDA detoxification process, both initiating transcriptional changes. Processes/enzymes in grey are deactivated. Solid lines show the reported pathways and dashed lines show suggested pathway from the current work results.

Our results also contradict the previously reported OPDA signaling capacity in *Arabidopsis* (Park et al., 2013; Ribot et al., 2008; Taki et al., 2005), and this discrepancy comes from four main aspects: (i) the availability of the *opr2/3* double mutant where JA biosynthesis is uncoupled from that of OPDA unlike the previously used “leaky” *opr3* single mutant (Chehab et al., 2011; Chini et al., 2018; Wasternack and Hause, 2018); (ii) the use of the *aos* mutant to identify the OPDA/JA independent responses that could be inadvertently attributed to OPDA; (iii) taking into consideration the conversion of OPDA into JA through the *OPR2/OPR1* cytosolic route when exogenously supplied to tissue (Chini et al., 2023, 2018); and (iv) addressing the



function of the endogenous OPDA formation in comparison to the exogenous supply of the compound.

Further investigation of OPDA signaling in other processes like seed germination and stomatal closure in *Arabidopsis* could be addressed using the *opr2/3* double mutant to clarify whether its function goes beyond being a JA precursor. Isolation of OPDA effects using OPDA treatment of tissue would be uncoupled from JA only when using genetic backgrounds where JA-production through cytosolic OPRs is abolished, for instance an *opr3opr2opr1* triple mutant in *Arabidopsis*. Investigation of the biological significance of OPDA's interactions as reactive electrophilic oxylipin with nucleophilic targets such as GSH, CYP20-3 and thioredoxins (Knieper et al., 2022; Maynard et al., 2021; Ohkama-Ohtsu et al., 2011; Park et al., 2013), would also clarify whether it has a specific function as a signaling molecule or whether it triggers a general detoxification response like other reactive electrophilic species due to its cytotoxicity (Mueller and Berger, 2009; Mueller et al., 2008).

### **3.2 Can OPDA as a signaling molecule translocate to other cell compartments?**

The results from our transcriptomic approach question the putative independent signaling of OPDA in *Arabidopsis* and favor OPDA functioning only as a JA precursor. Another way to address the same question was to hypothesize that *cis*-OPDA or *dn*-OPDA should translocate to the nucleus if it directly mediates gene transcription, as is the case of JA-Ile. To test this hypothesis the *opr2/3* double mutant was complemented by OPR3 targeted to the nucleus and other cell compartments. Restitution of JA production is only expected if OPR3 substrate is present in the tested compartment. Previous work demonstrated that when three plastid-localized enzymes responsible for tocopherol biosynthesis were mutated, the disruption was restored by redirecting these enzymes to the ER and this finding suggests that enzymes located in the ER may have the ability to interact with their metabolites pool found in the plastids (Mehrshahi et al., 2013).

#### **3.2.1 Incorporation of targeting signals to the primary sequence of OPR3 defines its subcellular destination.**

OPR3, responsible for the reduction of *cis*-OPDA and *dn*-OPDA in *A. thaliana*, is a peroxisome lumen-located enzyme. Its import into the peroxisome occurs through the peroxisome targeting signal 1 (PTS1) branch, which relies on its SRL C-terminal tripeptide and is mediated by the main receptor for PTS1-import branch, PEX5 (Brocard and Hartig, 2006; Kaur et al., 2009). Reports of PTS1-independent import to peroxisomes, despite the deletion of the C-terminal tripeptide, have indicated the involvement of other adjacent sequences in the import process (Brocard and Hartig, 2006; Parkes et al., 2003). However, for OPR3, the deletion of the SRL C-terminal peptide alone was sufficient to cease its import into peroxisomes. Integration of a plastid and a mitochondrial transit peptide at the N-terminus was sufficient for its import into

the chloroplast stroma and the mitochondria, respectively (Eseverri et al., 2020; Komiya et al., 1994). Import into the nucleus and the exclusion from it to keep a cytosolic localization were effectively mediated by the nuclear localization (NLS) and export (NES) signals from the HIV Rev protein, respectively (Kosugi et al., 2008; Raikhel, 1992). Although YFP-tagged OPR3 $\Delta$ SRL is capable of translocating into the nucleus through the nuclear membrane pore due to its size, an NLS sequence was attached to ensure selective nuclear uptake of OPR3 $\Delta$ SRL. Conversely, for cytosolic targeting, an NES was attached to OPR3 to ensure its export out of the nucleus through exportins. Furthermore, the targeting of OPR3 to the ER and its retention in the ER lumen were mediated by an N-terminal signal peptide and a C-terminal retention signal, respectively (De Meyer and Depicker, 2014; Kunze and Berger, 2015). Further validation of the ER localization of the ER-targeted OPR3 $\Delta$ SRL indicates that it is localized in the ER bodies of young seedlings (data not shown). The ER bodies, which are subdomains of the ER, constitute a continuity of the ER network and have not been fully characterized yet (Matsushima et al., 2003; Nakano et al., 2014). The import mechanism by which OPR3 is translocated to each of the tested cell compartments is expected to occur by the recognition of the targeting signal either during protein translation in the cytosol or after translation, and in the case of peroxisomes, after protein folding (Kunze and Berger, 2015). The well-established studies on targeting signals has provided robust knowledge that led to the production of collections of fluorescent organelle markers used for subcellular localization and other applications (Nelson et al., 2007; Kim et al., 2013).

### **3.2.2 Nucleus, cytosol, chloroplast, and mitochondria located OPR3 can reconstitute JA biosynthesis in the *opr2/3* double mutant.**

OPR3 located in plastids and ER should reconstitute JA biosynthesis by accessing the pool of OPDA in the chloroplast stroma and possibly in the ER, respectively. The latter might be achieved through the proposed model of transporter based or hemi-fusion based translocation of plastid-derived non polar compounds to the ER (Mehrshahi et al., 2014). It was further speculated that - if OPDA translocates to the nucleus to exert its signaling function - reconstitution of JA biosynthesis would be possible through the production of OPC-8 in the nucleus followed by its movement to the peroxisome for further metabolization into JA. Surprisingly, the results showed complementation of the *opr2/3* double mutant by OPR3 targeted to the nucleus, cytosol, chloroplast, and even to the mitochondria, where such reconstitution of JA biosynthesis was not expected. Initial experiments using the *aos* mutant for complementation with ER- and peroxisome-localized OPR3 (data not shown) did not result in reconstitution of its fertility, confirming that the complementation of the *opr2/3* double mutant necessarily relies on the products of the AOS branch, namely *cis*-OPDA and *dn*-OPDA. Thus, the reconstitution of *opr2/3* fertility by OPR3 in all the tested compartments, and the demonstrated leaf JA production in the case of ER, nucleus, and cytosol, suggest that the substrates of OPR3, *cis*-OPDA/*dn*-

OPDA, are available in these compartments. Whether they translocate there through transporters or by other means cannot be speculated at this stage. Further characterization of JA biosynthesis restitution in these complementation lines is of importance, including quantification of the JA biosynthesis intermediates such as 4,5-ddh-JA. This data is necessary to clarify the route of JA biosynthesis in these complementation experiments.

Since YFP-tagged OPR3 was used to complement the double mutant, subcellular localization and co-localization of OPR3 were performed to validate its correct targeting. The results showed exclusive localization of OPR3 $\Delta$ SRL to the targeted cell compartment, excluding the possibility of mis-localization. This finding validates that the observed complementation of the *opr2/3* double mutant results from a functional OPR3 and its substrate being available in the subsequent cell organelle. Additionally, the tested double-membrane-bound organelles, such as the nucleus, chloroplast, and mitochondria, suggest the translocation of OPR3's substrate through the membranes of the corresponding organelles. Grafting experiments revealed that OPDA acts as a long-distance mobile signal, translocating from damaged shoots to intact roots (Schulze et al., 2019), supporting the possible mobility of OPDA. Our results suggest that the substrate of OPR3 can translocate to different cell compartments.

Another important aspect is that no data is available regarding the affinity of OPR3 towards 4,5-ddh-JA. As demonstrated by Chini et al., 2018, in the absence of OPR3 OPDA is able to engage in  $\beta$ -oxidation leading to the formation 4,5-ddh-JA. Hence, it is also possible that 4,5-ddh-JA is the translocating compound rather than OPDA. We can only conclude that one of the substrates OPDA or 4,5-ddh-JA is able to translocate to different cell compartments. To determine which of the compounds is translocating an enzymatic assay should be performed to assess the ability of OPR3 to metabolize 4,5-ddh-JA. A second approach to complement this work and to answer which of the substrates is mobile, would be to use the substrate specificities of OPR2 and OPR1. As OPR1 has no activity towards 4,5-ddh-JA and OPR2 preferably metabolizes 4,5-ddh-JA than OPDA according to Chini et al., 2018, by targeting both enzymes to the tested organelles, we would be able to uncover which of the substrates is translocating. Initial experiments with OPR2 and OPR1 targeting to the peroxisome resulted in the complementation of the *opr2/3* sterility phenotype, while mitochondrial OPR2 but not OPR1 complemented *opr2/3* sterility (data not shown), hinting towards 4,5-ddh-JA being the substrate able to translocate to the tested organelles and possible ability of OPR3 to convert 4,5-ddh-JA to JA.

### **3.2.3 Is the substrate of OPR3 translocating to different organelles or the OPR3 directed to various organelles might occur also within the cytosol?**

One interesting observation in the current complementation approach was that the ER localization of OPR3 $\Delta$ SRL, unlike the other tested organelles, led to a partial complementation

of the *opr2/3* mutant phenotype, with lower restitution of fertility and partial restoration of JA biosynthesis and signaling in flowers and after wounding of vegetative tissue. Whether the differences in the organelles' pH affected OPR3 activity in the ER is improbable, since the ER was reported to have a pH around 7.1, similar to the cytosol at 7.2 (Shen et al., 2013). This pH would fit to the pH optimum of the OPR3 activity, which exhibits a broad optimum pH spectrum around pH 7-8 (F. Schaller et al., 2000). Moreover, OPR3 can self-inactivate by forming self-dimers (Breithaupt et al., 2006) and a monomeric form of AtOPR3 has been characterized (Nadja Sperling, 2012). However, the ER-localized OPR3 monomer variant OPR3<sub>(E292K)</sub>, also led to a partial restitution of fertility in the *opr2/3* mutant (data not shown). This rules out that a missing activator regulating OPR3 monomerization in the ER would be the reason for the partial restitution of JA biosynthesis in these lines.

The import of OPR3 to the ER was reported to mainly occur through a co-translational mechanism (De Meyer and Depicker, 2014), while for all other organelles, import happens after translation is finalized in the cytosol. Therefore, it might be possible that the reconstitution of JA biosynthesis in our complementation approach is due to a cytosolic activity of OPR3 before import in case of targeting to all organelles except ER. Reports of protein folding in the cytosol occurring before unfolding while being imported to organelles like mitochondria and chloroplasts support this assumption (Matouschek, 2003). Hence, this hypothesis suggests that the restoration of JA biosynthesis does not rely on OPR3's substrate reaching all tested organelles but rather being available in the cytosol, where JA biosynthesis is reconstituted through the action of *de novo* formed proteins before import. To investigate this hypothesis, a BiFC method was employed, and the results indicated probable dimerization of organelle-targeted OPR3 with a cytosolic-OPR3. However, it cannot be definitively determined whether the reconstitution of the YFP signal is solely dependent on the dimerization of OPR3 or also influenced by the self-assembly of the YFP halves. It should be noted that the stickiness of the YFP halves can be a limitation in the use of the BiFC system (Gookin and Assmann, 2014; Horstman et al., 2014). The BiFC results contradict the subcellular localization results from OPR3 targeting in *N. benthamiana* and in stable Arabidopsis lines which did not show any occurrence of the YFP signal in the cytosol but rather only to the organelle that OPR3 was targeted to.

### **3.2.4 The fertility of the *opr2/3* double mutant can be restored by cytosolic OPR3, whereas native cytosolic OPR2 is insufficient for the fertility of the *opr3* mutant.**

A question arising from the complementation assay regards the cytosolic OPR3 being able to complement JA biosynthesis in the *opr2/3* double mutant, whereas the native, cytosolic OPR2 does not since the *opr3* single mutant is sterile. Production of low JA levels by OPR2 was demonstrated, although via an alternative pathway using 4,5-ddh-JA (Chini et al., 2018). In our

complementation assays even ER-localized OPR3 resulted in the synthesis of low JA/JA-Ile levels, which led to the partial restitution of fertility of the *opr2/3* double mutant. This indicates that restitution of JA-Ile signaling might be dose-dependent. Comparing transcript levels, *OPR3* showed higher expression levels in reproductive organs of *A. thaliana* than *OPR2* and *OPR1*. We speculated that overexpression of OPR2 in the same tissues as *OPR3*, e.g., by using the *OPR3* promoter, OPR2-dependent JA production will enable restitution of fertility to the *opr2/3* double mutant. Indeed, the cytosolic OPR2 route of JA production replaced OPR3 function when expressed in the correct tissue. Further determination of JA/JA-Ile levels and additionally 4,5-ddh-JA levels would confirm this claim. These results highlight the importance of the OPR1/OPR2 cytosolic route of JA production, which was suggested by recent data to be ubiquitous in plant species and to precede the OPR3 route of JA biosynthesis (Chini et al., 2023).

While the obtained results from the organelle complementation approach could not precisely determine if OPDA is able to translocate to other cell compartments due to the lack of in-depth characterization of the complementation lines and of the enzymatic activity of OPR3, it shed light on the possible translocation of either OPDA, 4,5-ddh-JA, or both. Since it was demonstrated that OPR1 has no activity towards 4,5-ddh-JA and low activity towards *cis*-OPDA, additional determination of which of the substrates is translocating to other cell compartments could be done by complementing the *opr2/3* double mutant with OPR1 targeted to different organelles. In the case of OPR1 not complementing the double mutant when targeted to another organelle, it could suggest that the translocating substrate is 4,5-ddh-JA; conversely, the opposite scenario could indicate that OPDA is the translocating substrate.

### **3.3 The export of OPDA from the chloroplast inner envelope.**

It was initially hypothesized that OPDA would have a signaling capacity leading to the mediation of gene transcription and, consequently, OPDA would mediate the transcriptional regulation of its transporters. The prediction of OPDA transporters falling onto the list of OPDA-responsive genes comes from the notion that signaling molecules usually regulate their own transport. This is evident in the case of JA/JA-Ile transporters GTR1 and JAT1, whose transcription is enhanced by JA treatment (Li et al., 2017; Saito et al., 2015). However, with the current work, it was established that OPDA has no signaling capacity; consequently, as it functions solely as a JA precursor, it would be expected that its transport is transcriptionally regulated by JA-Ile.

The identification of several transporters from diverse transporter families which showed a JA-dependent responsiveness to wounding was possible, but it was not clear which transporter family could be preferentially involved in OPDA transport. So far, the identified chloroplast exporters of OPDA, JASSY in Arabidopsis and OPDAT1 in Poplar, belong to different gene

families and reside in the outer and inner envelopes of the chloroplast, respectively. JASSY does not belong to a known transporter family but has steroidogenic acute regulatory protein-related lipid transfer (START) domain which is predicted to bind and/or transport hydrophobic molecules (Guan et al., 2019). OPDAT1 belongs to the *Populus trichocarpa* orthologs of the Arabidopsis fatty acid exporter family (FAX) (Zhao et al., 2021). In Arabidopsis only FAX1 was characterized and was shown to export free fatty acids from the chloroplast through the inner envelope membrane (Li et al., 2015). Similarly, the JA/JA-Ile characterized transporters, JAT1 and GTR1 belong to the ATP-binding cassette ABCG family and the nitrate transporter 1/peptide transporter family (NPF), respectively. Only a few of the selected transporter candidates induced by wounding exhibited predictions for chloroplast localization. The utilized prediction databases demonstrated reliability in these predictions, particularly when different databases were cross-referenced, such as *ChloroP* and *SUBA*. Transporters that showed no chloroplast localization by both predictions, such as those belonging to the DTX family, showed no plastid subcellular localization in transient assays. Furthermore, candidates like STR1, which showed plastid localization according to *ChloroP* but had no prediction with *SUBA*, displayed dual ER-chloroplast localization.

The DTX family of transporters comprise 58 members in Arabidopsis which are poorly characterized and only few were attributed a function in the transport of different kinds of compounds (Legong Li et al., 2002). DTX30 plays a role auxin homeostasis in Arabidopsis roots (Kar and Datta, 2020), while DTX50 was found to facilitate ABA efflux (Zhang et al., 2014) and DTX47/EDS5 is involved in salicylic acid signaling but its is not known which substrate it transports (Nawrath et al., 2002). In this work, *DTX37* showed co-expression with JA biosynthesis and signaling components, with a JA-mediated amplification of expression upon wounding. Due to the disposition of its putative 12 transmembrane domains, its subcellular localization with C-terminal GFP showed aggregate formation in the ER, hinting not only towards a misfolding of the protein (Li and Sun, 2021) but also indicating that *DTX37* is a plausible secretory protein rather than being located in the plastid. STR1, like JASSY, possesses a START domain which has putative lipid transport function and was characterized as wound-responsive and JA-responsive not only in this work but also by previous reports (Satheesh et al., 2014; Yan et al., 2007). STR1 showed a very interesting dual localization to the ER and to the chloroplast, and this observation is validated by an independent work where both subcellular localization and western blot from chloroplast fractions consolidated this dual localization (Banday et al., 2022). This dual localization might indicate a function in lipid trafficking between chloroplast and ER, especially that *STR1* co-expresses with the monogalactosyldiacylglycerol (MGDG) synthase (*MGD1*) in addition to JA-related genes. As a result, this candidate is likely to be promising for galactolipid trafficking between the chloroplast and the ER (Kelly and Dörmann, 2004), rather than being directly involved in JA biosynthesis.



Additionally, the characterization of such an ER-chloroplast dually targeted protein would be a novelty.

The only candidate with an inner-envelope localization and showing a response to wounding exclusively in the presence of JA, was *PEC1*. Since it was characterized as a potassium channel with passive calcium transport (Volkner et al., 2021), it was not clear if it would have a function in relation to OPDA export. *PEC1* showed tight co-expression with OPDA biosynthetic enzymes *LOX2*, *AOS* and *AOC2* and accumulation at the transcriptional and protein levels were JA dependent (pers. comm. H.-H. Kunz). Loss of function of *PEC1/PEC2* leads to accumulation of lower levels of OPDA in response to wounding and to priming with wounding or MeJA treatment indicating putative involvement in OPDA formation. In the case of alteration of OPDA transport, it is expected that it leads to a lower JA formation due to limited pool of OPDA moving out from the plastid. However, *PEC1/PEC2* loss of function led to lower OPDA levels but did not impact JA or JA-Ile formation, implying other means of compensation. The involvement of calcium transporters in modulating jasmonate dynamics was previously reported, with the vacuolar cation channel *TPC1* gain-of-function, *fou2*, shown to induce JA synthesis/signaling (Beyhl et al., 2009; Bonaventure et al., 2007). Similarly, *PEC1* could be involved in the activation of *LOX2* by regulating calcium homeostasis in the plastid stroma. Further determination of *PEC1* function in relation to OPDA accumulation and JA responses will be addressed by mRNA sequencing of the *pec1* loss of function (collaboration with H.-H. Kunz).

In summary, the use of a transcriptional approach to identify a putative OPDA transporter led to the identification of an interesting candidate involved in OPDA accumulation, *PEC1*, whose exact function is yet to be characterized. The overall screening for an OPDA transporter using the transcriptome relies, however, on predictions for the localization of putative chloroplast-located candidates. Additionally, the lack of information about membrane proteins and about the variation in substrate specificity among members of the same transporter family (Barbier-Brygoo et al., 2001; Diallinas, 2014), makes the identification of transporters of specific substrates challenging. Several protein families with transmembrane domains and substrate transport ability are not yet characterized or conventionally classified as transporters, as seen in the case of *JASSY* (Guan et al., 2019). An alternative strategy to identify a transporter would be the use of a proteomic approach, and in the case of putative OPDA transporters screening could be performed from isolated chloroplast membranes to get higher specificity (Barbier-Brygoo et al., 2001). For functional characterization of candidate genes by reverse genetics, the screening for T-DNA lines was of limited success, since for certain genes suitable T-DNA lines were not available and for others predicted knock-out lines showed persistent gene

transcription. Therefore, generation of knock-out lines by gene editing tools like CRISPR-Cas9 will be the more favorable approach for future research.

### 3.4 Summary and conclusion

The recent findings regarding jasmonate biosynthesis and the contribution of different routes of JA formation in addition to the main characterized OPR3 canonical pathway, resulted in questioning of the previous findings which attributed signaling functions to OPDA that are independent from JA signaling. Hence, several roles were attributed to OPDA in addition to its role as a JA precursor in *Arabidopsis thaliana* despite the lack of knowledge on the mechanism of its signaling. Most of the previous work did not achieve to uncouple OPDA's production from that of JA. However, with the availability of a JA deficient background such as the *opr2/3* double mutant it is possible to re-evaluate the previous findings through confirmation or re-adjustment. With this work, we addressed the function of OPDA as a signaling molecule to induce transcriptional change at basal levels and upon its burst formation following mechanical wounding of Arabidopsis. The results hinted towards the absence of such signaling function when the transcriptome of different mutants affected in the production of JA and/or OPDA were compared. Additionally, the transcriptomic data coupled with determination of hormone levels highlighted limitations in the use of exogenous OPDA treatment as an experimental design to characterize OPDA signaling. Application of OPDA led through a not yet fully characterized route to the production of JA-Ile in the *opr2/3* double mutant, which we speculate to be through OPR1. Further experiments to substantiate these results are needed.

The complementary approach to investigate OPDA signaling by addressing its translocation to other cell compartments, and most importantly to the nucleus, to exert direct mediation of transcriptional change, demonstrated possible translocation of OPDA or 4,5-ddh-JA to different cell compartments. Further experiments are needed to unravel which of these substrates is translocating to the tested compartments. Interestingly, this approach led to a further characterization of the OPR3-independent pathway of JA formation, since the findings support that OPR2 can take over OPR3 function if expressed in the same tissues. The transcriptional and the trans-organellar complementation approaches even though designed to uncover OPDA signaling, unintentionally intersected in unraveling some aspects of OPR1 OPR2 cytosolic pathway of JA production. This indicates a high importance of this route of JA production not in terms of its contribution to the total JA production but rather to its interference with the identification of processes like OPDA signaling in JA-deficient mutants when its presence is not taken into account.

The use of the same transcriptomic data to identify a putative chloroplast located OPDA transporter, despite not identifying an OPDA transporter, led to the identification of a potassium/calcium channel with a function in JA pathway and specifically in OPDA formation.

The role of this channel in the JA pathway and its significance are, however, yet to be uncovered.

This work lays a basis for further evaluation of OPDA signaling in Arabidopsis and other angiosperms to uncover its function(s) whether as being solely a JA precursor or as a signaling molecule with independent function(s) from JA. It also highlights plausible translocation of JA precursors in the cell, to other compartments than those of their biosynthesis. Mobility of such JA precursors was previously demonstrated, however the mechanism behind it is still unknown. Further characterization of the mobility of JA precursors would shed light on the dynamics of JA biosynthesis and the role of its precursors within the plant cell.

## **4 The flower-specific transcription factors MYB21 and MYB24 are wound-responsive.**

### **4.1 Introduction**

Jasmonic acid (JA) is a plant hormone that plays a significant role in various aspects of plant growth, development, and responses to environmental stresses. As its primary functions are related to defense responses against herbivores and pathogens, it also plays a key role in the regulation of flowering in different plant species. While in *Arabidopsis thaliana* JA orchestrates key processes of male fertility by regulating the elongation of stamen filaments, anther dehiscence, and pollen maturation (Thines et al., 2013), in tomato JA regulates female fertility in addition to stamen and pollen development (Dobritzsch et al., 2015; Schubert et al., 2019).

#### **4.1.1 Flower development in Arabidopsis.**

Flower development is a well-studied process in *A. thaliana* and involves a series of stages which are controlled by a complex network of genes, hormones, and environmental cues. The onset of flowering is marked by the transition of the shoot apical meristems into flower meristems (Alvarez-Buylla et al., 2010). The floral meristem produces floral organs in a sequential manner through coordinated patterns and rates of cell division and expansion which occur in the different layers of cells within the meristem. As these cells divide and differentiate, they dynamically acquire distinct fates determining the types of floral organs they will eventually become (sepals, petals, stamens, or carpels) (Alvarez-Buylla et al., 2010; Irish, 2010). Based on specific cellular and physiological events, the process of development of the *A. thaliana* flower has been divided into twenty stages (Smyth et al., 1990; Alvarez-Buylla et al., 2010) (Fig. 4.1). The precursors of the flower organs, and specifically of stamens and petals, start to appear in the stage five of flower development and develop into a bud fully enclosed by both medial and lateral sepals at the stage six (Smyth et al., 1990). Stage eight is marked by the appearance of the anther locules on short stamens and is followed by a rapid lengthening of all organs at stage nine. During stage ten, the petals elongate to reach the top of the stamens and the stigma starts to form at the top of the gynoecium, and by stage eleven the stigmatic papillae forms (Alvarez-Buylla et al., 2010). The final stage of flower development corresponds to stage twelve and is characterized by a rapid elongation of the stamen filaments and the anthers almost reaching their mature length. This stage concludes with the sepals opening and culminates in anthesis when fertilization occurs. The latter is followed by the floral bud opening at stage fourteen (Smyth et al., 1990; Alvarez-Buylla et al., 2010). Stage fourteen also marks the beginning of silique and seeds developments translating in the extension of the stigma above the mature anthers. Up to the stage seventeen further expansion of the silique occurs and is accompanied by withering of sepals and petals and starting from stage eighteen ripening

of the siliques commences which ends by the mature seeds being ready to be dispersed at stage twenty (Alvarez-Buylla et al., 2010).

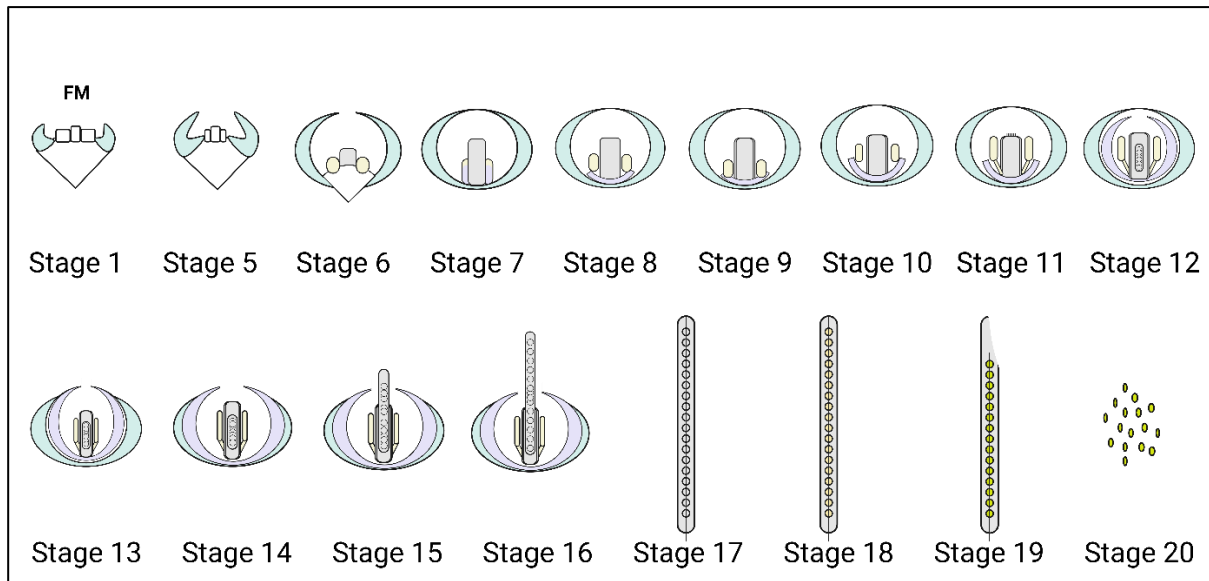


**Fig. 4.1 Schematic representation of the developmental stages of Arabidopsis flowers.**

The flower primordium is formed at stage 1 and continues to grow to form visible petal and stamen primordia at stage 5. Organ development continues until stage 12 where petals and stamens reach similar lengths. Fertilization occurs at anthesis by stage 13 and leads to flower opening (stage 14). At stage 17, the siliques reach their mature size, then turn yellow at stage 18 (stage 20) and fall by stage 20. Floral meristems (FM); sepals, green; petals, purple; stamens, yellow; gynoecia, grey; seeds orange. (adapted from Alvarez-Buylla et al., 2010).

#### 4.1.2 JA regulation of flowering.

Genetic studies have characterized the involvement of JA in the coordination of flower developmental processes lying within stages 10 and 13 of flower development (Fig. 5.1.1). Late flower developmental events consisting of stamen filament elongation, anther dehiscence, pollen maturation and flower opening were shown to be tightly related to intact JA biosynthesis and signaling (Ishiguro et al., 2001; Mandaokar et al., 2006). Mutants affected in JA signaling in *A. thaliana* like the *coi1* mutant and in JA biosynthesis like the *aos* and the *opr3* mutants are male sterile (Devoto et al., 2002; Ishiguro et al., 2001; Stintzi and Browse, 2000; Von Malek et al., 2002). Given that JA derives from chloroplast membrane lipids, also defects in JA fatty acid precursors results in male sterility as shown by the fatty acid desaturases triple mutant, *fad3 fad7 fad8*, and the lipase mutant *dad1* (Ishiguro et al., 2001; McConn and Browse, 1996). The male sterility of the previously mentioned JA mutants can be rescued by exogenous application of JA to flower buds, except for the *coi1* mutant which is JA insensitive due to the defect of the JA receptor COI1. This collection of mutants suggested the role of JA in coordinating late flower developmental events.

#### 4.1.3 The role of MYB21/MYB24 in Arabidopsis flower development.

The transcription factors MYB21 and MYB24 belong to the clade 19 of the R2R3-MYB gene family which encloses the MYB genes containing two repeats and constitutes the largest MYB gene family in plants (Stracke et al., 2001). MYB21 and MYB24 were isolated in a Yeast Two-Hybrid screening system for JAZ-interacting proteins, and were shown to interact with JAZ1, JAZ8, and JAZ11 through their N-terminal R2R3 DNA Binding Domain (Song et al., 2011). Both transcription factors were initially identified in a transcriptional profiling of the stamens from JA-treated flower buds of the JA-deficient *opr3* mutant (Mandaokar et al., 2006). The *myb21-1* mutant showed a male sterility phenotype consisting of shorter anther filaments and delayed anther dehiscence; phenotypes that were exacerbated by the crossing of the *myb21-1* with the *myb24-1* mutant and were not rescued by exogenous JA application (Mandaokar et al., 2006). The complementation of the *coi1* mutant with overexpression of the MYB21 coding sequence only partially recovered its fertility (Song et al., 2011). Similarly, overexpression of MYB24 can rescue the *opr3* mutant sterility, however, only moderate and not excessive levels of MYB24 complement the phenotype (Huang et al., 2017). MYB21 and MYB24 show flower-specific expression and are mainly localizing to sepals, petals, stamen filaments, and carpels (Reeves et al., 2012).

The auxin-related transcription factors, AUXIN RESPONSE FACTOR 6 (ARF6) and ARF8, are known to regulate Arabidopsis flowering by promoting male and female organs developments. Their corresponding mutants, the *arf6* and *arf8*, share similar defects with the *myb21myb24* double mutant consisting of delayed stamen filament elongation and decreased fertility (Nagpal et al., 2005). Expression and genetic studies had identified the ARF6 and ARF8 to be acting upstream of the MYB21 and MYB24 by inducing jasmonate production in flowers, which in turn triggers the expression of the latter transcription factors and promote flower development (Reeves et al., 2012). Hence a regulatory network was characterized for flower maturation involving a tight coordination between the auxin-responsive ARF transcription factors and the JA-induced MYB21 and MYB24 (Fig. 4.2).

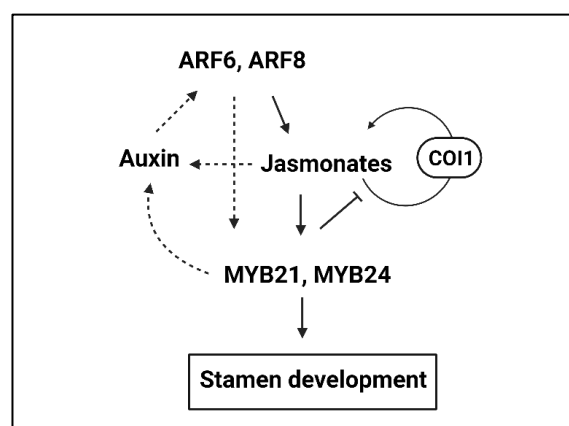


Fig. 4.2 The regulatory network for stamen development in Arabidopsis.



At flower stage 12, jasmonate biosynthesis is promoted by the ARF6 and 8 auxin response factors, and in turn triggers a COI1-dependent JA positive feedback loop to activate JA biosynthesis and promote stamen development through MYB21 and MYB24. Starting from stage 13, MYB21 engages in a JA negative feedback to repress JA biosynthesis and arrest flower maturation processes. Solid and dashed arrows indicate established and potential events, respectively (adapted from Reeves et al., 2012).

#### **4.1.4 Aims and objectives**

Following the identification of *MYB21* and *MYB24* as wound-responsive in Arabidopsis seedlings and leaves in our RNAseq data and considering the absence of any data referring to any putative function of these transcription factors in vegetative tissue, further investigation of this wound response was undertaken to understand their up-regulation in the seedlings and leaves. Both transcription factors are known to be flower-specific and their functions in flower organs has been well illustrated (Cheng et al., 2009; Huang et al., 2017, 2020; Mandaokar et al., 2006; Reeves et al., 2012; Schubert et al., 2019), hence the characterization of putative additional functions that they might exert in other tissues than flowers would better clarify the dynamics of their activity in Arabidopsis. Since MYB21 and MYB24 regulate JA pathway in flowers, this work could help further characterize JA dynamics in vegetative tissue if these TF perform the same molecular function as in flowers. Consequently, this work could be a first step to setting a bigger picture on their biological significance.

The development of this work in parallel with the main PhD project was achieved by the inclusion of a M.Sc. thesis work design which was performed by Olivia Putri Herdani in the laboratory of Prof. Dr. Bettina Hause at the Leibniz Institute of Plant Biochemistry.

##### **(I) Characterization of the wounding response of *MYB21* and *MYB24* in vegetative tissue.**

The wound-responsiveness of *MYB21* and *MYB24* should be validated by characterizing the kinetics of their transcriptional wound responses in vegetative tissues and by investigating their tissue-specific expression upon wounding. To understand the biological significance of the wound-induction of both transcription factors, we investigated the dynamics of their involvement in the JA pathway upon wounding, as inferred from their functions in flowers, using previously characterized *myb21* and *myb24* mutants.

##### **(I) Identification of other putative functions of *MYB21* and *MYB24* in vegetative tissues by screening of phenotypes in the mutants.**

To consolidate the possibility of *MYB21* and *MYB24* having additional function(s) beside flower development, we performed a screening for developmental phenotypes in the *myb21* and *myb24* mutants. The identification of developmental defects in these mutants would constitute initial indications towards possible implications of these TF in vegetative processes and might lead to the identification of agronomically important traits.

## 4.2 Results

### 4.2.1 MYB21 and MYB24 are wound-inducible in a JA-dependent manner.

When dissecting the wounding transcriptional response in Col-0 and the JA-deficient mutants *opr2/3* and *aos* (Section 2.1.3.3), within the differentially expressed genes in a strictly JA-dependent manner, two flower-specific transcription factors (TF) *MYB21* and *MYB24* appeared to be highly up-regulated upon wounding in seedlings and adult leaves of Col-0. These TFs were characterized as jasmonate signaling components responsible for the stamen elongation in *Arabidopsis thaliana* (Cheng et al., 2009; Huang et al., 2020; Reeves et al., 2012; Song et al., 2011). No previous data had reported expression or function of these genes in vegetative tissues in *A. thaliana* or other plant species and were therefore designated as flower specific (Reeves et al., 2012). Hence, the wound-induction of *MYB21* and *MYB24* in vegetative tissues in our experiments suggested putative uncharacterized tissue expressions and function(s), which as a novelty was relevant to be further examined.

Our wounding experiments performed with 10-day-old seedlings and 4-week-old rosettes permitted the characterization of the JA-specific transcriptomic response to wounding when we compared Col-0 to the JA-deficient *opr2/3* and *aos* mutants. Within the JA-dependent wounding response, which was only present in Col-0, for both developmental stages *MYB21* and *MYB24* showed high fold change in expression levels at 1h following wounding, (Table 4.1). Characterization of the up regulation of both TFs in terms of expression levels indicated that their transcripts accumulated only upon wounding since at control condition the levels were undetectable or close to zero for Col-0 and undetectable in the mutants *opr2/3* and *aos* (Fig. 4.3A and B). Upon wounding, both transcripts are induced, but in the absence of JA (in *opr2/3* and *aos*) no transcript induction of the TFs was detected. Hence *MYB21* and *MYB24* are wound responsive in a JA-dependent manner.

**Table 4.1: MYB21 and MYB24 are up-regulated upon wounding in the seedlings and adult leaves of Col-0.**

| AGI                         | Gene name    | Log2 FC <sup>A</sup> | p-value <sup>B</sup> | Adjusted p-value <sup>C</sup> |
|-----------------------------|--------------|----------------------|----------------------|-------------------------------|
| <b>10-day-old seedlings</b> |              |                      |                      |                               |
| AT3G27810                   | <i>MYB21</i> | 5.60                 | 2.26E-05             | 1.09E-04                      |
| AT5G40350                   | <i>MYB24</i> | 4.92                 | 2.46E-03             | 8.24E-03                      |
| <b>4-week-old rosettes</b>  |              |                      |                      |                               |
| AT3G27810                   | <i>MYB21</i> | 8.51                 | 8.57E-12             | 1.66E-10                      |
| AT5G40350                   | <i>MYB24</i> | 7.41                 | 2.10E-16             | 6.15E-15                      |

<sup>A</sup> Fold-change is expressed in log2 FC and was calculated from mean FKPM of three biologically independent experiments.

<sup>B</sup> False discovery rate

<sup>C</sup> Corrected false discovery rate

Determination of the kinetics of the wounding induction of *MYB21* and *MYB24* was performed in an independent experiment using 14-day-old seedlings grown in sterile media. Seedlings were wounded with forceps and samples were taken at 1-, 3-, 8- and 24-hours after wounding

(Fig. 4.3C). Both TFs showed the highest induction at 1 h post-wounding, which lowered throughout the time-course for *MYB24* and lowered while sustaining significantly higher levels at 8 and 24 h for *MYB21*. To investigate whether these TF are also JA responsive in the leaf, 4-week-old adult leaves from Col-0 and the JA-deficient mutants were treated with 50  $\mu$ M MeJA and relative transcript accumulation of *MYB21* and *MYB24* was determined by qRT-PCR (Fig. S25). Both TF-encoding genes were transcriptionally induced in response to MeJA with the highest levels detectable at 1 h after spraying of the rosette leaf with MeJA. Interestingly, their induction in the JA deficient mutants was higher than Col-0, hinting towards a negative regulation of their transcripts through the JA positive feedback loop, which is absent in the JA-deficient mutants.

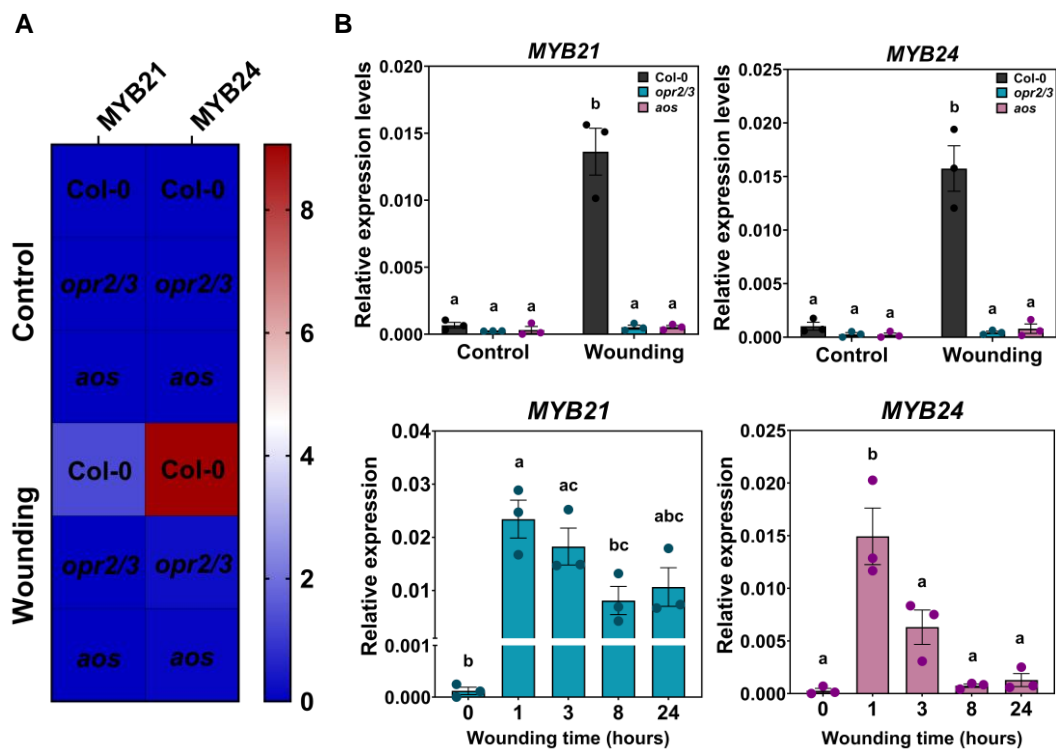


**Fig. 4.3** *MYB21* and *MYB24* are wound-inducible in leaf and seedlings in a JA-dependent manner.

**A:** The wounding response of *MYB21* and *MYB24* from the RNAseq data of 4-week-old rosette leaves of Col-0, *opr2/3* and *aos*. Heatmap shows the expression levels of the genes at control and 1 h following wounding with FPKM values averaged from three biological replicates.

**B:** The wounding response of *MYB21* and *MYB24* in 10-day-old seedlings of Col-0, *opr2/3* and *aos*. Data corresponds to qRT-PCR technical validation of the RNAseq data from 10-day-old seedlings with relative expression levels normalized to *PP2A*.

**C:** Time course of *MYB21* and *MYB24* transcript accumulation at 0, 1, 3, 8 and 24 h after wounding in two-week-old seedlings of Col-0.

Bars represent means of three biological replicates (single dots;  $\pm$ SEM). Different letters denote statistically significant differences among genotypes as determined by Two-way Anova in (B) and One-way ANOVA in (C) followed by Tukey HSD ( $p < 0.05$ ).

#### 4.2.1.1 Tissue-specific expression of *MYB21* and *MYB24* by promoter-GUS lines.

*MYB21* showed basal expression only in trichomes and hydathodes (Fig. 4.4A), the latter are structures found at the tips of leaf teeth and contain water pores, xylem ends, and small cells (Yagi et al., 2021). *MYB21* trichome/hydathode specific expression would explain its general

low expression levels in Col-0. At 2 h after wounding, *MYB21* showed clear induction only in the wounded area of the leaf, where the GUS signal appeared in the leaf margin and mid vein in addition to a strong signal in the podium and the skirt cells of trichomes (Fig. 4.4B). This induction is not present anymore in the wounded area at 24 h after wounding except from a small portion of the mid vein where wounding occurred. The GUS-staining obtained from *MYB21(7kb)pro::GUS* plants is in accordance with the expression levels and kinetics determined by qRT-PCR. It is also important to note that when using the *MYB21(2kb)pro::GUS* reporter lines no signal was detected neither at basal levels nor upon wounding (Fig. S26A).

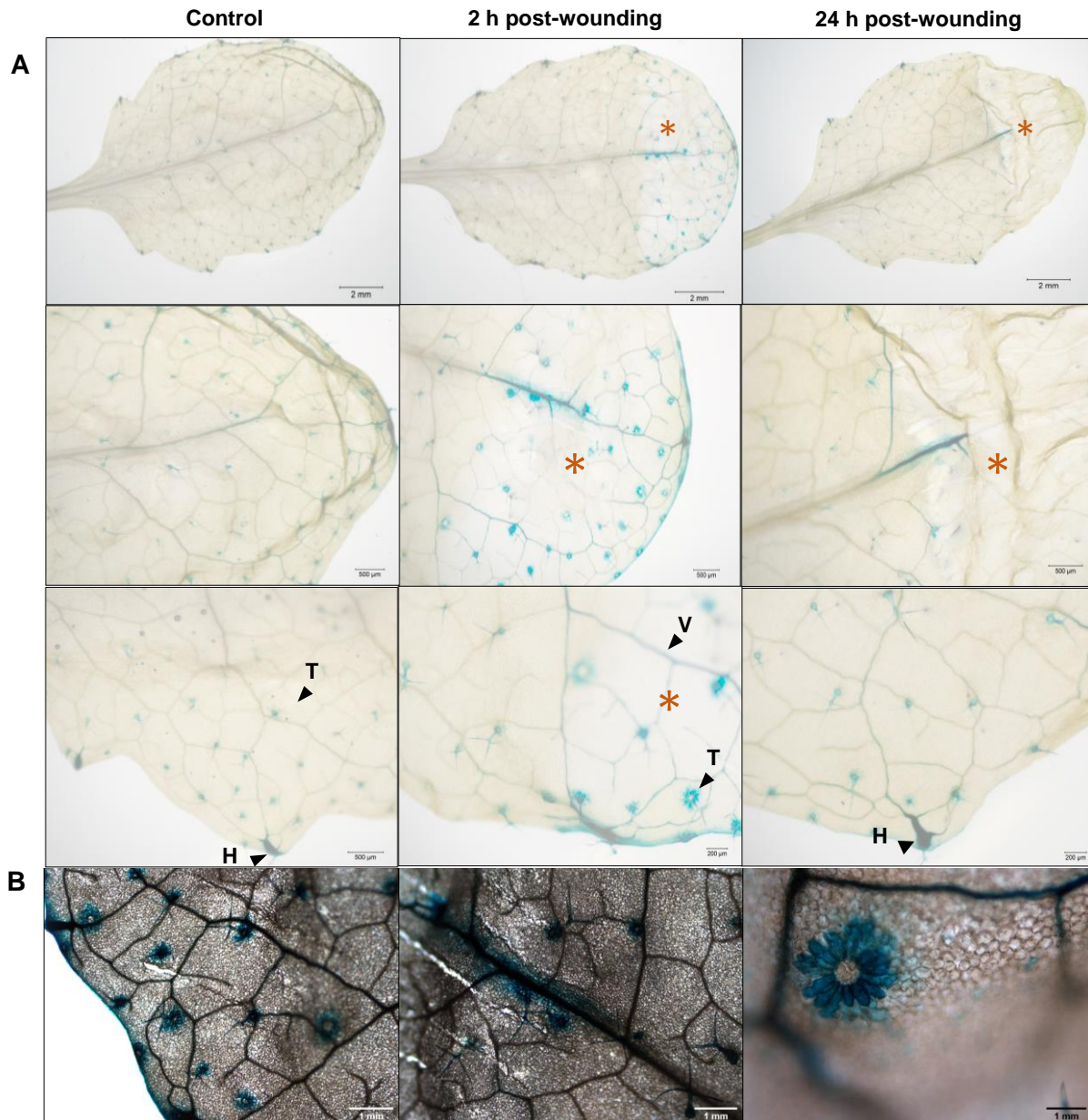


**Fig. 4.4 Expression of *MYB21(7kb)pro::GUS* reporter gene in 4-week-old rosette leaf at control and after wounding.**

Leaves were wounded with forceps (orange asterisks) and tissue fixation was performed at 2 h and 24 h post-wounding with control leaves kept unwounded. X-Gluc (5-bromo-4-chloro-3-indolyl-β-D-glucuronide) was used for histochemical staining to monitor GUS activity.

**A:** *MYB21(7kb)pro::GUS* expressing in trichomes (T) and hydathodes (H) of the leaf at basal levels and induced in trichomes (T) and leaf veins (V) upon wounding.

**B:** Close-up on the wounded area at 2h post wounding.



Similarly, the *MYB24(2kb)pro::GUS* lines did not show GUS signal in adult leaves (Fig. S26B). This indicates that *MYB21* and *MYB24* expressions in leaves are controlled by their promoter sequences upstream of 2 kb. Since GUS reporter lines with longer *MYB24*-promoter region were not available, investigation of *MYB24* tissue expression in leaves was not possible.

#### 4.2.1.2 The dynamics of the JA pathway in the wounded *myb21* and *myb24* mutants

Since *MYB21* and *MYB24* were identified as the components of JA signaling in flowers with *MYB21* being the TF that negatively feeds-back JA-biosynthesis (Reeves et al., 2012), determination of the levels of OPDA, JA and JA-Ile in addition of the transcript levels of JA-inducible genes in the *myb21-5* and *myb24-5* mutants was performed (Fig. 4.5).

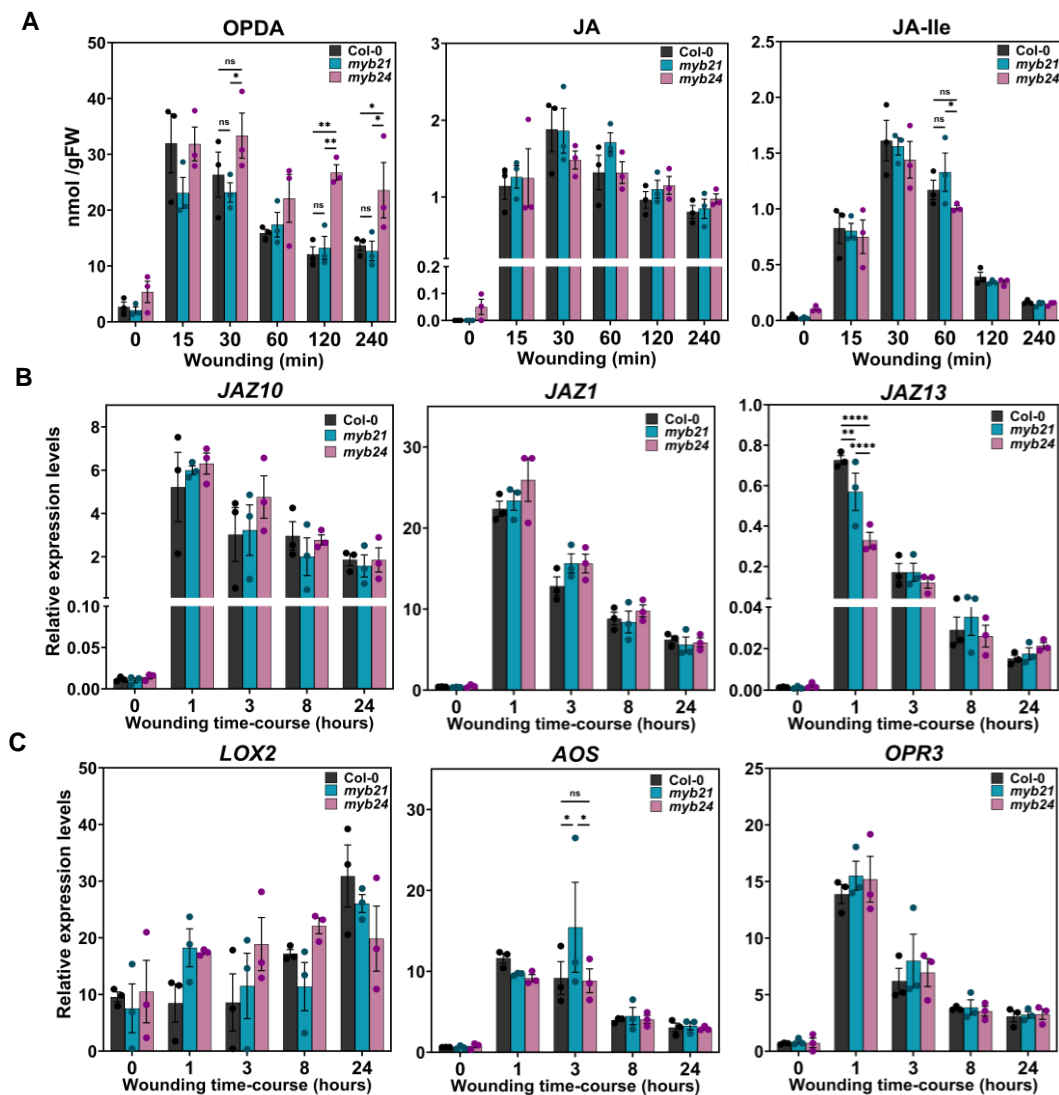


**Fig. 4.5** The dynamics of the JA pathway upon wounding do not show remarkable differences between the mutants *myb21* and *myb24* and Col-0.

Two-week-old seedlings of Col-0, and the *myb21* and *myb24* mutants were grown in sterile liquid media and wounded with forceps.

**A:** *cis*-OPDA, JA and JA-Ile accumulation in Col0 and the *myb21* and *myb24* mutants at 0, 15, 30-, 60-, 120- and 240-minutes post wounding.

**B:** Transcripts accumulation of the JA-responsive genes, *JAZ1*, *JAZ10* and *JAZ13*, upon wounding in Col-0 and the *myb21* and *myb24* mutants. The expression levels were determined by qRT-PCR and calculated in relation to *PP2A*.

**C:** Transcripts accumulation of the JA-responsive genes, *LOX2*, *AOS* and *OPR3*, in Col-0 and the *myb21* and *myb24* mutants. expression levels were determined relative to *PP2A* levels. Bars represent means of three biological replicates (single dots) with around 15-30 seedlings each. Differences between genotypes was determined at each time point (within the time-points) by One-way Anova and Tukey HSD ( $p < 0.05$ ). Statistical results are shown on graphs only when significant (\*  $p < 0.05$ , \*\*  $p < 0.01$ , \*\*\*  $p < 0.001$ , and \*\*\*\*  $p < 0.0001$ ).

While JA and JA-Ile levels did not show statistically significant differences in their accumulation in *myb21* and *myb24* seedlings upon wounding, it is to be noted that in *myb21* JA and JA-Ile were slightly but not significantly higher than in Col-0 at 1 h following wounding. OPDA accumulated in significantly higher levels in *myb24* in comparison to *myb21* and Col-0 specifically at 2 and 4 h following wounding without inducing changes in JA and JA-Ile levels (Fig. 4.5A). In accordance with the hormone levels, significant differences were not observed in the expression of *JAZ*-genes or the genes encoding JA biosynthesis enzymes when the mutants were compared to Col-0 (Fig. 4.5B, C), except for *JAZ13* which showed significantly lower relative expression at 1 h after wounding in both *myb21* and *myb24* mutants in comparison to Col-0. These results indicated that both TFs did not affect JA biosynthesis upon wounding in seedlings. Nevertheless, despite being not statistically significant, a tendency of higher JA/JA-Ile production in the *myb21* mutant is observed at 1 h following wounding in addition to a tendency of higher JA signaling through higher transcriptional induction of JA-responsive genes like *JAZ10*, *JAZ1*, *LOX2* and *OPR3*. It should also be noted that even though both TFs had very clear induction upon wounding, they expressed at low levels in seedlings and adult leaves, and this is due to a specific tissue/cell type expression as shown by the GUS experiment for *MYB21*, hence their effects on JA biosynthesis and signaling pathways could be masked in a whole seedling/leaf tissue set-up.

*MYB21* and *MYB24* were shown to be involved in the regulation of biosynthesis of flavanols in the flower's stamens (Zhang et al., 2021). Therefore, accumulation of anthocyanins in leaves following detachment from the rosette was determined (Fig. S27). Anthocyanins content in leaf number six accumulated following detachment from the rosette; however, no significant differences were recorded between the *myb21* and *myb24* mutant plants in comparison to Col-0 (Fig. S27B). This indicated no putative function of either TFs in the accumulation of anthocyanins in leaves post-detachment from the rosette.

#### **4.2.2 Analysis of developmental phenotypes of *myb21* and *myb24* mutant plants.**

Since *MYB21* and *MYB24* have a putative role, not yet fully characterized, in response to wounding in the seedlings and leaves of *A. thaliana*, further investigation to determine whether they could be involved in any developmental processes in vegetative tissues was performed by phenotyping of the *myb21* and *myb24* mutants.



One initial phenotype that was clearly observed while growing the mutants in sterile media or on soil, was that the *myb21* mutant had a bigger size than Col-0 and *myb24* as it is shown in Fig. 4.6A. Quantification of the rosette size was performed by measuring the rosette leaf length and area. It indicated that *myb21* had a significantly bigger rosette than Col-0 (Fig. 4.6B-C). The bigger true leaves of *myb21* had additionally a higher trichome number in comparison to Col-0 (Fig. 4.6D). Besides having bigger shoots, *myb21* also had longer roots confirming that the mutant was generally bigger in size in comparison to Col-0 (Fig. 4.6E), a phenotype that is also characteristic of JA-deficient mutants in *A. thaliana*. MYB21 is therefore likely to play a role in growth repression in the previously tested tissues. The *myb24* mutant plants, however, were not distinguishable from Col-0.

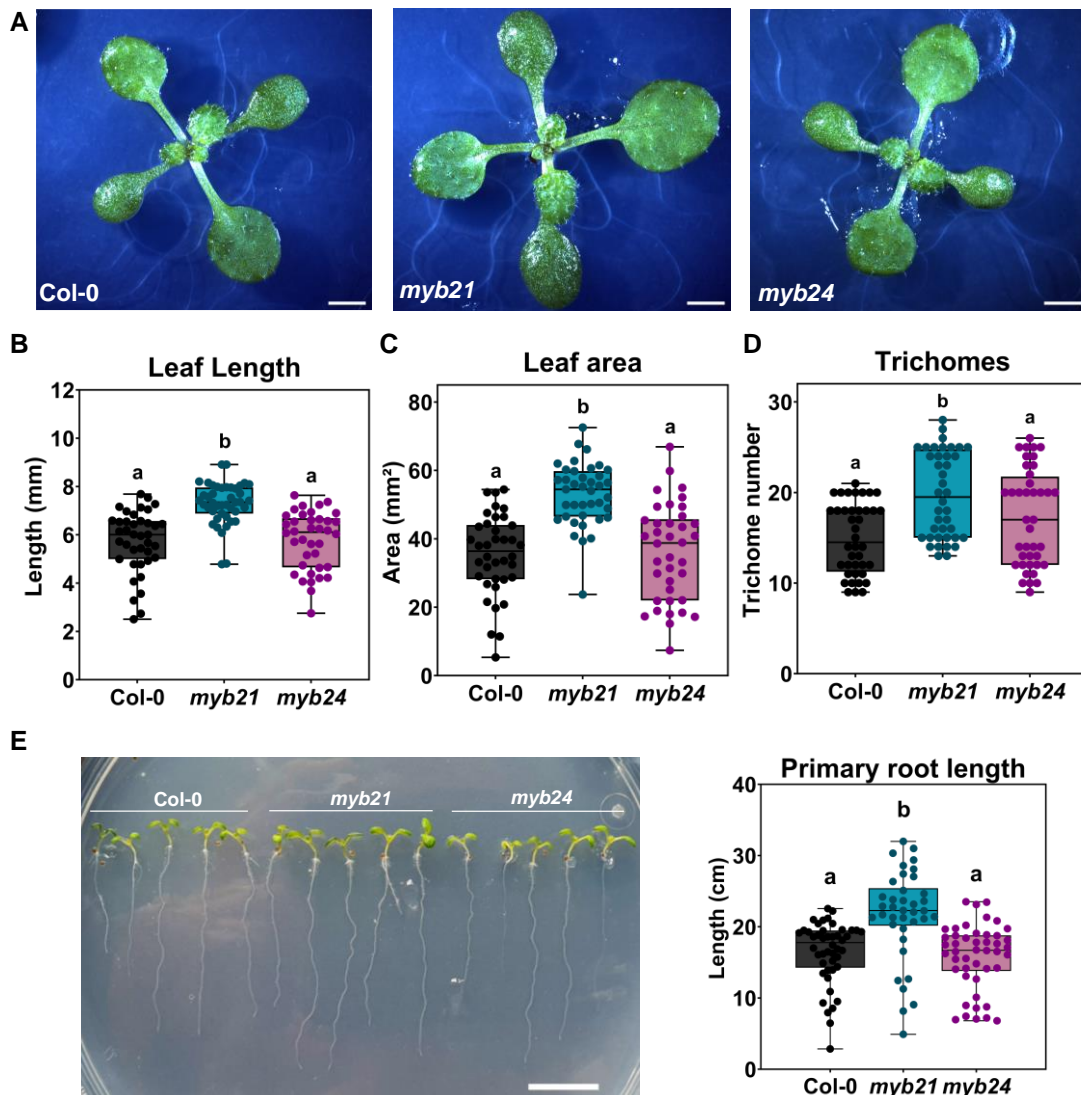


**Fig. 4.6** The *myb21* mutant plants have bigger rosettes, higher trichome number per leaf and longer roots than Col-0.

Two-week old seedlings from Col-0 and the *myb21* and *myb24* mutants were grown on sterile media and phenotyped using Image-J. Scale bars: 2 mm.

**A:** The *myb21* mutant shows bigger rosette size in comparison to Col-0 and *myb24*.

**B-D:** Leaf length (leaf blade + petiole), leaf area and number of trichomes per leaf. The box plots are from 38 to 43 individuals per genotype (single dots) with standard deviations and means depicted in solid lines.

**E:** Primary root length. The box plots are from 38 to 46 individuals per genotype (single dots) with standard deviations and means depicted in solid lines. Scale bars: 2 mm. Different letters denote statistically significant differences among genotypes as determined by One-way ANOVA followed by Tukey HSD ( $p < 0.05$ ).

Since JA is a growth repressor and MYB21 is a component of its signaling in flowers, root growth inhibition by MeJA was tested in the mutants and Col-0 (Fig. 4.7). MeJA inhibited the growth of the primary roots of Col-0, and the *myb21* and *myb24* seedlings. Interestingly, despite *myb21* exhibiting significantly increased root length compared to Col-0 at control condition, no significant differences in the root length were observed under MeJA condition (Fig. 4.7B). This result suggests a higher root inhibition in *myb21* and consequently a higher sensitivity of this mutant to MeJA. To avoid MeJA affecting differently the seed germination of the mutants and Col-0, the root inhibition growth experiment was repeated by transferring the seedlings to MeJA at 3 days post-germination (Fig. S28). This experimental setup yielded similar root inhibition results as the previous one. At control condition, however, *myb21*'s roots had the same length as Col-0. Interestingly, this means that the gentle “touching/wounding” with forceps during the transfer, resulted in higher inhibition of root growth in the *myb21* compared to Col-0. Both experiments highlight higher sensitivity of *myb21* to JA.

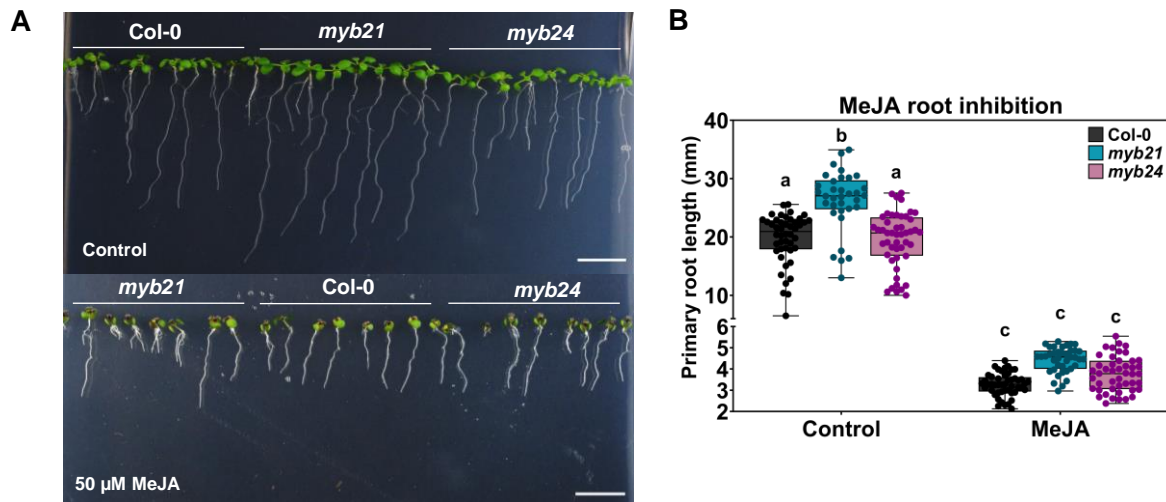


**Fig. 4.7 MeJA-mediated root growth inhibition of Col-0 and the *myb21* and the *myb24* mutants**

Two-week-old seedlings were grown on solid media at control condition and with media supplied with 50  $\mu$ M MeJA.

**A:** Seedlings of Col-0, *myb21* and *myb24* show shorter primary roots following growth on MeJA. Scale bars: 2 mm.

**B:** Growth inhibition of the primary root by MeJA. Seedlings were grown for 10 days at control and MeJA conditions. The box plots are from 39 to 49 replicates (single dots). The solid lines within the box plots depict standard deviations and means. Different letters denote statistically significant differences among genotypes as determined by Two-way ANOVA followed by Tukey HSD ( $p < 0.05$ ).

#### 4.2.3 Seedlings etiolation in the *myb21* and *myb24* mutants

When grown in darkness, seedlings undergo skotomorphogenesis, which translates into the elongation of the hypocotyl and non-opening of the cotyledons (Fig. 4.8A), and JA was shown to suppress hypocotyl elongation in etiolated seedlings (Zheng et al., 2017). To test whether MYB21 and MYB24 could have a role in JA-mediated hypocotyl elongation suppression,

seedlings from Col-0, and the *myb21* and *myb24* mutants were grown in the dark and hypocotyl length was determined in the three genotypes (Fig. 4.8B). The *myb21* mutant had a significantly longer hypocotyl than Col-0 and *myb24*, however considered that *myb21* seedlings were generally bigger in size the longer hypocotyl does not necessarily imply a function of MYB21 in etiolation. The etiolated seedlings of the *myb21* and *myb24* mutants did not show differences in the cotyledons opening or in the hypocotyl hook angles when compared to Col-0.

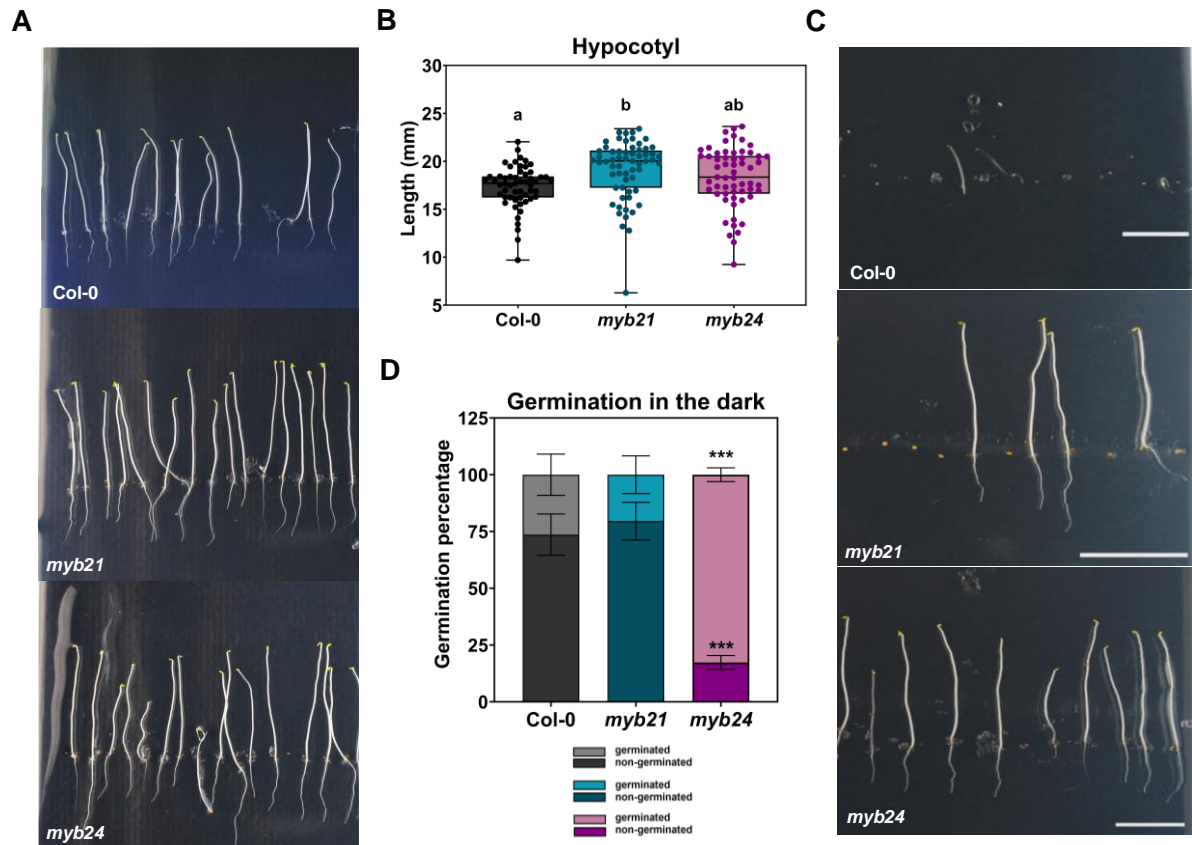


**Fig. 4.8 Etiolated seedlings of the *myb21* mutant have longer hypocotyl than Col-0 and *myb24* seeds can germinate in the dark.**

7-day-old seedlings from Col-0, and the *myb21* and *myb24* mutants were grown on sterile media and phenotyped using Image-J.

**A:** Etiolated seedlings of Col-0 and the *myb21* and *myb24* mutants. Seeds were grown in the dark after exposure to light for 3 h to alleviate seed dormancy.

**B:** Hypocotyl length of etiolated seedlings. The box plots are from 55-61 individuals per genotype (single dots) with standard deviations and means depicted in solid lines.

**C:** Etiolated seedlings of Col-0 and the *myb21* and *myb24* mutants. Seeds were grown directly in the dark without alleviating seed dormancy with exposure to light. Scale bars: 0.5 cm

**D:** Percentage of seed germination in the dark without light exposure. Bars represent means of three replications with around 25 seeds per biological replicate. Data represents the percentage of germinated and non-germinated seeds over the total number of seeds.

Statistically significant differences among genotypes were determined by One-way ANOVA followed by Tukey HSD ( $p < 0.05$ ) (**B**, **D**) and are shown in (**B**) with different letters, and in (**D**) only when significance was found (\*\* $p < 0.001$ )

To study etiolation and growth in darkness in *A. thaliana*, it is necessary to expose the seeds to light for a few hours before transferring them to darkness in order to alleviate seed dormancy. The termination of seed dormancy in *A. thaliana* is needed for seed germination is a light-dependent process and (Hennig et al., 2002; Stawska and Oracz, 2019). During our etiolation experiments, due to a handling mistake, the exposure of the seeds to light before growth in darkness was overlooked. and resulted in the inhibition of the seeds germination in Col-0 (Fig. 4.8C-D). However, this led to uncover an interesting phenotype in the *myb24* mutant which is that 80% of the seeds of the *my24* mutant can germinate in the dark without the need for light treatment (Fig. 4.8C-D). Hence MYB24 is likely to be involved in sustaining seed dormancy and consequently inhibiting seed germination in the absence of light.

#### 4.2.4 Seed development in the *myb21* and *myb24* mutants

Since *MYB24* showed a putative role in seed dormancy, investigation of the seed germination rate of each of the genotypes was determined by monitoring of the seed germination and seedling initial development stages. The seed germination process was monitored at 24, 30, 54, 48 and 72 h post sowing on ½ MS media and was divided into six main stages starting from unbroken seed and ending by the emergence of the whole seedling (Fig. 4.9A).

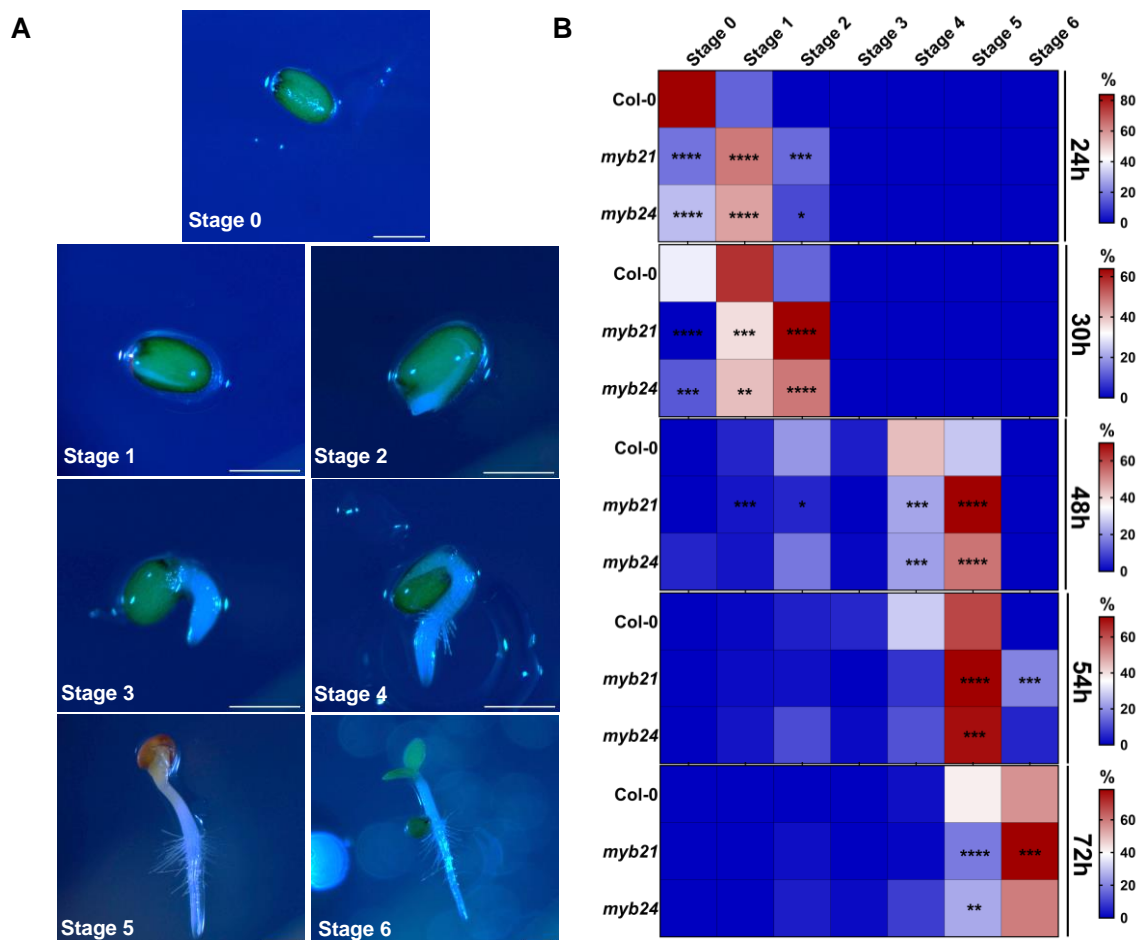


Fig. 4.9 Seeds of *myb21* and *myb24* mutants germinate faster than Col-0.



Seed germination and development were monitored at 24, 30, 48, 54 and 72 h after seeds sowing on plates with ½ MS medium.

**A:** Seed germination process up to 72 h after sowing was divided into six stages as following: 0 - unbroken seed, 1 – testa rupture, 2 – radical protrusion, 3 –primary root emergence, 4 – appearance of root hairs, 5 – whole root emergence, 6 – cotyledons emergence. Scale bars: 0.5 mm.

**B:** Quantification of the occurrence of each of the seed stages from 0 to 6 (**A**) in Col-0, *myb21* and *myb24* with the observations performed at 24, 30, 48, 54 and 72 h after sowing. The occurrence of each stage is expressed in percentage in relation to the total number of sown seeds and represented in a heatmap showing means of three replications with 36-50 seeds per biological replicate. The mutants were compared to Col-0 in terms of occurrence of every germination stage at each observation time point using One-way Anova and Tukey HSD ( $p < 0.05$ ). Statistical significance results are shown on the graphs only when significance was found with \*  $p < 0.05$ , \*\*  $p < 0.01$ , \*\*\*  $p < 0.001$ , and \*\*\*\*  $p < 0.0001$ .

The *myb21* and *myb24* mutant seeds showed earlier germination in comparison to Col-0 at 24 h after sowing. Here, a significant percentage of the seeds reached the stage1 and 2 of germination, while Col-0 started germinating at 30 h (Fig. 4.9B). At 48-54 h after sowing both mutants were at stage 5 with an emerged whole root, seeds germination rate was therefore higher in the mutants than in Col-0. These indicated a putative role of both TFs in the process of seed germination. Interestingly, despite germinating faster than Col-0, the *myb21* and *myb24* mutants reached the flowering stage later than Col-0, implying that the earlier germination in the mutants did not lead to faster development of the mutant until flowering (Fig. S29).

### 4.3 Discussion

MYB21 and MYB24 are mainly known as flower-specific transcription factors and their functions in stamen and flower development have been characterized. The detection of their up-regulated transcripts in response to wounding in vegetative tissue in the RNAseq data led us to hypothesize that they would have additional functions beside their main functions in flowers. Thus, this work aims to further characterize the wound-response of these transcription factors and identify its putative function in addition to explore potential involvement of these transcription factors in other vegetative developmental processes.

#### 4.3.1 MYB21 and MYB24 are wound-responsive in vegetative tissue.

In the transcriptional response to wounding, specifically at 1 h after wounding, the up-regulation of *MYB21* and *MYB24* was clearly detectable in seedlings and in adult leaves with high fold-inductions. The wound-induction of both transcription factors was found to be JA-dependent as it occurred in Col-0 but not in the JA-deficient mutants *opr2op3* and *aos*. The expression levels were, however, notably low, indicating limited tissue expression of *MYB21* and *MYB24* compared to flowers. This observation aligns with available expression data from databases (Expression Atlas, Genevestigator, and CoNekT), where transcripts for *MYB21* and *MYB24* are present at very low levels in seedlings and adult leaves. The near absence of their transcripts at control condition in Col-0 might indicate that they are repressed in normal condition in vegetative tissue and upon JA induction by wounding they get de-repressed in

specific tissues. *MYB21* was shown to be transcriptionally repressed in seedlings by a light-signaling component, CONSTITUTIVE PHOTOMORPHOGENIC 1 (COP1), however the signal or stimulus inducing the de-repression of *MYB21* in seedlings was not identified (Shin et al., 2002).

The wound-induction of *MYB21* and *MYB24* reached its highest levels at 1 h after wounding which coincided with the highest peak of JA accumulation after wounding (Hoo et al., 2008). Similarly, following MeJA treatment in adult leaves, the accumulation of *MYB21* and *MYB24* transcripts also peaked at 1 hour after spraying, further supporting their JA-dependent transcript accumulation.

Tissue expression analysis using beta-glucuronidase (GUS) reporter lines with the promoters of *MYB21* and *MYB24* revealed that their vegetative expressions are likely regulated by *cis*-acting elements situated more than 2 kb upstream of the start codon. The common use of portions of genes' promoters for transcriptional reporter assays in addition to the low levels of expression of both genes may explain their unnoticed expressions in vegetative tissues. Transgenic expression of *MYB21* in the *coi1-1* mutant using the 35S promoter could only partially restore its fertility (Song et al., 2011), and more importantly the expression of *MYB21* gene sequence under the control of 7 kb of its endogenous promoter in the *myb21-5* mutant led also to a partial complementation of the flower phenotype (Schubert et al., 2019). Both experiments indicate the complexity of the regulation of *MYB21*, and potential importance of regulatory elements neighboring the gene.

Generation of GUS transcriptional fusion lines with larger promoter region for *MYB24* would reveal its tissue expression in the leaf upon wounding, similar to *MYB21*. The very localized expression of *MYB21* in specific structures exclusively within the wounded area of the leaf, namely the midvein, the leaf margin, the skirt cells of the trichomes and the hydathodes, suggests a specialized function in certain cell types. This pattern aligns with its very low transcript levels in whole leaf mRNA extracts. The occurrence of *MYB21* expression in the midvein in addition to the hydathodes which contain pores that are directly connected to the vascular tissue (Paauw et al., 2023; Tena, 2023), could signify a regulation function for exudation and defense. Hydathodes have been proposed as an initial defense barrier against leaf-invading microbes (Paauw et al., 2023).

In *Arabidopsis*, trichomes are mechanosensory structures, contributing to an early layer of plant immunity by sensing mechanical stimuli, thereby anticipating pathogen infections (Matsumura et al., 2022). Trichomes were shown to activate immunity by initiating intercellular calcium waves, a process triggered by mechanical stimulation, and occurring primarily in the skirt cells. This stimulation results in an alkaline shift in the skirt and epidermal cell apoplasts (Matsumura et al., 2022; Zhou et al., 2017). Although the precise significance of this pH shift



remains to be fully characterized, it is suggested to favor the production of defense compounds or induce changes in cell wall compounds (Matsumura et al., 2022; Zhou et al., 2017). Considering that MYB21 is known as a regulator of JA production in flowers (Reeves et al., 2012) and that JA positively regulates trichome formation in *A. thaliana* (An et al., 2011), our results hint at a potential function for JA-related transcription factors, such as MYB21, in trichomes, along with a potential wound-induced JA regulation in these cells. Further investigation into the cell-specific expression of *MYB21* in the midvein and trichomes, as well as the surrounding cells, would help in identifying its putative function in the context of wounding.

#### **4.3.2 Are MYB21 and MYB24 not regulating the JA-pathway in wounded leaves, or their effect is not detected due to the experimental design?**

While almost no statistically significant differences were detected in the JA/JA-Ile accumulation in the wounded leaves of the *myb21* and *myb24* mutants compared to Col-0, there was a tendency towards a higher JA/JA-Ile production in the *myb21* mutant coinciding with a down-regulation of *JAZ13* transcripts at 1 h after wounding. Notably, *JAZ13* acts as a negative regulator of JA signaling (Thireault et al., 2015), and previous studies have shown that MYB21 interacts with other JAZ proteins, specifically *JAZ1*, *JAZ8* and *JAZ11* (Song et al., 2011). This suggests a possible regulation of JA pathway by MYB21 which may be masked due to the use of a whole leaf tissue. As the *MYB21* promoter GUS-reporter transcriptional fusion expressed only in the wounded area and exclusively in certain tissues of this area while JA-biosynthesis enzymes are known to be present at higher levels in the entire leaf (Hause et al., 2003; Stenzel et al., 2003a), it is plausible that the effects of *myb21* knockout on JA biosynthesis and signaling in these tissues cannot be observed due to differing JA dynamics in other leaf tissues. Consequently, a different experimental setup focusing on either the wounded area or the midvein may be necessary to clarify this point. Ideally, a single-cell transcriptomic approach would provide a more in-depth characterization of cell-specific differences between the *myb21* and *myb24* mutants and Col-0 within the leaf tissue.

#### The putative involvement of MYB21 in vegetative growth

The *myb21* mutant displayed developmental phenotypes related to growth, including a larger leaf area, longer primary root and a higher trichome number. These processes are known to be regulated by JA, with the first two processes being repressed by JA and the last being promoted by JA (Wasternack and Hause, 2013b). These growth phenotypes align with previous reports of MYB21 ectopic expression in adult plants resulting in dwarfism (shorter stems and smaller and narrower leaves) (Shin et al., 2002). In dark-grown seedlings, the *myb21* mutant exhibited a longer hypocotyl compared to Col-0; result that is consistent with the shorter hypocotyl phenotype of the dark-grown seedlings ectopically expressing MYB21

(Zheng et al., 2017). The shorter hypocotyl phenotype was attributed to decreased cell expansion in the hypocotyl (Zheng et al., 2017). Hence, MYB21's potential role in inhibiting cell expansion warrants further investigation, and it could be achieved through transversal sectioning of the *myb21* mutant leaf/root and determination of the shape/number of cells in the tissue layers.

To further investigate the involvement of MYB21 in growth in relation to JA, a root growth inhibition experiment was performed using MeJA. The results indicated an increased inhibition of the primary root of the *myb21* mutant compared to Col-0, suggesting a higher sensitivity to JA and implying a potential repressive role of MYB21 in the JA pathway. However, another explanation of this phenotype would be that if the longer primary root in *myb21* at control condition is due to higher cell expansion, the cells of *myb21* would be exposed to higher MeJA levels since they occupy a bigger area on the MeJA-supplied media. Thus, the higher inhibition would correspond to exposure of the cells to higher MeJA rather than higher sensitivity to MeJA. Complementation of the *coi1* mutant with MYB21 coding sequence under the control of the 35S promoter did not rescue its insensitivity to JA inhibition of root growth indicating no involvement of MYB21 in the JA-root growth inhibition process (Song et al., 2011). Nevertheless, knowing the importance of the *cis*-regulatory elements in the *MYB21* promoter for its expression in vegetative tissue from our GUS experiment and in the reported complementation assays (Schubert et al., 2019; Song et al., 2011), we cannot rule out a putative function of MYB21 in this process. Further examination of the dynamics of JA signaling would complement the root measurements data of the MeJA root inhibition experiment.

#### The putative involvement of MYB21 and MYB24 in seed germination.

The *myb21* and *myb24* mutants exhibited phenotypes related to seed germination. While both mutants germinated at faster rates compared to Col-0 at normal conditions, the seeds from *myb24* displayed the ability to germinate in the absence of light. These higher germination rates in the mutants coincide with the known JA delaying role of seed germination process (Pan et al., 2020). Interestingly, this phenotype contradicts the very low and almost non-detectable expressions of both transcription factors in seeds, as indicated by available expression databases. However, as suggested by MYB21's cell-specific expression in leaves upon wounding, it is possible that *MYB21* and *MYB24* are expressed in specific cells and/or during specific stages of seed germination. Considering that both *myb21* and *myb24* mutants could germinate faster than Col-0 while only *myb21* showed increased vegetative size, validated that its growth phenotype is not related to its faster germination rate. Since seed germination is a light-dependent process, the seed germination phenotypes of the *MYB21* and *MYB24* loss-of-function mutants can suggest potential involvement of both transcription factors in plant light responses. This hypothesis aligns with MYB21 being identified as regulated by

the light-signaling component COP1 (Shin et al., 2002), and COP1 has been shown to act as a positive regulator of seed germination (Lee et al., 2022). To further support this hypothesis, additional experiments should address *MYB21* and *MYB24* tissue expression and their relation to light-signaling components during the process of seed germination.

#### **4.4 Summary and conclusion**

The flower specific MYB21 and MYB24 play significant roles in Arabidopsis and tomato reproductive processes during flower maturation and show primary functions in flower organs. To date, there have been no reports of their expression in vegetative tissues or the characterization of any functions outside of flowers. In this work we identified a JA-dependent wound-responsiveness of *MYB21* and *MYB24* in seedlings and adult leaves of *A. thaliana*, with specific expression of *MYB21* in the wounded area of the leaf as determined by GUS reporter lines. The phenotyping of the *myb21* and *myb24* mutants suggested involvement of these transcription factors in other vegetative processes, such as plant growth and seed dormancy/germination. Importantly, these processes are known to be JA-regulated, suggesting a potential JA-mediated function of MYB21 and MYB24 in these vegetative developmental processes. Further examinations of the identified phenotypes are necessary to determine whether MYB21 and MYB24 do play any significant role in the above-mentioned processes. Such investigations could reveal new function(s) for these transcription factors in addition to their primary role in plant reproduction.

## 5 General summary

In Angiosperms, jasmonic acid (JA) is a defense hormone, and its bioactive conjugate JA-Ile accumulates in wounded plant tissues to mediate defense responses. JA-Ile biosynthesis involves sequential enzymatic reactions in the chloroplast, the peroxisome, and the cytosol. One major intermediate in JA production is *cis*-12-oxophytodienoic acid (OPDA). Produced in the chloroplast, OPDA is known to exert independent functions from JA despite its signaling mechanism being missing. The characterization of OPDA's functions relied on the use of a mutant, in which the function of OPDA-REDUCTASE3 (OPR3) is abolished. JA-Ile and OPDA productions were thought to be uncoupled in the *opr3* mutant until recently this mutant was shown to be "leaky". An OPR3-bypass to JA-Ile biosynthesis through the cytosolic OPR2 was identified, questioning the previously characterized OPDA functions.

In this study, we addressed OPDA putative signaling in *Arabidopsis thaliana* by characterizing its ability to mediate gene expression using the JA-deficient *opr2opr3* double mutant in comparison to the wild-type Col-0 and the OPDA-deficient mutant affected in the ALLENE OXIDE SYNTHASE (AOS), named *aos*. One limitation when using the *opr2opr3* double mutant was the reduced OPDA levels compared to Col-0. We established that this decrease resulted from the interruption of the JA positive feedback loop occurring during development. By mimicking this feedback loop through MeJA-pretreatment of the plants during development, the capacity of the *opr2opr3* mutant to accumulate the biosynthesis enzymes and to produce higher background and wound-induced OPDA levels was restituted.

A transcriptional comparative analysis during wounding enabled the dissection of the wounding response in terms of JA, OPDA and other signals-mediated transcriptional responses. The previously reported JA signaling showed a clear signature in the modulation of the transcriptome by inducing a specific set of JA-responsive genes. For OPDA, however, the reported OPDA-responsive genes did not show an OPDA-dependent transcriptional induction since it occurred also in the absence of OPDA in the *aos* background. Additionally, the analysis of the whole transcriptome showed a very high similarity between the *opr2opr3* and the *aos* mutants and very little number of genes being differentially expressed suggesting the absence of an OPDA signaling in Arabidopsis. Further determination of the differences between our experimental approach and the previously used approaches to characterize OPDA signaling, indicated that the exogenous application of OPDA leads to significant JA-Ile formation through the cytosolic OPR3-bypass pathway. Thus, we show that such experimental design leads to JA-Ile signaling that could be inadvertently attributed to OPDA signaling or function.

The divergence between the endogenous and exogenous rise of OPDA suggested its compartmentalization when endogenously produced. To address the subcellular distribution of OPDA, a complementation approach of the *opr2opr3* double mutant with different organelle

targeted OPR3 was performed. The complementation lines showed reconstitution of JA biosynthesis through restitution of fertility in the flower buds at stage 12 and silique formation. Furthermore, JA-Ile production and signaling upon wounding were also rescued in leaves. The ability of JA production to resume from other cell compartments than peroxisomes, namely the nucleus, cytosol, ER, chloroplast and mitochondria, suggested either a translocation of OPDA to these compartments or rather an entry of OPDA to  $\beta$ -oxidation followed by the translocation of 4,5-ddh-JA to these compartments. Future work to uncover which of JA intermediates is translocating to different compartments, would rely on the OPR2 and OPR1 enzymes specificities to these two substrates using the same complementation approach.

To test whether JA biosynthesis reconstitution from other organelles than peroxisomes is due to undetectable cytosolic occurrence of OPR3, a BiFC approach was tested in *N. benthamiana*. The results hinted towards such occurrence however were not conclusive due to possible stickiness of YFP halves. Since cytosolic OPR3 enabled the reconstitution of JA biosynthesis, the question why OPR2 despite producing JA from 4,5-ddh-JA in the cytosol is not sufficient to reconstitute JA responses, arose. Expression of OPR2 under the *CaMV 35S* and OPR3 promoters in the *opr2opr3* double background resulted in the reconstitution of JA biosynthesis and flower fertility, indicating that OPR2 can replace OPR3 function when expressed in the right tissues and to high levels.

The use of the generated transcriptomic data to screen for a plastid inner-membrane transporter for OPDA, showed only preliminary non-conclusive results. Identification of a DTX transporter family widely responsive to wounding and a plastid-ER colocalizing START-domain containing protein did not lead to characterizing their functions due to unsuccessful screen for proper mutants. Nevertheless, the plastid inner envelope located PEC1 channel showed putative function in relation to OPDA accumulation as the mutant accumulated significantly lower OPDA levels upon wounding and priming of seedlings. As a potassium/calcium channel, the investigation of its function in relation to OPDA accumulation is yet to be uncovered.

The dissection of the wounding transcriptomic data led to uncover a wound-responsiveness in seedlings and adult leaves of the flower-specific transcription factors (TF) MYB21 and MYB24. Their wound-induction was JA dependent and MYB21 showed a specific expression in the wounded area, mainly in leaf veins and the skirt-cells of the trichomes. Dissection of possible regulation of JA biosynthesis/signaling in this area showed no difference in JA accumulation and JA-responsive JAZs transcripts. Phenotyping of the mutants however, suggested involvement of the TFs in other vegetative processes including seed germination and leaf/root growth, both processes being known to be JA-regulated.

## 6 Material and methods

### 6.1 Plant material and growth conditions

#### 6.1.1 Seedling material

All *Arabidopsis thaliana* lines were in the ecotype Columbia-0 (Col-0) background, except for *opr3*, which was in the ecotype Wassilewskija (Ws). The different genotypes used in this study and the origin of the seed stocks are listed in the Appendix (Table S5). Arabidopsis seeds were sterilized in a 4% bleach solution containing Tween 20, washed with sterile water, and then stratified at 4°C for three days. Wounding experiments with 10-day-old seedlings from the Col-0, *opr2/3* and *aos* genotypes, were performed with seedlings that were grown in liquid half-strength Murashige and Skoog (MS) medium with a pH of 5.7 and 1 % sucrose (Fig. 6.1). Twelve to twenty seeds were sown into 2 ml of medium per well in a 24-well tissue culture plates (TPP, 92424). Phenotyping and seed germination experiments of Col-0, *myb21* and *myb24* were performed using solid half-strength MS medium supplemented with 1 % sucrose, and 0.8% plant agar (Duschefa).

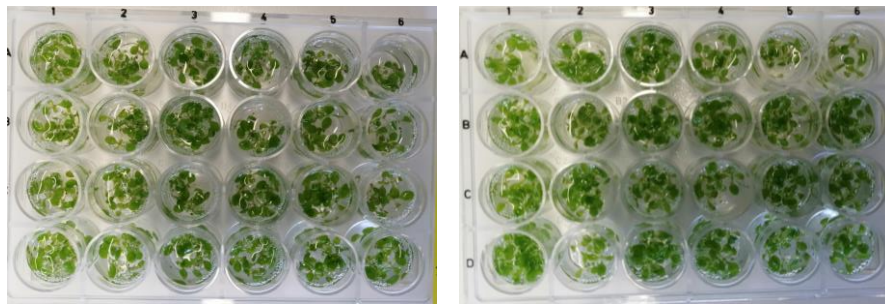


**Fig. 6.1 Ten-day-old seedlings grown in liquid media**

Sterilized seeds are sown directly into 2 ml MS medium with 12 to 20 seedlings per well. Seeds sowing and growth are carried out in sterile conditions.

#### 6.1.2 Adult plant material

Experiments performed on adult rosettes were conducted using 4-week-old plants grown on individual pots containing steam-sterilized clay mixed with coir fiber and vermiculite. *N. benthamiana* plants which were used for the subcellular localization and BiFC assays were also grown under long day conditions in a fully acclimatized greenhouse.

#### 6.1.3 Growth conditions

Both *Arabidopsis* seedlings and adult plants were grown under a controlled diurnal growth cycle combining 10 hours of daylight at 21°C with a light intensity of 120  $\mu\text{E m}^{-2} \text{s}^{-1}$ , with 14 hours of darkness at 19°C. For assays involving flowering plants, plant transformation and seed propagation, a long-day growth cycle was employed, comprising 16 hours of daylight at 22°C and 8 hours of darkness at 21°C. Seedlings and adult plants were maintained in controlled humidity of 65 % and were periodically rotated within the phytocabinets for



randomizations purposes. Seedlings were grown with a day interval between biological replicates while adult plants were grown with a week interval between biological replicates.

#### **6.1.4 Plant propagation**

Propagation of the JA-deficient mutants (*opr3*, *opr2/3* and *aos*) was carried out by applying MeJA to flower buds, while propagation of the sterile *myb21* mutant was performed through hand-pollination by tapping the anther on the stigma of the same flower buds.

### **6.2 Plant treatments**

#### **6.2.1 Wounding**

All wounding experiments were performed in the morning from 9 to 11 am to avoid variations associated to the circadian rhythm (Grundy et al., 2015). Seedlings grown in liquid media were wounded by crushing the grouped seedlings eight times using forceps with serrated teeth. For whole adult rosettes or the eighth leaf of the rosette, a single bruise was inflicted in the middle of each leaf using a double hemostat with serrated teeth. The counting of leaf number eight was performed as described by Farmer et al. (2013).

#### **6.2.2 Phytohormone application**

Phytohormone applications were always performed in the morning. To equalize the AOC proteins contents in Arabidopsis seedlings, MeJA pretreatment was carried out on day four and day six of development for 10-day-old seedlings, and on the second, third and fourth week of development for adult plants with a 3 days/week frequency. 1  $\mu$ M MeJA was added to the liquid MS medium for the treated samples while water alone was added to the untreated ones. For adult plants 1  $\mu$ M MeJA mixed with 0.025% Silwet L-77 was sprayed twice on the rosette of the treated plants using 50 ml brown glass bottles to ensure full coverage. Untreated rosettes were sprayed with water mixed with 0.025% Silwet L-77.

OPDA application to seedlings of the *opr2/3* mutants grown on liquid media was performed by directly adding OPDA ( $\geq 95\%$ , Cayman chemicals) to the liquid MS media at a concentration of 25  $\mu$ M for the treated samples, while untreated samples received water.

For root growth inhibition assays, the MS medium was supplemented with MeJA at a concentration of 50  $\mu$ M before solidification. For propagation of the JA-deficient mutants *opr3*, *opr2/3* and *aos*, application of a mixture of 450  $\mu$ M MeJA and 0.05% (v/v) Tween to the flower buds was carried out every two days after the first flowers failed to produce siliques according to Ishiguro et al. (2001).

#### **6.2.3 Seedlings etiolation in the dark**

Sterilized seeds of Col-0, *myb21* and *myb24* were sown in square petri dishes and exposed to light for three hours as described by An et al. (2012) before being covered with a layer of black

paper and in addition to a second aluminum foil layer to prevent light penetration. Plates were grown vertically in a short-day program phytocabinet with the lights turned off.

### 6.3 Molecular biology methods

#### 6.3.1 Genomic DNA isolation

For EMS mutant lines requiring genotyping by DNA sequencing, genomic DNA isolation was carried out using the NucleoSpin Plant II Mini kit (Macherey-Nagel) following the manufacturer's protocol, starting with 20-50 mg of frozen tissue. Alternatively, genomic DNA was extracted using a one-step protocol as described by Kasajima et al. (2004).

#### 6.3.2 Genotyping

The genotyping of the T-DNA insertion lines *opr2opr3*, *str1*, *pec1.3*, *dtx37* and *myb24* was carried out according to the procedure described by Malley et al. (2015). The genotyping primers were generated as recommended on the SALK primer design tool (<http://signal.salk.edu/tdnaprimers.2.html>). A two-step PCR assay was conducted to amplify the WT amplicon and a portion of the T-DNA insertion separately and was performed by directly adding small, excised leaf pieces to the Phire™ Plant Direct PCR Master Mix (Thermo Scientific™) following the manufacturer's protocol. For the SALK lines and GABI-Kat lines the left border primers LBb1.3 and o8474 were used in combination with their corresponding right primers, respectively. In the case of the *myb21-5* and *aos* EMS mutants, gene sequence amplification from extracted genomic DNA was performed using ALLin™ Red Taq Mastermix (HighQu) according to the manufacturer's instructions and was followed by the sequencing of the PCR amplicon. The mutant lines and their corresponding genotyping primers are listed in the Appendix (Table S5).

The genotyping of the generated transgenic lines was based on the Red Fluorescent Protein (RFP) seed coat plant selective marker (Shimada *et al.*, 2010). Seed selection was carried out by visualizing fluorescent seeds under a Zeiss Axioplan Fluorescence microscope. Segregation analysis was performed by counting the ratio of fluorescent seeds to non-fluorescent ones using ImageJ software. A minimum of 100 seeds were analyzed in each seed pool and a ratio of 3:1 (fluorescent:non-fluorescent) indicated a single-insertion line.

#### 6.3.3 RNA isolation and cDNA synthesis

Total RNA was extracted from 50 to 60 mg of previously homogenized frozen material using the RNeasy Plant Mini Kit (Qiagen) in accordance with the manufacturer's protocol, including two-time elution with 40 ml of water. Genomic DNA removal from 10 µg of total RNA in 50 µl total reactions was carried out using the DNA-free™ DNA Removal Kit (Invitrogen, AM1906) and following the rigorous rDNAse I treatment protocol provided by the manufacturer. RNA quality and integrity were assessed using the NanoDrop 1000 Spectrophotometer (Peqlab)

and by separating the ribosomal RNA (rRNA) bands on a 1.5% Agarose gel at 80 V, respectively.

For mRNA sequencing, total RNA was isolated as mentioned above, and RNA quality and integrity were determined using the RNA 6000 Nano Kit for standard RNA sensitivity (Agilent). Two microliters of 200 ng/μl total RNA were loaded onto the Chip priming station and run on the Agilent 2100 Bioanalyzer (Agilent) according to the manufacturer's instructions. RNA samples with an RNA Integrity Number (RIN) between 7 and 9 were considered of good quality and were sent on dry ice for sequencing to Novogene ([www.novogene.com](http://www.novogene.com)). Following the quality check, 1 μg of DNA-free RNA was used to synthesize cDNA using the RevertAid H Minus First Strand cDNA Synthesis Kit (Thermo Scientific™) according to the manufacturer's instructions with oligo d(T) primers.

#### 6.3.4 Gene expression analysis

For qPCR analysis, 3 μl of diluted cDNA was loaded into Hard-Shell® 96-Well PCR Plates (Biorad) and supplemented with 7 μl qPCR reactions prepared as follows:

2 μl 5x QPCR Mix EvaGreen® (No Rox)  
 1 μl forward primer (2 μM)  
 1 μl reverse primer (2 μM)  
 up to 10 μl water

The amplification was carried out on the CFX Connect Real-Time PCR Detection System (Bio-Rad) using the following protocol:

|           |      |        |
|-----------|------|--------|
| 1 cycle   | 95°C | 15 min |
| 40 cycles | 95°C | 15 s   |
|           | 60°C | 30 s   |

Post-PCR DNA melt curve analysis was generated by detection of the dye signal between 65°C and 95°C with a 0.5°C increment per 0.5 s.

All qPCR primers were designed using the Primer3Plus software with a 20 bp length, a melting temperature of 60°C, and a PCR amplicon size between 75-120 bp. Examination of hairpin and dimers formation was conducted using the Beacon Designer software. Primers' specificity within Arabidopsis genome was verified using the BLAST function on the NCBI platform.

Relative gene expression was determined using the  $2^{-\Delta C_T}$  method (Schmittgen and Livak, 2008) in relation to the reference gene AT1G13320 corresponding to the *PP2A* subunit (Czechowski et al., 2005; Wang et al., 2014), where  $\Delta C_T = C_T \text{ target gene} - C_T \text{ reference gene}$ .

#### 6.3.5 mRNA sequencing and transcriptome analysis

Next generation sequencing and bioinformatic data analysis were provided by Novogene and was carried out on three biological replicates of the Arabidopsis seedlings and adult rosettes

from the wounding experiments. mRNA short-read sequencing was conducted on an Illumina NovaSeq 6000 Sequencing System according to Novogene's sequencing pipeline. The pipeline involved library preparation, paired-end sequencing of 150 bp length, and raw data generation and quality check. The bioinformatic analysis was also carried out by Novogene according to their standard analysis pipeline and included the mapping of the short reads to the *A. thaliana* TAIR10 reference genome. Estimation of gene expression levels was performed by normalization of the read counts using the FPKM (Fragments per kilobase per million) method. The differential expression analysis was carried out according to Novogene's standard procedures from normalized read counts and pairwise comparisons were performed by model dependent p-value estimation and FDR value estimation based on multiple hypothesis testing. Enrichment analysis was performed for differentially expressed genes using Gene Ontology (GO) and KEGG databases.

Supplementary bioinformatic analysis was performed on the iDEP .96 and iDEP 1.1 software (Ge et al., 2018) using the read counts and FPKM values generated by Novogene. The analysis comprised generation of gene expression and gene differential expression data in addition to the generation of principle component analysis (PCA), expression heatmaps, gene clustering and enrichment analysis for differentially expressed genes using Gene Ontology (GO) and KEGG databases.

Technical validation of some selected genes from the RNAseq data was carried out by qPCR using cDNA synthesized from the same RNA samples which were sent for sequencing. cDNA synthesis and gene expression analysis were performed as described in sections 6.3.3 and 6.3.4, respectively.

### **6.3.6 Polymerase chain reaction (PCR)**

For DNA fragments destined for cloning, high-fidelity PCR with a proof-reading polymerase was performed. 50 ng and 5 ng of cDNA and plasmid DNA templates, respectively, were added to 25 µl PCR reactions of the Q5® High-Fidelity DNA Polymerase (Bio Labs, M0491) with the reaction setup assembled as indicated by the manufacturer. The PCRs were carried out on a Thermal cycler C1000 Touch (Bio-Rad) with 35 cycles and thermocycling conditions as instructed by the manufacturer. The PCR products were cleaned using PCR cleanup Kit (Macherey-Nagel) following the manufacturer's protocol.

Routine PCRs, such as genotyping PCRs and colony PCRs, were carried out using ALLin™ Red Taq Mastermix (HighQu). The 20 µl reaction setup was prepared following the manufacturer's instructions and guidelines and ran on the Thermal cycler C1000 Touch (Bio-Rad).

### 6.3.7 Golden Gate cloning

The complementation constructs, the transporters subcellular localization constructs and the split-YFP constructs were all performed using the Golden Gate system (Engler et al., 2014). This cloning system relies on the type IIS restriction endonucleases *BsaI* and *BpiI* and their ability to cut outside of their recognition sites. Hence, target DNA sequences containing *BsaI* and *BpiI* recognition sites were modified by removal of these sites by silent mutations. Amplification of target DNA sequences was carried out using high fidelity polymerase and was followed by assembly of the complete target DNA sequence in level 0 vectors. Generation of transcription cassettes was carried out by assembling promoter, coding sequence, fluorescent tag, and terminator modules in level 1 Golden Gate vectors. The Octopine synthase terminator (*tOcs*) was used for transcript termination. Level 1 constructs were used for transient assays in *N. benthamiana* leaves to evaluate the expression and subcellular localization of the generated fusion protein. The Oleosin 1 (OLE1) seed selection marker was used as a plant selective marker. The inclusion of the selective marker *OLE1p::OLE1:RFP* (pAGH1009) to the expression cassettes was carried out in level 2 Golden Gate vectors, which were subsequently used for *A. thaliana* plant transformation (Fig. 6.2).

All the constructs in this study were generated by assembling target sequences amplified from *A. thaliana* cDNA or genomic DNA into Golden Gate vectors which were kindly provided by Dr. Sylvestre Marillonnet (Engler et al., 2014). The cloning procedure including the digestion ligation reaction setup, *E. coli* transformation and clones examination were performed as described by Marillonnet and Grützner (2020).

#### 6.3.7.1 Cloning of *OPR3* for subcellular targeting

The coding sequence of *OPR3* (1176 bp) contained one *BsaI* and one *BpiI* restriction site, which were modified by silent mutations C205G and G1109C, respectively. To allow the targeting of *OPR3* to other cell compartments the SRL peroxisomal signal was removed from the coding sequence in addition to the stop codon (TGA). Depending on the targeting process of each organelle, the position of the targeting sequence was either at N or C-terminus of *OPR3* sequence or both. Additional removal of the ATG start codon from *OPR3* sequence was performed when the targeting signal was positioned at the N-terminus. The sequences of the targeting signals added, and their respective positions are listed in table 6.1. For each cell compartment, two fusion proteins were designed with the YFP coding sequence either at the N-terminus or the C-terminus of *OPR3* sequence. A two-amino acid (Gly-Ser) linker sequence was incorporated into the recombinant fusion protein to link *OPR3* sequence with YFP and with certain targeting sequences (Fig. 6.2).

The monomeric *OPR3* variant *OPR3*<sup>E292K</sup> was generated by gene synthesis using the GeneArt tool by Thermo Scientific. The variant mutation was designed as described by Sperling *et al.*

(2012), by introducing a single base change G874A. A 4X Myc-tag (EQKLISEEDL) was added at the carboxy-end of OPR3 sequence and was followed by the HDEL ER-retention signal. The OPR3<sup>E292K</sup> was designed for targeting the ER, hence was assembled with the signal peptide under the control of *CaMV 35S* promoter and the *tOcs* terminator sequences in the level 1 plasmid pAGH1330.

Following the detection of the fusion protein in transient *N. benthamiana* assay, the generated expression cassettes (see constructs' list in Appendix, Table S8) were assembled with the plant selective marker *OLE1p::OLE1:RFP* in a Golden Gate level 2 plasmid. Control lines were generated by transforming Col-0 and *opr2/3* with an empty level 1 vector also assembled with *OLE1p::OLE1:RFP* cassette in level 2 Golden Gate.

**Table 6.1 Targeting sequences used for OPR3 and their corresponding cell compartments.**

| Targeting signal                   | Targeting sequence   | Cell compartment | Position   | Reference sequence             |
|------------------------------------|----------------------|------------------|------------|--------------------------------|
| Signal peptide (SIP)               | First 24 amino acids | ER               | N-terminus | <i>AtCAPE3</i><br>(AT4G33720)  |
| Retention signal                   | HDEL                 | ER               | C-terminus | NA                             |
| Nuclear localization signal (NLS)  | PKKKRKV              | Nucleus          | N-terminus | simian virus 40<br>(SV40)      |
| Nuclear export signal (NES)        | LQLPPLERLTLD         | Cytosol          | C-terminus | HIV-1 rev protein              |
| Chloroplast transit peptide (cTP)  | First 51 amino acids | Plastid stroma   | N-terminus | <i>AtRECA1</i><br>(AT1G79050)  |
| Mitochondria transit peptide (mTP) | First 31 amino acids | Mitochondria     | N-terminus | <i>AtHSP60</i><br>(AT3G23990), |

### 6.3.7.2 Cloning of OPR3 promoter sequence

2299 bp upstream of the start codon in the *OPR3* promoter region were selected for cloning. Since the promoter sequence contained three *Bpil* sites, potential transcription factor binding sites were determined using the PlantPAN database (see Appendix Fig. S30). Introduced single nucleotide mutations of the *Bpil* restriction sites did not disrupt TF binding sites. The promoter sequence was amplified using high fidelity PCR and inserted into the pUC19-derived vector pICH41295. To evaluate the activity of the cloned promoter region, a transcriptional fusion construct was designed (*OPR3p::YFP*) and transiently expressed in *N. benthamiana* leaves. The responsiveness of the promoter to MeJA was tested by spraying infiltrated leaves with MeJA and was examined in terms of YFP signal and protein accumulation, using confocal fluorescent microscopy (Zeiss LSM880) and immunoblotting, respectively



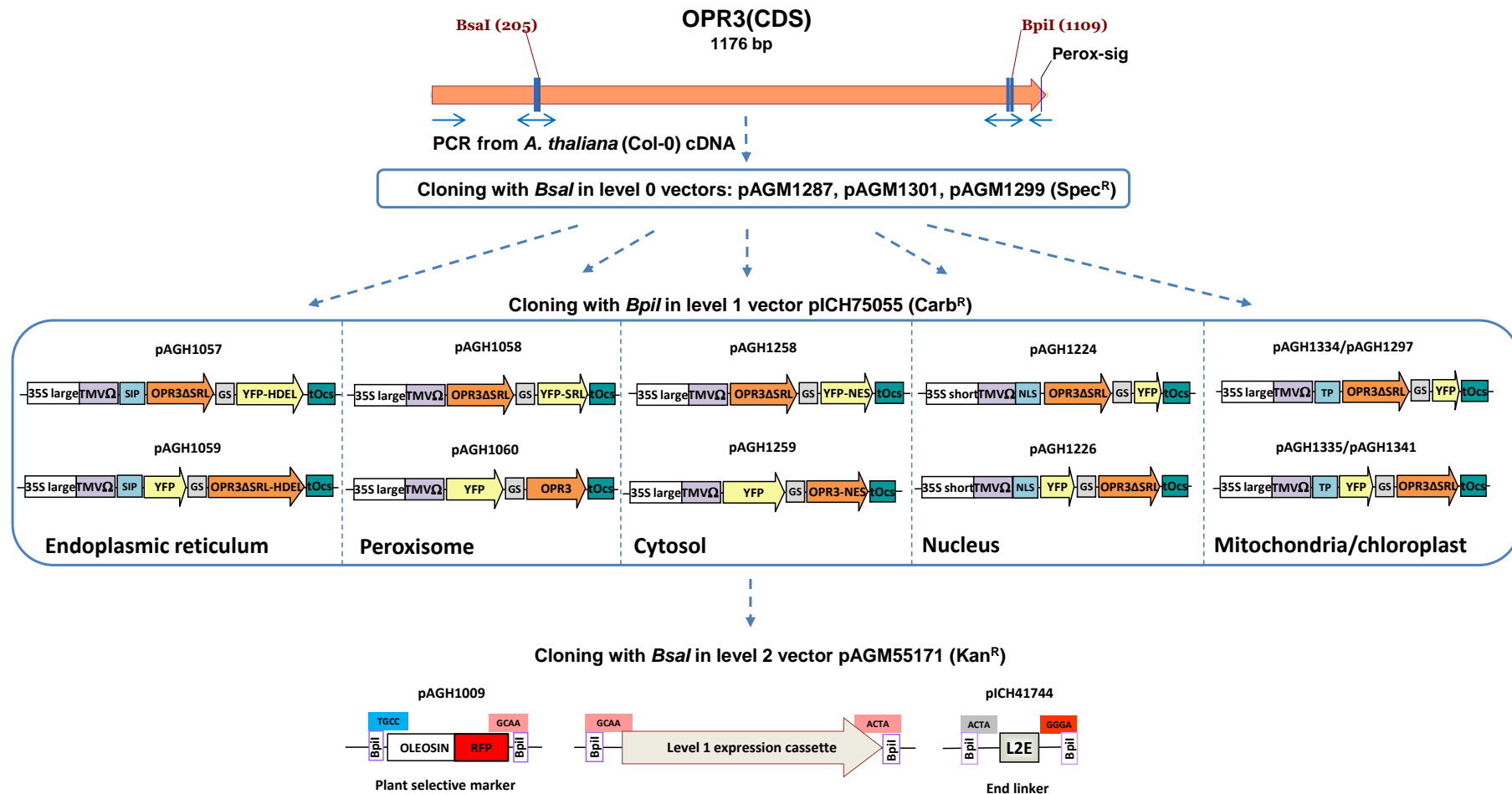


**Fig. 6.2 Golden Gate cloning strategy for the targeting of OPR3 fused to YFP to different cell compartments.**

Horizontal blue arrows represent the positions of the PCR primers used for cloning OPR3 coding sequence and the removal of the *BsaI* and *BpiI* restriction sites. Depending on the position of OPR3 in relation to YFP and the targeting sequences the PCR product was inserted in the Golden Gate level 0 vectors pAGM1287, pAGM1299 and pAGM1301 with Spectinomycin resistance. The generation of for the other modules (YFP, promoter, terminator and targeting sequences) was similarly performed in level 0. The assembly of the different modules to form the expression cassette was carried out in level 1 Golden Gate vector pICH75055 with Carbenicillin resistance. The assembly of expression cassette with the plant selective marker Oleosin-RFP was carried out in level 2 Golden Gate vector pAGM55171 with Kanamycin resistance: SIP, signal peptide; NES, nuclear exclusion signal; NLS, nuclear localization signal; TP, transit peptide; GS, Gly-Ser

### 6.3.7.3 Cloning of *OPR2*

*OPR2* coding sequence (1125 bp) did not contain any *Bsal* or *Bpil* restriction sites and was cloned into Golden Gate level 0 vector pAG1287. *OPR2*-YFP fusion protein was assembled in the Golden Gate level 1 vector pICH75055 by adding YFP sequence at the C-terminus of *OPR3* with a two-amino acid linker Gly-Ser. Two different constructs, pAGH1482 and pAGH1489, were designed using *OPR3*(2299 bp) and *CaMV 35S* promoters, respectively (Appendix, Table S8). The inclusion of the plant selective marker *OLE1p::OLE1-RFP* (pAGH1009) to the expression cassettes was carried out in level 2 Golden Gate vectors, which were subsequently used for *A. thaliana* plant transformation.

### 6.3.7.4 Cloning of transporter candidates

For subcellular localization of the selected transporters candidate, the coding sequences were amplified from Col-0 cDNA with high fidelity enzyme. Removal of *Bsal* and *Bpil* was performed by designing additional pair of primers introducing silent mutations. The coding sequences with omitted stop codons were fused to GFP at the C-terminal region in the Golden Gate level 1 vector pICH75055 (Carb<sup>R</sup>) and were assembled with the *CaMV 35S* promoter and *tOcs* terminator encoded on the pICH51266 and pICH41432 plasmids, respectively. The pAGT5745 plasmid containing the *GFP* coding sequence preceded by a short linker sequence was provided by Dr. Tom Schreiber.

### 6.3.8 Colony screening, plasmid purification and verification

Initial screening for positive *E. coli* colonies was carried out by colony PCR using the ALLin™ Red Taq Mastermix, 2X (HighQu). A single white *E. coli* colony was picked up with a pipette tip and transferred to the PCR mix containing 10 µl of the master mix supplemented with 8 µl of Nuclease-free water, 0.5 µM of forward and reverse primers (see PCR primers list in Appendix, Table S6). The PCR reactions were run on a thermocycler following the manufacturer's instructions. Positive colonies were selected for overnight culture in LB liquid medium. Pelleted *E. coli* cultures were used for isolation of plasmid DNA with the Mini preparation kit NucleoSpin® Plasmid EasyPure (Macherey-Nagel). DNA purification was performed as described in the protocol provided by the manufacturer, except for the elution which was performed twice with 40 µl of Nuclease-free water instead of Buffer AE.

To ensure the presence of the insert, restriction digest of the recombinant plasmids was performed using the FastDigest restriction enzymes (Thermo Fisher Scientific, Waltham, MA, USA). 0.8 to 1 µg of plasmid DNA was digested with the proper restriction enzyme in a thermocycler at 37°C for 40 min then immediately loaded onto an agarose gel. The preparation of the digestion reaction was carried out following the manufacturer's instructions.

The final verification step for the generated plasmids was carried out by DNA sequencing. Purified plasmids were sent to Eurofins genomics or Genewiz (Azenta Life Sciences) following the sample preparation protocol for the corresponding companies. Depending on the Golden Gate level, the appropriate forward and reverse primers were added to the sample. For instance, level 0 plasmids were sequenced using the MoClo primers as described by Marillonnet and Grütznér (2020). The resulting sequenced inserts were examined in terms of sequencing quality and aligned with the expected inserts on Geneious software.

### 6.3.9 Plant transformation

Plant transformation was performed by floral dip with the *Agrobacterium tumefaciens* strain GV3101 according to the protocol described by Zhang et al., (2006). The floral dip of JA-deficient mutants *aos*, *opr3* and *opr2/3* was followed by MeJA application to the flower buds starting from 48 h after dipping. Transformed seeds expressing *RFP* in T1, T2 and T3 generations were selected by fluorescence microscopy. A minimum of two independent single insertion lines from T3 generation for each construct were used for subsequent experiments. In addition to the RFP plant selective marker, all the generated transgenic lines were examined in terms of occurrence of the YFP tag in the vegetative tissue.

### 6.3.10 Subcellular localization in *N. benthamiana* leaves

The subcellular localization of organelle targeted OPR3 and OPR2 in addition to the transporter candidates STR1, DTX37, DTX36, DTX28 and DTX9 was carried out with transient assays in *N. benthamiana* leaves (Table 6.2). *A. tumefaciens* strain GV3101 carrying the fusion constructs was cultured in LB medium supplemented with the corresponding antibiotics for 48 hours. The pelleted bacteria were then resuspended in MMA infiltration media and infiltrated into *N. benthamiana* leaves, following the protocol described by Norkunas et al. (2018). Three days after infiltration, imaging of infiltrated leaves was carried out by mounting slides containing 1 cm diameter leaf disks with a drop of distilled water on the confocal fluorescent microscopes LSM880 and LSM900 (Carl Zeiss). Additionally, leaf pieces from the same infiltrated leaves were frozen in liquid nitrogen for subsequent immunoblot analysis.

**Table 6.2 List of the constructs used for subcellular localization in *N. benthamiana* leaves.**

| Subcellular targeting of OPR3              |                                    |
|--|------------------------------------|
| 35S::SP-OPR3 $\Delta$ SRL-YFP-HDEL         | 35S::SP-YFP-OPR3 $\Delta$ SRL-HDEL |
| 35S::OPR3 $\Delta$ SRL-YFP-SRL             | 35S::YFP-OPR3                      |
| 35S::cTP-OPR3 $\Delta$ SRL-YFP             | 35S::cTP-YFP-OPR3 $\Delta$ SRL     |
| 35S::NLS-OPR3 $\Delta$ SRL-YFP             | 35S::NLS-YFP-OPR3 $\Delta$ SRL     |
| 35S::OPR3 $\Delta$ SRL-YFP-NES             | 35S::YFP-OPR3 $\Delta$ SRL-NES     |
| 35S::mTP-OPR3 $\Delta$ SRL-YFP             | 35S::mTP-YFP-OPR3 $\Delta$ SRL     |
| 35S::SIP-OPR3E292K $\Delta$ SRL-4XMyC-HDEL |                                    |
| Subcellular targeting of OPR2              |                                    |
| 35S::OPR2-YFP                              | OPR3p::OPR2-YFP                    |

| Subcellular localization of putative transporters |                |
|---|----------------|
| 35S::STR1-GFP                                     | 35S::DTX28-GFP |
| 35S::DTX37-GFP                                    | 35S::DTX9-GFP  |
| 35S::DTX36-GFP                                    |                |

### 6.3.11 Co-localization in *N. benthamiana* protoplasts

To validate the subcellular targeting of OPR3 to the different cell compartments, the targeting constructs that were designed as described in section 6.3.7.2, were used for a co-localization study out in *N. benthamiana* protoplasts. The protoplasts were co-transfected with the level 1 plasmids of OPR3 targeting (listed in the Appendix, Table S9) and organelle markers provided by Hagen Stellmach (Stellmach et al., 2022) which are listed in table 6.3. The co-localization in protoplasts was carried out by Fiona Smith (Bachelor thesis) under the technical assistance of Hagen Stellmach.

Protoplasts isolation and co-transformation were performed according to the protocol from Janik et al. (2019) using third and fourth leaves of 4-week-old *N. benthamiana* plants as instructed. Following isolation, 200 µl of the protoplast suspension were mixed with 10 µg of DNA for protoplast transformation with PEG and left overnight incubated at room temperature as described by Janik et al. (2019). The next day, protoplasts were imaged using the LSM880 confocal laser scanning microscope (Carl Zeiss).

**Table 6.3 List of the organelle markers used for co-localization studies of OPR3 targeting.**

| Cell compartment | Plasmid name | Construct                      |
|------------------|--------------|--------------------------------|
| ER               | pAGH1020     | <i>NOSp::WAK2-mCherry-KDEL</i> |
| Peroxisome       | pAGH836      | <i>NOSp::mCherry-SKL</i>       |
| Nucleus          | pAGH840      | <i>NOSp::HTA6-mCherry</i>      |
| Cytosol          | pAGH1345     | <i>NOSp::mScarlett</i>         |
| Stroma           | pAGH567      | <i>NOSp::RubisCO-mCherry</i>   |
| Mitochondria     | pAGH838      | <i>NOSp::mtRi-mCherry</i>      |

### 6.3.12 Bimolecular fluorescence complementation (BiFC) in *N. benthamiana* leaves

A BiFC system was designed in Golden Gate vectors using the previously established targeting system of OPR3 to different cell compartments to test whether OPR3 with different subcellular localizations could interact and dimerize. OPR3 fusions with nYFP (465 bp) and cYFP (255 bp) halves targeted to two different organelles were assembled in the Golden Gate level M with a nuclear localized m-Cherry expression cassette added as a transformation control. The Golden Gate design for the BiFC was performed with the help of Dr. Tom Schreiber and the cloning and expression in *N. benthamiana* were carried out by Fiona Smith in the frame of her Bachelor thesis. For consistency reasons, two nYFP and cYFP combinations were tested for each cell compartment in addition to two negative controls, one for each half of YFP. Positive controls were also designed for each organelle so the two YFP halves are targeted to the same

compartment (see Fig. 6.3). Three expression cassettes were assembled in the Golden Gate level M vector pAGM8043 (Spec<sup>R</sup>) using *BpiI* restriction enzyme, comprising OPR3-nYFP in cell compartment 1, with OPR3-nYFP in cell compartment 2 and nuclear-targeted mCherry. For the ER, peroxisome, and mitochondria, the Split-YFP was tested with the cytosol as a second compartment in order to determine whether organelle-targeted OPR3 can meet a cytosolic targeted OPR3 as explained with the example in Fig. 6.3.

To validate that the reconstitution of the YFP signal relies on the dimerization of OPR3 rather than only the stickiness of the two YFP halves, an additional negative control was designed using the monomeric variant OPR3<sup>E292K</sup>. The OPR3<sup>E292K</sup>-nYFP and OPR3<sup>E292K</sup>-cYFP were both targeted to the peroxisomes.

The level M constructs with the different BiFC combinations were used for transient expression in *N. benthamiana* leaves and were visualized three days after infiltration with confocal laser microscopy. The infiltrated leaves were also used in downstream immunoblot analysis to validate the expression of the BiFC fusion proteins.

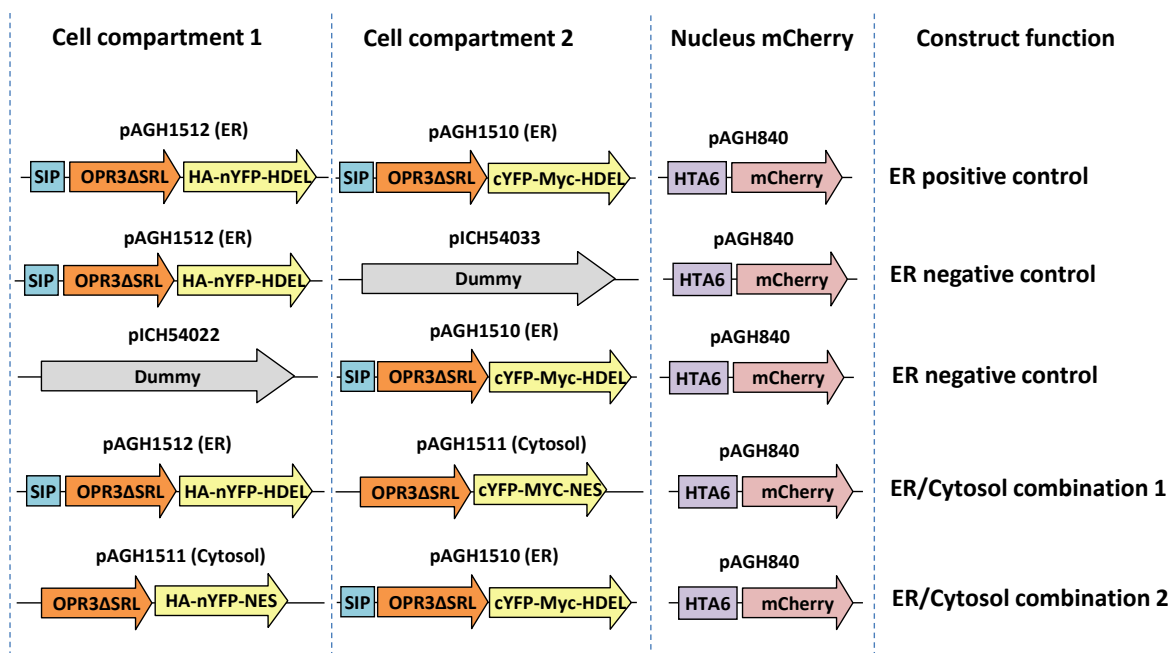


**Fig. 6.3 The BiFC constructs design for organelle targeting of OPR3 with YFP halves.**

The Golden Gate multigene constructs used to express simultaneously ER-targeted OPR3-half YFP with cytosolic-targeted OPR3-half YFP and the transformation control nuclear-mCherry with their corresponding positive and negative controls. The same design was carried out for all the tested compartments (peroxisome, cytosol, and mitochondria). The dummy is an empty transcriptional unit to fill the corresponding position. SIP, signal peptide.

## 6.4 Biochemical methods

### 6.4.1 Protein extraction

For subsequent protein detection without prior quantification, 200  $\mu$ l of extraction buffer (4% SDS, 20 mM Tris base), supplemented with 2x Halt<sup>TM</sup> Protease and Phosphatase Inhibitor

Cocktail (Thermo Scientific™), were added to 50 mg of powdered frozen material. After 20 min incubation at room temperature, samples were centrifuged at 12,000xg for 5 min and 10 µl of the resulting supernatant were used for subsequent protein detection assays.

For subsequent protein detection with prior quantification, 250 µl of extraction buffer (Raorane et al., 2016) were added to 50 mg of powdered frozen material. The samples were heated at 95°C for 10 min, then transferred to ice and supplemented with 2 µl 100x Halt™ Protease and Phosphatase Inhibitor Cocktail (Thermo Scientific™). Following a 2-hour incubation on ice with medium-speed shaking, the samples were centrifuged at 12,000xg for 15 min at 4°C and the resulting supernatant was used for protein quantification.

#### **6.4.2 Protein quantification assay**

Protein quantification was carried out using the Coomassie Plus (Bradford) Assay Kit (Thermo Scientific™) following the manufacturer's Standard Microplate protocol. In triplicates, 10 µl of 1:10 diluted protein samples were distributed into Nunc™ MicroWell™ 96 Wells microplates (Thermo Scientific™). Triplicates of blank samples and BSA standards at the following amounts: 0.15, 0.3, 0.6, 1.25, 2.5, 5 and 10 µg, were also loaded onto the microplates. 210 µl of Pierce™ Coomassie Plus (Thermo Scientific™). were added to each well and incubated for 10 min at room temperature after a brief vortexing. Protein amounts were measured photometrically at 595 nm using the SPARK® multimode microplate reader (TECAN). Protein concentrations were determined from the BSA standard curves, which were generated using linear or curvilinear regressions with an R-Squared value higher than 0.97. Typically, 10 µg of total proteins were used for immunoblotting analysis.

#### **6.4.3 Immunoblot Analysis**

Protein separation was carried out on SDS-PAGE (Laemmli, 1970) with a 4% acrylamide stacking gel and a 12% acrylamide resolving gel, prepared as previously described (Gallagher, 2012). Protein samples were mixed with 2x Laemmli buffer (0,004 % Bromophenol Blue, 10 % β-Mercaptoethanol, 20 % Glycerin, 4% SDS, 0,125 M Tris-HCl) in a 1:1 ratio and denatured at 95°C for 5 min before loading on the SDS-PAGE. For anti-AOC immunoblotting sample denaturation was performed at 96°C for 10 to dissolve AOC trimers. Electrophoresis was performed at 130 V in Tris-glycine buffer (25 mM Tris-Cl, 250 mM glycine, 0.1% SDS). The gels were then blotted on 0.45 µm PVDF membranes and "sandwiched" between two Blot papers in a Trans-Blot SD Semi-Dry Transfer Cell (BioRad). The semi-dry transfer was performed at 18 V for 30 min in Towbin buffer (25 mM Tris-Cl, 192 mM glycine, 20% (v/v) methanol).

For most experiments protein staining was carried out using Ponceau S (1.3 mM Ponceau S, 0.874 M acetic acid) for 10 min after each transfer to ensure successful protein transfer. Alternatively, the No-Stain™ Protein Labeling Reagent (Thermo Scientific™) was used for



protein staining according to the manufacturer's instructions. After staining, membranes were blocked for 30 min in 5% (w/v) BSA in TBST (20 mM Tris–Cl pH 7.8, 150 mM NaCl, 0.05% [v/v] Tween) before subsequent incubations with the primary and secondary antibodies, respectively.

Immunostaining of the fusion proteins, from the subcellular localization of the transporter candidates assays in *N. benthamiana* leaves, was performed using anti-GFP antibody (SC9996, Santa Cruz Biotechnology) at a 1:5000 dilution. Immunostaining of the OPR3-YFP and YFP-OPR3 fusion proteins from transient assays in *N. benthamiana* and from stable *Arabidopsis* lines was performed using anti-C-YFP antibody (AS11 1775, Agrisera) at a 1:3000 dilution. The same anti-YFP antibody was also used for the detection of the YFP halves from the Split-YFP assay in *N. benthamiana*, in addition to the anti-c-Myc (AS09601, Agrisera) primary antibody (1:4000 dilution) and the anti-HA (AS12 2220, Agrisera) primary antibody (1:4000 dilution). Immunostaining of AOC was performed using anti-AOC antibody (1:5000 dilution) raised against recombinant AtAOC2 (Stenzel et al., 2003). Anti-Actin (plant) antibody (A0480, Sigma-Aldrich) was used with a 1:3000 dilution. The detection step involved incubation of the membranes in either anti-rabbit or anti-mouse IgG antibodies conjugated with alkaline phosphatase (1:4000, Sigma-Aldrich) followed by incubation in the Immun-Star™ AP (BioRad) substrate following the manufacturer's instructions. The visualization of the chemiluminescent signal was done with a Fusion FX Imaging system (Vilber, [www.vilber.com](http://www.vilber.com)).

#### **Immunoblot normalization for AOC proteins detection.**

For subsequent quantification of the endogenous AOC levels from *Arabidopsis* seedlings and adult leaves of Col-0 and the *opr2opr3* and *aos* mutants, a normalization of the anti-AOC immunoblotting, performed as above-mentioned, was carried out to ensure a linear detection range of the AOC proteins in relation to total protein amounts in *Arabidopsis* tissues (Fig. 6.4 A, B). Quantification of band intensities was performed using the Gels Submenu of ImageJ software as described on the software's website (<https://imagej.nih.gov/ij/index.html>).

Determination of the R-Squared values from the plotted regressions across the serial dilutions of total protein samples under different treatments (control, MeJA), showed a range between 0.95 and 0.98, suggesting a linear detection range of AOC proteins in relation to the used total protein amounts (Fig. 6.4 B). Consequently, immunoblot loading amounts of 7 to 10 µg of total protein were set for determining endogenous AOC proteins levels from *Arabidopsis* tissues.

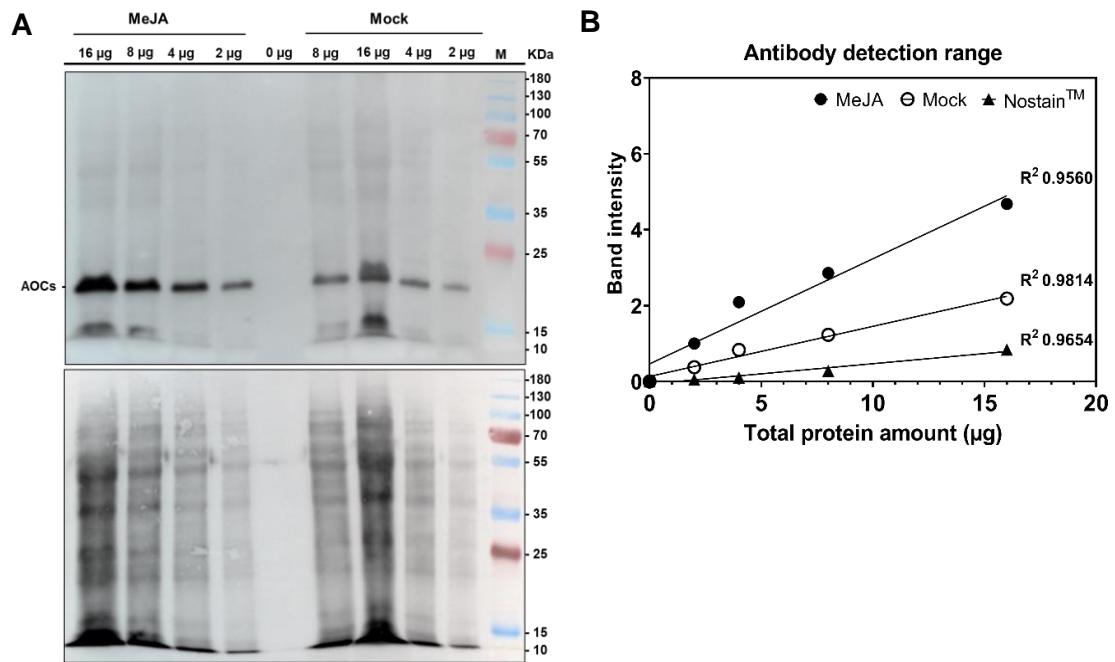


**Fig. 6.4 Determination of the anti-AOC immunoblot detection range.**

Ten-day-old seedlings from Col-0 were pretreated with MeJA or with water (Mock) during development. **A:** anti-AOCs immunoblot with 0, 2, 4, 8 and 16 µg of total proteins from Mock and MeJA pretreated seedlings. Total protein loading detection with NoStain™ was used as loading control. Immunolabeling was carried out by chemiluminescence. M= protein marker.

**B:** Determination of the detection range of AOC proteins across samples in relation to the total protein loading amounts (NoStain™). Protein band intensity was determined by Image J and linear regressions were plotted for the anti-AOCs antibody and the NoStain™ total protein control with their corresponding R-squared values.

#### 6.4.4 Histochemical detection of GUS activity

The *MYB24p(2-kb)::GUSplus*, *MYB21p(2-kb)::GUSplus* and *MYB21p(7-kb)::GUSplus* reporter lines, developed by Dr. Ivan F. Acosta, were grown on soil for four weeks before a single pinching was performed on the leaf with a hemostat. 2 h and 24 h following wounding, leaves were detached from the rosettes and fixed on ice with ice-cold 90% acetone for 60 min. GUS staining of the leaves was carried out according to Stenzel et al. (2012) and incubated at 37°C overnight. The microscopic analysis of the colored leaves was carried out in chloral hydrate: glycerol: water solution (8: 2: 1) and imaged with a Stemi 2000-C stereo microscope (Carl Zeiss) in combination with an AxioCam MRc5 camera (Carl Zeiss).

#### 6.4.5 Phytohormone measurements

Measurements of *cis*-OPDA, dnOPDA, JA, and JA-Ile were performed on 10-day-old seedlings grown in sterile liquid media, on whole rosettes or the eighth leaf of 4-week-old plants grown on soil in addition to flower buds from stage 12. The quantification was based on a standardized Ultra-performance liquid chromatography–tandem Mass Spectrometry (UPLC–MS/MS)-based method according to Balcke et al. (2012) using approximately 50 mg powdered frozen tissue. The sample preparation was performed by Hagen Stellmach, and involved extraction with 500 µl 100% LC-MS methanol supplied with 50ng of [<sup>2</sup>H<sub>5</sub>]OPDA, [<sup>2</sup>H<sub>6</sub>]JA, and

[<sup>2</sup>H<sub>2</sub>]JA-Ile as internal standards. After centrifugation, the supernatant was brought to a methanol:water ratio of 10:90 with LC-MS water, subjected to solid phase extraction on HR-XC (Chromabond, Macherey-Nagel, Düren, Germany) and eluted with 900 ml acetonitrile. 10 µl of the eluate were subjected to UPLC–MS/MS and analyte content was determined in relation to the internal standard peak heights. dnOPDA content was determined using [<sup>2</sup>H<sub>5</sub>]OPDA as internal standard.

## 6.5 Plant phenotyping

### 6.5.1 Root length and leaf area measurements

Sterile seeds of Col-0, *myb21* and *myb24* were placed at 1 cm distance on square petri dishes containing solid MS medium. For root and leaf growth, seeds were grown vertically and horizontally, respectively, in phytocabinets. Following two weeks of growth, seedlings were visualized and recorded on a Stemi 2000-C stereo microscope (Carl Zeiss) in combination with an AxioCam MRc5 camera (Carl Zeiss) and the resulting images were processed by ImageJ software for measurements determination using the function Measure in the submenu. The root length experiments comprised five seedlings per genotype, conducted across ten repetitions. The leaf area experiments were conducted in triplicate, with each repetition consisting of 10 seedlings per genotype and were used to count the trichome number per leaf.

### 6.5.2 Main stem length determination and flowers and siliques counting

At 58 days following germination, transgenic plant lines of Col+EV, *opr2/3*+ER-OPR3, and *opr2/3*+Px-OPR3 were fixed on a carton board with tape to allow proper length measurements. The length of the main stem was directly measured with a ruler and the number of open flowers from stages 13 to 15 were counted directly from the stems. Siliques number was also counted directly from stems at 70 days post-germination. Determination of the length of the siliques was performed from photos of the plants taken with a digital camera by adding a ruler as a length reference. Measurement of the lengths was carried out on ImageJ software.

Imaging of open flowers was carried out on Stemi 2000-C stereo microscope (Carl Zeiss) in combination with an AxioCam MRc5 camera (Carl Zeiss), with determination of the flower stage 13 according to Smyth et al. (1990).

### 6.5.3 Flowering time determination

For flowering time determination, plants were grown in long day conditions as described in section 2.1. The flowering time was determined by counting the days from germination until the appearance of the flower stem at 1 cm above the rosette.

### 6.5.4 Seeds germination assay

Seed stocks of Col-0, *myb21* and *myb24* harvested in the same year, were sterilized, and grown on solid media at short day conditions as described in section 6.1. Monitoring of the

different steps of seed germination was carried-out at 24, 30, 48, 54 and 72 hours after the introduction of the seeds to the growth cabinets. The different stages of seed germination were designated according to Maia et al. (2011). Visualization and recording of the germination stages was carried out on an Axioskop microscope equipped with a MRc 5 camera (Zeiss).

### 6.5.5 Pollen germination assay

For the transgenic plant lines of Col-0+EV, *opr2/3*+ER-OPR3, and *opr2/3*+Px-OPR3, pollen germination assay was carried out in germination media with pH 7 (18% sucrose, 1.62 mM boric acid, 1 mM CaCl<sub>2</sub>, 1 mM Ca(NO<sub>3</sub>)<sub>2</sub>, 1 mM MgSO<sub>4</sub>, 1 mM KCl, 0.8% agar) according to (Bou Daher et al., 2009). Hot agar-containing medium was poured onto a microscope slide to form a layer with a thickness of about 0.5 mm and left to cool. Open flower buds were rubbed on the media surface to sprinkle the pollen. The slides were incubated in a humid chamber which was mounted as described by Rodriguez-Enriquez et al., (2013). The incubation was performed at room temperature for 16 hours before visualization of the pollen on Axio Imager.Z1 (Carl Zeiss). The counting of the pollen tubes was performed on ImageJ software.

## 6.6 Microscopy

Confocal microscopy was carried out on the LSM880 and LSM900 laser scanning microscopes from Zeiss using usually a 40x objective. Laser lines with 488 nm (GFP), 514 nm (YFP) and 561 nm (mCherry) were used to excite the fluorophores, which were detected at the wavelength of 493–531 nm, 510–560 nm, and 570–650 nm, respectively. Images were captured and processed using the microscopy software ZEN (version 3.4, 2021, Zeiss, Jena, Germany). All images shown within one experiment were taken by analyzing different leaf areas and several individuals.

## 6.7 Figures and statistical analysis

Figures with schematic illustrations were designed on BioRender (<https://www.biorender.com>) and gene structure illustrations were designed on the Exon-Intron Graphic Maker (<http://wormweb.org/exonintron>). The statistical analyses applied to the different datasets are specified in the respective figures and were carried out on GraphPad Prism.

Venn diagrams were obtained using the VENNY 2.1 tool (<https://bioinfogp.cnb.csic.es/tools/venny/>).

## References

- Adio, A. M., Casteel, C. L., de Vos, M., Kim, J. H., Joshi, V., Li, B., Juárez, C., Daron, J., Kliebenstein, D. J., and Jander, G.** (2011). Biosynthesis and defensive function of N $\delta$ -Acetylornithine, a jasmonate-induced arabidopsis metabolite. *Plant Cell*, 23(9), 3303–3318. <https://doi.org/10.1105/tpc.111.088989>
- Alvarez-Buylla, E. R., Benítez, M., Corvera-Poiré, A., Chaos Cador, Á., de Folter, S., Gamboa de Buen, A., Garay-Arroyo, A., García-Ponce, B., Jaimes-Miranda, F., Pérez-Ruiz, R. V., Piñeyro-Nelson, A., and Sánchez-Corrales, Y. E.** (2010). Flower Development. *The Arabidopsis Book*, 8(8), e0127. <https://doi.org/10.1199/tab.0127>
- Améras, E., Stolz, S., Vollenweider, S., Reymond, P., Mène-Saffrané, L., and Farmer, E. E.** (2003). Reactive electrophile species activate defense gene expression in Arabidopsis. *Plant Journal*, 34(2), 205–216. <https://doi.org/10.1046/j.1365-313X.2003.01718.x>
- An, F., Zhang, X., Zhu, Z., Ji, Y., He, W., Jiang, Z., Li, M., and Guo, H.** (2012). Coordinated regulation of apical hook development by gibberellins and ethylene in etiolated Arabidopsis seedlings. *Cell Research*, 22(5), 915–927. <https://doi.org/10.1038/cr.2012.29>
- An, L., Zhou, Z., Yan, A., and Gan, Y.** (2011). Progress on trichome development regulated by phytohormone signaling. *Plant Signaling and Behavior*, 6(12), 1959–1962. <https://doi.org/10.4161/psb.6.12.18120>
- Antico, C. J., Colon, C., Banks, T., and Ramonell, K. M.** (2012). Insights into the role of jasmonic acid-mediated defenses against necrotrophic and biotrophic fungal pathogens. *Frontiers in Biology*, 7(1), 48–56. <https://doi.org/10.1007/s11515-011-1171-1>
- Balcke, G. U., Handrick, V., Bergau, N., Fichtner, M., Henning, A., Stellmach, H., Tissier, A., Hause, B., and Frolov, A.** (2012). An UPLC-MS/MS method for highly sensitive high-throughput analysis of phytohormones in plant tissues. *Plant Methods*, 8(1), 1–11. <https://doi.org/10.1186/1746-4811-8-47>
- Banday, Z. Z., Cecchini, N. M., Speed, D. Q. J., Scott, A. T., Parent, C., Hu, C. T., Filzen, R. C., Agbo, E., and Greenberg, J. T.** (2022). Friend or foe: Hybrid proline-rich proteins determine how plants respond to beneficial and pathogenic microbes. *Plant Physiology*, 190(1), 860–881. <https://doi.org/10.1093/plphys/kiac263>
- Bannenberg, G., Martínez, M., Hamberg, M., and Castresana, C.** (2009). Diversity of the enzymatic activity in the lipoxygenase gene family of arabidopsis thaliana. *Lipids*, 44(2), 85–95. <https://doi.org/10.1007/s11745-008-3245-7>
- Barbier-Brygoo, H., Gaymard, F., Rolland, N., and Joyard, J.** (2001). Strategies to identify transport systems in plants. *Trends in Plant Science*, 6(12), 577–585. [https://doi.org/10.1016/S1360-1385\(01\)02149-5](https://doi.org/10.1016/S1360-1385(01)02149-5)
- Barros-Galvão, T., Dave, A., Cole, A., Harvey, D., Langer, S., Larson, T. R., Vaistij, F. E., and Graham, I. A.** (2019). Cis-12-Oxo-phytodienoic acid represses Arabidopsis seed germination in shade conditions. *Journal of Experimental Botany*, 70(20), 5919–5927. <https://doi.org/10.1093/jxb/erz337>
- Beyhl, D., Hörtensteiner, S., Martinoia, E., Farmer, E. E., Fromm, J., Marten, I., and Hedrich, R.** (2009). The fou2 mutation in the major vacuolar cation channel TPC1 confers tolerance to inhibitory luminal calcium. *Plant Journal*, 58(5), 715–723. <https://doi.org/10.1111/j.1365-313X.2009.03820.x>
- Beynon, E. R., Symons, Z. C., Jackson, R. G., Lorenz, A., Rylott, E. L., and Bruce, N. C.** (2009). The role of oxophytodienoate reductases in the detoxification of the explosive 2,4,6-trinitrotoluene by Arabidopsis. *Plant Physiology*, 151(1), 253–261. <https://doi.org/10.1104/pp.109.141598>
- Birkett, M. A., Campbell, C. A. M., Chamberlain, K., Guerrieri, E., Hick, A. J., Martin, J. L., Matthes, M., Napier, J. A., Pettersson, J., Pickett, J. A., Poppy, G. M., Pow, E. M., Pye, B. J., Smart, L. E., Wadhams, G. H., Wadhams, L. J., and Woodcock, C. M.** (2000). New roles for cis-jasmone as an insect semiochemical and in plant defense. *Proceedings of the National Academy of Sciences of the United States of America*, 97(16), 9329–9334.

<https://doi.org/10.1073/pnas.160241697>

- Blée, E., and Joyard, J.** (1996). Envelope membranes from spinach chloroplasts are a site of metabolism of fatty acid hydroperoxides. *Plant Physiology*, *110*(2), 445–454. <https://doi.org/10.1104/pp.110.2.445>
- Bonaventure, G., Gfeller, A., Rodríguez, V. M., Armand, F., and Farmer, E. E.** (2007). The *fou2* gain-of-function allele and the wild-type allele of Two Pore Channel 1 contribute to different extents or by different mechanisms to defense gene expression in *Arabidopsis*. *Plant and Cell Physiology*, *48*(12), 1775–1789. <https://doi.org/10.1093/pcp/pcm151>
- Bou Daher, F., Chebli, Y., and Geitmann, A.** (2009). Optimization of conditions for germination of cold-stored *Arabidopsis thaliana* pollen. *Plant Cell Reports*, *28*(3), 347–357. <https://doi.org/10.1007/s00299-008-0647-1>
- Breithaupt, C., Kurzbauer, R., Lilie, H., Schaller, A., Strassner, J., Huber, R., Macheroux, P., and Clausen, T.** (2006). Crystal structure of 12-oxophytodienoate reductase 3 from tomato: Self-inhibition by dimerization. *Proceedings of the National Academy of Sciences of the United States of America*, *103*(39), 14337–14342. <https://doi.org/10.1073/pnas.0606603103>
- Brocard, C., and Hartig, A.** (2006). Peroxisome targeting signal 1: Is it really a simple tripeptide? *Biochimica et Biophysica Acta - Molecular Cell Research*, *1763*(12), 1565–1573. <https://doi.org/10.1016/j.bbamcr.2006.08.022>
- Brown, R. L., Kazan, K., McGrath, K. C., Maclean, D. J., and Manners, J. M.** (2003). A role for the GCC-box in jasmonate-mediated activation of the PDF1.2 gene of *Arabidopsis*. *Plant Physiology*, *132*(2), 1020–1032. <https://doi.org/10.1104/pp.102.017814>
- Browse, J., and Howe, G. A.** (2008). New weapons and a rapid response against insect attack. *Plant Physiology*, *146*(3), 832–838. <https://doi.org/10.1104/pp.107.115683>
- Browse, J., and Wallis, J. G.** (2019). *Arabidopsis* flowers unlocked the mechanism of Jasmonate signaling. *Plants*, *8*(8), 1–11. <https://doi.org/10.3390/plants8080285>
- Bruce, T. J. A., Matthes, M. C., Chamberlain, K., Woodcock, C. M., Mohib, A., Webster, B., Smart, L. E., Birkett, M. A., Pickett, J. A., and Napier, J. A.** (2008). *cis*-Jasmone induces *Arabidopsis* genes that affect the chemical ecology of multitrophic interactions with aphids and their parasitoids. *Proceedings of the National Academy of Sciences of the United States of America*, *105*(12), 4553–4558. <https://doi.org/10.1073/pnas.0710305105>
- Brunkard, J. O., Runkel, A. M., and Zambryski, P. C.** (2015). Chloroplasts extend stromules independently and in response to internal redox signals. *Proceedings of the National Academy of Sciences of the United States of America*, *112*(32), 10044–10049. <https://doi.org/10.1073/pnas.1511570112>
- Brunoni, F., Široká, J., Mik, V., Pospíšil, T., Kralová, M., Ament, A., Pernisová, M., Karady, M., Htítich, M., Ueda, M., Floková, K., Wasternack, C., Strnad, M., and Novák O.** (2023). Conjugation of *cis*-OPDA with amino acids is a conserved pathway affecting *cis*-OPDA homeostasis upon stress responses. *bioRxiv* 2023.07.18.549545. <https://doi.org/10.1101/2023.07.18.549545>
- Cai, X. T., Xu, P., Zhao, P. X., Liu, R., Yu, L. H., and Xiang, C. Bin.** (2014). *Arabidopsis* ERF109 mediates cross-talk between jasmonic acid and auxin biosynthesis during lateral root formation. *Nature Communications*, *5*(May), 1–13. <https://doi.org/10.1038/ncomms6833>
- Chang, P. L., Liu, D., Narasimhan, M. L., Raghothama, K. G., Hasegawa, P. M. and Bressan, R. A.** (1994). Plant Defense Genes Are Synergistically Induced by Ethylene and Methyl Jasmonate. *Plant Cell*, *6*(August), 1077–1085.
- Chang, Y., Shi, M., Sun, Y., Cheng, H., Ou, X., Zhao, Y., Zhang, X., Day, B., Miao, C., and Jiang, K.** (2023). Light-induced stomatal opening in *Arabidopsis* is negatively regulated by chloroplast-originated OPDA signaling. *Current Biology*, *33*(6), 1071-1081.e5. <https://doi.org/10.1016/j.cub.2023.02.012>
- Charpentier, M., Bredemeier, R., Wanner, G., Takeda, N., Schleiff, E., and Parniske, M.** (2008). Lotus japonicus Castor and Pollux are ion channels essential for perinuclear calcium spiking in



- legume root endosymbiosis. *Plant Cell*, 20(12), 3467–3479. <https://doi.org/10.1105/tpc.108.063255>
- Chehab, E. W., Kim, S., Savchenko, T., Kliebenstein, D., Dehesh, K., and Braam, J.** (2011). Intronic T-DNA insertion renders arabidopsis opr3 a conditional jasmonic acid-producing mutant. *Plant Physiology*, 156(2), 770–778. <https://doi.org/10.1104/pp.111.174169>
- Chen, H., Yang, R., Chen, J., Luo, Q., Cui, X., Yan, X., and Gerwick, W. H.** (2019). 1-Octen-3-ol, a self-stimulating oxylipin messenger, can prime and induce defense of marine alga. *BMC Plant Biology*, 19(1), 1–16. <https://doi.org/10.1186/s12870-019-1642-0>
- Chen, Q., Sun, J., Zhai, Q., Zhou, W., Qi, L., Xu, L., Wang, B., Chen, R., Jiang, H., Qi, J., Li, X., Palme, K., and Li, C.** (2011). The basic helix-loop-helix transcription factor myc2 directly represses plethora expression during jasmonate-mediated modulation of the root stem cell niche in arabidopsis. *Plant Cell*, 23(9), 3335–3352. <https://doi.org/10.1105/tpc.111.089870>
- Cheng, H., Song, S., Xiao, L., Soo, H. M., Cheng, Z., Xie, D., and Peng, J.** (2009). Gibberellin acts through jasmonate to control the expression of MYB21, MYB24, and MYB57 to promote stamen filament growth in arabidopsis. *PLoS Genetics*, 5(3), 20–22. <https://doi.org/10.1371/journal.pgen.1000440>
- Chini, A., Boter, M., and Solano, R.** (2009). Plant oxylipins: COI1/JAZs/MYC2 as the core jasmonic acid-signalling module. *FEBS Journal*, 276(17), 4682–4692. <https://doi.org/10.1111/j.1742-4658.2009.07194.x>
- Chini, A., Monte, I., Zamarreño, A. M., García-Mina, J. M., and Solano, R.** (2023). Evolution of the jasmonate ligands and their biosynthetic pathways. *New Phytologist*, 238(5), 2236–2246. <https://doi.org/10.1111/nph.18891>
- Chini, A., Monte, I., Zamarreño, A. M., Hamberg, M., Lassueur, S., Reymond, P., Weiss, S., Stintzi, A., Schaller, A., Porzel, A., García-Mina, J. M., and Solano, R.** (2018). An OPR3-independent pathway uses 4,5-didehydrojasmonate for jasmonate synthesis. *Nature Chemical Biology*, 14(2), 171–178. <https://doi.org/10.1038/nchembio.2540>
- Colling, J., Pollier, J., Makunga, N. P., and Goossens, A.** (2013). *Jasmonate Signaling*. 1011, 13–23. <https://doi.org/10.1007/978-1-62703-414-2>
- Creelman, R. A., and Mulpuri, R.** (2002). The Oxylipin Pathway in Arabidopsis. *The Arabidopsis Book*, 1, e0012. <https://doi.org/10.1199/tab.0012>
- Czechowski, T., Stitt, M., Altmann, T., Udvardi, M. K., and Scheible, W.-R.** (2005). Genome-Wide Identification and Testing of Superior Reference Genes for Transcript Normalization in Arabidopsis. *Plant Physiology*, 139(1), 5–17. <https://doi.org/10.1104/pp.105.063743>
- Dabrowska, P., and Boland, W.** (2007). iso-OPDA: An early precursor of cis-Jasmone in plants? *ChemBioChem*, 8(18), 2281–2285. <https://doi.org/10.1002/cbic.200700464>
- Dave, A., and Graham, I. A.** (2012). Oxylipin signaling: A distinct role for the jasmonic acid precursor cis-(+)-12-oxo-phytodienoic acid (cis-OPDA). *Frontiers in Plant Science*, 3(MAR), 1–6. <https://doi.org/10.3389/fpls.2012.00042>
- Dave, A., Hernández, M. L., He, Z., Andriotis, V. M. E., Vaistij, F. E., Larson, T. R., and Graham, I. A.** (2011). 12-Oxo-phytodienoic acid accumulation during seed development represses seed germination in Arabidopsis. *Plant Cell*, 23(2), 583–599. <https://doi.org/10.1105/tpc.110.081489>
- Davletova, S., Schlauch, K., Coutu, J., and Mittler, R.** (2005). The zinc-finger protein Zat12 plays a central role in reactive oxygen and abiotic stress signaling in Arabidopsis. *Plant Physiology*, 139(2), 847–856. <https://doi.org/10.1104/pp.105.068254>
- De Meyer, T., and Depicker, A.** (2014). Trafficking of endoplasmic reticulum-retained recombinant proteins is unpredictable in Arabidopsis thaliana. *Frontiers in Plant Science*, 5(SEP), 1–7. <https://doi.org/10.3389/fpls.2014.00473>
- Delessert, C., Wilson, L. W., Van Der Straeten, D., Dennis, E. S., and Dolferus, R.** (2004). Spatial and temporal analysis of the local response to wounding in Arabidopsis leaves. *Plant Molecular Biology*, 55(2), 165–181. <https://doi.org/10.1007/s11103-004-0112-7>

- Deniaud, A., Panwar, P., Frelet-Barrand, A., Bernaudat, F., Juillan-Binard, C., Ebel, C., Rolland, N., and Pebay-Peyroula, E. (2012). Oligomeric status and nucleotide binding properties of the plastid ATP/ADP transporter 1: Toward a molecular understanding of the transport mechanism. *PLoS ONE*, 7(3). <https://doi.org/10.1371/journal.pone.0032325>
- Devoto, A., Nieto-Rostro, M., Xie, D., Ellis, C., Harmston, R., Patrick, E., Davis, J., Sherratt, L., Coleman, M., and Turner, J. G. (2002). COI1 links jasmonate signalling and fertility to the SCF ubiquitin-ligase complex in Arabidopsis. *Plant Journal*, 32(4), 457–466. <https://doi.org/10.1046/j.1365-313X.2002.01432.x>
- Diallinas, G. (2014). Understanding transporter specificity and the discrete appearance of channel-like gating domains in transporters. *Frontiers in Pharmacology*, 5 AUG(September), 1–17. <https://doi.org/10.3389/fphar.2014.00207>
- Dobritzsch, S., Weyhe, M., Schubert, R., Dindas, J., Hause, G., Kopka, J., and Hause, B. (2015). Dissection of jasmonate functions in tomato stamen development by transcriptome and metabolome analyses. *BMC Biology*, 13(1), 1–18. <https://doi.org/10.1186/s12915-015-0135-3>
- Ellis, C., and Turner, J. G. (2002). A conditionally fertile coi1 allele indicates cross-talk between plant hormone signalling pathways in Arabidopsis thaliana seeds and young seedlings. *Planta*, 215(4), 549–556. <https://doi.org/10.1007/s00425-002-0787-4>
- Engelberth, J., Alborn, H. T., Schmelz, E. A., and Tumlinson, J. H. (2004). Airborne signals prime plants against insect herbivore attack. *Proceedings of the National Academy of Sciences of the United States of America*, 101(6), 1781–1785. <https://doi.org/10.1073/pnas.0308037100>
- Engler, C., Youles, M., Gruetzner, R., Ehnert, T. M., Werner, S., Jones, J. D. G., Patron, N. J., and Marillonnet, S. (2014). A Golden Gate modular cloning toolbox for plants. *ACS Synthetic Biology*, 3(11), 839–843. <https://doi.org/10.1021/sb4001504>
- Eseverri, Á., Baysal, C., Medina, V., Capell, T., Christou, P., Rubio, L. M., and Caro, E. (2020). Transit Peptides From Photosynthesis-Related Proteins Mediate Import of a Marker Protein Into Different Plastid Types and Within Different Species. *Frontiers in Plant Science*, 11(September), 1–14. <https://doi.org/10.3389/fpls.2020.560701>
- Eudes, A., Kunji, E. R. S., Noiriel, A., Klaus, S. M. J., Vickers, T. J., Beverley, S. M., Gregory III, J. F., and Hanson, A. D. (2010). Identification of transport-critical residues in a folate transporter from the Folate-Biopterin Transporter (FBT) family. *Journal of Biological Chemistry*, 285(4), 2867–2875. <https://doi.org/10.1074/jbc.M109.063651>
- Facchinelli, F., and Weber, A. P. M. (2011). The metabolite transporters of the plastid envelope: An update. *Frontiers in Plant Science*, 2(SEP), 1–18. <https://doi.org/10.3389/fpls.2011.00050>
- Farmer, E. E., and Ryan, C. A. (1990). Interplant communication: Airborne methyl jasmonate induces synthesis of proteinase inhibitors in plant leaves. *Proceedings of the National Academy of Sciences of the United States of America*, 87(19), 7713–7716. <https://doi.org/10.1073/pnas.87.19.7713>
- Farmer, E., Farmer, E., Mousavi, S., and Lenglet, A. (2013). Leaf numbering for experiments on long distance signalling in Arabidopsis. *Protocol Exchange*, 1–7. <https://doi.org/10.1038/protex.2013.071>
- Farmer, Edward E., and Davoine, C. (2007). Reactive electrophile species. *Current Opinion in Plant Biology*, 10(4), 380–386. <https://doi.org/10.1016/j.pbi.2007.04.019>
- Farmer, Edward E., and Goossens, A. (2019). Jasmonates: What ALLENE OXIDE SYNTHASE does for plants. *Journal of Experimental Botany*, 70(13), 3373–3378. <https://doi.org/10.1093/jxb/erz254>
- Feys, B. J. F., Benedetti, C. E., Penfold, C. N., and Turner, J. G. (1994). Arabidopsis mutants selected for resistance to the phytotoxin coronatine are male sterile, insensitive to methyl jasmonate, and resistant to a bacterial pathogen. *Plant Cell*, 6(5), 751–759. <https://doi.org/10.2307/3869877>
- Förster, S., Schmidt, L. K., Kopic, E., Anschütz, U., Huang, S., Schlücking, K., Köster, P., Waadt, R., Larriau, A., Batistic, O., Rodriguez, P. L., Gril, E., Kudla, J., and Becker, D. (2019). Wounding-Induced Stomatal Closure Requires Jasmonate-Mediated Activation of GORK K<sup>+</sup> Channels by a Ca<sup>2+</sup> Sensor-Kinase CBL1-CIPK5 Complex. *Developmental Cell*, 48(1), 87–99.e6.

<https://doi.org/10.1016/j.devcel.2018.11.014>

- Froehlich, J. E., Itoh, A., and Howe, G. A.** (2001). Tomato allene oxide synthase and fatty acid hydroperoxide lyase, two cytochrome P450s involved in oxylipin metabolism, are targeted to different membranes of chloroplast envelope. *Plant Physiology*, *125*(1), 306–317. <https://doi.org/10.1104/pp.125.1.306>
- Gallagher, S. R.** (2012). SDS-polyacrylamide gel electrophoresis (SDS-PAGE). *Current Protocols in Essential Laboratory Techniques*, *2012*(SUPPL.6). <https://doi.org/10.1002/9780470089941.et0703s06>
- Ge, S. X., Son, E. W., and Yao, R.** (2018). iDEP: An integrated web application for differential expression and pathway analysis of RNA-Seq data. *BMC Bioinformatics*, *19*(1), 1–24. <https://doi.org/10.1186/s12859-018-2486-6>
- Geng, S., Misra, B. B., de Armas, E., Huhman, D. V., Alborn, H. T., Sumner, L. W., and Chen, S.** (2016). Jasmonate-mediated stomatal closure under elevated CO<sub>2</sub> revealed by time-resolved metabolomics. *Plant Journal*, *88*(6), 947–962. <https://doi.org/10.1111/tpj.13296>
- Glauser, G., Grata, E., Dubugnon, L., Rudaz, S., Farmer, E. E., and Wolfender, J. L.** (2008). Spatial and temporal dynamics of jasmonate synthesis and accumulation in Arabidopsis in response to wounding. *Journal of Biological Chemistry*, *283*(24), 16400–16407. <https://doi.org/10.1074/jbc.M801760200>
- Goodspeed, D., Chehab, E. W., Min-Venditti, A., Braam, J., and Covington, M. F.** (2012). Arabidopsis synchronizes jasmonate-mediated defense with insect circadian behavior. *Proceedings of the National Academy of Sciences of the United States of America*, *109*(12), 4674–4677. <https://doi.org/10.1073/pnas.1116368109>
- Gookin, T. E., and Assmann, S. M.** (2014). Significant reduction of BiFC non-specific assembly facilitates in planta assessment of heterotrimeric G-protein interactors. *Plant Journal*, *80*(3), 553–567. <https://doi.org/10.1111/tpj.12639>
- Gould, S. J., Keller, G. A., Hosken, N., Wilkinson, J., and Subramani, S.** (1989). A conserved tripeptide sorts proteins to peroxisomes. *Journal of Cell Biology*, *108*(5), 1657–1664. <https://doi.org/10.1083/jcb.108.5.1657>
- Grundy, J., Stoker, C., and Carré, I. A.** (2015). Circadian regulation of abiotic stress tolerance in plants. *Frontiers in Plant Science*, *6*(AUG), 1–15. <https://doi.org/10.3389/fpls.2015.00648>
- Guan, L., Denkert, N., Eisa, A., Lehmann, M., Sjuts, I., Weiberg, A., Soll, J., Meinecke, M., and Schwenkert, S.** (2019). JASSY, a chloroplast outer membrane protein required for jasmonate biosynthesis. *Proceedings of the National Academy of Sciences of the United States of America*, *116*(21), 10568–10575. <https://doi.org/10.1073/pnas.1900482116>
- Guo, H. M., Li, H. C., Zhou, S. R., Xue, H. W., and Miao, X. X.** (2014). Cis-12-Oxo-phytodienoic acid stimulates rice defense response to a piercing-sucking insect. *Molecular Plant*, *7*(11), 1683–1692. <https://doi.org/10.1093/mp/ssu098>
- Guo, Q., Yoshida, Y., Major, I. T., Wang, K., Sugimoto, K., Kapali, G., Havko, N. E., Benning, C., and Howe, G. A.** (2018). JAZ repressors of metabolic defense promote growth and reproductive fitness in Arabidopsis. *Proceedings of the National Academy of Sciences of the United States of America*, *115*(45), E10768–E10777. <https://doi.org/10.1073/pnas.1811828115>
- Han, B. W., Malone, T. E., Kim, D. J., Bingman, C. A., Kim, H. J., Fox, B. G., and Phillips, G. N.** (2011). Crystal structure of Arabidopsis thaliana 12-oxophytodienoate reductase isoform 3 in complex with 8-iso prostaglandin A 1. *Proteins: Structure, Function and Bioinformatics*, *79*(11), 3236–3241. <https://doi.org/10.1002/prot.23153>
- Han, G. Z.** (2017). Evolution of jasmonate biosynthesis and signalling mechanisms. *Journal of Experimental Botany*, *68*(6), 1323–1331. <https://doi.org/10.1093/jxb/erw470>
- Harada, E., Yamaguchi, Y., Koizumi, N., and Hiroshi, S.** (2002). Cadmium stress induces production of thiol compounds and transcripts for enzymes involved in sulfur assimilation pathways in Arabidopsis. *Journal of Plant Physiology*, *159*(4), 445–448. <https://doi.org/10.1078/0176-1617-00733>

- Hause, B., Stenzel, I., Miersch, O., and Wasternack, C.** (2003). Occurrence of the allene oxide cyclase in different organs and an tissues of *Arabidopsis thaliana*. *Phytochemistry*. [https://doi.org/10.1016/S0031-9422\(03\)00447-3](https://doi.org/10.1016/S0031-9422(03)00447-3)
- Hennig, L., Stoddart, W. M., Dieterle, M., Whitelam, G. C., and Schäfer, E.** (2002). Phytochrome E controls light-induced germination of arabidopsis. *Plant Physiology*, *128*(1), 194–200. <https://doi.org/10.1104/pp.010559>
- Hofmann, E., Zerbe, P., and Schaller, F.** (2006). The crystal structure of *Arabidopsis thaliana* allene oxide cyclase: Insights into the oxylipin cyclization reaction. *Plant Cell*, *18*(11), 3201–3217. <https://doi.org/10.1105/tpc.106.043984>
- Hoo, S. C., Koo, A. J. K., Gao, X., Jayanty, S., Thines, B., Jones, A. D., and Howe, G. A.** (2008). Regulation and function of arabidopsis JASMONATE ZIM-domain genes in response to wounding and herbivory. *Plant Physiology*, *146*(3), 952–964. <https://doi.org/10.1104/pp.107.115691>
- Horstman, A., Tonaco, I. A. N., Boutilier, K., and Immink, R. G. H.** (2014). A Cautionary note on the use of split-YFP/BiFC in plant protein-protein interaction studies. *International Journal of Molecular Sciences*, *15*(6), 9628–9643. <https://doi.org/10.3390/ijms15069628>
- Howarth, J. R., Parmar, S., Barraclough, P. B., and Hawkesford, M. J.** (2009). A sulphur deficiency-induced gene, *sdi1*, involved in the utilization of stored sulphate pools under sulphur-limiting conditions has potential as a diagnostic indicator of sulphur nutritional status. *Plant Biotechnology Journal*, *7*(2), 200–209. <https://doi.org/10.1111/j.1467-7652.2008.00391.x>
- Howe, G. A.** (2004). Jasmonates as signals in the wound response. *Journal of Plant Growth Regulation*, *23*(3), 223–237. <https://doi.org/10.1007/s00344-004-0030-6>
- Howe, G. A., and Jander, G.** (2008). Plant immunity to insect herbivores. *Annual Review of Plant Biology*, *59*, 41–66. <https://doi.org/10.1146/annurev.arplant.59.032607.092825>
- Huang, H., Gao, H., Liu, B., Qi, T., Tong, J., Xiao, L., Xie, D., and Song, S.** (2017). Arabidopsis MYB24 regulates jasmonate-mediated stamen development. *Frontiers in Plant Science*, *8*(September), 1–8. <https://doi.org/10.3389/fpls.2017.01525>
- Huang, H., Gong, Y., Liu, B., Wu, D., Zhang, M., Xie, D., and Song, S.** (2020). The della proteins interact with MYB21 and MYB24 to regulate filament elongation in Arabidopsis. *BMC Plant Biology*, *20*(1), 1–9. <https://doi.org/10.1186/s12870-020-2274-0>
- Hughes, R. K., De Domenico, S., and Santino, A.** (2009). Plant cytochrome CYP74 family: Biochemical features, endocellular localisation, activation mechanism in plant defence and improvements for industrial applications. *ChemBioChem*, *10*(7), 1122–1133. <https://doi.org/10.1002/cbic.200800633>
- Incarbone, M., Ritzenthaler, C., and Dunoyer, P.** (2018). Peroxisomal targeting as a sensitive tool to detect protein-small RNA interactions through in vivo piggybacking. *Frontiers in Plant Science*, *9*(February), 1–13. <https://doi.org/10.3389/fpls.2018.00135>
- Irish, V. F.** (2010). The flowering of Arabidopsis flower development. *Plant Journal*, *61*(6), 1014–1028. <https://doi.org/10.1111/j.1365-313X.2009.04065.x>
- Ishiguro, S., Kawai-Oda, A., Ueda, J., Nishida, I., and Okada, K.** (2001). The defective in anther dehiscence1 gene encodes a novel phospholipase A1 catalyzing the initial step of jasmonic acid biosynthesis, which synchronizes pollen maturation, anther dehiscence, and flower opening in Arabidopsis. *Plant Cell*, *13*(10), 2191–2209. <https://doi.org/10.1105/tpc.13.10.2191>
- Janik, K., Stellmach, H., Mittelberger, C., and Hause, B.** (2019). Characterization of phytoplasmal effector protein interaction with proteinaceous plant host targets using bimolecular fluorescence complementation (BiFC). In *Methods in Molecular Biology* (Vol. 1875, pp. 321–331). [https://doi.org/10.1007/978-1-4939-8837-2\\_24](https://doi.org/10.1007/978-1-4939-8837-2_24)
- Kariola, T., Brader, G., Li, J., and Palva, E. T.** (2005). Chlorophyllase 1, a damage control enzyme, affects the balance between defense pathways in plants. *Plant Cell*, *17*(1), 282–294. <https://doi.org/10.1105/tpc.104.025817>
- Kasajima, I., Ide, Y., Ohkama-Ohtsu, N., Hayashi, H., Yoneyama, T., and Fujiwara, T.** (2004). A



- protocol for rapid DNA extraction from *Arabidopsis thaliana* for PCR analysis. *Plant Molecular Biology Reporter*, 22(1), 49–52. <https://doi.org/10.1007/BF02773348>
- Kaur, N., Reumann, S., and Hu, J.** (2009). Peroxisome Biogenesis and Function. *The Arabidopsis Book*, 7, e0123. <https://doi.org/10.1199/tab.0123>
- Kelly, A. A., and Dörmann, P.** (2004). Green light for galactolipid trafficking. *Current Opinion in Plant Biology*, 7(3), 262–269. <https://doi.org/10.1016/j.pbi.2004.03.009>
- Kim, D. H., Xu, Z. Y., and Hwang, I.** (2013). Generation of transgenic *Arabidopsis* plants expressing mcherry-fused organelle marker proteins. *Journal of Plant Biology*, 56(6), 399–406. <https://doi.org/10.1007/s12374-013-0348-3>
- Knieper, M., Vogelsang, L., Guntelmann, T., Sproß, J., Gröger, H., Viehhauser, A., and Dietz, K. J.** (2022). OPDAylation of Thiols of the Redox Regulatory Network In Vitro. *Antioxidants*, 11(5). <https://doi.org/10.3390/antiox11050855>
- Koch, T., Bandemer, K., and Boland, W.** (1997). Biosynthesis of cis-Jasmone: A Pathway for the Inactivation and the Disposal of the Plant Stress Hormone Jasmonic Acid to the Gas Phase? *Helvetica Chimica Acta*, 80(3), 838–850. <https://doi.org/10.1002/hlca.19970800318>
- Komiya, T., Hachiya, N., Sakaguchi, M., Omura, T., and Mihara, K.** (1994). Recognition of mitochondria-targeting signals by a cytosolic import stimulation factor, MSF. *Journal of Biological Chemistry*, 269(49), 30893–30897. [https://doi.org/10.1016/s0021-9258\(18\)47365-6](https://doi.org/10.1016/s0021-9258(18)47365-6)
- Koo, A. J. K., Gao, X., Daniel Jones, A., and Howe, G. A.** (2009). A rapid wound signal activates the systemic synthesis of bioactive jasmonates in *Arabidopsis*. *Plant Journal*, 59(6), 974–986. <https://doi.org/10.1111/j.1365-313X.2009.03924.x>
- Koo, A. J. K., and Howe, G. A.** (2009). The wound hormone jasmonate. *Phytochemistry*, 70(13–14), 1571–1580. <https://doi.org/10.1016/j.phytochem.2009.07.018>
- Kosugi, S., Hasebe, M., Tomita, M., and Yanagawa, H.** (2008). Nuclear export signal consensus sequences defined using a localization-based yeast selection system. *Traffic*, 9(12), 2053–2062. <https://doi.org/10.1111/j.1600-0854.2008.00825.x>
- Kunze, M., and Berger, J.** (2015). The similarity between N-terminal targeting signals for protein import into different organelles and its evolutionary relevance. *Frontiers in Physiology*, 6(SEP), 1–27. <https://doi.org/10.3389/fphys.2015.00259>
- Laemmli, U. K.** (1970). Cleavage of Structural Proteins during the Assembly of the Head of Bacteriophage T4. *Nature*, 227, 680–685.
- Lee, B. D., Yim, Y., Cañibano, E., Kim, S. H., García-León, M., Rubio, V., Fonseca, F., and Paek, N. C.** (2022). CONSTITUTIVE PHOTOMORPHOGENIC 1 promotes seed germination by destabilizing RGA-LIKE 2 in *Arabidopsis*. *Plant Physiology*, 189(3), 1662–1676. <https://doi.org/10.1093/plphys/kiac060>
- Li, H., and Sun, S.** (2021). Protein aggregation in the ER: Calm behind the storm. *Cells*, 10(12), 1–23. <https://doi.org/10.3390/cells10123337>
- Li, Legong, He, Z., Pandey, G. K., Tsuchiya, T., and Luan, S.** (2002). Functional cloning and characterization of a plant efflux carrier for multidrug and heavy metal detoxification. *Journal of Biological Chemistry*, 277(7), 5360–5368. <https://doi.org/10.1074/jbc.M108777200>
- Li, Lei, Li, C., Lee, G. I., and Howe, G. A.** (2002). Distinct roles for jasmonate synthesis and action in the systemic wound response of tomato. *Proceedings of the National Academy of Sciences of the United States of America*, 99(9), 6416–6421. <https://doi.org/10.1073/pnas.072072599>
- Li, N., Gügel, I. L., Giavalisco, P., Zeisler, V., Schreiber, L., Soll, J., and Philippar, K.** (2015). FAX1, a Novel Membrane Protein Mediating Plastid Fatty Acid Export. *PLoS Biology*, 13(2), 1–37. <https://doi.org/10.1371/journal.pbio.1002053>
- Li, Q., Zheng, J., Li, S., Huang, G., Skilling, S. J., Wang, L., Li, L., Li, M., Yuan, L., and Liu, P.** (2017). Transporter-Mediated Nuclear Entry of Jasmonoyl-Isoleucine Is Essential for Jasmonate Signaling. *Molecular Plant*, 10(5), 695–708. <https://doi.org/10.1016/j.molp.2017.01.010>

- Li, W., Cui, X., Meng, Z., Huang, X., Xie, Q., Wu, H., Jin, H., Zhang, D., and Liang, W. (2012). Transcriptional regulation of arabidopsis MIR168a and ARGONAUTE1 homeostasis in abscisic acid and abiotic stress responses. *Plant Physiology*, 158(3), 1279–1292. <https://doi.org/10.1104/pp.111.188789>
- Lister, R., Chew, O., Lee, M. N., Heazlewood, J. L., Clifton, R., Parker, K. L., Millar, A. H., and Whelan, J. (2004). A Transcriptomic and Proteomic Characterization of the Arabidopsis Mitochondrial Protein Import Apparatus and Its Response to Mitochondrial Dysfunction. *Plant Physiology*, 134(2), 777–789. <https://doi.org/10.1104/pp.103.033910>
- Lou, Y. R., Bor, M., Yan, J., Preuss, A. S., and Jander, G. (2016). Arabidopsis NATA1 acetylates putrescine and decreases defense-related hydrogen peroxide accumulation. *Plant Physiology*, 171(2), 1443–1455. <https://doi.org/10.1104/pp.16.00446>
- Lu, J., Wu, T., Zhang, B., Liu, S., Song, W., Qiao, J., and Ruan, H. (2021). Types of nuclear localization signals and mechanisms of protein import into the nucleus. *Cell Communication and Signaling*, 19(1), 1–10. <https://doi.org/10.1186/s12964-021-00741-y>
- Lyons, R., Manners, J. M., and Kazan, K. (2013). Jasmonate biosynthesis and signaling in monocots: A comparative overview. *Plant Cell Reports*, 32(6), 815–827. <https://doi.org/10.1007/s00299-013-1400-y>
- Maia, J., Dekkers, B. J. W., Provart, N. J., Ligterink, W., and Hilhorst, H. W. M. (2011). The re-establishment of desiccation tolerance in germinated arabidopsis thaliana seeds and its associated transcriptome. *PLoS ONE*, 6(12). <https://doi.org/10.1371/journal.pone.0029123>
- Malabarba, J., Reichelt, M., Pasquali, G., and Mithöfer, A. (2019). Tendril Coiling in Grapevine: Jasmonates and a New Role for GABA? *Journal of Plant Growth Regulation*, 38(1), 39–45. <https://doi.org/10.1007/s00344-018-9807-x>
- Mandaokar, A., Thines, B., Shin, B., Markus Lange, B., Choi, G., Koo, Y. J., Yoo, Y. J., Choi, Y. D., Choi, G., and Browse, J. (2006). Transcriptional regulators of stamen development in Arabidopsis identified by transcriptional profiling. *Plant Journal*, 46(6), 984–1008. <https://doi.org/10.1111/j.1365-313X.2006.02756.x>
- Marillonnet, S., and Grützner, R. (2020). Synthetic DNA Assembly Using Golden Gate Cloning and the Hierarchical Modular Cloning Pipeline. *Current Protocols in Molecular Biology*, 130(1). <https://doi.org/10.1002/cpmb.115>
- Matouschek, A. (2003). Protein unfolding - An important process in vivo? *Current Opinion in Structural Biology*, 13(1), 98–109. [https://doi.org/10.1016/S0959-440X\(03\)00010-1](https://doi.org/10.1016/S0959-440X(03)00010-1)
- Matsumura, M., Nomoto, M., Itaya, T., Aratani, Y., Iwamoto, M., Matsuura, T., Hayashi, Y., Mori, T., Skelly, M. J., Yamamoto, Y. Y., Kinoshita, T., Mori, I. C., Suzuki, T., Betsuyaku, S., Spoel, S. H., Toyota, M., and Tada, Y. (2022). Mechanosensory trichome cells evoke a mechanical stimuli-induced immune response in Arabidopsis thaliana. *Nature Communications*, 13(1), 1–15. <https://doi.org/10.1038/s41467-022-28813-8>
- Matsushima, R., Hayashi, Y., Yamada, K., Shimada, T., Nishimura, M., and Hara-Nishimura, I. (2003). The ER body, a novel endoplasmic reticulum-derived structure in Arabidopsis. *Plant and Cell Physiology*, 44(7), 661–666. <https://doi.org/10.1093/pcp/pcg089>
- Matthes, M., Bruce, T., Chamberlain, K., Pickett, J., and Napier, J. (2011). Emerging roles in plant defense for cis-jasmone-induced cytochrome P450 CYP81D11. *Plant Signaling and Behavior*, 6(4), 563–565. <https://doi.org/10.4161/psb.6.4.14915>
- Matthes, M. C., Bruce, T. J. A., Ton, J., Verrier, P. J., Pickett, J. A., & Napier, J. A. (2010). The transcriptome of cis-jasmone-induced resistance in Arabidopsis thaliana and its role in indirect defence. *Planta*, 232(5), 1163–1180. <https://doi.org/10.1007/s00425-010-1244-4>
- Maynard, D., Viehhauser, A., Knieper, M., Dreyer, A., Manea, G., Telman, W., Butter, F., Chibani, K., Scheibe, R., and Dietz, K. J. (2021). The in vitro interaction of 12-oxophytodienoic acid and related conjugated carbonyl compounds with thiol antioxidants. *Biomolecules*, 11(3), 1–21. <https://doi.org/10.3390/biom11030457>
- McConn, M., and Browse, J. (1996). The critical requirement for linolenic acid is pollen development,



- not photosynthesis, in an arabidopsis mutant. *Plant Cell*, 8(3), 403–416. <https://doi.org/10.2307/3870321>
- Mehrshahi, P., Johnny, C., and DellaPenna, D.** (2014). Redefining the metabolic continuity of chloroplasts and ER. *Trends in Plant Science*, 19(8), 501–507. <https://doi.org/10.1016/j.tplants.2014.02.013>
- Mehrshahi, P., Stefano, G., Andaloro, J. M., Brandizzi, F., Froehlich, J. E., and DellaPenna, D.** (2013). Transorganellar complementation redefines the biochemical continuity of endoplasmic reticulum and chloroplasts. *Proceedings of the National Academy of Sciences of the United States of America*, 110(29), 12126–12131. <https://doi.org/10.1073/pnas.1306331110>
- Mittler, R., Kim, Y. S., Song, L., Coutu, J., Coutu, A., Ciftci-Yilmaz, S., Lee, H., Stevenson, B., and Zhu, J. K.** (2006). Gain- and loss-of-function mutations in Zat10 enhance the tolerance of plants to abiotic stress. *FEBS Letters*, 580(28–29), 6537–6542. <https://doi.org/10.1016/j.febslet.2006.11.002>
- Mizoi, J., Kanazawa, N., Kidokoro, S., Takahashi, F., Qin, F., Morimoto, K., Shinozaki, K., and Yamaguchi-Shinozaki, K.** (2019). Heat-induced inhibition of phosphorylation of the stress-protective transcription factor DREB2A promotes thermotolerance of *Arabidopsis thaliana*. *Journal of Biological Chemistry*, 294(3), 902–917. <https://doi.org/10.1074/jbc.RA118.002662>
- Monte, I., Caballero, J., Zamarreño, A. M., Fernández-Barbero, G., García-Mina, J. M., and Solano, R.** (2022). JAZ is essential for ligand specificity of the COI1/JAZ co-receptor. *Proceedings of the National Academy of Sciences*, 119(49), 2017. <https://doi.org/10.1073/pnas.2212155119>
- Monte, I., Ishida, S., Zamarreño, A. M., Hamberg, M., Franco-Zorrilla, J. M., García-Casado, G., Gouhier-Darimont, C., Reymond, P., Takahashi, K., García-Mina, J. M., Nishihama, R., Kohchi, T., and Solano, R.** (2018). Ligand-receptor co-evolution shaped the jasmonate pathway in land plants. *Nature Chemical Biology*, 14(5), 480–488. <https://doi.org/10.1038/s41589-018-0033-4>
- Monte, I., Kneeshaw, S., Franco-Zorrilla, J. M., Chini, A., Zamarreño, A. M., García-Mina, J. M., and Solano, R.** (2020). An Ancient COI1-Independent Function for Reactive Electrophilic Oxylipins in Thermotolerance. *Current Biology*, 30(6), 962–971.e3. <https://doi.org/10.1016/j.cub.2020.01.023>
- Mueller, M. J., and Berger, S.** (2009). Reactive electrophilic oxylipins: Pattern recognition and signalling. *Phytochemistry*, 70(13–14), 1511–1521. <https://doi.org/10.1016/j.phytochem.2009.05.018>
- Mueller, S., Hilbert, B., Dueckershoff, K., Roitsch, T., Krischke, M., Mueller, M. J., and Berger, S.** (2008). General detoxification and stress responses are mediated by oxidized lipids through TGA transcription factors in arabidopsis. *Plant Cell*, 20(3), 768–785. <https://doi.org/10.1105/tpc.107.054809>
- Müller, S. M., Wang, S., Telman, W., Liebthal, M., Schnitzer, H., Viehhauser, A., Sticht, C., Delatorre, C., Wirtz, M., Hell, R., and Dietz, K. J.** (2017). The redox-sensitive module of cyclophilin 20-3, 2-cysteine peroxiredoxin and cysteine synthase integrates sulfur metabolism and oxylipin signaling in the high light acclimation response. *Plant Journal*, 91(6), 995–1014. <https://doi.org/10.1111/tpj.13622>
- Munemasa, S., Mori, I. C., and Murata, Y.** (2011). Methyl jasmonate signaling and signal crosstalk between methyl jasmonate and abscisic acid in guard cells. *Plant Signaling and Behavior*, 6(7), 939–941. <https://doi.org/10.4161/psb.6.7.15439>
- Nadja Sperling.** (2012). Regulation der Jasmonsäure-Synthese durch reversible Dimerisierung der Oxophytodiensäurereductase 3 (OPR3). Doctoral dissertation, Universität Hohenheim.
- Nagpal, P., Ellis, C. M., Weber, H., Ploense, S. E., Barkawi, L. S., Guilfoyle, T. J., Hagen, G., Alonso, J. M., Cohen, J. D., Farmer, E. E., Ecker, J. R., and Reed, J. W.** (2005). Auxin response factors ARF6 and ARF8 promote jasmonic acid production and flower maturation. *Development*, 132(18), 4107–4118. <https://doi.org/10.1242/dev.01955>
- Nakano, R. T., Yamada, K., Bednarek, P., Nishimura, M., and Hara-Nishimura, I.** (2014). ER bodies

- in plants of the Brassicales order: Biogenesis and association with innate immunity. *Frontiers in Plant Science*, 5(MAR), 1–17. <https://doi.org/10.3389/fpls.2014.00073>
- Nawrath, C., Heck, S., Parinthewong, N., and Métraux, J. P.** (2002). EDS5, an essential component of salicylic acid-dependent signaling for disease resistance in Arabidopsis, is a member of the MATE transporter family. *Plant Cell*, 14(1), 275–286. <https://doi.org/10.1105/tpc.010376>
- Nelson, B. K., Cai, X., and Nebenführ, A.** (2007). A multicolored set of in vivo organelle markers for co-localization studies in Arabidopsis and other plants. *Plant Journal*, 51(6), 1126–1136. <https://doi.org/10.1111/j.1365-313X.2007.03212.x>
- Nguyen, T. N., Tuan, P. A., and Ayele, B. T.** (2022). Jasmonate regulates seed dormancy in wheat via modulating the balance between gibberellin and abscisic acid. *Journal of Experimental Botany*, 73(8), 2434–2453. <https://doi.org/10.1093/jxb/erac041>
- Norkunas, K., Harding, R., Dale, J., and Dugdale, B.** (2018). Improving agroinfiltration-based transient gene expression in *Nicotiana benthamiana*. *Plant Methods*, 14(1), 1–14. <https://doi.org/10.1186/s13007-018-0343-2>
- O'Malley, R. C., Barragan, C. C., and Ecker, J. R.** (2015). HHMI Author Manuscript A User's Guide to the Arabidopsis T-DNA Insertional Mutant Collections. *Methods in Molecular Biology*, 323–342.
- Ohkama-Ohtsu, N., Sasaki-Sekimoto, Y., Oikawa, A., Jikumaru, Y., Shinoda, S., Inoue, E., Kamide, Y., Yokoyama, T., Hirai, M. Y., Shirasu, K., Kamiya, Y., Oliver, D. J., and Saito, K.** (2011). 12-Oxo-phytodienoic acid-glutathione conjugate is transported into the vacuole in Arabidopsis. *Plant and Cell Physiology*, 52(1), 205–209. <https://doi.org/10.1093/pcp/pcq181>
- Otto, M., Naumann, C., Brandt, W., Wasternack, C., and Hause, B.** (2016). Activity regulation by heteromerization of Arabidopsis allene oxide cyclase family members. *Plants*. <https://doi.org/10.3390/plants5010003>
- Paauw, M., van Hulten, M., Chatterjee, S., Berg, J. A., Taks, N. W., Giesbers, M., Richard, M. M.S., and van den Burg, H. A.** (2023). Hydathode immunity protects the Arabidopsis leaf vasculature against colonization by bacterial pathogens. *Current Biology*, 33(4), 697–710.e6. <https://doi.org/10.1016/j.cub.2023.01.013>
- Pan, J., Hu, Y., Wang, H., Guo, Q., Chen, Y., Howe, G. A., and Yu, D.** (2020). Molecular mechanism underlying the synergistic effect of jasmonate on abscisic acid signaling during seed germination in Arabidopsis. *Plant Cell*, 32(12), 3846–3865. <https://doi.org/10.1105/tpc.19.00838>
- Park, J. H., Halitschke, R., Kim, H. B., Baldwin, I. T., Feldmann, K. A., and Feyereisen, R.** (2002). A knock-out mutation in allene oxide synthase results in male sterility and defective wound signal transduction in Arabidopsis due to a block in jasmonic acid biosynthesis. *Plant Journal*, 31(1), 1–12. <https://doi.org/10.1046/j.1365-313X.2002.01328.x>
- Park, S. W., Li, W., Viehhauser, A., He, B., Kim, S., Nilsson, A. K., Andersson, M. X., Kittle, J. D., Ambavaram, M. M. R., Luan, S., Esker, A. R., Tholl, D., Cimini, D., Ellerström, M., Coaker, G., Mitchell, T. K., Pereira, A., Dietz, K. J., and Lawrence, C. B.** (2013). Cyclophilin 20-3 relays a 12-oxo-phytodienoic acid signal during stress responsive regulation of cellular redox homeostasis. *Proceedings of the National Academy of Sciences of the United States of America*, 110(23), 9559–9564. <https://doi.org/10.1073/pnas.1218872110>
- Parkes, J. A., Langer, S., Hartig, A., and Bakert, A.** (2003). PTS1-independent targeting of isocitrate lyase to peroxisomes requires the PTS1 receptor Pex5p. *Molecular Membrane Biology*, 20(1), 61–69. <https://doi.org/10.1080/0968768031000047859>
- Pedranzani, H., Sierra-De-Grado, R., Vigliocco, A., Miersch, O., and Abdala, G.** (2007). Cold and water stresses produce changes in endogenous jasmonates in two populations of *Pinus pinaster* Ait. *Plant Growth Regulation*, 52(2), 111–116. <https://doi.org/10.1007/s10725-007-9166-2>
- Pollmann, S., Springer, A., Rustgi, S., Von Wettstein, D., Kang, C. H., Reinbothe, C., and Reinbothe, S.** (2019). Substrate channeling in oxylipin biosynthesis through a protein complex in the plastid envelope of Arabidopsis thaliana. *Journal of Experimental Botany*, 70(5), 1497–1511. <https://doi.org/10.1093/jxb/erz015>
- Prasad, A., Sedlářová, M., Balukova, A., Rác, M., and Pospíšil, P.** (2020). Reactive Oxygen Species

- as a Response to Wounding: In Vivo Imaging in *Arabidopsis thaliana*. *Frontiers in Plant Science*, 10(January), 1–10. <https://doi.org/10.3389/fpls.2019.01660>
- Raikhel, N.** (1992). Nuclear targeting in plants. *Plant Physiology*, 100(4), 1627–1632. <https://doi.org/10.1104/pp.100.4.1627>
- Raorane, M. L., Narciso, J. O., and Kohli, A.** (2016). Total soluble protein extraction for improved proteomic analysis of transgenic rice plant roots. *Methods in Molecular Biology*, 1385, 139–147. [https://doi.org/10.1007/978-1-4939-3289-4\\_10](https://doi.org/10.1007/978-1-4939-3289-4_10)
- Reeves, P. H., Ellis, C. M., Ploense, S. E., Wu, M. F., Yadav, V., Tholl, D., Chételat, A., Haupt, I., Kennerley, B. J., Hodgens, C., Farmer, E. E., Nagpal, P., and Reed, J. W.** (2012). A regulatory network for coordinated flower maturation. *PLoS Genetics*, 8(2). <https://doi.org/10.1371/journal.pgen.1002506>
- Reymond, P., Bodenhausen, N., Van Poecke, R. M. P., Krishnamurthy, V., Dicke, M., and Farmer, E. E.** (2004). A conserved transcript pattern in response to a specialist and a generalist herbivore. *Plant Cell*, 16(11), 3132–3147. <https://doi.org/10.1105/tpc.104.026120>
- Reymond, P., Weber, H., Damond, M., and Farmer, E. E.** (2000). Differential gene expression in response to mechanical wounding and insect feeding in *Arabidopsis*. *Plant Cell*, 12(5), 707–719. <https://doi.org/10.1105/tpc.12.5.707>
- Ribot, C., Zimmerli, C., Farmer, E. E., Reymond, P., and Poirier, Y.** (2008). Induction of the *Arabidopsis* PHO1;H10 gene by 12-oxo-phytodienoic acid but not jasmonic acid via a Coronatine Insensitive1-dependent pathway. *Plant Physiology*, 147(2), 696–706. <https://doi.org/10.1104/pp.108.119321>
- Rodriguez-Enriquez, M. J., Mehdi, S., Dickinson, H. G., and Grant-Downton, R. T.** (2013). A novel method for efficient in vitro germination and tube growth of *Arabidopsis thaliana* pollen. *New Phytologist*, 197(2), 668–679. <https://doi.org/10.1111/nph.12037>
- Rowan, B. A., Oldenburg, D. J., and Bendich, A. J.** (2010). RecA maintains the integrity of chloroplast DNA molecules in *Arabidopsis*. *Journal of Experimental Botany*, 61(10), 2575–2588. <https://doi.org/10.1093/jxb/erq088>
- Saito, H., Oikawa, T., Hamamoto, S., Ishimaru, Y., Kanamori-Sato, M., Sasaki-Sekimoto, Y., Utsumi, T., Chen, J., Kanno, Y., Masuda, S., Kamiya, Y., Seo, M., Uozumi, N., Ueda, M., and Ohta, H.** (2015). The jasmonate-responsive GTR1 transporter is required for gibberellin-mediated stamen development in *Arabidopsis*. *Nature Communications*, 6, 1–11. <https://doi.org/10.1038/ncomms7095>
- Sakuma, Y., Maruyama, K., Qin, F., Osakabe, Y., Shinozaki, K., and Yamaguchi-Shinozaki, K.** (2006). Dual function of an *Arabidopsis* transcription factor DREB2A in water-stress-responsive and heat-stress-responsive gene expression. *Proceedings of the National Academy of Sciences of the United States of America*, 103(49), 18822–18827. <https://doi.org/10.1073/pnas.0605639103>
- Satheesh, V., Chidambaranathan, P., Jagannadham, P. T., Kohli, D., Jain, P. K., Bhat, S. R., and Srinivasan, R.** (2014). A polyketide cyclase/dehydrase and lipid transport superfamily gene of *Arabidopsis* and its orthologue of chickpea exhibit rapid response to wounding. *Indian Journal of Genetics and Plant Breeding*, 74(4), 463–470. <https://doi.org/10.5958/0975-6906.2014.00871.2>
- Schaller, A., and Stintzi, A.** (2008). Jasmonate biosynthesis and signaling for induced plant defense against herbivory. *Induced Plant Resistance to Herbivory*, 349–366. [https://doi.org/10.1007/978-1-4020-8182-8\\_17](https://doi.org/10.1007/978-1-4020-8182-8_17)
- Schaller, A., and Stintzi, A.** (2009). Enzymes in jasmonate biosynthesis - Structure, function, regulation. *Phytochemistry*, 70(13–14), 1532–1538. <https://doi.org/10.1016/j.phytochem.2009.07.032>
- Schaller, F., Biesgen, C., Müssig, C., Altmann, T., and Weiler, E. W.** (2000). 12-oxophytodienoate reductase 3 (OPR3) is the isoenzyme involved in jasmonate biosynthesis. *Planta*, 210(6), 979–984. <https://doi.org/10.1007/s004250050706>
- Schaller, F., Hennig, P., and Weiler, E. W.** (1998). 12-oxophytodienoate- 10, 11-reductase: Occurrence of two isoenzymes of different specificity against stereoisomers of 12-oxophytodienoic

- acid. *Plant Physiology*, 118(4), 1345–1351. <https://doi.org/10.1104/pp.118.4.1345>
- Schmittgen, T. D., and Livak, K. J.** (2008). Analyzing real-time PCR data by the comparative CT method. *Nature Protocols*, 3(6), 1101–1108. <https://doi.org/10.1038/nprot.2008.73>
- Scholz, S. S., Reichelt, M., Boland, W., and Mithöfer, A.** (2015). Additional evidence against jasmonate-induced jasmonate induction hypothesis. *Plant Science*, 239, 9–14. <https://doi.org/10.1016/j.plantsci.2015.06.024>
- Schrack, K., Nguyen, D., Karlowski, W. M., and Mayer, K. F. X.** (2004). START lipid/sterol-binding domains are amplified in plants and are predominantly associated with homeodomain transcription factors. *Genome Biology*, 5(6), 1–16. <https://doi.org/10.1186/gb-2004-5-6-r41>
- Schubert, R., Dobritsch, S., Gruber, C., Hause, G., Athmer, B., Schreiber, T., Marillonnet, S., Okabe, Y., Ezura, H., Acosta, I. F., Tarkowska, D., and Hause, B.** (2019). Tomato myb21 acts in ovules to mediate jasmonate-regulated fertility. *Plant Cell*, 31(5), 1043–1062. <https://doi.org/10.1105/tpc.18.00978>
- Schulze, A., Zimmer, M., Mielke, S., Stellmach, H., Melnyk, C. W., Hause, B., and Gasperini, D.** (2019). Wound-Induced Shoot-to-Root Relocation of JA-Ile Precursors Coordinates Arabidopsis Growth. *Molecular Plant*, 12(10), 1383–1394. <https://doi.org/10.1016/j.molp.2019.05.013>
- Schuman, M. C., Meldau, S., Gaquerel, E., Diezel, C., McGale, E., Greenfield, S., and Baldwin, I. T.** (2018). The active jasmonate JA-Ile regulates a specific subset of plant jasmonate-mediated resistance to herbivores in nature. *Frontiers in Plant Science*, 9(June). <https://doi.org/10.3389/fpls.2018.00787>
- Sheard, L. B., Tan, X., Mao, H., Withers, J., Ben-Nissan, G., Hinds, T. R., Kobayashi, Y., Hsu, F. F., Sharon, M., Browse, J., He, S. Y., Rizo, J., Howe, G. A., and Zheng, N.** (2010). Jasmonate perception by inositol-phosphate-potentiated COI1-JAZ co-receptor. *Nature*, 468(7322), 400–407. <https://doi.org/10.1038/nature09430>
- Shen, J., Zeng, Y., Zhuang, X., Sun, L., Yao, X., Pimpl, P., and Jiang, L.** (2013). Organelle pH in the arabidopsis endomembrane system. *Molecular Plant*, 6(5), 1419–1437. <https://doi.org/10.1093/mp/sst079>
- Shi, H., Wang, X., Ye, T., Chen, F., Deng, J., Yang, P., Zhang, Y., and Chan, Z.** (2014). The cysteine2/histidine2-type transcription factor zinc finger of arabidopsis thaliana6 modulates biotic and abiotic stress responses by activating salicylic acid-related genes and c-repeat-binding factor genes in arabidopsis. *Plant Physiology*, 165(3), 1367–1379. <https://doi.org/10.1104/pp.114.242404>
- Shimada, T. L., Shimada, T., and Hara-Nishimura, I.** (2010). A rapid and non-destructive screenable marker, FAST, for identifying transformed seeds of Arabidopsis thaliana: TECHNICAL ADVANCE. *Plant Journal*, 61(3), 519–528. <https://doi.org/10.1111/j.1365-313X.2009.04060.x>
- Shin, B., Choi, G., Yi, H., Yang, S., Cho, I., Kim, J., Lee, S., Paek, N-C., Kim, J-H., Song, P-S., and Choi, G.** (2002). AtMYB21, a gene encoding a flower-specific transcription factor, is regulated by COP1. *Plant Journal*, 30(1), 23–32. <https://doi.org/10.1046/j.1365-313X.2002.01264.x>
- Shoji, T., Inai, K., Yazaki, Y., Sato, Y., Takase, H., Shitan, N., Yazaki, K., Goto, Y., Toyooka, K., Matsuoka, K., and Hashimoto, T.** (2009). Multidrug and toxic compound extrusion-type transporters implicated in vacuolar sequestration of nicotine in tobacco roots. *Plant Physiology*, 149(2), 708–718. <https://doi.org/10.1104/pp.108.132811>
- Simeoni, F., Skiryycz, A., Simoni, L., Castorina, G., Souza, L. P. De, Fernie, A. R., Alseekh, S., Giavalisco, P., Conti, L., Tonelli, C., and Galbiati, M.** (2022). The AtMYB60 transcription factor regulates stomatal opening by modulating oxylipin synthesis in guard cells. *Scientific Reports*, (0123456789), 1–12. <https://doi.org/10.1038/s41598-021-04433-y>
- Simm, S., Papasotiriou, D. G., Ibrahim, M., Leisegang, M. S., Müller, B., Schorge, T., Karas, M., Mirus, O., Sommer, M. S., and Schleiff, E.** (2013). Defining the core proteome of the chloroplast envelope membranes. *Frontiers in Plant Science*, 4(FEB), 1–18. <https://doi.org/10.3389/fpls.2013.00011>
- Singh, P., Dave, A., Vaistij, F. E., Worrall, D., Holroyd, G. H., Wells, J. G., Kaminski, F., Graham, I.**



- A., and Roberts, M. R.** (2017). Jasmonic acid-dependent regulation of seed dormancy following maternal herbivory in *Arabidopsis*. *New Phytologist*, 214(4), 1702–1711. <https://doi.org/10.1111/nph.14525>
- Smyth, D. R., Bowman, J. L., and Meyerowitz, E. M.** (1990). Early flower development in *Arabidopsis*. *The Plant Cell*, 2(8), 755–767. <https://doi.org/10.1105/tpc.2.8.755>
- Song, S., Qi, T., Huang, H., Ren, Q., Wu, D., Chang, C., Peng, W., Liu, Y., Peng, J., & Xie, D.** (2011). The jasmonate-ZIM domain proteins interact with the R2R3-MYB transcription factors MYB21 and MYB24 to affect jasmonate-regulated stamen development in *Arabidopsis*. *Plant Cell*, 23(3), 1000–1013. <https://doi.org/10.1105/tpc.111.083089>
- Staswick, P. E., Su, W., and Howell, S. H.** (1992). Methyl jasmonate inhibition of root growth and induction of a leaf protein are decreased in an *Arabidopsis thaliana* mutant. *Proceedings of the National Academy of Sciences of the United States of America*, 89(15), 6837–6840. <https://doi.org/10.1073/pnas.89.15.6837>
- Statello, L., Guo, C. J., Chen, L. L., and Huarte, M.** (2021). Gene regulation by long non-coding RNAs and its biological functions. *Nature Reviews Molecular Cell Biology*, 22(2), 96–118. <https://doi.org/10.1038/s41580-020-00315-9>
- Stawska, M., and Oracz, K.** (2019). Phyb and hy5 are involved in the blue light-mediated alleviation of dormancy of *Arabidopsis* seeds possibly via the modulation of expression of genes related to light, ga, and aba. *International Journal of Molecular Sciences*, 20(23). <https://doi.org/10.3390/ijms20235882>
- Stellmach, H., Hose, R., Råde, A., Marillonnet, S., and Hause, B.** (2022). A New Set of Golden-Gate-Based Organelle Marker Plasmids for Colocalization Studies in Plants. *Plants*, 11(19). <https://doi.org/10.3390/plants11192620>
- Stelmach, B. A., Müller, A., Hennig, P., Laudert, D., Andert, L., and Weiler, E. W.** (1998). Quantitation of the octadecanoid 12-oxo-phytodienoic acid, a signalling compound in plant mechanotransduction. *Phytochemistry*, 47(4), 539–546. [https://doi.org/10.1016/S0031-9422\(97\)00547-5](https://doi.org/10.1016/S0031-9422(97)00547-5)
- Stenzel, I., Hause, B., Miersch, O., Kurz, T., Maucher, H., Weichert, H., Ziegler, J., Feussner, I., and Wasternack, C.** (2003). Jasmonate biosynthesis and the allene oxide cyclase family of *Arabidopsis thaliana*. *Plant Molecular Biology*, 51(6), 895–911. <https://doi.org/10.1023/A:1023049319723>
- Stenzel, I., Otto, M., Delker, C., Kirmse, N., Schmidt, D., Miersch, O., Hause, B., and Wasternack, C.** (2012). ALLENE OXIDE CYCLASE (AOC) gene family members of *Arabidopsis thaliana*: Tissue- and organ-specific promoter activities and in vivo heteromerization. *Journal of Experimental Botany*. <https://doi.org/10.1093/jxb/ers261>
- Stintzi, A., and Browse, J.** (2000). The *Arabidopsis* male-sterile mutant, opr3, lacks the 12-oxophytodienoic acid reductase required for jasmonate synthesis. *Proceedings of the National Academy of Sciences of the United States of America*, 97(19), 10625–10630. <https://doi.org/10.1073/pnas.190264497>
- Stintzi, A., Weber, H., Reymond, P., Browse, J., and Farmer, E. E.** (2001). Plant defense in the absence of jasmonic acid: The role of cyclopentenones. *Proceedings of the National Academy of Sciences of the United States of America*, 98(22), 12837–12842. <https://doi.org/10.1073/pnas.211311098>
- Stracke, R., Werber, M., & Weisshaar, B.** (2001). The R2R3-MYB gene family in *Arabidopsis thaliana*. *Current Opinion in Plant Biology*, 4(5), 447–456. [https://doi.org/10.1016/S1369-5266\(00\)00199-0](https://doi.org/10.1016/S1369-5266(00)00199-0)
- Suza, W. P., and Staswick, P. E.** (2008). The role of JAR1 in Jasmonoyl-l-isoleucine production during *Arabidopsis* wound response. *Planta*, 227(6), 1221–1232. <https://doi.org/10.1007/s00425-008-0694-4>
- Taki, N., Sasaki-Sekimoto, Y., Obayashi, T., Kikuta, A., Kobayashi, K., Ainai, T., Yagi, K., Sakurai, N., Suzuki, H., Masuda, T., Takamiya, K.-I., Shibata, D., Kobayashi, Y., and Ohta, H.** (2005). 12-Oxo-phytodienoic acid triggers expression of a distinct set of genes and plays a role in wound-

- induced gene expression in Arabidopsis. *Plant Physiology*. <https://doi.org/10.1104/pp.105.067058>
- Tena, G.** (2023). Hydathodes as security gates. *Nature Plants*, 9(2), 194. <https://doi.org/10.1038/s41477-023-01363-7>
- Theodoulou, F. L., Job, K., Slocombe, S. P., Footitt, S., Holdsworth, M., Baker, A., Larson, T. R., and Graham, I. A.** (2005). Jasmonic acid levels are reduced in COMATOSE ATP-binding cassette transporter mutants. Implications for transport of jasmonate precursors into peroxisomes. *Plant Physiology*. <https://doi.org/10.1104/pp.105.059352>
- Thireault, C., Shyu, C., Yoshida, Y., St. Aubin, B., Campos, M. L., and Howe, G. A.** (2015). Repression of jasmonate signaling by a non-TIFY JAZ protein in Arabidopsis. *Plant Journal*, 82(4), 669–679. <https://doi.org/10.1111/tpj.12841>
- Thoms, S.** (2015). Import of proteins into peroxisomes: Piggybacking to a new home away from home. *Open Biology*, 5(11), 0–3. <https://doi.org/10.1098/rsob.150148>
- Thuswaldner, S., Lagerstedt, J. O., Rojas-Stütz, M., Bouhidel, K., Der, C., Leborgne-Castel, N., Mishra, A., Marty, F., Schoefs, B., Adamska, I., Persson, B. L., and Spetea, C.** (2007). Identification, expression, and functional analyses of a thylakoid ATP/ADP carrier from Arabidopsis. *Journal of Biological Chemistry*, 282(12), 8848–8859. <https://doi.org/10.1074/jbc.M609130200>
- Truman, W., Bennet, M. H., Kubigsteltig, I., Turnbull, C., and Grant, M.** (2007). Arabidopsis systemic immunity uses conserved defense signaling pathways and is mediated by jasmonates. *Proceedings of the National Academy of Sciences of the United States of America*, 104(3), 1075–1080. <https://doi.org/10.1073/pnas.0605423104>
- Upadhyay, N., Kar, D., and Datta, S.** (2020). A multidrug and toxic compound extrusion (MATE) transporter modulates auxin levels in root to regulate root development and promotes aluminium tolerance. *Plant Cell and Environment*, 43(3), 745–759. <https://doi.org/10.1111/pce.13658>
- Varshney, V., and Majee, M.** (2021). JA Shakes Hands with ABA to Delay Seed Germination. *Trends in Plant Science*, 26(8), 764–766. <https://doi.org/10.1016/j.tplants.2021.05.002>
- Verhage, A., Vlaardingerbroek, I., Raaymakers, C., Van Dam, N. M., Dicke, M., Van Wees, S. C. M., and Pieterse, C. M. J.** (2011). Rewiring of the Jasmonate signaling pathway in Arabidopsis during insect herbivory. *Frontiers in Plant Science*, 2(SEP), 1–12. <https://doi.org/10.3389/fpls.2011.00047>
- Vijayan, P., Shockey, J., Lévesque, C. A., Cook, R. J., and Browse, J.** (1998). A role for jasmonate in pathogen defense of Arabidopsis. *Proceedings of the National Academy of Sciences of the United States of America*, 95(12), 7209–7214. <https://doi.org/10.1073/pnas.95.12.7209>
- Vincenti, S., Mariani, M., Alberti, J. C., Jacopini, S., de Caraffa, V. B. B., Berti, L., and Maury, J.** (2019). Biocatalytic synthesis of natural green leaf volatiles using the lipoxygenase metabolic pathway. *Catalysts*, 9(10). <https://doi.org/10.3390/catal9100873>
- Volkner, C., Holzner, L. J., Day, P. M., Ashok, A. D., De Vries, J., Bolter, B., and Kunz, H. H.** (2021). Two plastid POLLUX ion channel-like proteins are required for stress-triggered stromal Ca<sup>2+</sup> release. *Plant Physiology*, 187(4), 2110–2125. <https://doi.org/10.1093/plphys/kiab424>
- Von Malek, B., Van Der Graaff, E., Schneitz, K., and Keller, B.** (2002). The Arabidopsis male-sterile mutant *dde2-2* is defective in the ALLENE OXIDE SYNTHASE gene encoding one of the key enzymes of the jasmonic acid biosynthesis pathway. *Planta*, 216(1), 187–192. <https://doi.org/10.1007/s00425-002-0906-2>
- Wang, H., Wang, J., Jiang, J., Chen, S., Guan, Z., Liao, Y., and Chen, F.** (2014). Reference genes for normalizing transcription in diploid and tetraploid Arabidopsis. *Scientific Reports*, 4(Table 1), 1–8. <https://doi.org/10.1038/srep06781>
- Wang, Y., Hou, Y., Qiu, J., Wang, H., Wang, S., Tang, L., Tong, X., and Zhang, J.** (2020). Abscisic acid promotes jasmonic acid biosynthesis via a 'SAPK10-bZIP72-AOC' pathway to synergistically inhibit seed germination in rice (*Oryza sativa*). *New Phytologist*, 228(4), 1336–1353. <https://doi.org/10.1111/nph.16774>
- Wasternack, C.** (2007). Jasmonates: An update on biosynthesis, signal transduction and action in plant



- stress response, growth and development. *Annals of Botany*. <https://doi.org/10.1093/aob/mcm079>
- Wasternack, C., and Hause, B.** (2013). Jasmonates: Biosynthesis, perception, signal transduction and action in plant stress response, growth and development. An update to the 2007 review in *Annals of Botany*. *Annals of Botany*, 111(6), 1021–1058. <https://doi.org/10.1093/aob/mct067>
- Wasternack, Claus, and Feussner, I.** (2018). The Oxylipin Pathways: Biochemistry and Function. *Annual Review of Plant Biology*, 69, 363–386. <https://doi.org/10.1146/annurev-arplant-042817-040440>
- Wasternack, Claus, Forner, S., Strnad, M., and Hause, B.** (2013). Jasmonates in flower and seed development. *Biochimie*, 95(1), 79–85. <https://doi.org/10.1016/j.biochi.2012.06.005>
- Wasternack, Claus, and Hause, B.** (2018). A Bypass in Jasmonate Biosynthesis – the OPR3-independent Formation. *Trends in Plant Science*, 23(4), 276–279. <https://doi.org/10.1016/j.tplants.2018.02.011>
- Wasternack, Claus, Miersch, O., Kramell, R., Hause, B., Ward, J., Beale, M., Boland, W., Parthier, B., and Feussner, I.** (1998). Jasmonic acid: biosynthesis, signal transduction, gene expression. *Lipid - Fett*, 100(4–5), 139–146. [https://doi.org/10.1002/\(sici\)1521-4133\(19985\)100:4/5<139::aid-lipi139>3.3.co;2-x](https://doi.org/10.1002/(sici)1521-4133(19985)100:4/5<139::aid-lipi139>3.3.co;2-x)
- Wasternack, Claus, Stenzel, I., Hause, B., Hause, G., Kutter, C., Maucher, H., Neumerkel, J., Feussner, I., and Miersch, O.** (2006). The wound response in tomato - Role of jasmonic acid. *Journal of Plant Physiology*, 163(3), 297–306. <https://doi.org/10.1016/j.jplph.2005.10.014>
- Williams, R. E., and Bruce, N. C.** (2002). “New uses for an old enzyme” - The Old Yellow Enzyme family of flavoenzymes. *Microbiology*, 148(6), 1607–1614. <https://doi.org/10.1099/00221287-148-6-1607>
- Xie, X. D., Feys, B. F., James, S., Nieto-rostro, M., and Turnert, J. G.** (2017). COI1 : An Arabidopsis Gene Required for Jasmonate-Regulated Defense and Fertility. *Science*, 280,1091-1094(1998).DOI:10.1126/science.280.5366.1091
- Xu, L., Liu, F., Lechner, E., Genschik, P., Crosby, W. L., Ma, H., Peng, W., Huang, D., and Xie, D.** (2002). The SCFCO11 ubiquitin-ligase complexes are required for jasmonate response in Arabidopsis. *Plant Cell*, 14(8), 1919–1935. <https://doi.org/10.1105/tpc.003368>
- Yagi, H., Tamura, K., Matsushita, T., and Shimada, T.** (2021). Spatiotemporal relationship between auxin dynamics and hydathode development in Arabidopsis leaf teeth. *Plant Signaling and Behavior*, 16(12). <https://doi.org/10.1080/15592324.2021.1989216>
- Yan, J., Li, S., Gu, M., Yao, R., Li, Y., Chen, J., Yang, M., Tong, J., Xiao, L., Nan, F., and Xie, D.** (2016). Endogenous bioactive jasmonate is composed of a set of (+)-7-iso-JA-amino acid conjugates. *Plant Physiology*, 172(4), 2154–2164. <https://doi.org/10.1104/pp.16.00906>
- Yan, Y., Stolz, S., Chételat, A., Reymond, P., Pagni, M., Dubugnon, L., and Farmer, E. E.** (2007). A downstream mediator in the growth repression limb of the jasmonate pathway. *Plant Cell*, 19(8), 2470–2483. <https://doi.org/10.1105/tpc.107.050708>
- Zhang, H., Zhu, H., Pan, Y., Yu, Y., Luan, S., and Li, L.** (2014). A DTX/MATE-type transporter facilitates abscisic acid efflux and modulates ABA sensitivity and drought tolerance in Arabidopsis. *Molecular Plant*, 7(10), 1522–1532. <https://doi.org/10.1093/mp/ssu063>
- Zhang, Xiuren, Henriques, R., Lin, S. S., Niu, Q. W., and Chua, N. H.** (2006). Agrobacterium-mediated transformation of Arabidopsis thaliana using the floral dip method. *Nature Protocols*, 1(2), 641–646. <https://doi.org/10.1038/nprot.2006.97>
- Zhang, Xueying, He, Y., Li, L., Liu, H., and Hong, G.** (2021). Involvement of the R2R3-MYB transcription factor MYB21 and its homologs in regulating flavonol accumulation in Arabidopsis stamen. *Journal of Experimental Botany*, 72(12), 4319–4332. <https://doi.org/10.1093/jxb/erab156>
- Zhao, X., Li, N., Song, Q., Li, X., Meng, H., and Luo, K.** (2021). OPDAT1, a plastid envelope protein involved in 12-oxo-phytodienoic acid export for jasmonic acid biosynthesis in Populus. *Tree Physiology*, 41(9), 1714–1728. <https://doi.org/10.1093/treephys/tpab037>

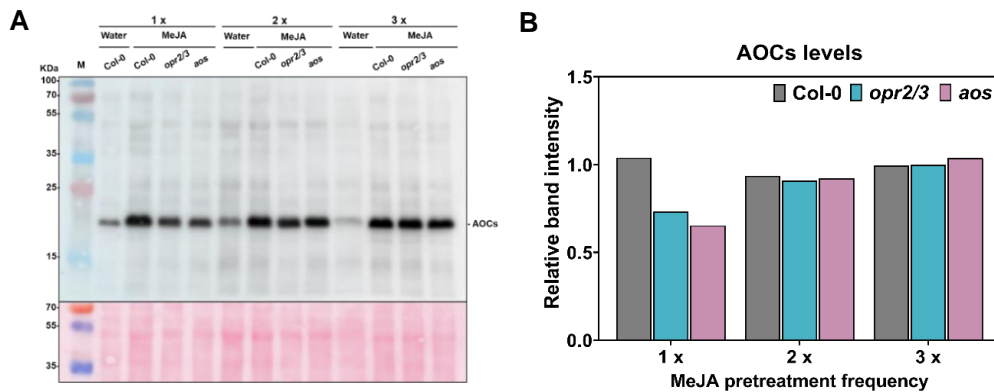
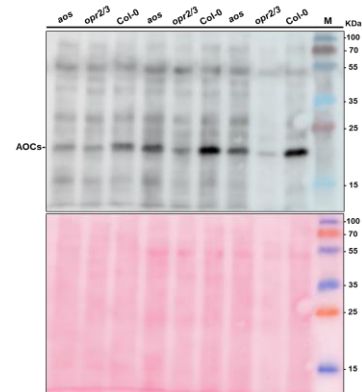
- Zheng, Y., Cui, X., Su, L., Fang, S., Chu, J., Gong, Q., Yang, J., and Zhu, Z.** (2017). Jasmonate inhibits COP1 activity to suppress hypocotyl elongation and promote cotyledon opening in etiolated *Arabidopsis* seedlings. *Plant Journal*, *90*(6), 1144–1155. <https://doi.org/10.1111/tpj.13539>
- Zhou, L. H., Liu, S. B., Wang, P. F., Lu, T. J., Xu, F., Genin, G. M., and Pickard, B. G.** (2017). The *Arabidopsis* trichome is an active mechanosensory switch. *Plant Cell and Environment*, *40*(5), 611–621. <https://doi.org/10.1111/pce.12728>

## Appendix

**Fig. S1 Anti-AOC immunoblots with four biological replicates.**

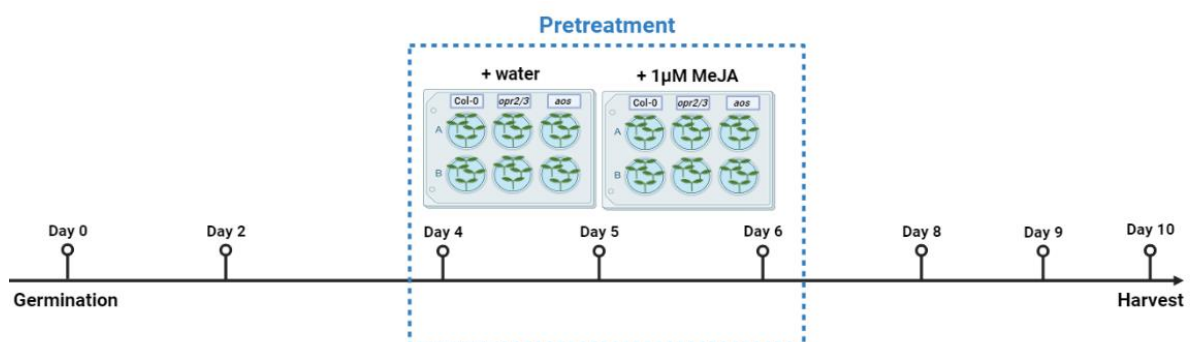
Ten-day-old seedlings from Col-0, *opr2/3* and *aos*.

Each lane represents a biological replicate. Ponceau staining was used as internal control to verify equal protein loading. Immunolabeling was done by chemiluminescence using an anti-rabbit-IgG antibody conjugated to Alkaline Phosphatase. M= protein marker.

**Fig. S2 AOC protein levels restitution in the mutants is MeJA-dose-dependent.**

**A:** Immunoblot showing AOCs protein content in seedlings of Col-0, *opr2/3* and *aos* subjected to MeJA pretreatment during development and Col-0 mock-pretreated as control. 1 $\mu$ M MeJA was added at different frequencies during the seedling's growth to the 10-days stage. Water was added instead for the Mock condition. Anti-AOCs primary antibody was used for the detection of the AOC proteins from the total protein extract. Ponceau S staining was used as internal control to verify equal proteins loadings. Immunolabeling was visualized by chemiluminescence using an anti-rabbit-IgG antibody conjugated to Alkaline Phosphatase. M= protein marker.

**B:** Relative AOCs protein levels in Col-0, *opr2/3* and *aos* mutants following MeJA pretreatment. AOCs band intensity was quantified from the immunoblot by Image J and normalized to the total protein intensity of the Ponceau S staining. Bars represent one biological replicate.

**Fig. S3 The MeJA pretreatment experimental setup to mimic the JA-positive feedback loop during development.**

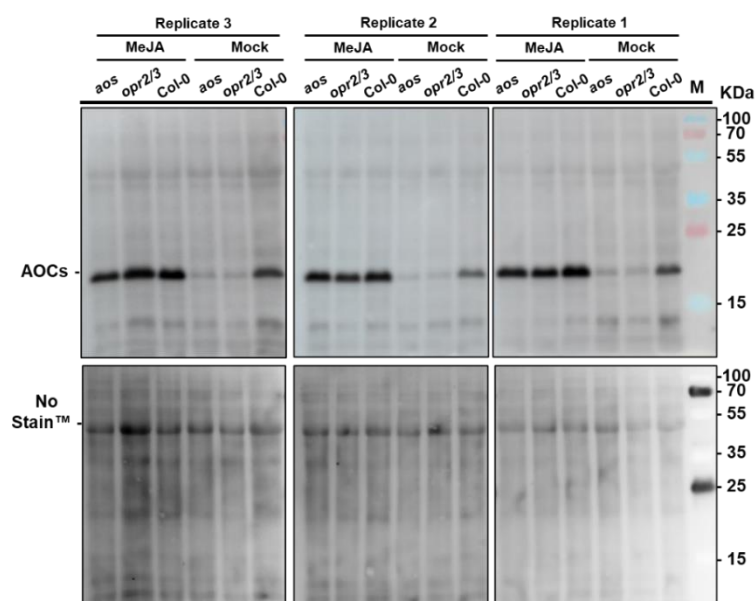


**Fig. S4 Anti-AOC proteins immunoblots with three biological replicates.**

Ten-day-old seedlings Col-0, *opr2/3* and *aos* seedlings were grown in liquid  $\frac{1}{2}$  MS medium. The schedule of the seedling's growth and the MeJA pretreatment during development. Samples pretreated with water (Mock) were used as controls for the pretreatment. Ten-day-old seedlings from Col-0, *opr2/3* and *aos* were pretreated with MeJA during development (MeJA) or with water (Mock). AOCs protein levels determination in Col-0, *opr2/3* and *aos* seedlings by immunoblotting from 7  $\mu$ g total protein extract using anti-AOCs primary antibody. Protein staining with NoStain™ was used as internal control. M= protein marker.

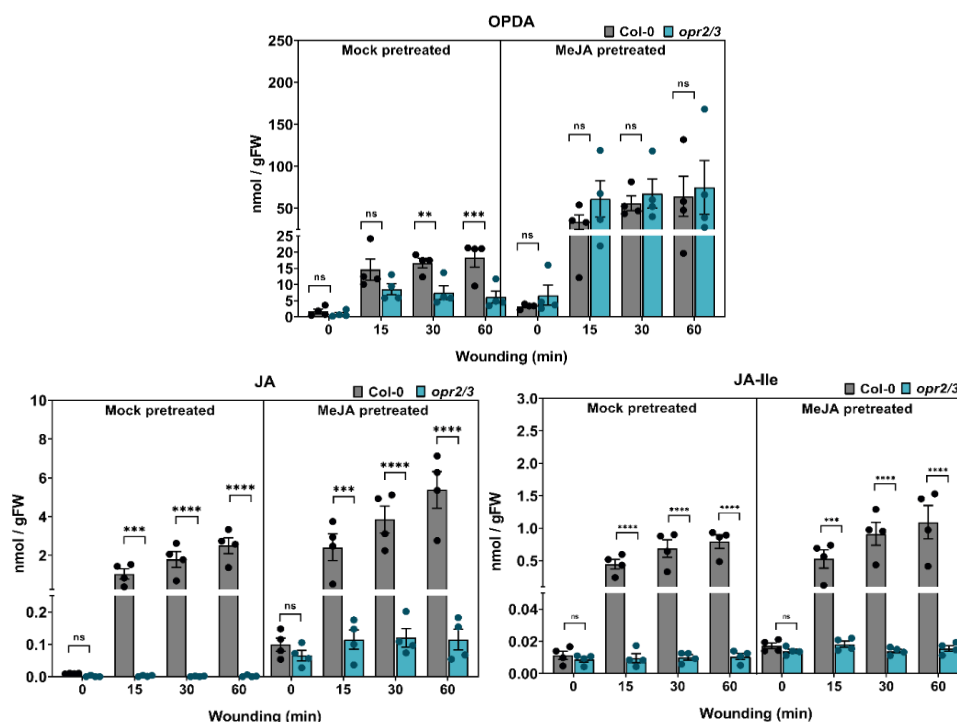


**Fig. S5 Time-course of OPDA, JA and JA-Ile accumulation upon wounding in seedlings of Col-0 and *opr2/3*.**

OPDA, JA and JA-Ile content in Col-0, *opr2/3* at 0, 15, 30 and 60 minutes after wounding. Seedlings were pretreated with MeJA or water (Mock) during development. JA and OPDA levels were determined by LC/MS and bars represent the average of four biological replicates with 30 seedlings each (single dots). Student t test was performed to determine statistical significance between genotypes at each condition with \*  $p < 0.05$ , \*\*  $p < 0.01$ , \*\*\*  $p < 0.001$ , \*\*\*\*  $p < 0.0001$  and ns not significant.

**Table S1 List of differentially expressed genes upon MeJA pretreatment during development.**  
For each genotype, the transcriptome after MeJA pretreatment was compared to the Mock pretreatment by water. DEGs were calculated from three biologically independent experiments.

| AGI  | Gene name | LogFC <sup>A</sup> |               |            | Adjusted p-value <sup>B</sup> |               |            | Description  |
|--|-----------|--------------------|---------------|------------|-------------------------------|---------------|------------|--|
|  |           | Col-0              | <i>opr2/3</i> | <i>aos</i> | Col-0                         | <i>opr2/3</i> | <i>aos</i> |  |
| <b>20 DEGs common in Col-0, <i>opr2/3</i> and <i>aos</i></b> |           |                    |               |            |                               |               |            |  |
| AT2G26010  | PDF1.3    | 1.79               | 3.50          | 3.47       | 2.0E-02                       | 2.6E-05       | 4.4E-05    | PR (pathogenesis-related) protein                        |
| AT5G44420  | PDF1.2A   | 2.23               | 3.02          | 2.48       | 4.2E-03                       | 1.1E-04       | 7.9E-04    | Ethylene- and jasmonate-responsive plant defensin        |
| AT3G49620  | DIN11     | 1.18               | 2.81          | 2.42       | 4.1E-03                       | 7.8E-07       | 3.4E-06    | Dark inducible 11  |
| AT3G44860  | FAMT      | 1.20               | 1.50          | 1.59       | 8.2E-03                       | 4.5E-04       | 3.7E-04    | Farnesoic acid carboxyl-o-methyltransferase (famt)       |
| AT1G52000  | JAL5      | 2.08               | 2.30          | 2.47       | 4.1E-06                       | 1.0E-06       | 1.0E-06    | Mannose-binding lectin superfamily protein               |
| AT1G19670  | CLH1      | 1.00               | 1.32          | 1.53       | 4.1E-03                       | 1.4E-04       | 5.1E-05    | Chlorophyllase 1   |
| AT5G25980  | TGG2      | 1.72               | 2.44          | 2.47       | 4.5E-04                       | 8.8E-06       | 1.2E-05    | Glucoside glucohydrolase 2                               |
| AT5G35940  | JAL41     | 1.13               | 1.37          | 1.05       | 1.5E-03                       | 9.4E-05       | 1.3E-03    | Mannose-binding lectin superfamily protein               |
| AT1G52400  | BGLU18    | 1.29               | 1.36          | 1.05       | 1.1E-04                       | 2.6E-05       | 3.7E-04    | Beta glucosidase 18                                      |
| AT1G73325  | -         | 1.26               | 1.97          | 1.91       | 1.5E-03                       | 1.1E-05       | 2.2E-05    | Kunitz family trypsin and protease inhibitor protein     |
| AT5G23840  | -         | 1.53               | 1.33          | 1.29       | 2.3E-04                       | 3.2E-04       | 5.8E-04    | MD-2-related lipid recognition domain-containing protein |
| AT5G23830  | -         | 1.16               | 1.54          | 1.23       | 3.2E-03                       | 9.4E-05       | 8.6E-04    | MD-2-related lipid recognition domain-containing protein |
| AT5G42580  | CYP705A12 | 1.34               | 1.45          | 1.46       | 7.3E-06                       | 2.6E-06       | 3.4E-06    | Cytochrome p450, family 705, polypeptide 12              |
| AT3G23550  | DTX18     | 1.32               | 1.15          | 1.26       | 7.0E-03                       | 7.7E-03       | 4.8E-03    | Detoxification 18  |
| AT4G17470  | CRSH      | 1.03               | 1.67          | 1.62       | 4.8E-03                       | 2.6E-05       | 5.1E-05    | CA2+-activated rela-spot homolog                         |
| AT5G38100  | -         | 1.18               | 1.40          | 1.26       | 2.3E-04                       | 2.3E-05       | 7.8E-05    | SABATH family methyltransferase                          |
| AT1G73500  | MKK9      | 1.19               | 1.26          | 1.59       | 4.6E-02                       | 1.3E-02       | 2.6E-03    | Map kinase kinase 9                                      |
| AT2G39330  | JAL23     | 1.52               | 1.20          | 1.02       | 1.5E-03                       | 4.4E-03       | 1.7E-02    | Jacalin-related lectin 23                                |
| AT1G66800  | -         | 1.03               | 1.25          | 1.16       | 1.0E-02                       | 7.0E-04       | 1.8E-03    | Unknown function   |
| AT3G45160  | -         | -1.14              | -1.05         | -1.29      | 1.7E-02                       | 1.2E-02       | 2.9E-03    | Putative membrane lipoprotein                            |
| <b>20 DEGs in <i>opr2/3</i> only</b>                         |           |                    |               |            |                               |               |            |  |
| AT5G19110  | -         | 0.81               | 1.20          | 0.83       | 1.3E-01                       | 5.5E-03       | 5.7E-02    | Eukaryotic aspartyl protease family protein              |
| AT1G06620  | -         | 0.61               | 1.17          | 1.00       | 7.8E-02                       | 2.0E-04       | 1.1E-03    | Similar to a 2-oxoglutarate-dependent dioxygenase        |
| AT1G66270  | BGLU21    | 0.68               | 1.05          | 0.98       | 3.4E-02                       | 4.2E-04       | 9.4E-04    | Beta-glucosidase 21                                      |
| AT5G26260  | -         | 0.50               | 1.04          | 0.76       | 4.6E-02                       | 4.4E-05       | 8.2E-04    | TRAF-like family protein                                 |
| AT3G17860  | JAZ3      | 0.38               | 1.04          | 0.97       | 2.8E-01                       | 2.9E-04       | 6.9E-04    | Jasmonate-zim-domain protein 3                           |
| AT4G15330  | CYP705A1  | 0.55               | 1.01          | 0.87       | 1.2E-01                       | 8.3E-04       | 3.5E-03    | Cytochrome P450, subfamily A, polypeptide 1              |
| AT1G45015  | -         | 0.94               | 1.06          | 0.19       | 1.4E-01                       | 4.6E-02       | 8.0E-01    | MD-2-related lipid recognition domain-containing protein |
| AT2G23110  | -         | 0.72               | 1.15          | 0.42       | 1.9E-01                       | 7.1E-03       | 3.8E-01    | Late embryogenesis abundant protein, group 6             |
| AT2G46650  | CYT5B5-C  | 0.11               | 1.06          | 0.97       | 8.9E-01                       | 1.7E-04       | 5.2E-04    | Cytochrome B5 isoform C (CB5-C)                          |
| AT1G62660  | BFRUCT3   | 0.57               | 1.01          | 0.86       | 2.2E-02                       | 6.4E-05       | 3.8E-04    | Vacuolar invertase 1                                     |
| AT2G23620  | MES1      | 0.30               | 1.15          | 0.69       | 6.1E-01                       | 8.6E-04       | 4.2E-02    | Methyl esterase 1  |

|                              |           |       |       |       |         |         |         |   |
|------------------------------|-----------|-------|-------|-------|---------|---------|---------|---|
| AT2G43100                    | IPMI2     | -0.01 | 1.23  | 0.88  | 1.0E+00 | 5.4E-06 | 1.2E-04 | Isopropylmalate isomerase 2   |
| AT5G14200                    | IMDH3     | 0.15  | 1.12  | 0.95  | 5.1E-01 | 7.5E-07 | 3.4E-06 | Isopropylmalate dehydrogenase 1   |
| AT1G62560                    | FMOGS-OX3 | 0.11  | 1.00  | 0.95  | 9.0E-01 | 4.8E-04 | 9.1E-04 | Flavin-monoxygenase glucosinolate s-oxygenase 3   |
| AT3G58990                    | IPMI1     | -0.05 | 1.14  | 0.83  | 9.8E-01 | 2.0E-04 | 4.1E-03 | Isopropylmalate isomerase 1   |
| AT5G07690                    | MYB29     | 0.32  | 1.04  | 0.69  | 7.1E-01 | 1.8E-02 | 1.2E-01 | Myb domain protein 29   |
| AT4G37700                    | -         | 0.63  | 1.00  | 0.26  | 1.6E-01 | 4.7E-03 | 5.2E-01 | Hypothetical protein  |
| AT2G32290                    | BAM6      | 0.22  | 1.02  | 0.67  | 8.1E-01 | 7.1E-03 | 8.1E-02 | Beta-amylase 6  |
| AT2G06255                    | EFL3      | 0.04  | 1.01  | 0.38  | 1.0E+00 | 4.4E-03 | 3.1E-01 | Elf4-like 3   |
| AT5G20790                    | -         | -0.52 | -1.08 | -0.88 | 3.1E-01 | 4.5E-03 | 2.2E-02 | Transmembrane protein   |
| <b>16 DEGs in Col-0 only</b> |           |       |       |       |         |         |         |   |
| AT3G55970                    | JRG21     | 2.01  | 0.60  | 0.42  | 4.5E-05 | 1.7E-01 | 3.0E-01 | Jasmonate-regulated gene 21   |
| AT2G38240                    | ANS       | 1.06  | 0.23  | -0.09 | 3.8E-02 | 8.5E-01 | 9.1E-01 | Jasmonate-induced oxygenase4  |
| AT2G39030                    | NATA1     | 1.61  | 0.51  | 0.40  | 8.6E-04 | 3.7E-01 | 3.9E-01 | N-acetyltransferase activity 1  |
| AT5G13220                    | JAZ10     | 1.06  | 0.03  | 0.07  | 5.5E-05 | 1.0E+00 | 8.4E-01 | JASMONATE ZIM-domain 10   |
| AT5G24770                    | VSP2      | 1.55  | 0.85  | 0.95  | 2.3E-04 | 1.6E-02 | 8.2E-03 | Vegetative storage protein 2  |
| AT1G52410                    | TSA1      | 1.03  | 0.97  | 0.68  | 6.6E-03 | 4.1E-03 | 4.6E-02 | N/a   |
| AT1G52040                    | MBP1      | 1.66  | 0.34  | 0.37  | 2.6E-05 | 4.3E-01 | 2.5E-01 | Myrosinase-binding protein 1  |
| AT5G42600                    | MRN1      | 1.87  | 0.69  | 0.67  | 2.7E-09 | 5.5E-05 | 9.1E-05 | Marneral synthase 1   |
| AT3G02620                    | 0         | 1.70  | 0.88  | 0.73  | 1.6E-06 | 3.7E-04 | 2.4E-03 | Stearoyl- <i>acp</i> desaturase   |
| AT5G24140                    | SQP2      | 1.29  | 0.92  | 0.65  | 2.3E-04 | 2.1E-03 | 3.0E-02 | Squalene monooxygenase 2  |
| AT1G52030                    | ATMBP     | 1.29  | 0.49  | 0.46  | 1.4E-04 | 9.4E-02 | 1.0E-01 | Myrosinase-binding protein 2  |
| AT4G37850                    | BHLH25    | 1.14  | 0.78  | 0.49  | 2.3E-04 | 3.1E-03 | 6.1E-02 | Basic helix-loop-helix (bhlh) DNA-binding superfamily protein                             |
| AT5G24780                    | VSP1      | 1.08  | 0.21  | 0.23  | 1.5E-03 | 7.4E-01 | 4.8E-01 | Vegetative storage protein 1  |
| AT5G24420                    | PGL5      | 1.05  | 0.11  | 0.16  | 1.4E-05 | 7.9E-01 | 4.0E-01 | 6-phosphogluconolactonase 5   |
| AT4G22210                    | LCR85     | 1.17  | 0.19  | 0.24  | 2.6E-05 | 6.2E-01 | 2.9E-01 | N/a   |
| AT5G62730                    | NPF4.7    | -1.16 | -0.78 | -0.80 | 4.1E-02 | 1.6E-01 | 1.1E-01 | Major facilitator superfamily protein   |
| <b>25 DEGs in aos only</b>   |           |       |       |       |         |         |         |   |
| AT1G72920                    | TN9       | 1.35  | 1.61  | 1.98  | 2.2E-01 | 6.8E-02 | 1.9E-02 | Toll-Interleukin-Resistance (TIR) domain family protein                                   |
| AT1G72910                    | TN8       | 1.33  | 1.39  | 1.77  | 2.3E-01 | 1.4E-01 | 4.2E-02 | Tir-nbs8  |
| AT1G27730                    | ZAT10     | 1.23  | 1.26  | 1.81  | 2.0E-01 | 1.2E-01 | 1.6E-02 | Salt tolerance zinc finger 10   |
| AT2G44840                    | ERF13     | 1.31  | 1.08  | 1.64  | 1.4E-01 | 2.0E-01 | 2.5E-02 | Ethylene-responsive element binding factor 13   |
| AT1G72900                    | TN7       | 1.38  | 1.13  | 1.49  | 7.0E-02 | 1.1E-01 | 2.3E-02 | Tir-nbs7  |
| AT5G39670                    | CML46     | 1.30  | 0.89  | 1.54  | 7.5E-02 | 2.3E-01 | 1.3E-02 | Calmodulin-like 46  |
| AT2G43530                    | ATTI3     | 0.76  | 0.96  | 1.03  | 2.7E-03 | 1.2E-04 | 9.4E-05 | Encodes a defensin-like (DEFL) family protein   |
| AT1G72940                    | TN11      | 1.15  | 1.11  | 1.37  | 1.3E-01 | 9.8E-02 | 3.1E-02 | Tir-nbs11   |
| AT4G12545                    | AIR1B     | 0.90  | 0.42  | 1.05  | 1.1E-01 | 6.2E-01 | 2.6E-02 | Bifunctional inhibitor/lipid-transfer protein/seed storage 2S albumin superfamily protein |



|           |           |       |       |       |         |         |         |   |
|-----------|-----------|-------|-------|-------|---------|---------|---------|---|
| AT4G23600 | CORI3     | 0.38  | 0.76  | 1.05  | 7.2E-01 | 2.3E-01 | 4.7E-02 | Coronatine induced 1                                    |
| AT4G13410 | CSLA15    | 0.57  | 0.65  | 1.07  | 6.4E-04 | 7.3E-05 | 1.4E-06 | Cellulose synthase like a15                             |
| AT4G27280 | KRP1      | 1.09  | 0.73  | 1.08  | 9.0E-02 | 2.8E-01 | 4.6E-02 | Ca2+-dependent modulator of icr1                        |
| AT2G20142 | -         | 0.92  | 0.63  | 1.28  | 7.7E-02 | 2.3E-01 | 4.4E-03 | Toll-Interleukin-Resistance (TIR) domain family protein |
| AT3G50930 | HSR4      | 0.86  | 0.84  | 1.01  | 1.2E-01 | 8.4E-02 | 2.9E-02 | Cytochrome bc1 synthesis                                |
| AT3G23570 | -         | 0.43  | 0.99  | 1.01  | 4.2E-02 | 1.5E-05 | 1.8E-05 | Alpha/beta-Hydrolases superfamily protein               |
| AT1G78370 | GSTU20    | 0.21  | 0.92  | 1.04  | 8.2E-01 | 1.5E-02 | 6.4E-03 | Glutathione s-transferase tau 20                        |
| AT1G62540 | FMOGS-OX2 | 0.59  | 0.83  | 1.07  | 2.0E-02 | 4.2E-04 | 5.8E-05 | Belongs to the flavin-monooxygenase (FMO) family        |
| AT3G50800 | -         | 0.94  | 0.30  | 1.07  | 1.3E-01 | 8.2E-01 | 3.8E-02 | PADRE protein   |
| AT3G55130 | ABCG19    | 0.50  | 0.76  | 1.12  | 1.4E-01 | 5.7E-03 | 2.8E-04 | Atp-binding cassette g19                                |
| AT2G23590 | MES8      | 0.60  | 0.86  | 1.02  | 1.3E-01 | 7.5E-03 | 2.4E-03 | Methyl esterase 8                                       |
| AT3G44260 | CAF1-9    | 0.76  | 0.67  | 1.01  | 1.0E-01 | 1.1E-01 | 9.1E-03 | CCR4- ASSOCIATED FACTOR 1A (atcaf1a)                    |
| AT1G33960 | AIG1      | 0.75  | 0.25  | 1.03  | 2.2E-01 | 8.5E-01 | 3.3E-02 | Immune associated nucleotide binding 8                  |
| AT2G03980 | -         | 0.41  | 0.65  | 1.00  | 2.7E-01 | 2.0E-02 | 7.7E-04 | GDSL-motif esterase/acyltransferase/lipase              |
| AT1G73010 | PS2       | -0.36 | -0.96 | -1.03 | 5.0E-01 | 4.8E-03 | 3.4E-03 | Phosphate starvation-induced gene 2                     |
| AT1G73330 | ATDR4     | -0.81 | -0.74 | -1.06 | 7.7E-02 | 6.6E-02 | 6.6E-03 | Drought-repressed 4                                     |

**1 DEG common to Col-0 and opr2/3**

|           |   |      |      |      |         |         |         |   |
|-----------|---|------|------|------|---------|---------|---------|---|
| AT4G33120 | - | 1.14 | 1.14 | 0.92 | 1.7E-04 | 6.4E-05 | 5.8E-04 | S-adenosyl-L-methionine-dependent methyltransferase |
|-----------|---|------|------|------|---------|---------|---------|---|

**27 DEGs common to opr2/3 and aos**

|           |          |      |      |      |         |         |         |   |
|-----------|----------|------|------|------|---------|---------|---------|---|
| AT5G42650 | AOS      | 0.71 | 1.66 | 1.37 | 4.5E-04 | 1.4E-07 | 1.0E-06 | Allene oxide synthase   |
| AT5G05600 | JOX2     | 0.92 | 1.86 | 1.89 | 1.0E-02 | 8.8E-06 | 1.1E-05 | Jasmonic acid oxidase 2   |
| AT3G25770 | AOC2     | 0.64 | 1.89 | 1.56 | 1.8E-02 | 7.5E-07 | 3.4E-06 | Allene oxide cyclase 2  |
| AT4G15210 | BAM5     | 0.67 | 2.46 | 2.32 | 3.4E-01 | 4.9E-05 | 1.1E-04 | Reduced beta amylase 1 (ram1)   |
| AT1G66280 | BGLU22   | 0.58 | 1.64 | 1.43 | 4.3E-02 | 3.3E-06 | 1.4E-05 | Glycosyl hydrolase superfamily protein  |
| AT5G48010 | THAS1    | 0.80 | 1.69 | 1.44 | 9.8E-03 | 6.0E-06 | 3.1E-05 | Thalianol synthase 1  |
| AT5G47990 | CYP705A5 | 0.76 | 1.69 | 1.41 | 1.8E-02 | 7.0E-06 | 4.7E-05 | Cytochrome p450, family 705, subfamily a, polypeptide 5                                   |
| AT1G19180 | JAZ1     | 0.81 | 1.17 | 1.49 | 5.7E-02 | 1.5E-03 | 2.7E-04 | Jasmonate-zim-domain protein 1  |
| AT2G26530 | AR781    | 1.26 | 1.67 | 1.90 | 1.4E-01 | 1.5E-02 | 6.4E-03 | Ar781   |
| AT1G16410 | CYP79F1  | 0.40 | 2.25 | 1.79 | 5.6E-01 | 1.5E-05 | 1.4E-04 | Cytochrome p450 79f1  |
| AT5G48000 | CYP708A2 | 0.66 | 1.43 | 1.31 | 7.8E-02 | 7.4E-05 | 2.4E-04 | Member of the CYP708A family of cytochrome P450 enzymes                                   |
| AT4G22610 | -        | 0.92 | 1.32 | 1.06 | 5.2E-02 | 1.6E-03 | 1.0E-02 | Bifunctional inhibitor/lipid-transfer protein/seed storage 2S albumin superfamily protein |
| AT3G45140 | LOX2     | 0.41 | 1.45 | 1.68 | 4.1E-01 | 1.6E-04 | 5.8E-05 | Lipoxygenase 2  |
| AT5G42590 | CYP71A16 | 0.79 | 1.50 | 1.18 | 3.6E-03 | 5.4E-06 | 5.1E-05 | Cytochrome p450, family 71, polypeptide 16  |
| AT4G13310 | CYP71A2- | 0.87 | 1.63 | 1.32 | 3.8E-02 | 8.2E-05 | 6.9E-04 | Cytochrome p450, family 71, polypeptide 20  |
| AT5G23010 | MAM1     | 0.33 | 1.69 | 1.49 | 4.2E-01 | 7.0E-06 | 3.1E-05 | Methylthioalkylmalate synthase 1  |
| AT3G22740 | HMT3     | 0.27 | 1.72 | 1.32 | 6.3E-01 | 1.5E-05 | 2.1E-04 | Homocysteine s-methyltransferase 3  |

|           |       |       |       |       |         |         |         |   |
|-----------|-------|-------|-------|-------|---------|---------|---------|---|
| AT3G05770 | -     | 0.61  | 1.10  | 1.10  | 2.3E-01 | 4.6E-03 | 5.0E-03 | Hypothetical protein                        |
| AT2G32487 | -     | 0.70  | 1.38  | 1.16  | 8.1E-02 | 1.9E-04 | 1.2E-03 | Hypothetical protein                        |
| AT2G43510 | ATTI1 | 0.76  | 1.19  | 1.01  | 6.6E-02 | 1.0E-03 | 4.8E-03 | Trypsin inhibitor protein 1                 |
| AT5G43580 | UPI   | 0.49  | 1.22  | 1.01  | 3.5E-01 | 1.4E-03 | 8.3E-03 | Unusual serine protease inhibitor           |
| AT3G44300 | NIT2  | 1.00  | 1.13  | 1.10  | 2.0E-03 | 2.3E-04 | 4.4E-04 | Nitrilase 2                                 |
| AT3G19710 | BCAT4 | 0.08  | 1.43  | 1.12  | 9.4E-01 | 1.3E-05 | 1.4E-04 | Branched-chain aminotransferase4            |
| AT3G02020 | AK3   | 0.13  | 1.34  | 1.09  | 9.1E-01 | 3.7E-04 | 2.8E-03 | Aspartate kinase 3                          |
| AT5G59310 | LTP4  | -1.13 | -1.41 | -1.52 | 6.1E-02 | 6.0E-03 | 4.1E-03 | Member of the lipid transfer protein family |
| AT5G59320 | LTP3  | -0.72 | -1.72 | -1.48 | 1.5E-01 | 1.2E-04 | 6.4E-04 | PR (pathogenesis-related) protein           |
| AT5G03545 | AT4   | -0.74 | -1.14 | -1.22 | 2.0E-02 | 1.9E-04 | 1.4E-04 | Induced by pi starvation 2                  |

#### 2 DEGs common to Col-0 and aos

|           |             |      |      |      |         |         |         |                                   |
|-----------|-------------|------|------|------|---------|---------|---------|-----------------------------------|
| AT5G44430 | PDF1.2<br>C | 2.29 | 0.96 | 1.41 | 7.3E-04 | 1.4E-01 | 1.7E-02 | PR (pathogenesis-related) protein |
| AT4G12550 | AIR1        | 1.59 | 1.15 | 1.38 | 2.8E-02 | 8.9E-02 | 3.3E-02 | Auxin-induced in root cultures 1  |

<sup>A</sup>DEGs in seedlings of Col-0, *opr2/3* and *aos* following MeJA pretreatment during development relative to Mock pretreated controls. An FDR of 0.05 and a minimum FC of 2 were applied as cutoffs. DEGs were classified according to the group they belong to in the Venn diagram comparisons (Fig. S4).

<sup>B</sup> False discovery rate corrected p-value.

N/A not annotated.

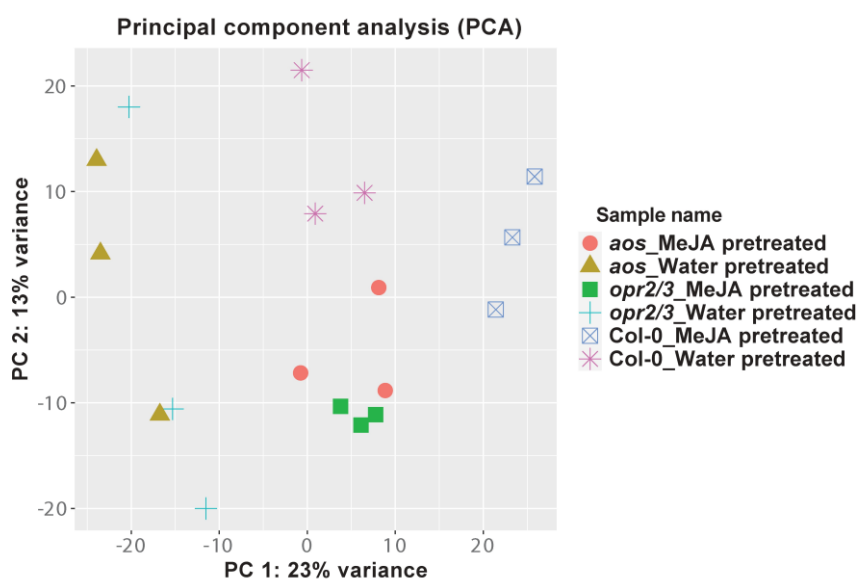


**Fig. S6 PCA projection of the seedlings' transcriptome of Col-0, *opr2/3* and *aos* following MeJA and water pretreatment.**

The PCA shows the effect of MeJA pretreatment during development on each genotype with PC1 and PC2 showing variation in the dataset due to pretreatment/genotypes.

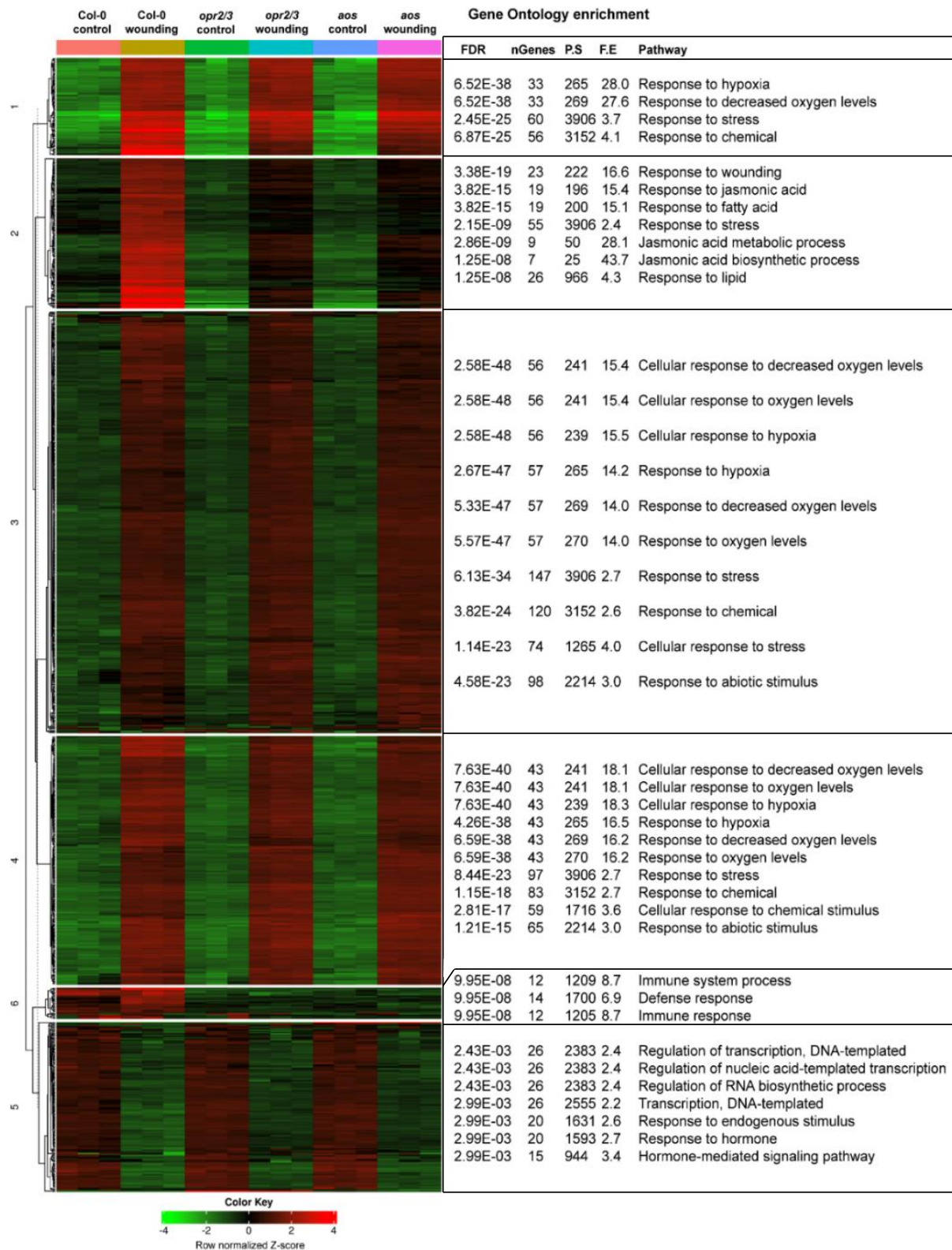


**Fig. S7 Clustering of the transcriptional wounding response in Col-0, *opr2/3* and *aos* seedlings pretreated with MeJA during development.**

K-means clustering of the 2000 most variable genes across all RNA-seq samples and enrichment analysis of each cluster with FDR: False Discovery rate, P.S: Pathway size and F.E: Fold enrichment. Gene Ontology (GO) biological process-based enrichment analysis.

**Table S2 List of wound-responsive genes which are independent from JA/OPDA pathway and classified under the GO term: cellular response to stress.**

Genes which are commonly differentially expressed upon wounding in Col-0, *opr2/3* and *aos* with similar fold change and expression levels (FPKM) and classified as stress-responsive genes. DEGs were calculated from three biologically independent experiments. Genes in bold were identified as OPDA-specific response genes (Taki et al., 2005).

| AGI                       | Gene name    | LogFC <sup>A</sup> |               |             | Adjusted p-value <sup>B</sup> |                |                | Description   |
|---------------------------|--------------|--------------------|---------------|-------------|-------------------------------|----------------|----------------|---|
|                           |              | Col-0              | <i>opr2/3</i> | <i>aos</i>  | Col-0                         | <i>opr2/3</i>  | <i>aos</i>     |   |
| <b>Up regulated genes</b> |              |                    |               |             |                               |                |                |   |
| AT3G47720                 | SRO4         | 6.09               | 5.86          | 6.07        | 7.0E-11                       | 1.4E-10        | 9.0E-11        | Probable inactive poly [ADP-ribose] polymerase      |
| AT4G01360                 | -            | 5.61               | 5.61          | 6.20        | 1.8E-14                       | 1.8E-14        | 5.7E-15        | BPS1-like protein                                   |
| AT1G15010                 | -            | 5.50               | 5.34          | 5.48        | 2.2E-13                       | 5.3E-13        | 3.7E-13        | Mediator of RNA polymerase II transcription subunit |
| AT5G62520                 | SRO5         | 5.15               | 5.04          | 5.42        | 6.9E-10                       | 1.1E-09        | 4.7E-10        | Probable inactive poly [ADP-ribose] polymerase SRO5 |
| <b>AT5G42380</b>          | <b>CML37</b> | <b>5.09</b>        | <b>4.94</b>   | <b>4.76</b> | <b>2.2E-13</b>                | <b>5.3E-13</b> | <b>6.3E-13</b> | <b>Calcium-binding protein CML37</b>                |
| AT5G39890                 | PCO2         | 4.99               | 5.26          | 5.64        | 2.3E-08                       | 1.6E-08        | 6.8E-09        | Plant cysteine oxidase 2                            |
| AT1G76650                 | CML38        | 4.78               | 4.84          | 5.11        | 6.1E-09                       | 6.5E-09        | 3.3E-09        | Calmodulin-like 38                                  |
| AT2G14247                 | -            | 4.57               | 5.00          | 5.17        | 2.1E-10                       | 1.1E-10        | 7.1E-11        | Expressed protein                                   |
| AT4G33070                 | PDC1         | 4.48               | 4.45          | 4.66        | 8.9E-12                       | 1.5E-11        | 8.0E-12        | Pyruvate decarboxylase 1                            |
| AT4G22780                 | ACR7         | 4.40               | 4.00          | 4.21        | 4.9E-12                       | 1.8E-11        | 1.0E-11        | ACT domain-containing protein ACR7                  |
| AT5G66985                 | HUP44        | 4.31               | 4.28          | 4.21        | 5.4E-09                       | 7.2E-09        | 8.2E-09        | Hypoxia response unknown protein 44                 |
| AT1G18300                 | NUDT4        | 4.15               | 3.82          | 3.68        | 3.9E-13                       | 1.4E-12        | 1.6E-12        | Nudix hydrolase 4                                   |
| AT5G42200                 | ATL23        | 4.11               | 3.59          | 3.87        | 4.6E-10                       | 2.7E-09        | 1.1E-09        | E3 ubiquitin-protein ligase ATL23                   |
| AT4G10265                 | WIP3         | 4.09               | 4.26          | 4.80        | 4.4E-06                       | 3.3E-06        | 8.8E-07        | Wound-induced polypeptide 3                         |
| AT5G65207                 | -            | 4.03               | 3.76          | 3.73        | 8.4E-10                       | 2.3E-09        | 2.4E-09        | Uncharacterized protein                             |
| AT2G47520                 | ERF071       | 4.01               | 3.67          | 3.86        | 6.4E-10                       | 2.2E-09        | 1.2E-09        | Ethylene-responsive transcription factor ERF071     |
| AT1G76600                 | -            | 3.93               | 4.12          | 4.13        | 1.4E-11                       | 1.2E-11        | 1.1E-11        | Poly polymerase                                     |
| AT3G23170                 | HUP39        | 3.84               | 3.88          | 3.82        | 6.4E-08                       | 6.7E-08        | 7.6E-08        | Hypoxia response unknown protein 39                 |
| AT4G24110                 | HUP40        | 3.77               | 4.22          | 4.40        | 3.3E-07                       | 1.1E-07        | 6.6E-08        | Hypoxia response unknown protein 40                 |
| AT1G19020                 | HUP35        | 3.77               | 3.51          | 3.64        | 6.5E-10                       | 1.8E-09        | 1.1E-09        | Hypoxia response unknown protein 35                 |
| <b>AT3G25250</b>          | <b>OXI1</b>  | <b>3.76</b>        | <b>3.84</b>   | <b>3.53</b> | <b>1.9E-11</b>                | <b>2.1E-11</b> | <b>4.9E-11</b> | <b>Serine/threonine-protein kinase OXI1</b>         |
| AT3G13310                 | DJC66        | 3.72               | 3.57          | 3.87        | 4.8E-09                       | 9.1E-09        | 3.5E-09        | DNA J protein C66                                   |
| AT2G36220                 | -            | 3.71               | 3.41          | 3.46        | 2.9E-10                       | 9.4E-10        | 7.3E-10        | hypothetical protein                                |
| AT4G33560                 | WIP5         | 3.70               | 3.94          | 3.99        | 1.8E-09                       | 1.2E-09        | 9.3E-10        | Wound-induced polypeptide 5                         |
| AT3G02550                 | LBD41        | 3.67               | 3.83          | 4.15        | 1.2E-06                       | 9.0E-07        | 3.6E-07        | LOB domain-containing protein 41                    |
| AT3G27220                 | -            | 3.67               | 3.81          | 4.13        | 4.1E-08                       | 3.0E-08        | 1.2E-08        | Kelch repeat-containing protein At3g27220           |
| AT3G06435                 | -            | 3.66               | 3.96          | 4.23        | 1.3E-08                       | 6.6E-09        | 3.0E-09        | Expressed protein                                   |
| AT5G57510                 | -            | 3.65               | 3.06          | 2.86        | 8.4E-10                       | 7.6E-09        | 1.5E-08        | Cotton fiber protein                                |
| AT4G29780                 | -            | 3.59               | 3.54          | 3.43        | 4.9E-12                       | 8.1E-12        | 1.0E-11        | Nuclease  |
| AT3G10040                 | -            | 3.58               | 3.98          | 4.21        | 6.6E-06                       | 2.5E-06        | 1.3E-06        | Sequence-specific DNA binding transcription factor  |

|                  |                    |             |             |             |                     |                     |                     |  |
|------------------|--------------------|-------------|-------------|-------------|---------------------|---------------------|---------------------|--|
| AT5G13080        | WRKY<br>75         | 3.56        | 3.83        | 3.37        | 1.2E-<br>08         | 6.2E-<br>09         | 2.4E-<br>08         | WRKY DNA-binding protein 75                          |
| <b>AT5G59820</b> | <b>ZAT12</b>       | <b>3.54</b> | <b>3.50</b> | <b>3.29</b> | <b>4.3E-<br/>10</b> | <b>6.3E-<br/>10</b> | <b>1.2E-<br/>09</b> | <b>Zinc finger protein ZAT12</b>                     |
| AT2G32200        | -                  | 3.48        | 3.12        | 3.47        | 5.5E-<br>13         | 2.3E-<br>12         | 1.0E-<br>12         | Unknown protein                                      |
| <b>AT5G35735</b> | -                  | <b>3.42</b> | <b>3.73</b> | <b>3.62</b> | <b>3.2E-<br/>11</b> | <b>1.7E-<br/>11</b> | <b>2.1E-<br/>11</b> | <b>Cytochrome B561</b>                               |
| <b>AT1G61340</b> | <b>FBS1</b>        | <b>3.40</b> | <b>3.44</b> | <b>3.52</b> | <b>1.2E-<br/>10</b> | <b>1.4E-<br/>10</b> | <b>1.0E-<br/>10</b> | <b>F-BOX stress induced 1</b>                        |
| AT5G47910        | RBOH<br>D          | 3.38        | 3.26        | 3.44        | 7.7E-<br>13         | 1.7E-<br>12         | 1.1E-<br>12         | Respiratory burst oxidase homolog protein D          |
| AT1G10140        | -                  | 3.35        | 2.53        | 2.64        | 2.1E-<br>12         | 4.8E-<br>11         | 2.9E-<br>11         | Uncharacterized conserved protein<br>UCP031279       |
| AT1G07135        | -                  | 3.31        | 3.04        | 2.76        | 1.6E-<br>09         | 5.1E-<br>09         | 1.4E-<br>08         | Glycine-rich protein                                 |
| AT4G30280        | XTH18              | 3.28        | 3.04        | 3.10        | 4.5E-<br>13         | 1.4E-<br>12         | 1.1E-<br>12         | Probable xyloglucan endotransglucosylase             |
| AT5G15120        | PCO1               | 3.26        | 3.62        | 3.76        | 3.0E-<br>08         | 1.1E-<br>08         | 6.9E-<br>09         | Plant cysteine oxidase 1                             |
| AT2G32210        | -                  | 3.25        | 3.17        | 3.06        | 5.3E-<br>09         | 8.3E-<br>09         | 1.2E-<br>08         | Cysteine-rich/transmembrane domain A-like<br>protein |
| <b>AT2G46400</b> | <b>WRKY<br/>46</b> | <b>3.14</b> | <b>3.31</b> | <b>3.25</b> | <b>2.6E-<br/>09</b> | <b>1.9E-<br/>09</b> | <b>2.1E-<br/>09</b> | <b>Probable WRKY transcription factor 46</b>         |
| <b>AT3G04640</b> | -                  | <b>3.11</b> | <b>3.01</b> | <b>3.11</b> | <b>9.7E-<br/>10</b> | <b>1.8E-<br/>09</b> | <b>1.2E-<br/>09</b> | <b>Glycine-rich protein</b>                          |
| AT1G09950        | RAS1               | 3.06        | 2.48        | 2.63        | 5.9E-<br>12         | 7.2E-<br>11         | 3.8E-<br>11         | Response to aba and salt 1                           |
| <b>AT5G05410</b> | <b>DREB2<br/>A</b> | <b>3.01</b> | <b>3.06</b> | <b>3.45</b> | <b>1.8E-<br/>10</b> | <b>2.0E-<br/>10</b> | <b>5.3E-<br/>11</b> | <b>Dehydration-responsive element-binding<br/>2A</b> |
| AT1G63090        | PP2A1<br>1         | 2.99        | 2.83        | 2.74        | 3.0E-<br>13         | 7.9E-<br>13         | 1.0E-<br>12         | F-box protein PP2-A11                                |
| AT3G15210        | ERF4               | 2.92        | 3.00        | 3.13        | 1.4E-<br>10         | 1.3E-<br>10         | 8.1E-<br>11         | Ethylene-responsive transcription factor 4           |
| AT1G20823        | ATL80              | 2.91        | 2.14        | 2.28        | 1.3E-<br>10         | 4.7E-<br>09         | 2.2E-<br>09         | RING-H2 finger protein ATL80                         |
| AT5G54470        | BBX29              | 2.89        | 3.28        | 3.36        | 8.4E-<br>11         | 2.9E-<br>11         | 2.1E-<br>11         | B-BOX domain protein 29                              |
| <b>AT2G22500</b> | <b>PUMP<br/>5</b>  | <b>2.89</b> | <b>2.74</b> | <b>2.82</b> | <b>1.4E-<br/>11</b> | <b>3.3E-<br/>11</b> | <b>2.2E-<br/>11</b> | <b>Mitochondrial uncoupling protein 5</b>            |
| AT3G23150        | ETR2               | 2.80        | 2.70        | 2.95        | 1.1E-<br>12         | 2.4E-<br>12         | 1.1E-<br>12         | Ethylene receptor 2                                  |
| AT1G53840        | PME1               | 2.73        | 2.51        | 2.74        | 6.9E-<br>15         | 1.8E-<br>14         | 5.7E-<br>15         | Pectinesterase                                       |
| AT1G14540        | PER4               | 2.73        | 3.64        | 3.83        | 1.1E-<br>06         | 5.2E-<br>08         | 2.8E-<br>08         | Peroxidase   |
| AT1G50740        | FAX5               | 2.73        | 2.80        | 2.76        | 2.2E-<br>12         | 2.4E-<br>12         | 2.5E-<br>12         | Protein fatty acid export 5                          |
| AT1G78070        | -                  | 2.72        | 2.81        | 3.00        | 3.6E-<br>13         | 5.3E-<br>13         | 2.6E-<br>13         | Transducin/WD40 repeat-like superfamily<br>protein   |
| AT1G76680        | OPR1               | 2.69        | 3.16        | 2.63        | 6.1E-<br>11         | 1.5E-<br>11         | 9.4E-<br>11         | 12-oxophytodienoate reductase 1                      |
| AT5G63790        | ANAC1<br>02        | 2.68        | 2.97        | 2.71        | 8.2E-<br>13         | 6.5E-<br>13         | 1.1E-<br>12         | NAC domain containing protein 102                    |
| AT5G20230        | BCB                | 2.67        | 2.15        | 2.18        | 9.2E-<br>11         | 1.2E-<br>09         | 9.3E-<br>10         | Blue copper binding protein                          |
| AT1G01720        | NAC00<br>2         | 2.62        | 2.87        | 2.82        | 5.3E-<br>12         | 3.0E-<br>12         | 3.0E-<br>12         | NAC domain-containing protein 2                      |
| AT1G33055        | -                  | 2.61        | 2.74        | 2.72        | 3.0E-<br>06         | 2.0E-<br>06         | 2.1E-<br>06         | Uncharacterized protein                              |
| AT5G44730        | -                  | 2.57        | 2.73        | 2.84        | 1.5E-<br>10         | 1.0E-<br>10         | 6.6E-<br>11         | Haloacid dehalogenase-like hydrolase<br>(HAD)        |
| <b>AT3G46080</b> | <b>ZAT8</b>        | <b>2.53</b> | <b>2.55</b> | <b>2.34</b> | <b>1.3E-<br/>08</b> | <b>1.5E-<br/>08</b> | <b>3.6E-<br/>08</b> | <b>Zinc finger protein ZAT8</b>                      |
| AT1G68620        | CXE6               | 2.53        | 3.17        | 2.81        | 5.2E-<br>09         | 5.5E-<br>10         | 1.9E-<br>09         | Probable carboxylesterase 6                          |
| AT4G27657        | -                  | 2.52        | 2.54        | 2.34        | 4.5E-<br>09         | 5.1E-<br>09         | 1.2E-<br>08         | hypothetical protein                                 |
| AT1G62300        | WRKY<br>6          | 2.51        | 2.84        | 2.75        | 5.6E-<br>11         | 2.0E-<br>11         | 2.5E-<br>11         | transcription factor WRKY6                           |
| AT4G01250        | WRKY<br>22         | 2.50        | 2.45        | 2.71        | 2.9E-<br>09         | 4.6E-<br>09         | 1.4E-<br>09         | WRKY transcription factor 22                         |



|                  |                |             |             |             |                |                |                |   |
|------------------|----------------|-------------|-------------|-------------|----------------|----------------|----------------|---|
| <b>AT1G66090</b> | -              | <b>2.49</b> | <b>2.71</b> | <b>2.56</b> | <b>1.4E-08</b> | <b>6.4E-09</b> | <b>1.1E-08</b> | <b>Disease resistance protein (TIR-NBS class)</b>   |
| AT1G03610        | -              | 2.47        | 2.44        | 2.63        | 2.2E-09        | 3.2E-09        | 1.3E-09        | Plant/protein (DUF789)                              |
| AT1G22220        | AUF2           | 2.42        | 1.97        | 2.32        | 1.2E-07        | 1.2E-06        | 2.1E-07        | AUXIN UP-REGULATED F-BOX PROTEIN 2                  |
| AT2G20880        | ERF053         | 2.41        | 2.13        | 2.59        | 8.6E-10        | 4.6E-09        | 4.7E-10        | Ethylene-responsive transcription factor ERF053     |
| AT5G13190        | -              | 2.40        | 2.44        | 2.40        | 1.3E-10        | 1.5E-10        | 1.6E-10        | necrosis factor alpha factor                        |
| <b>AT4G20860</b> | <b>FAD-OXR</b> | <b>2.39</b> | <b>2.54</b> | <b>2.50</b> | <b>1.6E-08</b> | <b>9.4E-09</b> | <b>1.1E-08</b> | <b>Berberine bridge enzyme-like 22</b>              |
| AT4G13395        | DVL10          | 2.37        | 2.08        | 1.93        | 5.0E-07        | 2.4E-06        | 5.3E-06        | Rotundifolia like 12                                |
| AT4G32480        | -              | 2.35        | 2.00        | 2.18        | 2.8E-10        | 2.1E-09        | 7.4E-10        | Phosphorus (P) stress inducible DUF506 gene family  |
| AT2G01180        | ATPAP1         | 2.34        | 2.15        | 2.20        | 5.2E-09        | 1.6E-08        | 1.2E-08        | Phosphatidic acid phosphatase 1                     |
| AT1G28380        | NSL1           | 2.32        | 1.93        | 1.92        | 1.7E-12        | 1.5E-11        | 1.4E-11        | Necrotic spotted lesions 1                          |
| AT3G47340        | ASN1           | 2.32        | 1.89        | 2.21        | 6.2E-08        | 6.6E-07        | 1.2E-07        | Dark inducible 6                                    |
| AT5G64260        | EXL2           | 2.30        | 2.09        | 2.26        | 6.7E-13        | 2.4E-12        | 1.1E-12        | Protein EXORDIUM-like 2                             |
| AT5G24590        | NAC091         | 2.29        | 2.25        | 2.38        | 2.6E-12        | 4.6E-12        | 2.3E-12        | NAC domain-containing protein 91                    |
| AT2G03240        | PHO1-H5        | 2.29        | 1.83        | 2.03        | 6.4E-11        | 8.9E-10        | 2.7E-10        | Phosphate transporter PHO1 homolog 5                |
| AT4G34131        | UGT73B3        | 2.26        | 2.90        | 2.61        | 5.3E-09        | 4.3E-10        | 1.2E-09        | UDP-glycosyltransferase 73B3                        |
| AT1G23710        | -              | 2.26        | 1.96        | 2.15        | 1.6E-10        | 9.4E-10        | 3.2E-10        | hypothetical protein                                |
| <b>AT4G24570</b> | <b>DIC2</b>    | <b>2.24</b> | <b>2.12</b> | <b>1.83</b> | <b>1.2E-09</b> | <b>2.9E-09</b> | <b>1.4E-08</b> | <b>DICARBOXYLATE CARRIER 2</b>                      |
| AT5G06320        | NHL3           | 2.23        | 2.20        | 2.17        | 5.2E-08        | 7.3E-08        | 8.0E-08        | NDR1/HIN1-LIKE 3                                    |
| AT5G04340        | ZAT6           | 2.22        | 2.07        | 2.15        | 5.4E-09        | 1.5E-08        | 9.0E-09        | Zinc finger protein ZAT6                            |
| AT1G13360        | -              | 2.20        | 2.14        | 2.12        | 6.2E-12        | 1.2E-11        | 1.2E-11        | hypothetical protein                                |
| AT1G19530        | -              | 2.19        | 2.53        | 2.68        | 2.0E-08        | 4.9E-09        | 2.4E-09        | DNA polymerase epsilon catalytic subunit A          |
| <b>AT5G27420</b> | <b>ATL31</b>   | <b>2.18</b> | <b>1.93</b> | <b>2.00</b> | <b>9.0E-08</b> | <b>4.0E-07</b> | <b>2.6E-07</b> | <b>E3 ubiquitin-protein ligase ATL31</b>            |
| AT5G19240        | -              | 2.16        | 2.46        | 2.55        | 2.7E-10        | 9.2E-11        | 5.9E-11        | Uncharacterized GPI-anchored protein At5g19240      |
| AT1G26270        | PI4KG5         | 2.16        | 2.32        | 2.60        | 1.3E-10        | 7.6E-11        | 2.2E-11        | Phosphatidylinositol 4-kinase gamma 5               |
| AT1G59870        | ABCG36         | 2.15        | 2.13        | 2.12        | 1.3E-09        | 1.9E-09        | 1.9E-09        | ABC transporter G family member 36                  |
| AT5G66650        | -              | 2.09        | 1.81        | 1.75        | 3.8E-10        | 2.4E-09        | 3.2E-09        | Calcium uniporter protein 3, mitochondrial          |
| AT2G41430        | ERD15          | 2.09        | 1.90        | 1.91        | 4.9E-12        | 1.8E-11        | 1.5E-11        | Early responsive to dehydration 15                  |
| AT3G50440        | MES10          | 2.09        | 1.46        | 1.33        | 1.3E-09        | 9.0E-08        | 2.3E-07        | Methylesterase 10                                   |
| AT1G35140        | EXL1           | 2.06        | 2.03        | 1.92        | 1.6E-09        | 2.5E-09        | 4.3E-09        | Protein EXORDIUM-like 1                             |
| AT2G31865        | PARG2          | 2.06        | 2.23        | 2.67        | 2.4E-07        | 1.2E-07        | 1.5E-08        | poly(ADP-ribose) glycohydrolase 2                   |
| AT4G30370        | ATL14          | 2.05        | 2.01        | 2.12        | 2.1E-08        | 3.0E-08        | 1.5E-08        | RING-H2 finger protein ATL14                        |
| AT4G30440        | GAE1           | 2.01        | 1.84        | 1.94        | 4.7E-10        | 1.6E-09        | 8.4E-10        | UDP-D-GLUCURONATE 4-EPIMERASE 1                     |
| <b>AT4G24160</b> | -              | <b>2.01</b> | <b>2.43</b> | <b>2.30</b> | <b>1.0E-10</b> | <b>1.8E-11</b> | <b>3.0E-11</b> | <b>1-acylglycerol-3-phosphate O-acyltransferase</b> |
| AT3G03280        | -              | 2.01        | 2.39        | 2.34        | 1.3E-08        | 2.4E-09        | 2.8E-09        | PADRE protein                                       |
| AT1G07150        | MAPKKK13       | 1.99        | 1.95        | 2.22        | 3.4E-09        | 5.3E-09        | 1.2E-09        | F10K1.14 protein                                    |
| AT2G15890        | MEE14          | 1.97        | 1.82        | 1.88        | 3.0E-07        | 7.9E-07        | 5.4E-07        | CCG-binding protein 1                               |



|                  |                |             |             |             |                |                |                |  |
|------------------|----------------|-------------|-------------|-------------|----------------|----------------|----------------|--|
| AT1G09070        | SRC2           | 1.97        | 2.01        | 1.97        | 1.1E-11        | 1.2E-11        | 1.4E-11        | Protein SRC2 homolog                                 |
| AT5G64905        | PEP3           | 1.97        | 2.75        | 2.95        | 3.8E-05        | 1.4E-06        | 6.1E-07        | Elicitor peptide 3                                   |
| AT1G07870        | -              | 1.97        | 2.23        | 2.49        | 2.1E-12        | 1.1E-12        | 4.1E-13        | Protein kinase superfamily protein                   |
| AT3G19130        | RBP47B         | 1.96        | 2.08        | 2.31        | 1.4E-11        | 1.1E-11        | 3.1E-12        | Polyadenylate-binding protein RBP47B                 |
| AT1G30040        | GA2OX2         | 1.96        | 1.51        | 1.67        | 9.4E-11        | 2.0E-09        | 6.1E-10        | Gibberellin 2-beta-dioxygenase 2                     |
| AT1G29690        | CAD1           | 1.94        | 2.14        | 2.08        | 4.2E-11        | 2.0E-11        | 2.4E-11        | MACPF domain-containing protein CAD1                 |
| AT2G40000        | HSPRO2         | 1.94        | 1.80        | 1.94        | 1.3E-07        | 3.4E-07        | 1.5E-07        | Nematode resistance protein-like HSPRO2              |
| AT5G54960        | PDC2           | 1.94        | 1.66        | 1.92        | 1.6E-11        | 1.2E-10        | 2.4E-11        | Pyruvate decarboxylase 2                             |
| AT1G68690        | PERK9          | 1.94        | 2.28        | 2.38        | 3.8E-09        | 8.0E-10        | 4.5E-10        | Proline-rich receptor-like protein kinase PERK9      |
| AT5G44070        | PCS1           | 1.85        | 1.99        | 2.15        | 2.3E-10        | 1.4E-10        | 6.2E-11        | PHYTOCHELATIN SYNTHASE 1                             |
| AT3G08720        | ATPK2          | 1.84        | 1.48        | 1.45        | 9.2E-11        | 1.2E-09        | 1.4E-09        | Serine/threonine-protein kinase AtPK2/AtPK19         |
| AT3G52800        | SAP6           | 1.84        | 1.49        | 1.42        | 4.6E-11        | 5.6E-10        | 8.3E-10        | A20/AN1-like zinc finger family protein              |
| AT2G47190        | ATMYB2         | 1.81        | 1.58        | 1.51        | 8.4E-07        | 4.1E-06        | 6.6E-06        | MYB domain protein 2                                 |
| AT3G02555        | -              | 1.81        | 1.65        | 1.72        | 1.0E-08        | 3.4E-08        | 2.1E-08        | hypothetical protein                                 |
| AT5G19230        | -              | 1.78        | 1.51        | 1.56        | 9.0E-10        | 7.5E-09        | 4.9E-09        | Uncharacterized GPI-anchored protein At5g19230       |
| AT3G49780        | PSK3           | 1.78        | 1.61        | 1.63        | 4.8E-08        | 1.7E-07        | 1.4E-07        | Phytosulfokines 3                                    |
| AT3G20600        | NDR1           | 1.77        | 1.84        | 1.77        | 2.7E-07        | 2.0E-07        | 3.0E-07        | Protein NDR1   |
| AT1G18390        | -              | 1.76        | 2.00        | 1.91        | 4.5E-10        | 1.5E-10        | 2.3E-10        | Protein kinase superfamily protein                   |
| AT1G72940        | -              | 1.75        | 1.21        | 1.09        | 2.5E-05        | 8.3E-04        | 1.8E-03        | At1g72940/F3N23_14                                   |
| AT1G14040        | PHO1; H3       | 1.75        | 2.17        | 1.96        | 4.5E-10        | 6.3E-11        | 1.7E-10        | Phosphate transporter PHO1 homolog 3                 |
| AT5G58070        | TIL            | 1.74        | 1.67        | 1.75        | 1.2E-10        | 2.3E-10        | 1.3E-10        | Temperature-induced lipocalin                        |
| AT4G30380        | -              | 1.73        | 1.84        | 2.21        | 2.0E-06        | 1.2E-06        | 1.6E-07        | Barwin-related endoglucanase                         |
| AT2G16900        | -              | 1.71        | 1.85        | 1.95        | 3.9E-12        | 2.4E-12        | 1.5E-12        | Expressed protein                                    |
| AT2G18670        | ATL56          | 1.71        | 1.82        | 2.01        | 3.6E-08        | 2.0E-08        | 6.5E-09        | RING-H2 finger protein ATL56                         |
| <b>AT5G57560</b> | <b>XTH22</b>   | <b>1.69</b> | <b>1.57</b> | <b>1.42</b> | <b>1.7E-08</b> | <b>4.6E-08</b> | <b>1.3E-07</b> | <b>Xyloglucan endotransglucosylase/hydrolase</b>     |
| AT3G55880        | SUE4           | 1.69        | 1.53        | 1.24        | 1.1E-07        | 3.8E-07        | 3.5E-06        | Alpha/beta hydrolase related protein                 |
| AT2G46500        | PI4KG4         | 1.68        | 1.80        | 1.95        | 7.1E-12        | 5.5E-12        | 2.2E-12        | Phosphatidylinositol 4-kinase gamma 4                |
| AT2G13790        | SERK4          | 1.67        | 1.81        | 1.93        | 1.0E-09        | 5.3E-10        | 2.5E-10        | Somatic embryogenesis receptor kinase 4              |
| AT4G34150        | -              | 1.66        | 1.67        | 1.86        | 2.8E-08        | 3.1E-08        | 9.0E-09        | Calcium-dependent lipid-binding (CaLB domain) family |
| AT1G74940        | FLZ13          | 1.65        | 1.60        | 1.63        | 3.6E-07        | 5.8E-07        | 4.7E-07        | FCS-Like Zinc finger 13                              |
| AT3G55980        | SZF1           | 1.65        | 1.03        | 1.12        | 1.5E-06        | 1.9E-04        | 8.1E-05        | Salt-inducible zinc finger 1                         |
| AT5G61780        | TSN2           | 1.65        | 1.18        | 1.24        | 8.3E-12        | 4.0E-10        | 2.1E-10        | Ribonuclease TUDOR 2                                 |
| <b>AT1G15520</b> | <b>ABC G40</b> | <b>1.64</b> | <b>1.69</b> | <b>1.33</b> | <b>6.6E-07</b> | <b>5.4E-07</b> | <b>7.2E-06</b> | <b>ABC transporter G family member 40</b>            |
| AT1G28760        | PNET2_A        | 1.64        | 1.74        | 1.96        | 4.8E-09        | 3.3E-09        | 8.1E-10        | Inner nuclear membrane protein A                     |
| AT2G41010        | CAMB P25       | 1.61        | 1.76        | 1.77        | 4.2E-10        | 2.2E-10        | 1.9E-10        | Calmodulin-binding protein 25                        |
| AT2G26190        | IQM4           | 1.59        | 1.87        | 1.88        | 1.4E-08        | 2.8E-09        | 2.4E-09        | IQ domain-containing protein IQM4                    |

|                  |                 |             |             |             |                |                |                |  |
|------------------|-----------------|-------------|-------------|-------------|----------------|----------------|----------------|--|
| AT4G19520        | -               | 1.58        | 1.72        | 1.83        | 6.7E-08        | 2.9E-08        | 1.4E-08        | Probable disease resistance protein At4g19520        |
| AT1G19310        | -               | 1.55        | 1.58        | 1.34        | 4.2E-08        | 4.1E-08        | 2.4E-07        | At1g19310/F18O14_14                                  |
| <b>AT5G54490</b> | <b>PBP1</b>     | <b>1.51</b> | <b>1.70</b> | <b>1.48</b> | <b>3.8E-07</b> | <b>1.2E-07</b> | <b>5.2E-07</b> | <b>Pinoid-binding protein 1</b>                      |
| AT1G21550        | CML44           | 1.49        | 1.48        | 1.51        | 9.0E-06        | 1.1E-05        | 9.0E-06        | Probable calcium-binding protein CML44               |
| AT1G73010        | PS2             | 1.49        | 1.11        | 1.39        | 2.3E-07        | 6.1E-06        | 5.2E-07        | Inorganic pyrophosphatase 1                          |
| <b>AT1G59660</b> | <b>NUP98B</b>   | <b>1.49</b> | <b>1.20</b> | <b>1.44</b> | <b>2.0E-08</b> | <b>2.6E-07</b> | <b>3.2E-08</b> | <b>Nuclear pore complex protein NUP98B</b>           |
| <b>AT1G59860</b> | <b>HSP17.6A</b> | <b>1.48</b> | <b>1.25</b> | <b>1.20</b> | <b>6.4E-06</b> | <b>4.3E-05</b> | <b>6.0E-05</b> | <b>17.6 kDa class I heat shock protein 1</b>         |
| AT1G61660        | BHLH12          | 1.48        | 1.26        | 1.24        | 6.7E-10        | 5.1E-09        | 5.6E-09        | Transcription factor bHLH112                         |
| AT4G12720        | AtNUD T7        | 1.45        | 1.69        | 1.83        | 1.1E-07        | 2.3E-08        | 9.4E-09        | MutT/nudix family protein                            |
| AT4G18880        | HSFA4A          | 1.45        | 1.66        | 1.53        | 1.6E-08        | 4.2E-09        | 9.7E-09        | Heat shock transcription factor A4A                  |
| AT5G45630        | -               | 1.45        | 1.63        | 1.40        | 3.1E-06        | 9.6E-07        | 5.0E-06        | Putative uncharacterized protein                     |
| AT2G41100        | CML12           | 1.44        | 1.65        | 1.70        | 1.0E-06        | 2.8E-07        | 1.9E-07        | Calmodulin-like protein 12                           |
| AT3G43190        | SUS4            | 1.44        | 1.45        | 1.45        | 6.9E-08        | 7.4E-08        | 7.3E-08        | Sucrose synthase 4                                   |
| AT1G17290        | ALAAT1          | 1.44        | 1.53        | 1.56        | 1.4E-08        | 8.0E-09        | 6.1E-09        | Alanine aminotransferase 1, mitochondrial            |
| AT5G58120        | -               | 1.43        | 1.64        | 1.73        | 2.0E-09        | 5.7E-10        | 3.1E-10        | Disease resistance protein (TIR-NBS-LRR class)       |
| AT1G57630        | -               | 1.43        | 1.84        | 1.67        | 2.6E-05        | 2.3E-06        | 6.0E-06        | Disease resistance protein RPP1-WsB, putative        |
| AT5G25250        | FLOT1           | 1.40        | 1.70        | 2.05        | 9.6E-06        | 1.4E-06        | 1.8E-07        | Flotillin-like protein 1                             |
| AT5G57220        | CYP81F2         | 1.38        | 1.83        | 1.80        | 1.4E-04        | 1.0E-05        | 1.2E-05        | Cytochrome P450 81F2                                 |
| AT4G02380        | SAG21           | 1.37        | 1.67        | 1.59        | 2.7E-07        | 3.5E-08        | 5.8E-08        | senescence-associated gene 21                        |
| AT2G26560        | PLP2            | 1.36        | 1.01        | 1.35        | 6.0E-04        | 6.5E-03        | 7.3E-04        | Patatin-like protein 2                               |
| AT1G14780        | -               | 1.36        | 1.91        | 2.21        | 1.0E-09        | 3.7E-11        | 7.8E-12        | MACPF domain-containing protein At1g14780            |
| <b>AT1G16030</b> | <b>HSP70-5</b>  | <b>1.35</b> | <b>1.37</b> | <b>1.41</b> | <b>2.5E-04</b> | <b>2.6E-04</b> | <b>1.9E-04</b> | <b>Heat shock protein 70-5</b>                       |
| AT3G60520        | -               | 1.35        | 1.55        | 1.73        | 4.2E-07        | 1.0E-07        | 2.9E-08        | zinc ion-binding protein                             |
| AT3G22830        | HSFA6B          | 1.32        | 1.72        | 2.11        | 3.8E-08        | 2.3E-09        | 2.3E-10        | Heat stress transcription factor A-6b                |
| AT3G47640        | BHLH47          | 1.32        | 1.45        | 1.66        | 3.1E-08        | 1.3E-08        | 2.8E-09        | Transcription factor bHLH47                          |
| AT5G47060        | -               | 1.32        | 1.55        | 1.70        | 3.2E-05        | 7.2E-06        | 2.5E-06        | Putative uncharacterized protein                     |
| AT2G33585        | -               | 1.31        | 1.35        | 1.16        | 4.7E-09        | 4.2E-09        | 1.9E-08        | unknown protein                                      |
| AT2G36580        | -               | 1.30        | 1.31        | 1.47        | 7.4E-09        | 8.2E-09        | 2.2E-09        | Pyruvate kinase                                      |
| AT1G18570        | MYB51           | 1.29        | 1.43        | 1.57        | 2.1E-05        | 8.5E-06        | 3.2E-06        | Transcription factor MYB51                           |
| AT2G30250        | WRKY25          | 1.28        | 1.40        | 1.58        | 2.7E-09        | 1.3E-09        | 3.3E-10        | Probable WRKY transcription factor 25                |
| AT5G03380        | HIPP06          | 1.26        | 1.16        | 1.00        | 6.9E-09        | 2.1E-08        | 1.1E-07        | Heavy metal-associated isoprenylated plant protein 6 |
| AT5G42050        | -               | 1.26        | 1.47        | 1.68        | 2.5E-08        | 5.3E-09        | 1.1E-09        | Development and Cell Death domain protein            |
| <b>AT5G45340</b> | <b>CYP707A3</b> | <b>1.26</b> | <b>1.64</b> | <b>1.56</b> | <b>6.0E-04</b> | <b>6.2E-05</b> | <b>9.8E-05</b> | <b>Abscisic acid 8'-hydroxylase 3</b>                |
| AT1G42990        | BZIP60          | 1.24        | 1.10        | 1.19        | 1.1E-08        | 5.0E-08        | 2.0E-08        | bZIP transcription factor 60                         |
| AT4G20380        | LSD1            | 1.24        | 1.33        | 1.32        | 4.0E-09        | 2.3E-09        | 2.3E-09        | LSD1 zinc finger family protein                      |
| AT1G14550        | PER5            | 1.21        | 1.20        | 1.57        | 4.7E-05        | 6.1E-05        | 3.8E-06        | Peroxidase 5   |

|                             |                 |              |              |              |                |                |                |   |
|-----------------------------|-----------------|--------------|--------------|--------------|----------------|----------------|----------------|---|
| AT2G38470                   | WRKY33          | 1.21         | 1.22         | 1.29         | 5.9E-05        | 6.1E-05        | 3.5E-05        | WRKY DNA-binding protein 33                       |
| AT1G16420                   | AMC8            | 1.19         | 1.42         | 1.19         | 1.7E-04        | 3.7E-05        | 1.9E-04        | Metacaspase-8                                     |
| AT4G34460                   | GB1             | 1.17         | 1.22         | 1.36         | 6.5E-10        | 5.5E-10        | 1.7E-10        | GTP binding protein beta 1                        |
| AT2G16060                   | AHB1            | 1.16         | 1.38         | 1.18         | 2.2E-05        | 4.4E-06        | 2.1E-05        | Class I hemoglobin                                |
| AT1G68760                   | NUDT1           | 1.16         | 1.34         | 1.65         | 1.4E-05        | 3.9E-06        | 3.8E-07        | Nudix hydrolase 1                                 |
| AT1G29395                   | COR413IM1       | 1.16         | 1.47         | 1.42         | 6.4E-03        | 1.3E-03        | 1.7E-03        | Cold-regulated 413 inner membrane protein 1       |
| AT3G49530                   | NAC062          | 1.16         | 1.33         | 1.42         | 1.9E-07        | 4.7E-08        | 2.1E-08        | NAC domain-containing protein 62                  |
| AT1G66880                   | -               | 1.11         | 1.32         | 1.35         | 1.4E-07        | 2.2E-08        | 1.7E-08        | Protein kinase superfamily protein                |
| AT4G14970                   | -               | 1.10         | 1.30         | 1.62         | 1.0E-06        | 2.0E-07        | 1.6E-08        | unknown protein                                   |
| AT4G27460                   | CBSX5           | 1.10         | 1.11         | 1.12         | 2.0E-06        | 2.1E-06        | 1.9E-06        | CBS domain containing protein 5                   |
| AT1G03220                   | -               | 1.10         | 1.16         | 1.14         | 2.2E-08        | 1.4E-08        | 1.7E-08        | Eukaryotic aspartyl protease family protein       |
| AT1G64280                   | NPR1            | 1.10         | 1.28         | 1.35         | 2.6E-09        | 6.1E-10        | 3.1E-10        | Regulatory protein NPR1                           |
| AT2G01150                   | RHA2B           | 1.08         | 1.65         | 1.73         | 3.7E-07        | 4.0E-09        | 2.2E-09        | RING-H2 finger protein 2B                         |
| AT1G55920                   | SAT1            | 1.06         | 1.89         | 1.41         | 4.1E-09        | 1.1E-11        | 2.3E-10        | Serine acetyltransferase 1, chloroplastic         |
| AT4G23210                   | CRK13           | 1.06         | 1.81         | 2.19         | 1.2E-03        | 1.0E-05        | 1.3E-06        | Cysteine-rich receptor-like protein kinase 13     |
| AT5G20480                   | EFR             | 1.05         | 1.50         | 1.42         | 3.4E-05        | 9.3E-07        | 1.6E-06        | LRR receptor-like serine/threonine-protein kinase |
| AT2G33120                   | SAR1            | 1.04         | 1.19         | 1.10         | 1.3E-08        | 3.3E-09        | 7.7E-09        | Synaptobrevin-related protein 1                   |
| AT5G46350                   | WRKY8           | 1.03         | 1.46         | 1.55         | 3.2E-05        | 1.0E-06        | 5.3E-07        | WRKY transcription factor 8                       |
| AT3G56880                   | -               | 1.03         | 1.48         | 1.64         | 9.9E-09        | 2.3E-10        | 7.5E-11        | VQ motif-containing protein                       |
| AT2G17520                   | IRE1A           | 1.01         | 1.14         | 1.21         | 2.9E-08        | 8.8E-09        | 4.5E-09        | Serine/threonine-protein                          |
| <b>Down regulated genes</b> |                 |              |              |              |                |                |                |   |
| AT1G05200                   | GLR3.4          | -1.04        | -1.04        | -1.35        | 8.7E-08        | 1.1E-07        | 5.4E-09        | Glutamate receptor                                |
| AT5G15410                   | CNGC2           | -1.06        | -1.08        | -1.18        | 3.0E-07        | 2.7E-07        | 1.0E-07        | Cyclic nucleotide-gated ion channel 2             |
| AT5G24660                   | LSU2            | -1.10        | -1.08        | -1.27        | 2.2E-04        | 3.0E-04        | 6.5E-05        | Protein response to low sulfur 2                  |
| AT5G56010                   | HSP90-3         | -1.24        | -1.31        | -1.18        | 1.2E-10        | 8.8E-11        | 2.3E-10        | Heat shock protein 90-3                           |
| AT4G13540                   | -               | -1.28        | -1.12        | -1.21        | 7.4E-06        | 3.2E-05        | 1.4E-05        | Golgin family A protein                           |
| AT3G12610                   | DRT100          | -1.28        | -1.21        | -1.22        | 3.7E-09        | 8.4E-09        | 7.3E-09        | DNA-damage repair/tolerant 100                    |
| AT4G28270                   | RMA2            | -1.38        | -1.31        | -1.35        | 9.9E-08        | 2.0E-07        | 1.4E-07        | E3 ubiquitin-protein ligase RMA2                  |
| AT1G21910                   | ERF012          | -1.44        | -1.67        | -1.60        | 1.2E-06        | 2.8E-07        | 4.3E-07        | Dehydration response element-binding protein      |
| AT4G26850                   | VTC2            | -1.44        | -1.58        | -1.68        | 6.6E-10        | 3.4E-10        | 1.6E-10        | GDP-L-galactose phosphorylase 1                   |
| AT2G21320                   | BBX18           | -1.46        | -1.52        | -1.65        | 5.1E-07        | 3.6E-07        | 1.5E-07        | B-box zinc finger protein 18                      |
| AT3G28270                   | AFL1            | -1.66        | -1.72        | -1.85        | 4.3E-05        | 3.5E-05        | 1.7E-05        | AT14A-LIKE1                                       |
| <b>AT1G78000</b>            | <b>SULTR1;2</b> | <b>-1.70</b> | <b>-1.35</b> | <b>-1.01</b> | <b>7.4E-07</b> | <b>9.8E-06</b> | <b>1.7E-04</b> | <b>Sulfate transporter 1.2</b>                    |
| AT5G20790                   | -               | -1.74        | -1.68        | -2.00        | 1.7E-07        | 2.8E-07        | 3.9E-08        | unknown protein                                   |
| AT5G39610                   | NAC92           | -1.75        | -1.72        | -1.75        | 5.7E-10        | 8.7E-10        | 6.9E-10        | NAC domain-containing protein 92                  |
| AT5G44680                   | -               | -1.89        | -2.07        | -2.07        | 4.8E-07        | 2.0E-07        | 2.0E-07        | DNA glycosylase superfamily protein               |

|           |            |       |       |       |             |             |             |   |
|-----------|------------|-------|-------|-------|-------------|-------------|-------------|---|
| AT3G56400 | WRKY<br>70 | -1.93 | -1.89 | -1.70 | 8.0E-<br>06 | 1.1E-<br>05 | 3.2E-<br>05 | Probable WRKY transcription factor 70         |
| AT1G72910 | TN8        | -2.59 | -2.54 | -2.83 | 3.5E-<br>07 | 4.7E-<br>07 | 1.5E-<br>07 | Similar to part of disease resistance protein |

<sup>A</sup>DEGs in seedlings of Col-0, *opr2/3* and *aos* one hour after wounding relative to control. All genotypes were pretreated with MeJA during development. An FDR of 0.1 and a minimum FC of 2 were applied as cutoffs. DEGs were classified according to their Gene Ontology enrichment and in many cases, genes may fall into more than one GO category.

<sup>B</sup> False discovery rate corrected p-value.

<sup>C</sup> Ratio between LogFC of Col-0 and the LogFC of *opr2/3* and *aos*.

N/A not annotated.

**Table S3 List of wound-responsive genes which are JA-dependent**

Wound-responsive DEGs which are differentially expressed in Col-0 in comparison to *opr2/3* and *aos*. DEGs were calculated from three biologically independent experiments and were classified according to their GO enrichment.

| AGI                              | Gene name     | LogFC <sup>A</sup> |               |              | Adjusted p-value <sup>B</sup> |                     |                     | Description   |
|----------------------------------|---------------|--------------------|---------------|--------------|-------------------------------|---------------------|---------------------|---|
|                                  |               | Col-0              | <i>opr2/3</i> | <i>aos</i>   | Col-0                         | <i>opr2/3</i>       | <i>aos</i>          |   |
| <b>Response to jasmonic acid</b> |               |                    |               |              |                               |                     |                     |   |
| AT1G17420                        | LOX3          | 4.76               | 4.43          | 3.83         | 1.1E-<br>-12                  | 3.3E-<br>12         | 1.3E-<br>11         | Lipoxygenase 3, chloroplastic                       |
| AT1G20510                        | 4CLL5         | 3.32               | 2.06          | 1.90         | 5.4E-<br>-14                  | 5.5E-<br>12         | 1.1E-<br>11         | 4-coumarate--CoA ligase-like 5                      |
| <b>AT1G28480</b>                 | <b>GRX480</b> | <b>5.62</b>        | <b>4.63</b>   | <b>4.44</b>  | <b>3.0E-<br/>-11</b>          | <b>3.1E-<br/>10</b> | <b>4.3E-<br/>10</b> | <b>Glutaredoxin-C9</b>                              |
| <b>AT1G30135</b>                 | <b>JAZ8</b>   | <b>5.94</b>        | <b>3.53</b>   | <b>3.72</b>  | <b>3.0E-<br/>-14</b>          | <b>4.7E-<br/>12</b> | <b>2.4E-<br/>12</b> | <b>Protein TIFY 5A</b>                              |
| AT1G61120                        | GES           | 2.41               | 0.25          | 0.13         | 1.6E-<br>-10                  | 8.3E-<br>02         | 3.9E-<br>01         | (E, E)-geranylinalool synthase                      |
| <b>AT1G70700</b>                 | <b>JAZ9</b>   | <b>2.30</b>        | <b>0.78</b>   | <b>0.74</b>  | <b>1.3E-<br/>-11</b>          | <b>2.1E-<br/>06</b> | <b>3.7E-<br/>06</b> | <b>TIFY7</b>  |
| <b>AT1G72450</b>                 | <b>JAZ6</b>   | <b>1.76</b>        | <b>0.57</b>   | <b>0.38</b>  | <b>2.6E-<br/>-08</b>          | <b>2.1E-<br/>03</b> | <b>2.7E-<br/>02</b> | <b>TIFY11B</b>                                      |
| <b>AT1G74950</b>                 | <b>JAZ2</b>   | <b>3.73</b>        | <b>2.06</b>   | <b>2.19</b>  | <b>3.2E-<br/>-14</b>          | <b>1.1E-<br/>11</b> | <b>5.4E-<br/>12</b> | <b>TIFY10B</b>                                      |
| AT3G09940                        | MDAR3         | 2.87               | 1.73          | 1.28         | 1.2E-<br>-12                  | 3.4E-<br>10         | 8.6E-<br>09         | Monodehydroascorbate reductase 3                    |
| AT3G15500                        | NAC055        | 2.42               | 0.71          | 0.67         | 1.6E-<br>-09                  | 6.7E-<br>04         | 1.0E-<br>03         | NAC3  |
| AT3G16470                        | JAL35         | 0.42               | -0.12         | -0.13        | 1.6E-<br>-02                  | 5.4E-<br>01         | 4.8E-<br>01         | Jacalin-related lectin 35                           |
| <b>AT3G22275</b>                 | <b>JAZ13</b>  | <b>3.88</b>        | <b>0.28</b>   | <b>0.15</b>  | <b>3.0E-<br/>-13</b>          | <b>2.8E-<br/>02</b> | <b>2.4E-<br/>01</b> | <b>Protein JAZ13</b>                                |
| AT3G23240                        | ERF1B         | 1.39               | 1.00          | 0.71         | 5.0E-<br>-07                  | 1.9E-<br>05         | 4.3E-<br>04         | Ethylene-responsive transcription factor 1B         |
| <b>AT3G45140</b>                 | <b>LOX2</b>   | <b>0.31</b>        | <b>-0.38</b>  | <b>-0.43</b> | <b>1.8E-<br/>-02</b>          | <b>6.3E-<br/>03</b> | <b>2.7E-<br/>03</b> | <b>Lipoxygenase 2, chloroplastic</b>                |
| AT3G53600                        | ZAT18         | 3.56               | 1.95          | 1.80         | 5.3E-<br>-10                  | 5.2E-<br>07         | 1.2E-<br>06         | Nuclear C2H2 zinc finger protein                    |
| AT5G09980                        | PEP4          | 2.55               | 0.76          | 0.98         | 2.3E-<br>-07                  | 1.3E-<br>02         | 2.5E-<br>03         | Elicitor peptide 4                                  |
| AT5G17490                        | RGL3          | 2.06               | 0.62          | 0.79         | 2.4E-<br>-10                  | 1.2E-<br>04         | 1.0E-<br>05         | DELLA protein RGL3                                  |
| AT5G55120                        | VTC5          | 1.36               | 0.24          | 0.30         | 1.8E-<br>-09                  | 2.2E-<br>02         | 5.8E-<br>03         | vitamin C defective 5                               |
| AT5G60300                        | LECRK19       | 1.94               | 0.38          | 0.39         | 2.0E-<br>-10                  | 3.5E-<br>03         | 2.7E-<br>03         | L-type lectin-domain containing receptor kinase I.9 |
| AT5G63970                        | RGLG3         | 2.05               | 1.36          | 0.86         | 7.1E-<br>-09                  | 8.1E-<br>07         | 8.7E-<br>05         | E3 ubiquitin-protein ligase RGLG3                   |
| <b>Response to wounding</b>      |               |                    |               |              |                               |                     |                     |   |
| AT1G51760                        | JR3           | 2.03               | 0.61          | 0.39         | 7.9E-<br>-12                  | 4.9E-<br>06         | 3.5E-<br>04         | jasmonic acid responsive 3                          |
| AT1G73500                        | MKK9          | 0.21               | -0.79         | -0.89        | 4.1E-<br>-01                  | 3.6E-<br>03         | 1.4E-<br>03         | Mitogen-activated protein kinase kinase 9           |
| AT1G74930                        | ERF018        | 3.93               | 1.94          | 1.40         | 4.9E-<br>-11                  | 1.4E-<br>07         | 4.6E-<br>06         | Ethylene-responsive transcription factor ERF018     |

|   |          |       |       |       |         |         |         |   |
|---|----------|-------|-------|-------|---------|---------|---------|---|
| AT1G80840   | WRKY40   | 4.52  | 3.83  | 3.72  | 3.0E-13 | 1.9E-12 | 2.1E-12 | Probable WRKY transcription factor 40             |
| AT2G22330   | CYP79B3  | 1.52  | 0.65  | 0.45  | 4.6E-09 | 5.3E-05 | 1.3E-03 | cytochrome P450, family 79, polypeptide 3         |
| AT2G46510   | AIB      | 2.97  | 1.03  | 1.11  | 4.0E-12 | 4.6E-07 | 2.1E-07 | Transcription factor ABA-inducible bHLH-TYPE      |
| AT2G46970   | PIL1     | -0.05 | 1.40  | 1.27  | 9.2E-01 | 2.6E-04 | 5.9E-04 | Transcription factor PIL1                         |
| AT4G08170   | ITPK3    | 2.12  | 0.78  | 0.55  | 3.2E-10 | 2.1E-05 | 4.9E-04 | Inositol-tetrakisphosphate 1-kinase 3             |
| AT4G10390   | -        | 1.00  | -0.33 | -0.30 | 1.7E-05 | 5.6E-02 | 8.9E-02 | Probable receptor-like protein kinase             |
| AT4G15440   | CYP74B2  | 1.42  | -0.42 | -0.20 | 3.0E-08 | 4.3E-03 | 1.4E-01 | Probable inactive linolenate hydroperoxide lyase  |
| AT4G24350   | -        | 1.90  | -0.01 | -0.17 | 3.5E-10 | 1.0E+00 | 1.8E-01 | Phosphorylase superfamily protein                 |
| AT4G39980   | DHS1     | 0.60  | -0.08 | -0.18 | 3.6E-07 | 2.6E-01 | 1.7E-02 | Phospho-2-dehydro-3-deoxyheptonate aldolase 1     |
| AT5G05730   | ASA1     | 1.21  | 0.51  | 0.40  | 5.4E-08 | 3.9E-04 | 3.0E-03 | Anthranilate synthase alpha subunit 1             |
| AT5G10300   | HNL      | 2.11  | 0.41  | 0.65  | 4.7E-10 | 6.0E-03 | 1.7E-04 | Alpha-hydroxynitrile lyase                        |
| AT5G47240   | atnudt8  | 2.70  | 1.13  | 1.18  | 2.2E-10 | 3.9E-06 | 2.5E-06 | nudix hydrolase homolog 8                         |
| AT5G53750   | -        | 1.64  | 0.55  | 0.34  | 2.1E-08 | 1.5E-03 | 3.1E-02 | CBS domain-containing protein                     |
| AT5G54170   | -        | 2.13  | 1.17  | 0.91  | 1.6E-11 | 1.3E-08 | 2.0E-07 | Polyketide cyclase/dehydrase and lipid transport  |
| AT5G63450   | CYP94B1  | 3.97  | 1.39  | 0.67  | 1.3E-10 | 1.4E-05 | 7.0E-03 | cytochrome P450 family 94, polypeptide 1          |
| <b>Indole-containing compound metabolic process</b> |          |       |       |       |         |         |         |   |
| AT1G25220   | ASB1     | 1.56  | 0.97  | 0.75  | 1.1E-08 | 2.2E-06 | 3.4E-05 | Anthranilate synthase beta subunit 1              |
| AT1G69370   | CM3      | 1.07  | -0.09 | -0.07 | 4.8E-06 | 6.3E-01 | 7.3E-01 | Chorismate mutase 3, chloroplastic                |
| AT4G27260   | GH3.5    | -0.19 | 0.58  | 1.02  | 1.4E-01 | 2.1E-04 | 7.7E-07 | Indole-3-acetic acid-amido synthetase GH3.5       |
| AT4G30530   | GGP1     | 1.40  | 0.68  | 0.54  | 2.2E-10 | 8.4E-07 | 9.9E-06 | Gamma-glutamyl peptidase 1                        |
| AT4G34410   | ERF109   | 4.78  | 3.67  | 3.45  | 3.0E-14 | 5.3E-13 | 9.1E-13 | Ethylene-responsive transcription factor ERF109   |
| AT4G37400   | CYP81F3  | 1.34  | 0.17  | 0.44  | 1.8E-08 | 1.7E-01 | 1.6E-03 | Cytochrome P450 81F3                              |
| AT4G39950   | CYP79B2  | 0.82  | 0.40  | 0.16  | 1.3E-04 | 2.9E-02 | 3.9E-01 | Cytochrome P450 family 79, polypeptide 2          |
| AT5G05590   | PAI2     | 0.82  | 0.58  | 0.35  | 3.3E-05 | 8.5E-04 | 2.4E-02 | N-(5'-phosphoribosyl) anthranilate isomerase 2    |
| AT5G27520   | PNC2     | 2.59  | 1.60  | 1.55  | 3.7E-11 | 7.9E-09 | 1.1E-08 | peroxisomal adenine nucleotide carrier 2          |
| AT5G60890   | MYB34    | 0.27  | -1.48 | -1.41 | 1.4E-01 | 5.7E-07 | 9.6E-07 | Transcription factor MYB34                        |
| <b>Toxin metabolic process</b>                      |          |       |       |       |         |         |         |   |
| AT1G17190   | GSTU26   | 3.96  | 1.78  | 1.35  | 5.3E-12 | 3.7E-08 | 7.4E-07 | Glutathione S-transferase U26                     |
| AT1G69930   | GSTU11   | 3.38  | 2.69  | 2.65  | 4.0E-11 | 5.7E-10 | 6.1E-10 | Glutathione S-transferase U11                     |
| AT1G78340   | GSTU22   | 0.61  | 1.49  | 1.42  | 7.7E-03 | 3.7E-06 | 6.1E-06 | Glutathione S-transferase U22                     |
| AT2G29450   | GSTU5    | 1.74  | 0.62  | 0.32  | 2.2E-10 | 1.9E-05 | 5.3E-03 | Glutathione S-transferase U5                      |
| <b>Response to hormone</b>                          |          |       |       |       |         |         |         |   |
| AT1G02340   | HFR1     | 0.32  | 1.25  | 1.75  | 4.1E-02 | 7.0E-07 | 1.7E-08 | Transcription factor HFR1                         |
| AT1G05100   | MAPKKK18 | 3.17  | 1.68  | 1.95  | 7.5E-11 | 9.9E-08 | 1.8E-08 | Mitogen-activated protein kinase kinase kinase 18 |
| AT1G08920   | ESL1     | 2.96  | 1.19  | 1.14  | 1.9E-10 | 5.0E-06 | 7.7E-06 | ERD (early response to dehydration) six-like 1    |
| AT1G12240   | BFRUCT4  | 0.38  | -0.72 | -0.81 | 5.8E-02 | 1.3E-03 | 4.9E-04 | Acid beta-fructofuranosidase 4, vacuolar          |

|                                      |          |       |       |       |         |         |         |  |
|--------------------------------------|----------|-------|-------|-------|---------|---------|---------|--|
| AT1G28370                            | ERF11    | 2.71  | 2.35  | 2.07  | 1.1E-09 | 6.7E-09 | 2.5E-08 | ERF domain protein 11                                |
| AT2G31230                            | ERF15    | 1.48  | 0.40  | 0.43  | 2.5E-06 | 6.2E-02 | 4.5E-02 | Ethylene-responsive transcription factor 15          |
| AT2G32510                            | MAPKKK17 | 2.04  | 0.81  | 0.89  | 5.7E-09 | 1.3E-04 | 5.0E-05 | Mitogen-activated protein kinase kinase 17           |
| AT2G44840                            | ERF13    | 2.17  | 0.65  | 0.49  | 3.3E-05 | 1.1E-01 | 2.4E-01 | Ethylene-responsive transcription factor 13          |
| AT2G44940                            | ERF034   | 2.16  | 0.90  | 1.01  | 7.7E-11 | 1.3E-06 | 3.6E-07 | Ethylene-responsive transcription factor ERF034      |
| AT3G23230                            | ERF098   | 2.97  | 1.95  | 1.76  | 2.6E-09 | 3.3E-07 | 1.0E-06 | Ethylene-responsive transcription factor ERF098      |
| AT3G60490                            | ERF035   | 3.24  | 1.34  | 1.52  | 3.3E-12 | 5.5E-08 | 1.3E-08 | Ethylene-responsive transcription factor ERF035      |
| AT4G05100                            | AtMYB74  | 3.45  | 1.99  | 2.36  | 7.5E-11 | 3.7E-08 | 5.4E-09 | Transcription factor MYB74                           |
| AT4G36900                            | RAP2-10  | 2.18  | 1.10  | 0.68  | 1.5E-10 | 3.4E-07 | 5.0E-05 | Ethylene-responsive transcription factor RAP2-10     |
| AT5G45820                            | CIPK20   | -1.15 | -0.38 | -0.19 | 1.6E-02 | 4.6E-01 | 7.4E-01 | CBL-interacting serine/threonine-protein kinase 20   |
| AT5G50760                            | SAUR55   | 0.83  | -0.82 | -0.61 | 2.4E-03 | 3.0E-03 | 2.0E-02 | Small auxin upregulated RNA 55                       |
| AT5G52900                            | MAKR6    | -1.08 | -0.15 | -0.11 | 2.0E-04 | 6.0E-01 | 7.2E-01 | Probable membrane-associated kinase regulator 6      |
| <b>Response to external stimulus</b> |          |       |       |       |         |         |         |  |
| AT1G11580                            | PMEPCRA  | 1.13  | 0.49  | 0.49  | 6.4E-11 | 8.3E-07 | 7.1E-07 | methyl esterase PCR A                                |
| AT1G16370                            | ATOCT6   | 2.71  | 2.41  | 2.31  | 2.4E-12 | 1.1E-11 | 1.5E-11 | Organic cation/carnitine transporter 6               |
| AT1G26730                            | PHO1-H7  | 4.02  | 3.00  | 3.17  | 2.1E-13 | 3.3E-12 | 1.9E-12 | Phosphate transporter PHO1 homolog 7                 |
| AT1G61800                            | GPT2     | -0.24 | -1.24 | -0.81 | 4.4E-01 | 3.3E-04 | 7.9E-03 | glucose-6-phosphate/phosphate translocator 2         |
| AT2G01340                            | AT17.1   | 1.85  | 0.68  | 0.73  | 4.8E-09 | 2.2E-04 | 1.2E-04 | PADRE protein  |
| AT2G06255                            | EFL3     | 1.53  | -0.26 | -0.26 | 4.0E-06 | 2.8E-01 | 2.7E-01 | Protein ELF4-LIKE 3                                  |
| AT2G22121                            | LCR35    | 2.40  | 0.26  | 0.56  | 8.4E-08 | 3.3E-01 | 3.1E-02 | Putative defensin-like protein 154                   |
| AT2G23560                            | MES7     | 1.07  | -0.37 | -0.61 | 8.9E-06 | 3.9E-02 | 1.6E-03 | methyl esterase 7                                    |
| AT2G33830                            | DRMH1    | 0.81  | 1.26  | 1.47  | 9.7E-03 | 4.1E-04 | 9.4E-05 | dormancy associated gene 2                           |
| AT3G06490                            | MYB108   | 2.89  | 1.69  | 1.69  | 7.9E-11 | 3.4E-08 | 3.3E-08 | Transcription factor MYB108                          |
| AT3G16400                            | NSP1     | 0.62  | 0.16  | -0.02 | 1.4E-04 | 2.3E-01 | 9.2E-01 | Nitrile-specifier protein 1                          |
| AT4G01895                            | -        | 1.41  | 0.15  | 0.12  | 2.2E-04 | 6.9E-01 | 7.6E-01 | systemic acquired resistance (SAR) regulator protein |
| AT4G10500                            | DLO1     | 1.39  | 0.10  | 0.41  | 6.5E-08 | 5.1E-01 | 6.7E-03 | Protein DMR6-like oxygenase 1                        |
| AT4G15330                            | CYP705A1 | 2.16  | 1.10  | 0.41  | 4.5E-08 | 6.5E-05 | 6.1E-02 | Cytochrome P450 705A1                                |
| AT4G22212                            | -        | 1.41  | 0.22  | 0.18  | 2.7E-07 | 1.9E-01 | 3.0E-01 | Defensin-like protein 98                             |
| AT4G22214                            | -        | 2.78  | 0.19  | 0.68  | 7.9E-10 | 3.6E-01 | 1.7E-03 | Defensin-like protein 99                             |
| AT4G22230                            | -        | 1.37  | 0.63  | 0.44  | 1.1E-03 | 9.8E-02 | 2.7E-01 | Defensin-like protein 96                             |
| AT4G29283                            | LCR21    | 2.10  | 0.00  | 0.17  | 2.2E-07 | 1.0E+00 | 5.4E-01 | Defensin-like protein 156                            |
| AT4G29285                            | LCR24    | 2.09  | 0.37  | 0.51  | 1.5E-09 | 1.9E-02 | 2.6E-03 | Defensin-like protein 163                            |
| AT5G01900                            | WRKY62   | 1.27  | 0.46  | 0.41  | 2.5E-06 | 1.5E-02 | 3.0E-02 | Uncharacterized protein At5g01900 (Fragment)         |
| AT5G09978                            | PEP7     | 1.63  | 0.46  | 0.16  | 1.1E-06 | 3.8E-02 | 5.2E-01 | Elicitor peptide 7                                   |
| AT5G12340                            | -        | 3.69  | 2.50  | 1.85  | 8.0E-10 | 7.7E-08 | 2.0E-06 | DUF4228 domain protein                               |
| AT5G19520                            | MSL9     | 1.73  | 0.29  | 0.64  | 9.5E-08 | 1.3E-01 | 2.0E-03 | Mechanosensitive ion channel protein 9               |



|           |          |       |       |       |         |         |         |  |
|-----------|----------|-------|-------|-------|---------|---------|---------|--|
| AT5G47990 | CYP705A5 | 0.51  | -0.57 | -0.75 | 6.2E-04 | 2.6E-04 | 1.9E-05 | thalian-diol desaturase                              |
| AT5G57685 | GDU3     | -1.69 | -1.06 | -0.98 | 2.0E-07 | 3.2E-05 | 6.6E-05 | Protein GLUTAMINE DUMPER 3                           |
| AT5G60310 | LECRK110 | 1.30  | 0.14  | 0.21  | 2.8E-07 | 3.9E-01 | 1.9E-01 | L-type lectin-domain containing receptor kinase I.10 |

<sup>A</sup>DEGs in seedlings of Col-0, *opr2/3* and *aos* one hour after wounding relative to control. All genotypes were pretreated with MeJA during development. An FDR of 0.1 and a minimum FC of 2 were applied as cutoffs. DEGs were classified according to their Gene Ontology enrichment and in many cases, genes may fall into more than one GO category.

<sup>B</sup> False discovery rate corrected p-value.

<sup>C</sup> Ratio between LogFC of Col-0 and the LogFC of *opr2/3* and *aos*.

Genes in bold were validated by qRT-PCR.

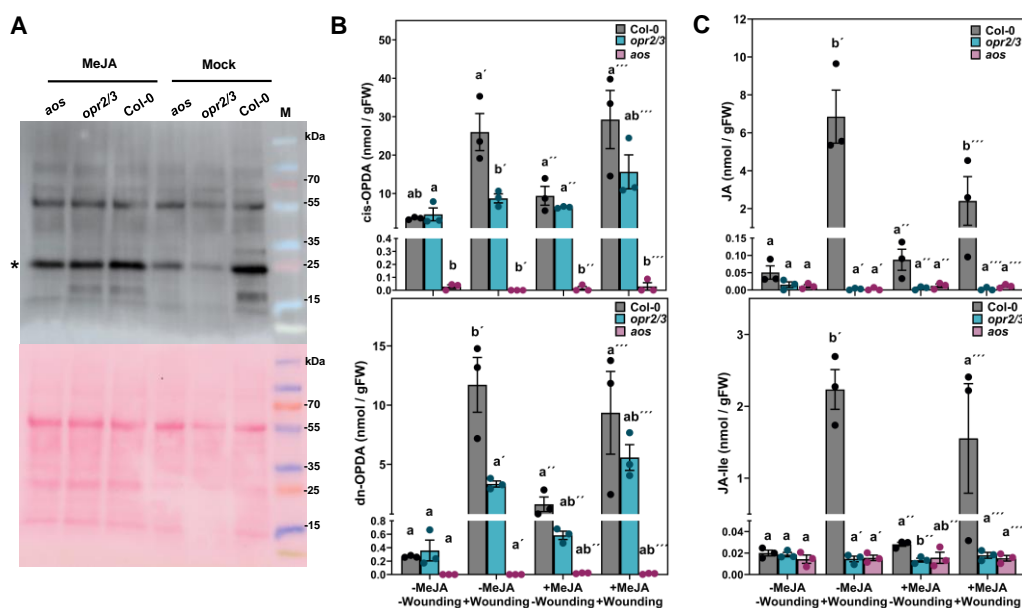


**Fig. S8 Mimicking of the JA feedback loop during development restitutes AOC proteins levels and OPDA in the *opr2/3* double mutant.**

4-week-old rosettes from Col-0, *opr2/3* and *aos* were pretreated with 1  $\mu$ M MeJA during development (MeJA) or with water (Mock).

**A:** AOC proteins levels determination in Col-0, *opr2/3* and *aos* seedlings by immunoblotting from 7  $\mu$ g total protein extract using anti-AOCs primary antibody. Protein staining with Ponceau S. was used as internal control. M= protein marker.

**B, C:** *cis*-OPDA, *dn*-OPDA, JA and JA-Ile levels were determined by LC/MS in Col-0, *opr2/3* and *aos* at control and 1h post-wounding (-wounding, +wounding). The plants were pretreated with water or MeJA during development (-MeJA, +MeJA). Bars represent means of three biological replicates with 3 rosettes each (single dots;  $\pm$ SEM). Different letters denote statistically significant differences among genotypes at each condition as determined by One-Way ANOVA followed by Tukey HSD ( $p < 0.05$ ).

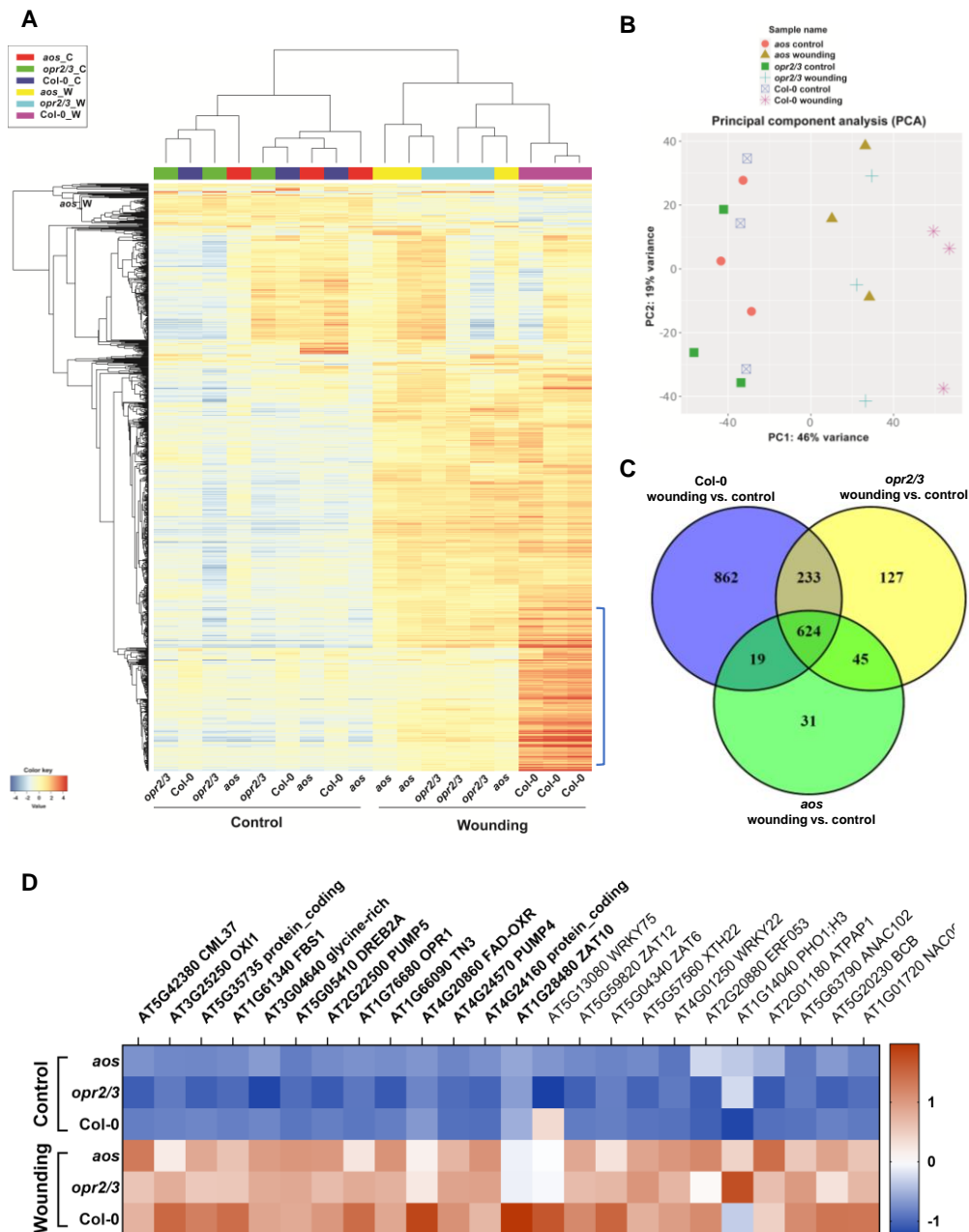


**Fig. S9 Hierarchical clustering and PCA of the wound-induced transcriptional change in adult leaves of Col-0, the JA-deficient *opr2/3* and *aos* mutants.**

4-week-old rosette leaves from Col-0, *opr2/3* and *aos* were pretreated with MeJA during development and were either unwounded (Control) or harvested 1h post wounding with forceps (wounding).

**A:** Hierarchical clustering with heatmap of the 1000 most variable genes based on RNAseq FPKM values transformed into Row normalized Z-score with a threshold of 4. The data is centered by subtracting the average expression level for each gene. The distance matrix is  $1 - r$ , where  $r$  is Pearson's correlation coefficient. The average linkage is used (Bottom 25% of genes regarding expression level are excluded). Regions marked with blue brackets show a different expression pattern between the genotypes.

**B:** PCA projection in two-dimensional space of the transcriptome data with PC1 showing variation in the dataset due to wounding while PC2 showing the variation due to the genotypes.

**C:** Venn diagram representing differentially expressed genes by wounding in Col-0 in comparison to *opr2/3* and *aos*. 624 DEGs were common to all genotypes and were identified by RNAseq using FDR and FC cutoffs of 0.1 and 2, respectively.

**D:** Heatmap illustrating DEGs commonly upregulated by wounding in all the genotypes. Genes in bold were previously identified as OPDA-responsive genes (Taki *et al.*, 2005). Average FPKM values of three independent biological replicates were transformed into row normalized Z-Score.

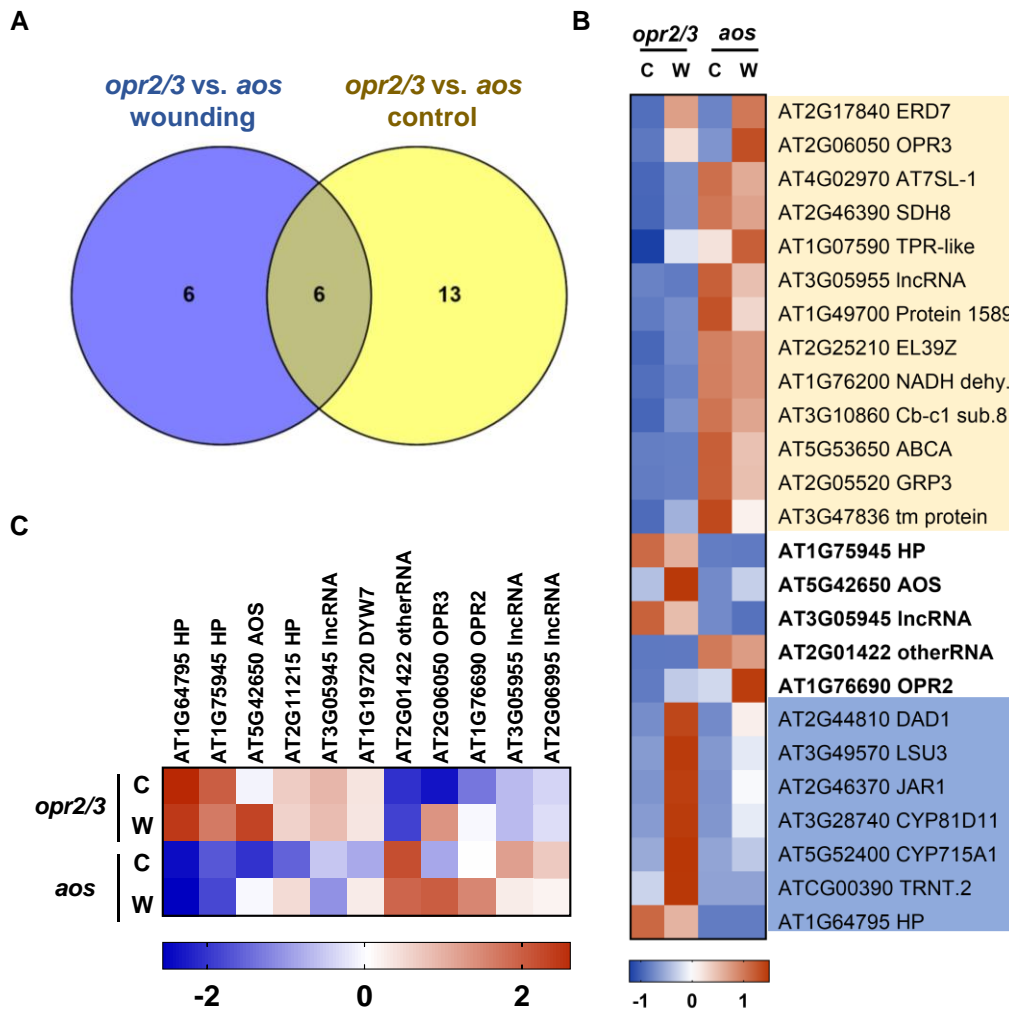


**Fig. S10 The OPDA-mediated transcriptional change in adult leaves.**

4-week-old rosette leaves from Col-0, *opr2/3* and *aos* were pretreated with MeJA during development and were either unwounded (C) or harvested 1h post wounding with forceps (W).

**A:** Venn diagram representing 19 differentially expressed genes in *opr2/3* when compared to *aos* with 6 out of the 19 being common to control and wounding conditions (FDR cutoff: 0.05 and FC cutoff: 2).

**B:** Heatmap illustrating the expression levels of the 25 DEGs in *opr2/3* in comparison to *aos* from (A). The Average FPKM values of three independent biological replicates were transformed into row-normalized Z-Score. Genes highlighted in yellow, and blue correspond to the groups from the Venn diagram in (A) and genes in bold are in the intersection. HP: hypothetical protein.

**C:** DEGs in the absence of MeJA pretreatment. Heatmap illustrating the expression levels of the differentially expressed genes in *opr2/3* in comparison to *aos* from adult leaves that were pretreated with water instead of MeJA during development. The Average FPKM values of three independent biological replicates were transformed into row-normalized Z-Score. HP: hypothetical protein.

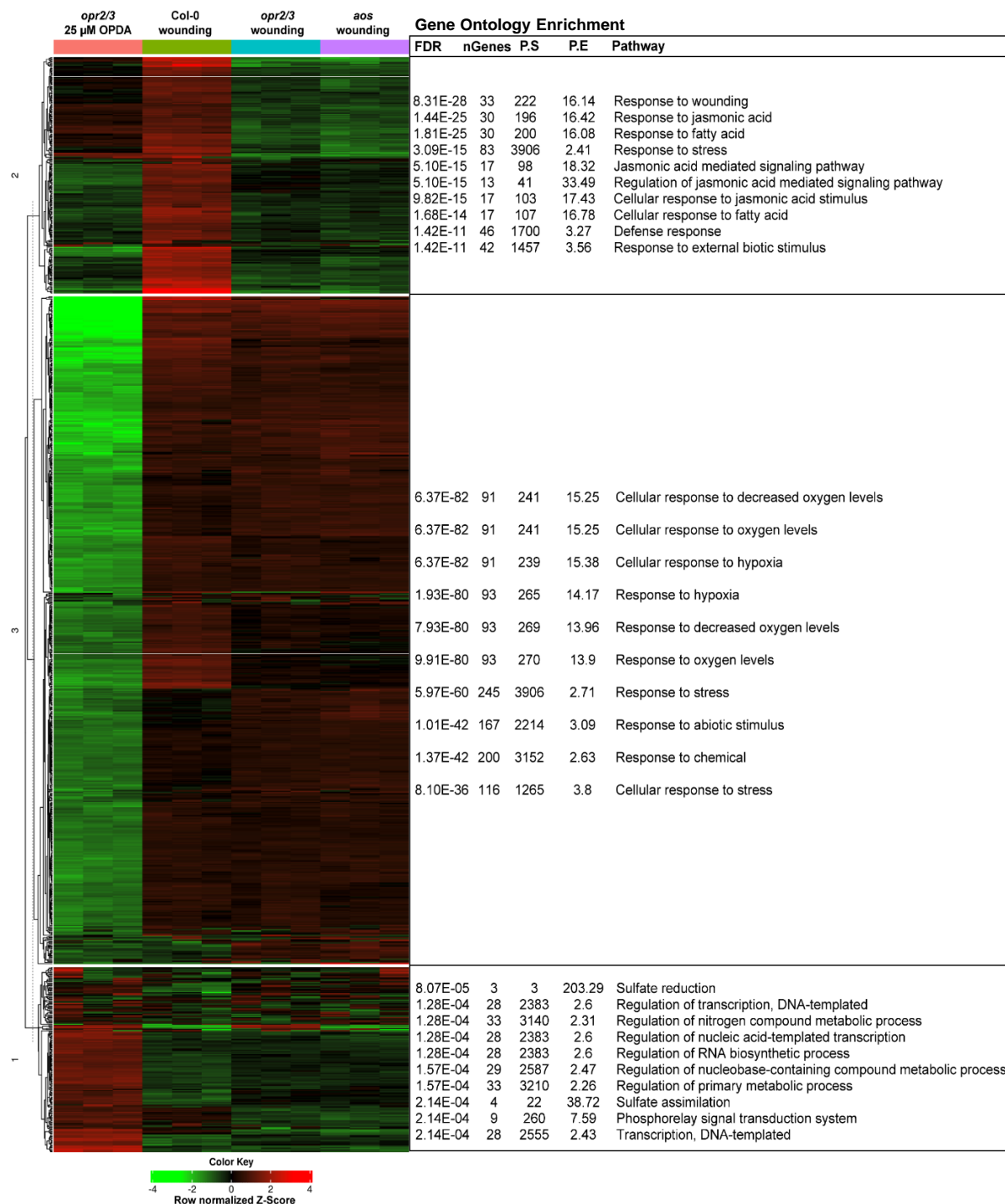


**Fig. S11 Clustering of the transcriptional response in *opr2/3* after treatment with OPDA with the wounding transcriptional response in *Col-0*, *opr2/3* and *aos* seedlings**

All seedlings were pretreated with MeJA during development. K-means clustering of the 1000 most variable genes across the RNA-seq samples and enrichment analysis of each cluster with FDR: False Discovery rate, P.S: Pathway size and F.E: Fold enrichment. Gene Ontology (GO) biological process-based enrichment analysis.

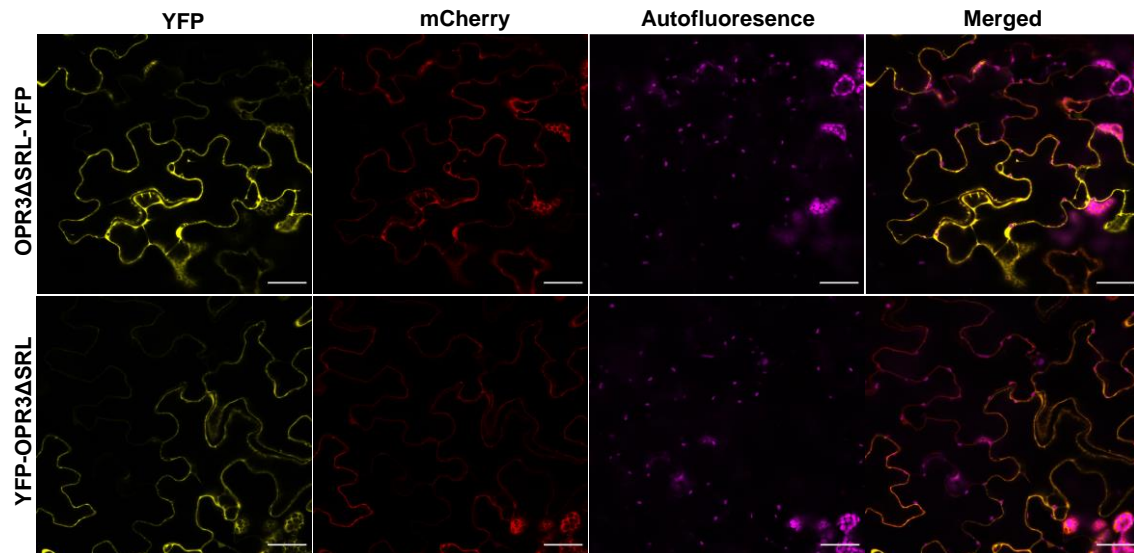


**Fig. S12 OPR3ΔSRL colocalizes with mCherry and shows a cytosolic localization.**

OPR3ΔSRL fused C- and N- terminally to YFP was transiently expressed under the *CaMV 35S* promoter, and co-expressed with mCherry in *N. benthamiana* leaves. The yellow signal corresponds to YFP, red corresponds to mCherry and the magenta corresponds to chlorophyll autofluorescence. Scale bars: 50  $\mu$ m.



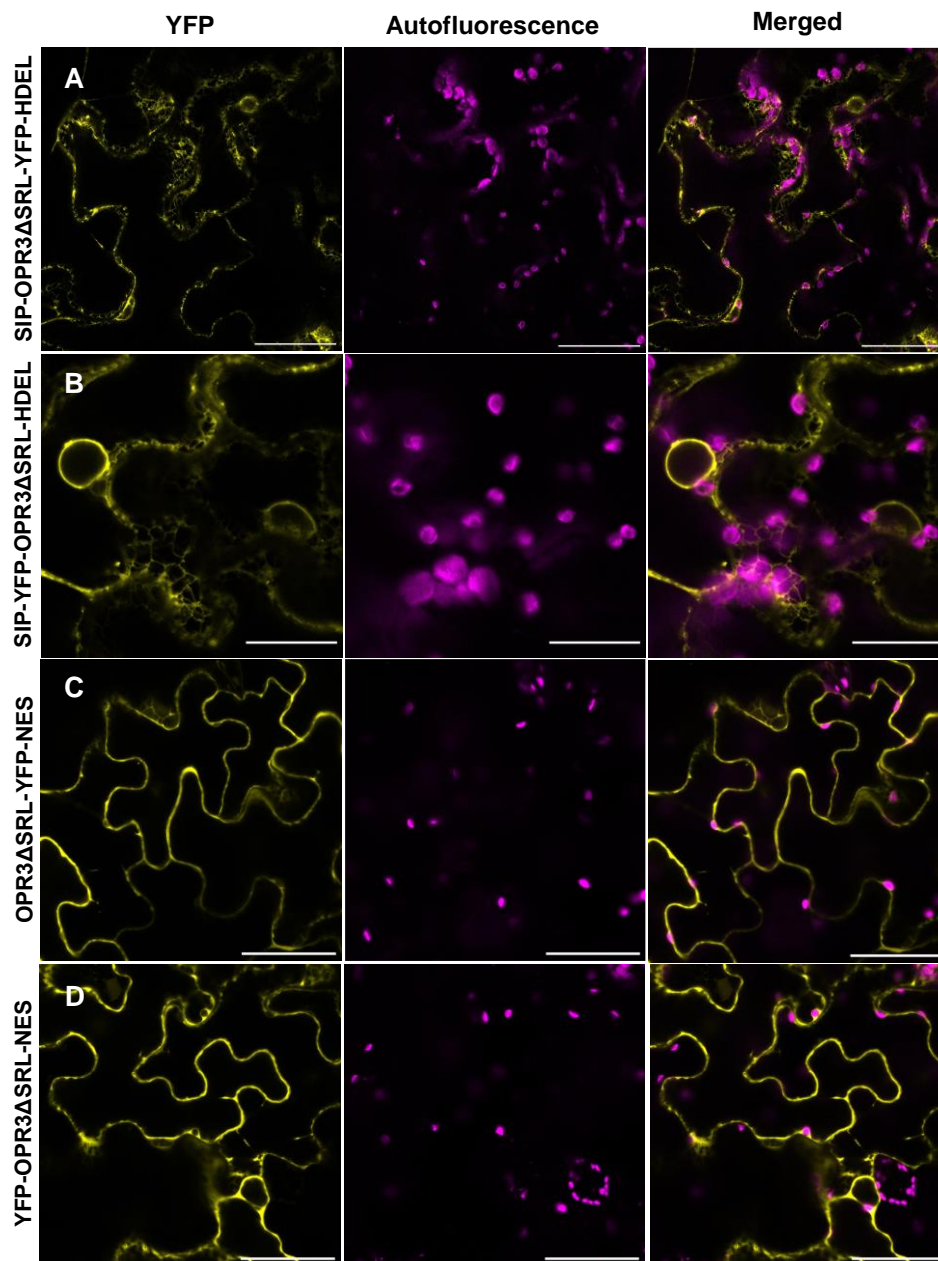


**Fig. S13 Targeting of OPR3 to the ER, cytosol, nucleus, chloroplast, and mitochondria showed successful subcellular localization when transiently expressed in *N. benthamiana* leaves.**

The *CaMV 35S* promoter and *tOCS* terminator were used to drive the expression of *OPR3ΔSRL-YFP* and *YFP-OPR3ΔSRL*. Fluorescence imaging was performed 48-72h post leaf infiltration. The yellow signal corresponds to YFP, and the magenta corresponds to chlorophyll autofluorescence. SIP: signal peptide, NES: nuclear exclusion signal, NLS: nuclear localization signal, cTP: chloroplast transit peptide, mTP: mitochondria transit peptide.

**A, B:** ER-targeted OPR3 shows ER net-like structure with SIP-OPR3ΔSRL-YFP-HDEL (**A**) and SIP-YFP-OPR3ΔSRL-HDEL (**B**). Scale bars: 50 μm in (**A**) and 20 μm in (**B**).

**C, D:** Cytosol-targeted OPR3 shows exclusive cytosolic localization due to the NES signal with OPR3ΔSRL-YFP-NES (**C**) and YFP-OPR3ΔSRL-NES (**D**). Scale bars: 100 μm.

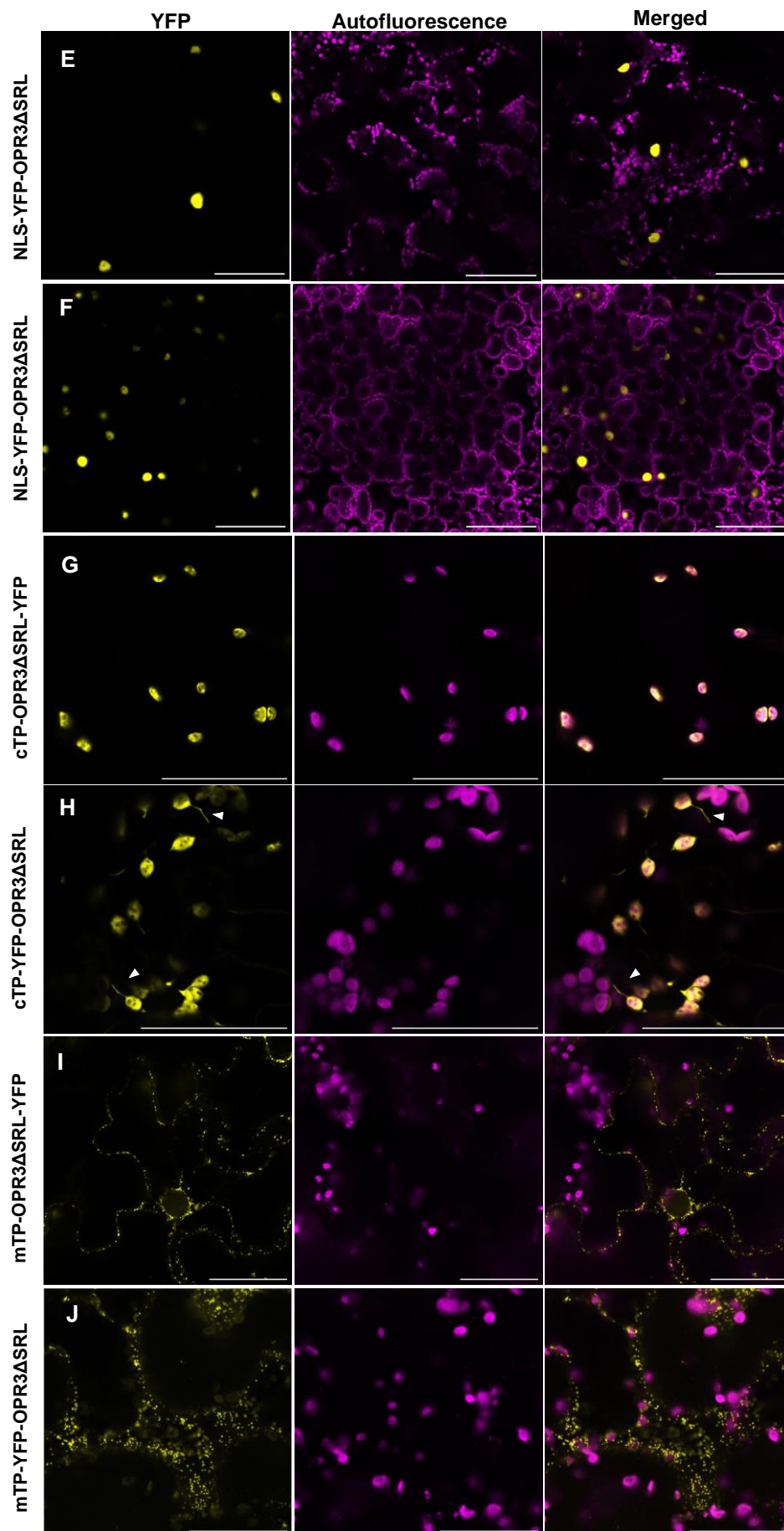
**E, F:** Nucleus-targeted OPR3 shows clear nuclear localization with NLS-OPR3ΔSRL-YFP (**E**) and NLS-YFP-OPR3ΔSRL (**F**). Scale bars: 100 μm.

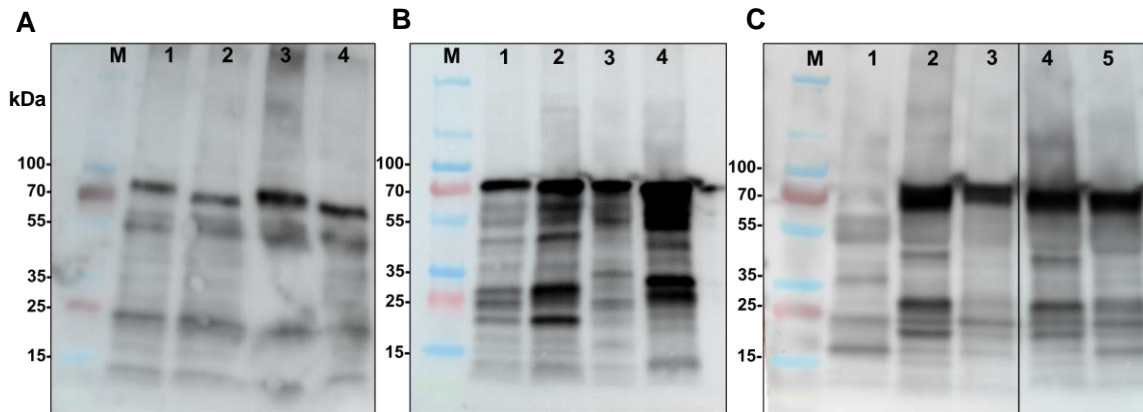
**G, H:** Plastid stroma-targeted OPR3 localizes to the plastids and their stromules (white arrowheads) with cTP-OPR3ΔSRL-YFP (**G**) and cTP-YFP-OPR3ΔSRL (**H**). Scale bars: 50 μm.

**I, J:** Mitochondria-targeted OPR3 localizes to mitochondria mTP-OPR3ΔSRL-YFP (**I**) and mTP-YFP-OPR3ΔSRL (**J**). Scale bars: 50 μm.

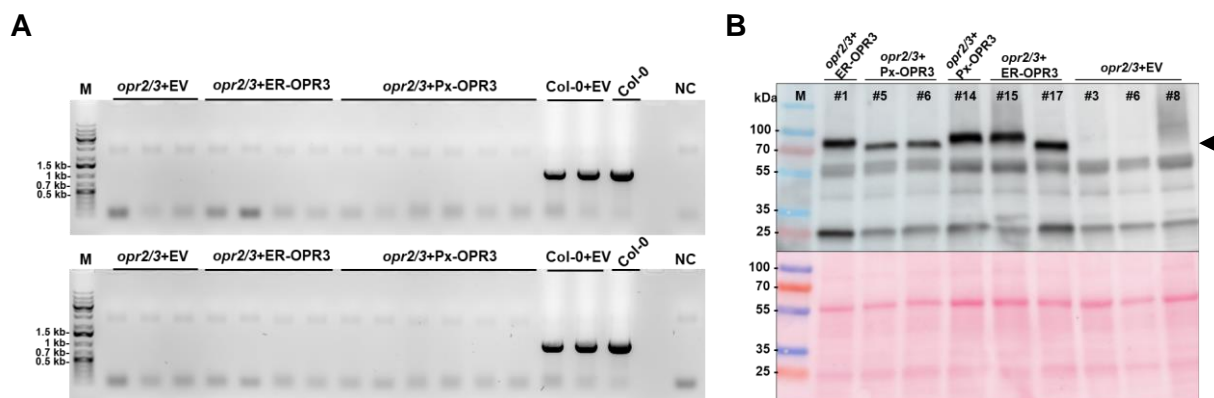


Fig. S13 (continued)





**Fig. S14 Detection of the organelles-targeted OPR3-YFP fusion proteins in *N. benthamiana***  
 Immunoblotting with anti-YFP antibody at 48-72 h post leaf infiltration. M= protein marker.  
**A:** ER-targeted OPR3 $\Delta$ SRL (72.67 kDa) with C-terminal YFP (1) and N-terminal YFP (3) and Peroxisome-targeted OPR3 (69.56 kDa) with C-terminal YFP (2) and N-terminal YFP (4)  
**B:** Nucleus-targeted OPR3 $\Delta$ SRL (71.12 kDa) with C-terminal YFP (1) and N-terminal YFP (3) and cytosol-targeted OPR3 (71.47 kDa) with C-terminal YFP (2) and N-terminal YFP (4)  
**C:** Chloroplast-targeted OPR3 $\Delta$ SRL (77.23 kDa) with C-terminal YFP (2) and N-terminal YFP (4) and mitochondria-targeted (73.45 kDa) OPR3 with C-terminal YFP (3) and N-terminal YFP (5). Line 1 corresponds to non-infiltrated leaves.



**Fig. S15 Genotyping and anti-YFP immunoblotting of the *opr2/3* complementation lines confirm that their phenotypes are due to the function of the organelle targeted OPR3.**

**A:** Genotyping of *opr2/3+EV*, *opr2/3+Px-OPR3*, and *opr2/3+ER-OPR3* confirms the interruption of the *OPR3* and *OPR2* genes. Col-0+EV and Col-0 were used as positive controls for the amplification of *OPR3* (1334 bp) and *OPR2* (1028 bp) in the first and second line, respectively. M= Marker (1kb plus DNA ladder).

**B:** Anti-YFP immunoblot shows similar amounts of OPR3-YFP in in rosette leaves of the *opr2/3+Px-OPR3* and *opr2/3+ER-OPR3* lines (7  $\mu$ g of total protein extract). Arrowhead points to the OPR3-YFP fusion protein. M= protein marker.

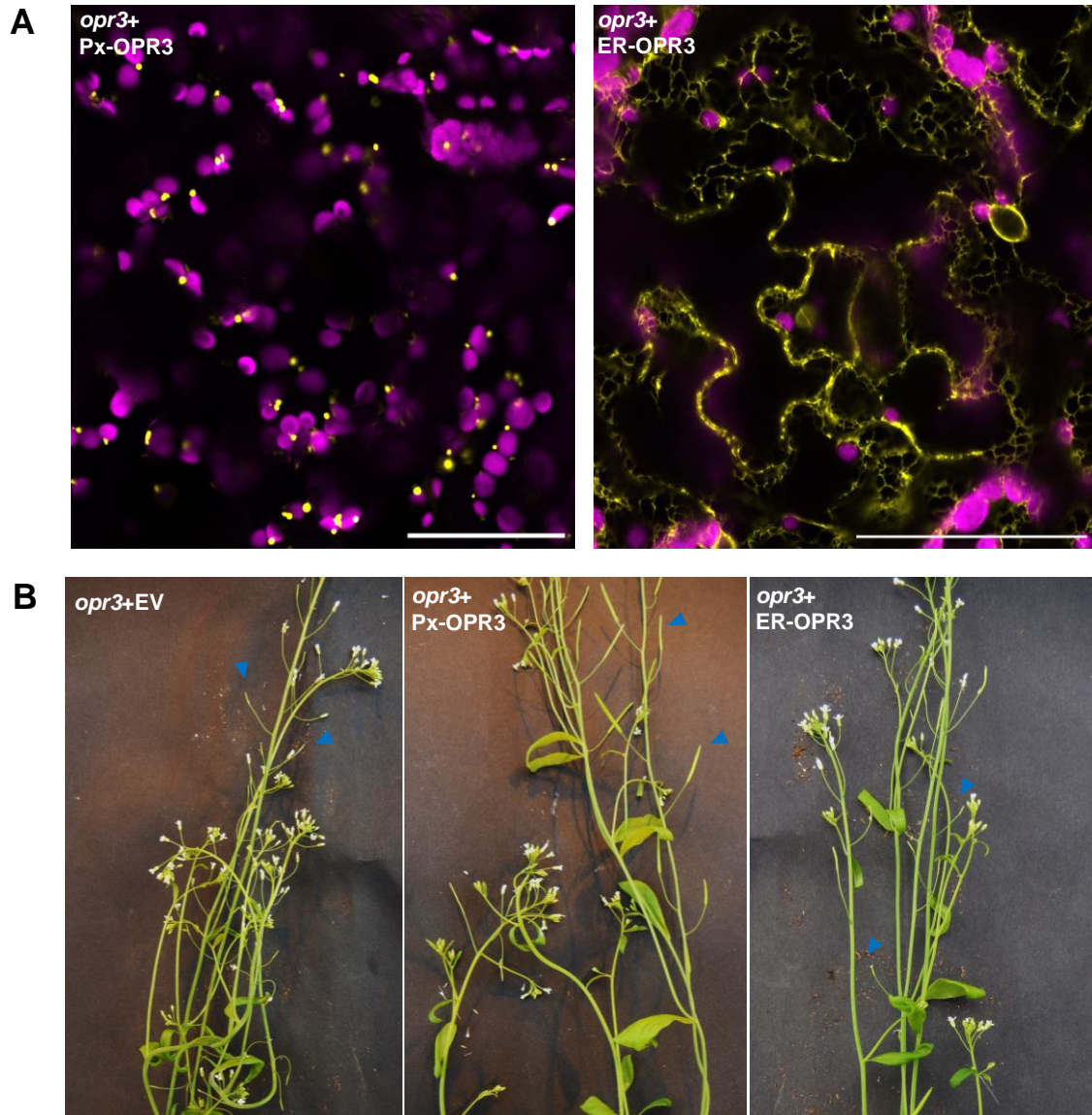


**Fig. S16 Complementation of the *opr3-1* single mutant with ER and Px-OPR3.**

*opr3+ER-OPR3-YFP* shows partial restitution of fertility phenotype. Images are from stable lines which are single insertion from the second generation. ER: endoplasmic reticulum, Px: peroxisome.

**A:** Selected lines showed a clear localization in the peroxisome for the *opr3+Px-OPR3* and ER-localization in the *opr3+ER-OPR3*. The yellow signal corresponds to YFP signal and the magenta to chlorophyll autofluorescence. Scale bars: 50  $\mu$ m.

**B:** The inflorescence of the *opr3+Px-OPR3* line shows full restitution of fertility in comparison to the sterile *opr3+EV*, whereas *opr3+ER-OPR3* plants show lower fertility through later and smaller silique formation. Blue arrowheads point to differences in siliques formation between the genotypes.

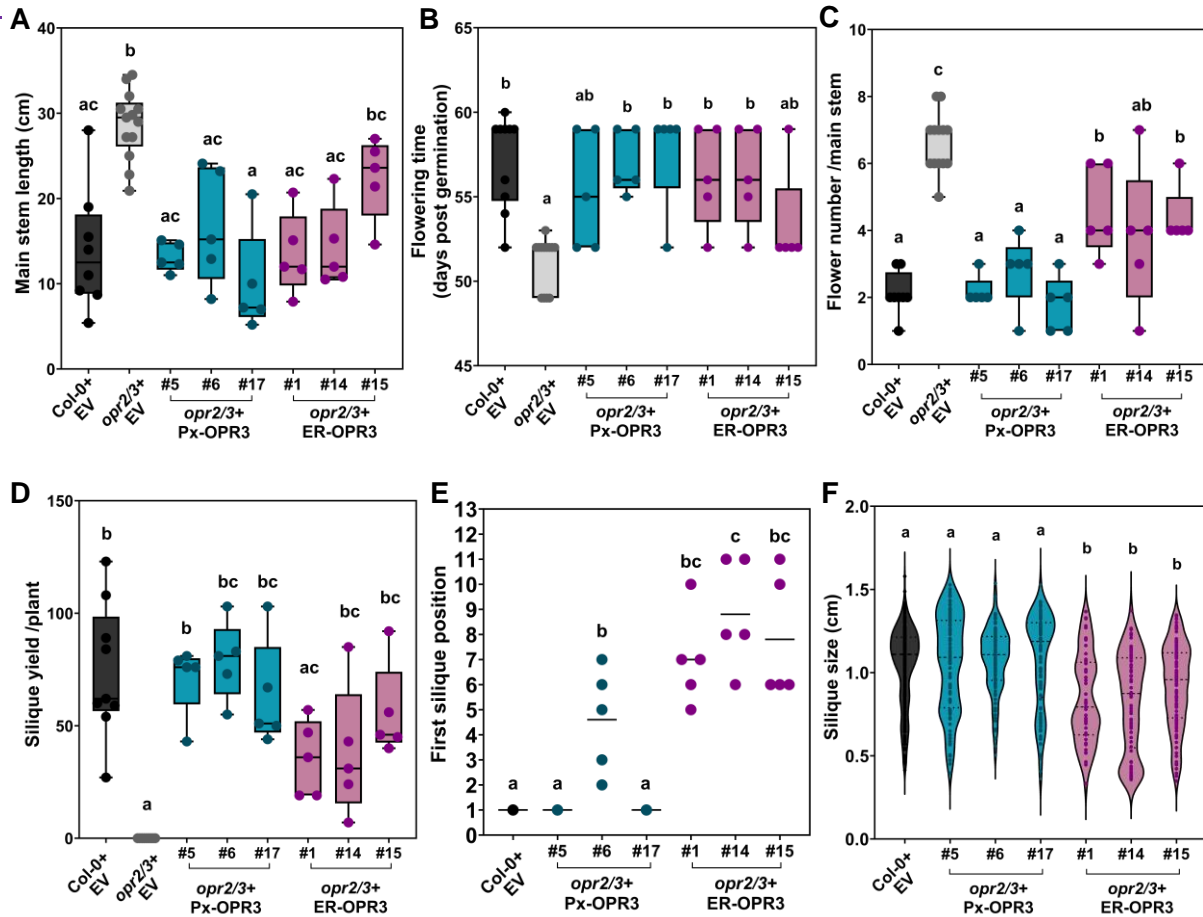


**Fig. S17 Phenotyping of the stem length and fertility-related parameters of the *opr2/3+ER-OPR3* lines shows partial fertility.**

The phenotyped lines are homozygous single-insertion lines from third generation. Data was collected from three independent transgenic lines for each of the complemented lines. For the empty-vector lines (EV), data was pooled from three and two independent lines for *opr2/3* and *Col-0*, respectively. Data is represented in box plots of five biological replicates with standard deviation and median depicted in solid lines (**A-D**), scatter plots of five biological replicates with means depicted in solid lines (**E**) and violin plots with median and quartiles represented in dashed lines (**F**). Different letters denote statistically significant differences among genotypes as determined by Two-way ANOVA followed by Tukey HSD ( $p < 0.05$ ).

**A:** Length of the plant main stem measured in centimeters from 58-day-old plants (plant age was counted in days post germination).

**B:** Plant flowering was defined as the plant floral stem reached 1 cm above the rosette. Flowering time was calculated in days post germination.

**C:** The number of open flowers (stage 13-14-15) were counted from the main stem of 58-day-old plants (plant age was counted in days post germination).

**D:** Number of siliques produced per plant were counted at day 70 post germination.

**E:** The position of the first developed silique on the main stem was determined by considering the silique present at the bottom of the stalk being at position one, whereas the high numbers are those of higher positions on the stem. Single dots coinciding with the mean bar on the scatter plot correspond to superposed values of five replicates.

**F:** Violin plot showing the distribution of silique sizes measured in centimeters. Data was collected from 117 to 246 siliques per biological replicate at day 70 post germination of the plants.



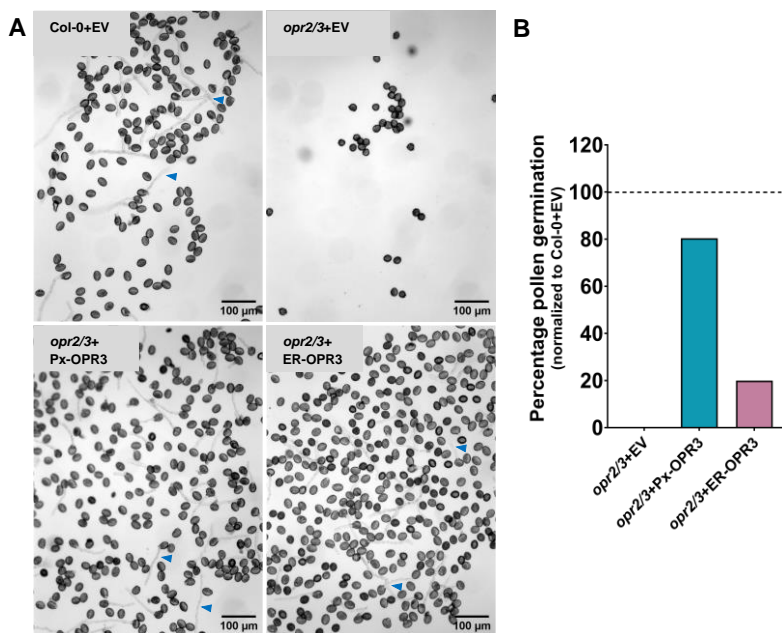


**Fig. S18 In vitro pollen germination assay shows restitution of the pollen germination in the *opr2/3+Px-OPR3* and *opr2/3+ER-OPR3* complementation lines.**

ER: endoplasmic reticulum, Px: peroxisome. Pollen was imaged 6 h post-incubation in germination media (blue arrowheads points toward pollen tubes) (A). The pollen germination rate (%) was determined relative to Col-0+EV (B). Data was collected from 500 to 900 pollen grains per line with one biological replication.

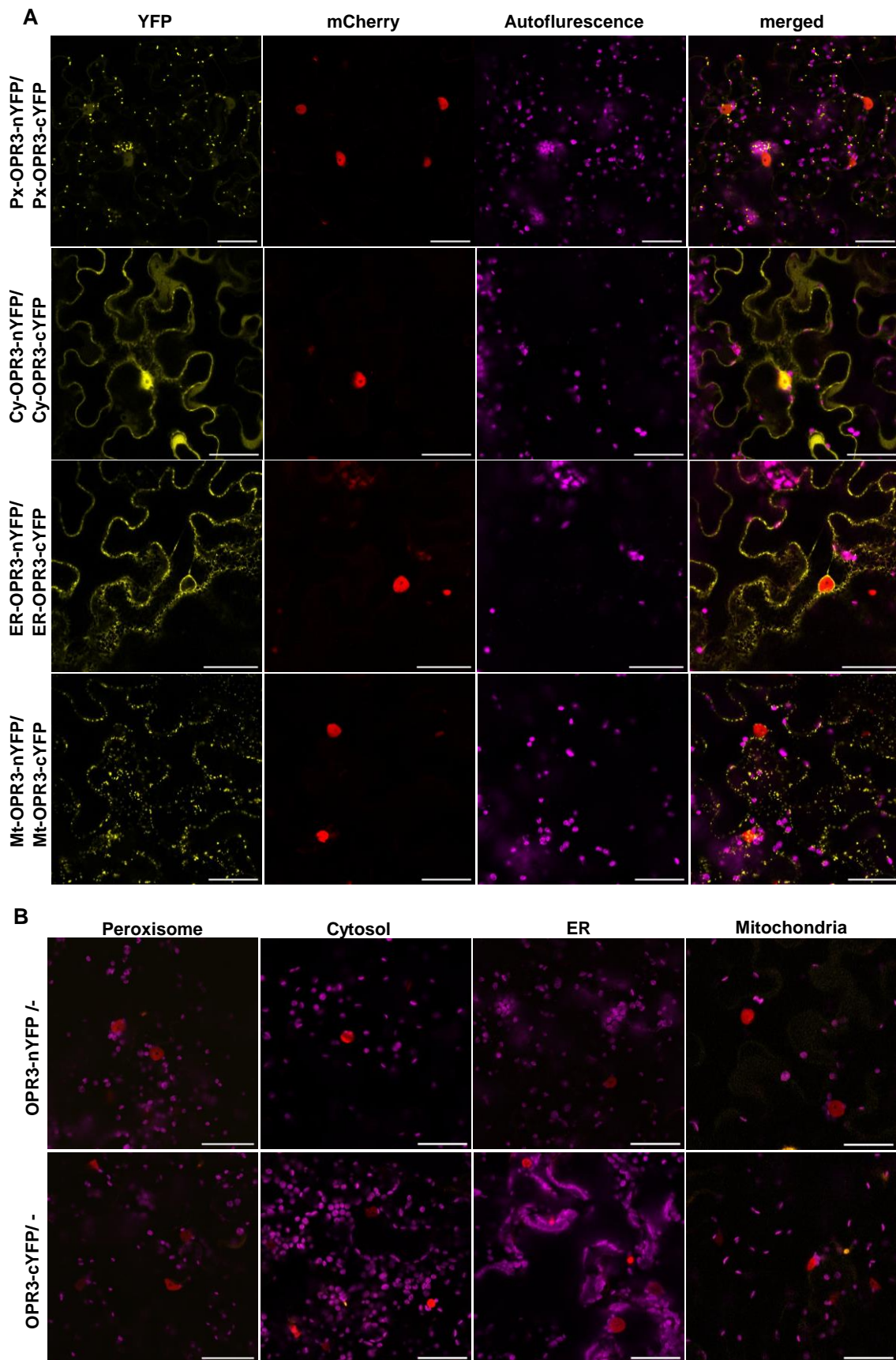


**Fig. S19 The BiFC positive and negative controls.**

Positive controls show reconstitution of the YFP signal in the corresponding organelles (A), while the negative controls do not lead to a signal (B) in *N. benthamiana* leaves at 48-72 h post infiltration. *N. benthamiana* leaves were infiltrated with a single construct expressing organelle-OPR3-nYFP,



organelle-OPR3-cYFP and the infiltration control NLS-mCherry. The yellow signal corresponds to YFP, red to mCherry and magenta to chlorophyll autofluorescence. Cy: cytosol, ER: endoplasmic reticulum, Mt: mitochondria, Px: peroxisome. Scale bars: 50  $\mu$ m. (Data from Fiona Smith's B.Sc., 2023).

**A:** For each of the organelles; peroxisome (Px), cytosol (Cy), endoplasmic reticulum (ER) and mitochondria (Mt), OPR3 fused to the nYFP and to the cYFP half was targeted to the same organelle using *35Spro::Organelle-OPR3-nYFP* and *35Spro::Organelle-OPR3-cYFP*.

**B:** The negative controls correspond to OPR3-nYFP and OPR3-cYFP targeted to each of the organelles in the absence of the corresponding other YFP half.

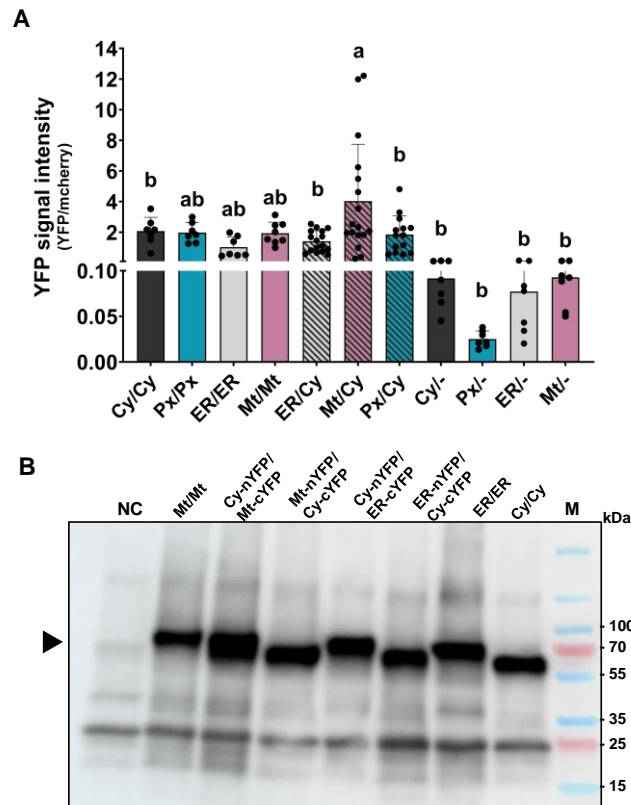


**Fig. S20 Quantification of the YFP signal indicates higher cytosolic “leakage” of OPR3 when targeted to the mitochondria.**

BiFC pairs are labeled according to the organelle and n/cYFP halves with Cy: cytosol, ER: endoplasmic reticulum, Mt: mitochondria, Px: peroxisome. (Data from Fiona Smith's B.Sc., 2023).

**A:** Quantification of the cytosolic YFP signal in each cell was normalized to the nuclear mCherry signal of the infiltration control. Comparisons between ER/cytosol, mitochondria/cytosol and peroxisome/cytosol BiFC pairs in addition to the positive and negative controls for each organelle (Fig. S19). Bars represent means of at least six cells (single dots) and differences were determined by One-Way ANOVA followed by Tukey's HSD test ( $p < 0.05$ ). Different letters denote statistically significant differences among samples.

**B:** Anti-YFP immunoblot validating the presence of the OPR3-n/cYFP in the total protein extracts of the infiltrated *N. benthamiana* leaves. Arrow points to the OPR3-n/cYFP fusion protein. NC= negative control (non-infiltrated leaves), M= protein marker.



**Fig. S21** The *opr3-1* single mutant is not fertile, even when grown until senescence.

*opr3-1* plants were grown for eight weeks. Note that the inflorescence shows only non-developed siliques. The photos are representative of five individuals.

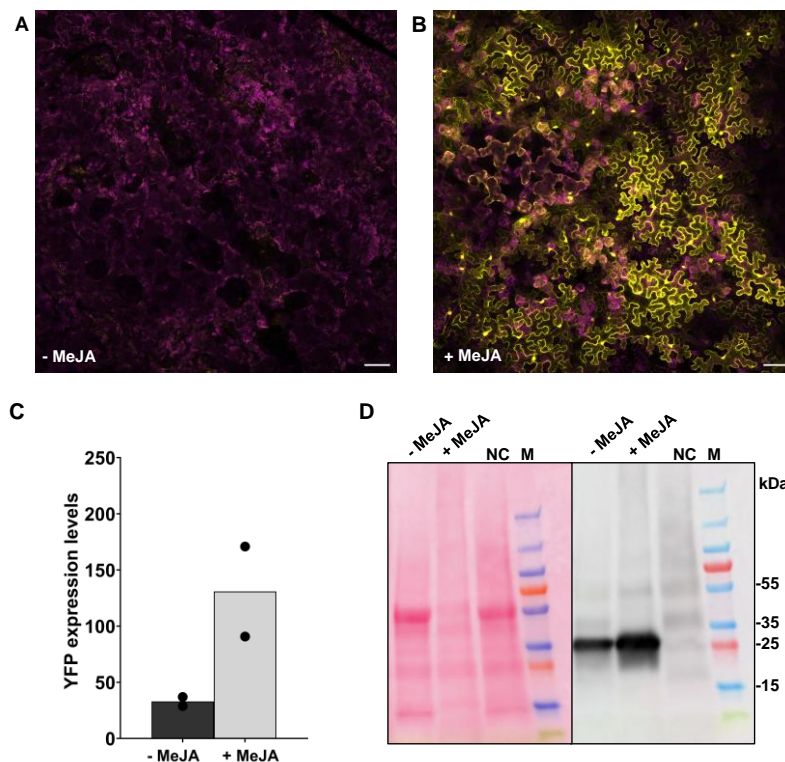


**Fig. S22** The *OPR3pro::YFP* shows induction of expression in response to MeJA in *N. benthamiana* leaves.

Transient assays in *N. benthamiana* leaves 48h after infiltration with *OPR3pro::YFP*. Leaves were sprayed with 10  $\mu$ M MeJA (+ MeJA) or with water (- MeJA).

**A, B:** Induction of the YFP signal in infiltrated *N. benthamiana* leaves, five hours after spraying of the leaves with 10  $\mu$ M of MeJA or water. The yellow signal corresponds to YFP and magenta to chlorophyll autofluorescence. Scale bars: 100  $\mu$ m.

**C:** qRT-PCR showing the increase of YFP transcripts 1 h after MeJA spraying of the infiltrated *N. benthamiana* leaves. Transcript levels were determined in relation to *NbUbe35* (Pombo *et al.*, 2019), and bars represent means of two biological replicates.

**D:** anti-YFP immunoblot showing the increase of YFP protein levels after MeJA spraying of the infiltrated *N. benthamiana* leaves. Immunolabeling was visualized by chemiluminescence using an anti-rabbit-IgG antibody conjugated with Alkaline Phosphatase. Arrow points to the OPR3-n/cYFP fusion protein. NC= negative control (non-infiltrated leaves), M= protein marker

Table S4 List of transporters candidates

| AGI              | Gene name | Description  | Leaf exp. <sup>A</sup> | Co-exp. <sup>B</sup> | Transporter superfamily <sup>C</sup>                           | Transporter family <sup>D</sup>                          | Transport type <sup>E</sup>      | cTP <sup>F</sup> | Localisation prediction <sup>G</sup> |
|------------------|-----------|--|------------------------|----------------------|--|--|----------------------------------|------------------|--------------------------------------|
| AT3G63380        | ACA12     | Calcium-transporting ATPase                                  | 11.82                  | N                    | P-type ATPase  | P2B-type calcium cation-transporting ATPase              | Primary active transport         | N                | Plasma membrane                      |
| <b>AT5G54170</b> | N/A       | Polyketide cyclase/dehydrase and lipid transport             | 72.52                  | Y                    | N/A  | N/A  | N/A                              | Y                | Plasma membrane                      |
| AT1G22570        | NPF5.15   | Protein NRT1/ PTR 5.15                                       | 100.51                 | N                    | MFS group (Major Facilitator Superfamily)                      | Nitrate transporter 1/peptide transporter (NTR1/PTR)     | Plant carrier-mediated transport | N                | Vacuole                              |
| AT1G11960        | OSCA 1.3  | Hyperosmolality-gated Ca <sup>2+</sup> permeable channel 1.3 | 56.34                  | Y                    | Channels   | Osmosensitive calcium (Ca <sup>2+</sup> ) channel (OSCA) | Plant channel-mediated transport | N                | Plasma membrane                      |
| AT1G66760        | DTX9      | Protein detoxification 9                                     | 47.29                  | Y                    | Multidrug/Oligosaccharidyl-lipid/Polysaccharide Flippase (MOP) | Multidrug efflux transporters (MATE)                     | Plant carrier-mediated transport | N                | Plasma membrane                      |
| AT5G44050        | DTX28     | Protein detoxification 28                                    | 4.48                   | Y                    | Multidrug/Oligosaccharidyl-lipid/Polysaccharide Flippase (MOP) | Multidrug efflux transporters (MATE)                     | Plant carrier-mediated transport | N                | Plasma membrane                      |
| AT3G23550        | DTX18     | Protein detoxification 18                                    | 7.32                   | Y                    | Multidrug/Oligosaccharidyl-lipid/Polysaccharide Flippase (MOP) | Multidrug efflux transporters (MATE)                     | Plant carrier-mediated transport | N                | Plasma membrane                      |
| AT1G79410        | OCT5      | Organic cation/carnitine transporter 5                       | 9.42                   | Y                    | MFS group (Major Facilitator Superfamily)                      | Organic cation transporter (OCT)                         | Plant carrier-mediated transport | N                | Vacuole                              |
| AT1G58200        | MSL3      | Mechanosensitive ion channel protein 3                       | 34.23                  | N                    | Channels   | Small Conductance Mechanosensitive Ion Channel (MscS)    | Channel-mediated transport       | N                | Plastid                              |
| AT5G26340        | STP13     | Sugar transport protein 13                                   | 156.75                 | N                    | MFS group (Major Facilitator Superfamily)                      | Sugar porter (SP)  | Plant carrier-mediated transport | N                | Plasma membrane                      |
| <b>AT5G02940</b> | PEC1      | Protein of unknown function (DUF1012)                        | 33.53                  | Y                    | Channels   | Voltage-gated ion channel (VIC)                          | Channel-mediated transport       | Y                | Plastid                              |
| AT1G10090        | N/A       | Hyperosmolality-gated Ca <sup>2+</sup> permeable channel 2.2 | 34.4                   | Y                    | Channels   | Osmosensitive calcium (Ca <sup>2+</sup> ) channel (OSCA) | Channel-mediated transport       | N                | Plasma membrane                      |
| AT4G19960        | KUP9      | K <sup>+</sup> uptake permease 9                             | 39.18                  | N                    | Other groups   | K <sup>+</sup> uptake permeases (KUP)                    | Carrier-mediated transport       | N                | Vacuole                              |
| AT2G36380        | ABCG34    | ABC transporter G family member 34                           | 10.51                  | Y                    | ABC group (ATP-Binding Cassette)                               | ABC-G group  | Primary active transport         | N                | Plasma membrane                      |
| AT1G27770        | ACA1      | Calcium-transporting ATPase                                  | 115.49                 | Y                    | P-type ATPase  | Type II ATPases (P2 group)                               | Primary active transport         | N                | Plastid, endoplasmic reticulum       |
| AT1G35350        | PHO1-H8   | Phosphate transporter PHO1 homolog 8                         | 44.92                  | Y                    | Other groups   | Phosphate permease (Pho1)                                | Carrier-mediated transport       | N                | Plasma membrane                      |
| AT3G25610        | ALA10     | Phospholipid-transporting ATPase 10                          | 35.84                  | Y                    | P-type ATPase  | Phospholipid flippase complex                            | Primary active transport         | N                | Plasma membrane                      |
| AT1G57990        | PUP18     | PURINE PERMEASE 18   | 785.53                 | Y                    | DMT group (Drug/Metabolite Transporter)                        | Plant organocation permease (POP)                        | Carrier-mediated transport       | N                | Plasma membrane                      |
| AT1G15520        | ABCG40    | ABC transporter G family member 40                           | 30.61                  | Y                    | ABC group (ATP-Binding Cassette)                               | ABC-G group  | Primary active transport         | N                | Plasma membrane                      |
| AT1G59820        | ALA3      | Phospholipid-transporting ATPase                             | 22.54                  | N                    | P-type ATPase  | Phospholipid flippase complex                            | Primary active transport         | Y                | Plasma membrane, golgi               |

Table S4 (continued)

| AGI       | Gene name | Description  | Leaf exp. <sup>A</sup> | Co-exp. <sup>B</sup> | Transporter superfamily <sup>C</sup>           | Transporter family <sup>D</sup>                  | Transport type <sup>E</sup> | cTP <sup>F</sup> | Localisation prediction <sup>G</sup> |
|-----------|-----------|--|------------------------|----------------------|--|--|-----------------------------|------------------|--------------------------------------|
| AT1G59870 | ABCG36    | ABC transporter G family member 36                       | 924.83                 | N                    | ABC group (ATP-Binding Cassette)               | ABC-G group                                      | Primary active transport    | Y                | Plasma membrane                      |
| AT4G37640 | ACA2      | Calcium ATPase 2   | 75.39                  | Y                    | P-type ATPase                                  | Type II ATPases (P2 group)                       | Primary active transport    | N                | Endoplasmic reticulum                |
| AT3G55640 | N/A       | Ca-dependent solute carrier-like protein                 | 15.11                  | Y                    | MC group (Mitochondrial Carrier)               | Mitochondrial carriers (MC)                      | Carrier-mediated transport  | N                | Mitochondrion                        |
| AT1G19770 | PUP14     | Purine permease 14                                       | 416.71                 | Y                    | DMT group (Drug/Metabolite Transporter)        | Plant organocation permease (POP)                | Carrier-mediated transport  | N                | Plasma membrane                      |
| AT4G01010 | CNGC13    | Putative cyclic nucleotide-gated ion channel 13          | 43.04                  | N                    | Channels                                       | Voltage-gated ion channel (VIC)                  | Channel-mediated transport  | N                | Golgi, mitochondrion                 |
| AT3G62150 | ABCB21    | ABC transporter B family member 21                       | 25.6                   | N                    | ABC group (ATP-Binding Cassette)               | ABC-B group                                      | Primary active transport    | N                | Plasma membrane                      |
| AT4G27870 | N/A       | Vacuolar iron transporter (VIT) family protein           | 37.94                  | N/A                  | Other groups                                   | Vacuolar Iron Transporter (VIT)                  | Carrier-mediated transport  | N                | Vacuole                              |
| AT1G08930 | ERD6      | Early response to dehydration 6                          | 450.35                 | N                    | MFS group (Major Facilitator Superfamily)      | Sugar porter (SP)                                | Carrier-mediated transport  | N                | Golgi                                |
| AT4G19450 | N/A       | Major facilitator superfamily protein                    | 39.42                  | Y                    | MFS group (Major Facilitator Superfamily)      | MFS-UMF23 family                                 | Carrier-mediated transport  | N                | Vacuole                              |
| AT3G10960 | AZG1      | AZA-guanine resistant1                                   | 3.8                    | N                    | APC group (Amino acid/Polyamine/organo-Cation) | NCS-2 family                                     | Carrier-mediated transport  | Y                | Plasma membrane                      |
| AT2G21120 | N/A       | Probable magnesium transporter                           | 61.72                  | Y                    | DMT group (Drug/Metabolite Transporter)        | The NIPA Mg <sup>2+</sup> Uptake Permease (NIPA) | Carrier-mediated transport  | N                | Plasma membrane                      |
| AT5G13750 | ZIFL1     | Zinc induced facilitator-like 1                          | 10.49                  | N                    | MFS group (Major Facilitator Superfamily)      | DHA-1 family                                     | Carrier-mediated transport  | N                | Vacuole                              |
| AT3G19553 | PUT5      | Polyamine uptake transporter 5                           | 82.85                  | N                    | APC group (Amino acid/Polyamine/organo-Cation) | Amino Acid-Polyamine-Organocation (APC)          | Carrier-mediated transport  | N                | Plasma membrane                      |
| AT1G80300 | AATP1     | ADP, ATP carrier protein 1                               | 244.49                 | N                    | MFS group (Major Facilitator Superfamily)      | ATP:ADP Antiporter (AAA)                         | Carrier-mediated transport  | Y                | Plastid                              |
| AT4G29900 | ACA10     | Calcium-transporting ATPase 10                           | 114.89                 | N                    | P-type ATPase                                  | Type II ATPases (P2 group)                       | Primary active transport    | N                | Plasma membrane                      |
| AT4G32060 | MICU      | Calcium uptake protein                                   | 230.78                 | N                    | Channels                                       | Mitochondrial calcium uniporter (MCU)            | Channel-mediated transport  | N                | Mitochondrion                        |
| AT2G39480 | ABCB6     | ABC transporter B 6                                      | 18.22                  | N                    | ABC group (ATP-Binding Cassette)               | ABC-B group                                      | Primary active transport    | N                | Plasma membrane                      |
| AT3G57330 | ACA11     | Putative calcium-transporting ATPase 11                  | 73.74                  | N                    | P-type ATPase                                  | Type II ATPases (P2 group)                       | Primary active transport    | N                | Vacuole                              |
| AT5G17020 | XPO1A     | Exportin 1A  | 27.42                  | N                    | N/A  | N/A  | N/A                         | N                | Nucleus                              |
| AT1G23130 | N/A       | Polyketide cyclase/dehydrase and lipid transport protein | 2524.43                | N                    | N/A  | N/A  | N/A                         | N                | Cytosol                              |

Table S4 (continued)

| AGI              | Gene name | Description  | Leaf exp. <sup>A</sup> | Co-exp. <sup>B</sup> | Transporter superfamily <sup>C</sup>                           | Transporter family <sup>D</sup>                        | Transport type <sup>E</sup>      | cTP <sup>F</sup> | Localisation prediction <sup>G</sup> |
|------------------|-----------|--|------------------------|----------------------|--|--|----------------------------------|------------------|--------------------------------------|
| AT1G16010        | MRS2-1    | Magnesium transporter MRS2-1                                 | 43.55                  | N                    | Channels   | Magnesium/cobalt transport protein (CorA)              | Channel-mediated transport       | N                | Plasma membrane                      |
| AT5G10190        | N/A       | Major facilitator superfamily protein                        | 33.69                  | N                    | MFS group (Major Facilitator Superfamily)                      | MFS-UMF15 family                                       | Carrier-mediated transport       | N                | Plasma membrane                      |
| AT2G22500        | PUMP5     | Mitochondrial uncoupling protein 5                           | 300.34                 | Y                    | MC group (Mitochondrial Carrier)                               | Mitochondrial carriers (MC)                            | Carrier-mediated transport       | N                | Mitochondrion                        |
| AT1G30360        | ERD4      | Hyperosmolality-gated Ca <sup>2+</sup> permeable channel 3.1 | 244.65                 | N                    | MFS group (Major Facilitator Superfamily)                      | Sugar porter (SP)                                      | Carrier-mediated transport       | N                | Plasma membrane                      |
| AT5G15240        | AVT1J     | Amino acid transporter AVT1J                                 | 4.88                   | Y                    | APC group (Amino acid/Polyamine/organo-Cation)                 | Amino Acid/Auxin Permease (AAAP)                       | Carrier-mediated transport       | N                | Vacuole                              |
| AT2G38290        | AMT2      | Ammonium transporter 2                                       | 24.32                  | Y                    | Channels   | Ammonia transporters (AMT)                             | Channel-mediated transport       | N                | Plasma membrane                      |
| AT5G52050        | DTX50     | Protein detoxification 50                                    | 47.98                  | Y                    | Multidrug/Oligosaccharidyl-lipid/Polysaccharide Flippase (MOP) | Multidrug efflux transporters (MATE)                   | Plant carrier-mediated transport | N                | Plasma membrane                      |
| AT3G56200        | AVT6C     | Amino acid transporter AVT6C                                 | 102.27                 | Y                    | APC group (Amino acid/Polyamine/organo-Cation)                 | Amino Acid/Auxin Permease (AAAP)                       | Carrier-mediated transport       | Y                | Plasma membrane                      |
| AT4G24570        | DIC2      | Dicarboxylate carrier 2                                      | 441.63                 | Y                    | MC group (Mitochondrial Carrier)                               | Mitochondrial carriers (MC)                            | Carrier-mediated transport       | N                | Mitochondrion                        |
| AT3G13050        | OCT7      | Organic cation/carnitine transporter 7                       | 17.95                  | Y                    | MFS group (Major Facilitator Superfamily)                      | Organic cation transporter (OCT)                       | Plant carrier-mediated transport | N                | Endoplasmic reticulum                |
| AT3G13100        | ABCC7     | ABC transporter C family member 7                            | 2.99                   | N                    | ABC group (ATP-Binding Cassette)                               | ABC-C group  | Primary active transport         | N                | Vacuole                              |
| <b>AT4G14500</b> | N/A       | Polyketide cyclase/dehydrase and lipid transport protein     | 43.94                  | N                    | N/A  | N/A  | N/A                              | N                | Plasma membrane                      |
| AT1G67300        | N/A       | Major facilitator superfamily protein                        | 17.76                  | N                    | MFS group (Major Facilitator Superfamily)                      | Sugar porter (SP)                                      | Carrier-mediated transport       | N                | Vacuole                              |
| AT3G13320        | CAX2      | Vacuolar cation/proton exchanger 2                           | 23.74                  | N                    | other cation carrier groups (CPA, CaCA, CDF, CaCA2)            | Ca <sup>2+</sup> : Cation Antiporter (CaCA)            | Carrier-mediated transport       | N                | Vacuole                              |
| AT2G13650        | GONST1    | GDP-mannose transporter (Fragment)                           | 19.01                  | N                    | DMT group (Drug/Metabolite Transporter)                        | NST-TPT-type group                                     | Carrier-mediated transport       | N                | Golgi                                |
| AT5G23660        | SWEET12   | Bidirectional sugar transporter SWEET12                      | 158                    | N                    | Other groups   | Sugars will eventually be exported transporter (SWEET) | Carrier-mediated transport       | Y                | Plasma membrane                      |
| AT5G15640        | N/A       | Mitochondrial substrate carrier family protein               | 31.07                  | N                    | MC group (Mitochondrial Carrier)                               | Mitochondrial carriers (MC)                            | Carrier-mediated transport       | N                | Mitochondrion                        |
| AT4G09640        | N/A       | Probable magnesium transporter NIPA5                         | 8.86                   | N                    | DMT group (Drug/Metabolite Transporter)                        | Mg <sup>2+</sup> Uptake Permease (NIPA)                | Carrier-mediated transport       | N                | Plasma membrane                      |
| AT2G03240        | PHO1-H5   | Phosphate transporter PHO1 homolog 5                         | 19.76                  | Y                    | Other groups   | Phosphate permease (Pho1)                              | Carrier-mediated transport       | N                | Golgi                                |
| AT1G64200        | ATENT6    | Equilibrative nucleoside transporter 6                       | 22.12                  | Y                    | V-type ATPase  | Vacuolar ATPase peripheral V1 subcomplex               | Primary active transport         | N                | Vacuole                              |



Table S4 (continued)

| AGI              | Gene name | Description  | Leaf exp. <sup>A</sup> | Co-exp. <sup>B</sup> | Transporter superfamily <sup>C</sup>                           | Transporter family <sup>D</sup>                        | Transport type <sup>E</sup>      | cTP <sup>F</sup> | Localisation prediction <sup>G</sup> |
|------------------|-----------|--|------------------------|----------------------|--|--|----------------------------------|------------------|--------------------------------------|
| AT4G18160        | TPK3      | Tandem-pore K+ channel 3                               | 14.04                  | Y                    | Channels   | Voltage-gated ion channel (VIC)                        | Channel-mediated transport       | N                | Vacuole                              |
| AT4G23030        | DTX49     | Protein detoxification 49                              | 3.82                   | N                    | Multidrug/Oligosaccharidyl-lipid/Polysaccharide Flippase (MOP) | Multidrug efflux transporters (MATE)                   | Plant carrier-mediated transport | N                | Plasma membrane                      |
| AT5G01500        | TAAC      | Thylakoid ADP, ATP carrier protein                     | 6.45                   | Y                    | MC group (Mitochondrial Carrier)                               | Mitochondrial carriers (MC)                            | Carrier-mediated transport       | Y                | Plastid                              |
| AT2G02860        | SUC3      | Sucrose transport protein SUC3                         | 18.46                  | Y                    | MFS group (Major Facilitator Superfamily)                      | Glycoside-Pentoside-Hexuronide (GPH): Cation Symporter | Plant carrier-mediated transport | N                | Golgi                                |
| AT5G67500        | VDAC2     | Voltage dependent anion channel 2                      | 82.49                  | N/A                  | Porins   | Mitochondrial processing peptidase (MPP)               | Channel-mediated transport       | N                | Mitochondrion                        |
| AT4G05120        | ENT3      | Equilibrative nucleotide transporter 3                 | 3.66                   | N                    | Other groups   | Equilibrative Nucleoside Transporter (ENT)             | Carrier-mediated transport       | N                | Plasma membrane                      |
| AT2G34355        | N/A       | Major facilitator superfamily protein                  | 2.8                    | Y                    | MFS group (Major Facilitator Superfamily)                      | MFS-UMF23 family                                       | Carrier-mediated transport       | N                | Plasma membrane                      |
| AT1G42540        | GLR3.3    | Glutamate receptor 3.3                                 | 7.73                   | N/A                  | Channels   | Glutamate-gated Ion Channel (GIC)                      | Channel-mediated transport       | N                | Plasma membrane                      |
| <b>AT1G04570</b> | N/A       | Probable folate-biopterin transporter 8                | 1.53                   | N/A                  | MFS group (Major Facilitator Superfamily)                      | Folate-biopterin transporter (FBT)                     | Carrier-mediated transport       | Y                | Plastid                              |
| AT5G66650        | N/A       | Calcium uniporter protein 3, mitochondrial             | 21.77                  | Y                    | Channels   | Mitochondrial calcium uniporter (MCU)                  | Channel-mediated transport       | N                | Mitochondrion                        |
| AT5G24030        | SLAH3     | S-type anion channel SLAH3                             | 8.66                   | Y                    | Channels   | Tellurite-Resistance/Dicarboxylate Transporter (TDT)   | Channel-mediated transport       | N                | Plasma membrane                      |
| AT3G47780        | ABCA7     | ABC transporter A family member 7                      | 9.47                   | Y                    | ABC group (ATP-Binding Cassette)                               | ABC-A group  | Primary active transport         | N                | Plasma membrane                      |
| AT1G16370        | OCT6      | Organic cation/carnitine transporter 6                 | 6.62                   | Y                    | MFS group (Major Facilitator Superfamily)                      | Organic cation transporter (OCT)                       | Plant carrier-mediated transport | N                | Plasma membrane                      |
| AT2G46520        | CAS       | Exportin-2   | 13.48                  | N                    | N/A  | N/A  | N/A                              | N                | Nucleus, cytosol                     |
| AT3G58730        | VHA-D     | V-type proton ATPase subunit D                         | 193.59                 | N/A                  | V-type ATPase  | Vacuolar ATPase peripheral V1 subcomplex               | Primary active transport         | N                | Vacuole, golgi                       |
| AT4G27730        | OPT6      | Oligopeptide transporter 6                             | 1.86                   | N                    | Other groups   | Oligopeptide transporter (OPT)                         | Carrier-mediated transport       | N                | Plasma membrane                      |
| AT1G57610        | N/A       | Calcium uniporter protein 5                            | 7.75                   | N/A                  | Channels   | Mitochondrial calcium uniporter (MCU)                  | Channel-mediated transport       | N                | Mitochondrion                        |
| AT3G56620        | UMAMI T10 | Usually multiple acids move in and out transporters 10 | 1.2                    | N                    | DMT group (Drug/Metabolite Transporter)                        | Drug/metabolite exporter (DME)                         | Carrier-mediated transport       | N                | Plasma membrane                      |
| AT4G15236        | ABCG 43   | ABC-2 and Plant PDR ABC-type transporter protein       | 0.41                   | N/A                  | ABC group (ATP-Binding Cassette)                               | ABC-G group  | Primary active transport         | N                | Vacuole                              |
| AT3G47960        | GTR1      | Glucosinolate transporter 1                            | 101.88                 | Y                    | MFS group (Major Facilitator Superfamily)                      | Nitrate transporter 1/peptide transporter (NTR1/PTR)   | Plant carrier-mediated transport | N                | Plasma membrane                      |
| AT5G17850        | CCX2      | Cation/calcium exchanger 2                             | 23.29                  | Y                    | Other cation carrier groups (CPA, CaCA, CDF, CaCA2)            | Ca <sup>2+</sup> : Cation Antiporter (CaCA)            | Carrier-mediated transport       | N                | Plasma membrane                      |

Table S4 (continued)

| AGI       | Gene name | Description                                    | Leaf exp. <sup>A</sup> | Co-exp. <sup>B</sup> | Transporter superfamily <sup>C</sup>                | Transporter family <sup>D</sup>  | Transport type <sup>E</sup>      | cTP <sup>F</sup> | Localisation prediction <sup>G</sup> |
|-----------|-----------|--|------------------------|----------------------|---|--|----------------------------------|------------------|--------------------------------------|
| AT5G48970 | N/A       | Mitochondrial thiamine diphosphate carrier 2   | 13.65                  | N                    | MC group (Mitochondrial Carrier)                    | Mitochondrial carriers (MC)  | Carrier-mediated transport       | N                | Mitochondrion                        |
| AT5G57100 | N/A       | Nucleotide-sugar uncharacterized transporter 1 | 10.81                  | N/A                  | DMT group (Drug/Metabolite Transporter)             | Nucleotide sugar transporters (NST)- triose-phosphate translocator (TPT) | Carrier-mediated transport       | N                | Endoplasmic reticulum,golgi          |
| AT4G27720 | GOSA MT2  | Golgi s-adenosyl methione transporter 2        | 16.34                  | N                    | MFS group (Major Facilitator Superfamily)           | Major facilitator superfamily domain containing protein (MFSD)           | Carrier-mediated transport       | N                | Golgi                                |
| AT5G61810 | N/A       | Mitochondrial substrate carrier family protein | 11.56                  | N/A                  | MC group (Mitochondrial Carrier)                    | Mitochondrial carriers (MC)  | Carrier-mediated transport       | N                | Peroxisome                           |
| AT2G47600 | MHX       | Magnesium/proton exchanger                     | 40.74                  | Y                    | Other cation carrier groups (CPA, CaCA, CDF, CaCA2) | Ca2+:Cation Antiporter (CaCA)  | Carrier-mediated transport       | N                | Vacuole                              |
| AT5G36290 | BICAT3    | Bivalent cation transporter 3                  | 57.23                  | N                    | other cation carrier groups (CPA, CaCA, CDF, CaCA2) | Ca2+:Cation Antiporter 2 (CaCA2)   | Carrier-mediated transport       | N                | Golgi                                |
| AT1G09575 | N/A       | Calcium uniporter protein 6                    | 4.76                   | N                    | Channels  | Mitochondrial calcium uniporter (MCU)                                    | Channel-mediated transport       | N                | Mitochondrion                        |
| AT1G73020 | TMEM 16   | Trans membrane protein 16                      | 1.86                   | N                    | Channels  | Calcium-dependent chloride channel (Ca-ClC)                              | Channel-mediated transport       | N                | Plasma membrane                      |
| AT3G13620 | PUT4      | Polyamine uptake transporter 4                 | 30.02                  | N/A                  | Channels  | Amino Acid-Polyamine-Organocation (APC)                                  | Channel-mediated transport       | N                | Plasma membrane                      |
| AT5G14570 | NRT2.7    | High affinity nitrate transporter 2.7          | 41.47                  | N                    | MFS group (Major Facilitator Superfamily)           | Nitrate/nitrite porter (NNP)   | Plant carrier-mediated transport | N                | Plasma membrane,vacuole              |
| AT1G76670 | URGT1     | UDP-rhamnose/UDP-galactose transporter 1       | 0.44                   | N                    | DMT group (Drug/Metabolite Transporter)             | Nucleotide sugar transporters (NST)- triose-phosphate translocator (TPT) | Carrier-mediated transport       | Y                | Golgi                                |
| AT1G53470 | MSL4      | Mechanosensitive ion channel protein 4         | 34.14                  | Y                    | Channels  | Small Conductance Mechanosensitive Ion Channel (MscS)                    | Channel-mediated transport       | N                | Plasma membrane                      |
| AT3G53960 | NPF5.7    | Protein NRT1/ PTR 5.7                          | 16.92                  | N/A                  | MFS group (Major Facilitator Superfamily)           | Nitrate transporter 1/peptide transporter (NTR1/PTR)                     | Plant carrier-mediated transport | N                | Plasma membrane                      |
| AT5G41800 | N/A       | Probable GABA transporter 2                    | 1.03                   | N                    | APC group (Amino acid/Polyamine/organo-Cation)      | Amino Acid/Auxin Permease (AAP)  | Carrier-mediated transport       | N                | Plasma membrane                      |
| AT4G36820 | MCU4      | Mitochondrial calcium channel.                 | 46.1                   | Y                    | Channels  | Mitochondrial calcium uniporter (MCU)                                    | Channel-mediated transport       | Y                | Mitochondrion                        |
| AT1G08920 | ESL1      | ERD (early response to dehydration) six-like 1 | 2.39                   | Y                    | MFS group (Major Facilitator Superfamily)           | Sugar porter (SP)  | Carrier-mediated transport       | N                | Vacuole                              |
| AT1G09960 | SUC4      | Sucrose transport protein SUC4                 | 60.31                  | N                    | MFS group (Major Facilitator Superfamily)           | Glycoside-Pentoside-Hexuronide (GPH): Cation Symporter                   | Plant carrier-mediated transport | Y                | Vacuole                              |
| AT1G69870 | NPF 2.13  | Protein NRT1/ PTR 2.13                         | 9.28                   | N/A                  | MFS group (Major Facilitator Superfamily)           | Nitrate transporter 1/peptide transporter (NTR1/PTR)                     | Plant carrier-mediated transport | N                | Plasma membrane                      |

Table S4 (continued)

| AGI       | Gene name | Description  | Leaf exp. <sup>A</sup> | Co-exp. <sup>B</sup> | Transporter superfamily <sup>C</sup>                           | Transporter family <sup>D</sup>                          | Transport type <sup>E</sup>      | cTP <sup>F</sup> | Localisation prediction <sup>G</sup> |
|-----------|-----------|--|------------------------|----------------------|--|--|----------------------------------|------------------|--------------------------------------|
| AT5G57110 | ACA8      | Calcium-transporting ATPase                            | 2.52                   | N                    | P-type ATPase  | Type II ATPases (P2 group)                               | Primary active transport         | N                | Plasma membrane                      |
| AT5G64700 | UMAMI T21 | Usually multiple acids move in and out transporters 21 | 8.91                   | Y                    | DMT group (Drug/Metabolite Transporter)                        | Drug/metabolite exporter (DME)                           | Carrier-mediated transport       | Y                | Plasma membrane                      |
| AT5G11800 | KEA6      | K(+) efflux antiporter 6                               | 0.02                   | N                    | other cation carrier groups (CPA, CaCA, CDF, CaCA2)            | Monovalent Cation:Proton Antiporter-2 (CPA2)             | Carrier-mediated transport       | N                | Plasma membrane                      |
| AT2G24610 | ATCNG C14 | cyclic nucleotide-gated channel 14                     | 0.26                   | N                    | Channels   | Voltage-gated ion channel (VIC)                          | Channel-mediated transport       | N                | Plasma membrane                      |
| AT1G09930 | OPT2      | Oligopeptide transporter 2                             | 0.26                   | Y                    | Other groups   | Oligopeptide transporter (OPT)                           | Carrier-mediated transport       | N                | Plasma membrane                      |
| AT3G16690 | SWEET 16  | Bidirectional sugar transporter SWEET                  | 3.06                   | Y                    | Other groups   | Sugars will eventually be exported transporter (SWEET)   | Carrier-mediated transport       | N                | Plasma membrane                      |
| AT4G27970 | SLAH2     | S-type anion channel SLAH2                             | 0.45                   | Y                    | Channels   | Tellurite-Resistance/Dicarboxylate Transporter (TDT)     | Channel-mediated transport       | N                | Plasma membrane                      |
| AT1G11670 | DTX36     | Protein detoxification 36                              | 1.83                   | Y                    | Multidrug/Oligosaccharidyl-lipid/Polysaccharide Flippase (MOP) | Multidrug efflux transporters (MATE)                     | Plant carrier-mediated transport | N                | Plasma membrane                      |
| AT1G62320 | N/A       | CSC1-like protein                                      | 0.16                   | N                    | channels   | Osmosensitive calcium (Ca <sup>2+</sup> ) channel (OSCA) | Channel-mediated transport       | N                | Plasma membrane                      |
| AT3G45700 | NPF2.4    | Protein NRT1/ PTR 2.4                                  | 0                      | N/A                  | MFS group (Major Facilitator Superfamily)                      | Nitrate transporter 1/peptide transporter (NTR1/PTR)     | Plant carrier-mediated transport | N                | Plasma membrane                      |
| AT5G19520 | MSL9      | Mechanosensitive ion channel protein 9                 | 0                      | N                    | Channels   | Small Conductance Mechanosensitive Ion Channel (MscS)    | Channel-mediated transport       | N                | Plasma membrane                      |
| AT3G59340 | N/A       | Solute carrier family 35 protein (DUF914)              | 0                      | N/A                  | DMT group (Drug/Metabolite Transporter)                        | Thiamine Pyrophosphate Transporter (TPPT)                | Carrier-mediated transport       | N                | Endoplasmic reticulum                |
| AT1G12950 | DTX31     | Protein detoxification 31                              | 0.05                   | Y                    | Multidrug/Oligosaccharidyl-lipid/Polysaccharide Flippase (MOP) | Multidrug efflux transporters (MATE)                     | Plant carrier-mediated transport | N                | Plasma membrane                      |
| AT1G61890 | DTX37     | Protein detoxification 37                              | 727.25                 | Y                    | Multidrug/Oligosaccharidyl-lipid/Polysaccharide Flippase (MOP) | Multidrug efflux transporters (MATE)                     | Plant carrier-mediated transport | N                | Vacuole                              |

Candidate transporters were selected from up-regulated genes by wounding common to seedlings and leaf RNAseq datasets and annotated as transporter or not assigned by Mercator4 V2.

<sup>A</sup> *A. thaliana* leaf tissue expression. Raw expression values (normalized transcript per kilobase million TPM) from CoNekT database.

<sup>B</sup> Co-expression with the JA-biosynthetic enzymes (LOXs, AOS, AOCs and OPRs) and/or JAZs signaling transcription factors in ATTED-II database with Y: yes, and N: no. A gene was considered co-expressing with any of the JA component if it co-expressed with at least one gene of the JA-cited groups.

<sup>C, D, E</sup> Transporter superfamily, family, and group of transport classification according to the plant permeome on Aramemnon database.

<sup>F</sup> Chloroplast transit peptide (cTP) prediction using ChloroP 1.1 prediction server with Y: a transit peptide and its cleavage site were predicted and N: no.

<sup>G</sup> Subcellular localization prediction using SUBA5 database. The cell compartment with the highest SUBAcon score was selected.

Genes which identifiers (AGI) are in bold were selected for further experiments.

Candidate genes highlighted in purple were found in the proteome of the chloroplast envelopes (Simm *et al.*, 2013).

N/A: not assigned.

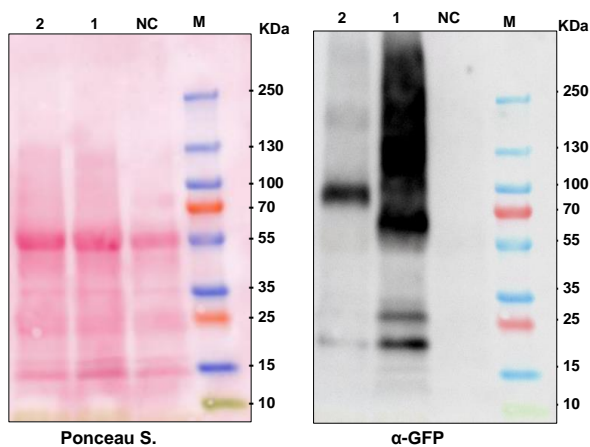


**Fig. S23** Detection of the transporter-GFP fusion proteins after transient expression in *N. benthamiana* leaves.

Detection of DTX37-GFP with expected size of 83.53 kDa (1), At5g54170-GFP with a size of 77.81 kDa. (2) and non-infiltrated leaf served as negative control (NC).

Immunoblot was done using anti-GFP primary antibody. Protein staining with Ponceau S was used as internal control. M= protein marker.

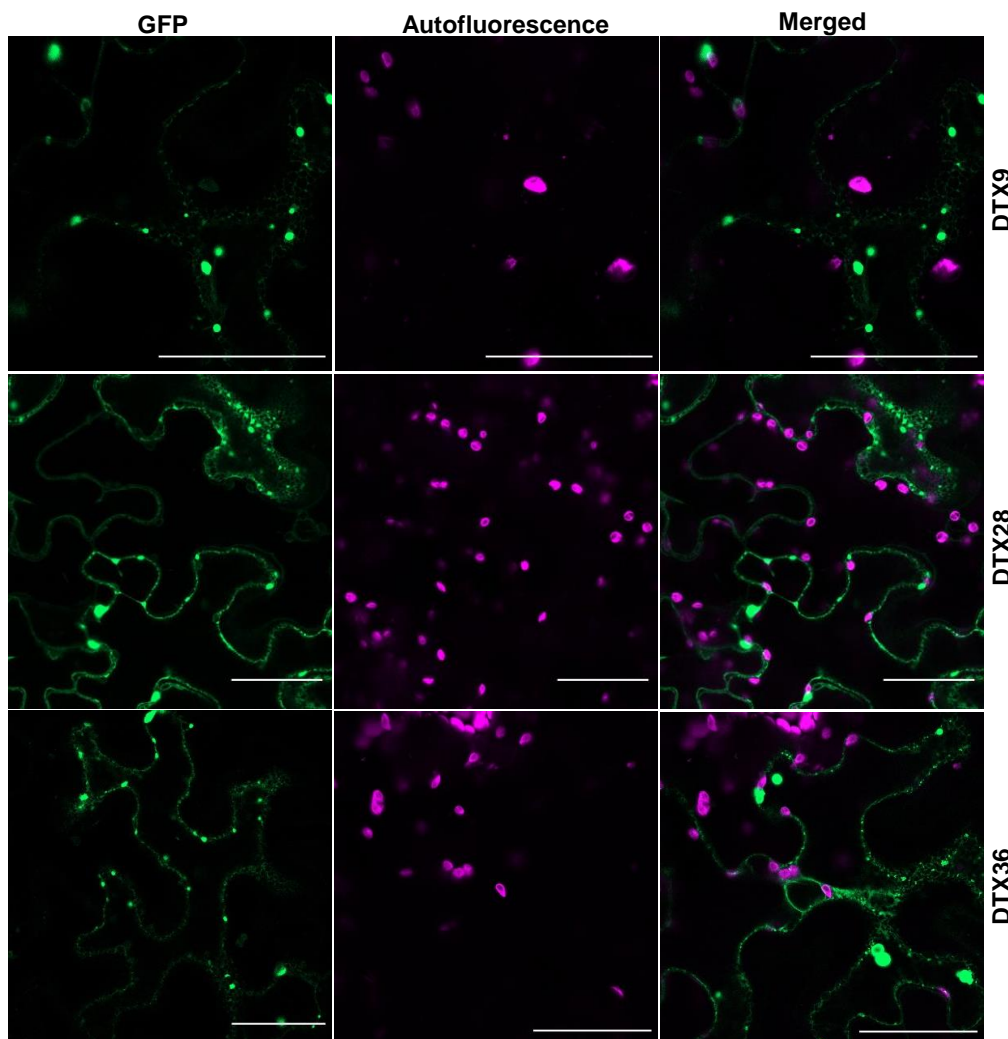


**Fig. S24** Subcellular localization of DTX9, DTX28 and DTX36.

The respective transporters were C-terminally fused to GFP and expressed transiently in *Nicotiana benthamiana* leaves using the *CaMV* 35S promoter. The green signal corresponds to GFP and the magenta corresponds to chlorophyll autofluorescence. Scale bars: 50  $\mu$ M.

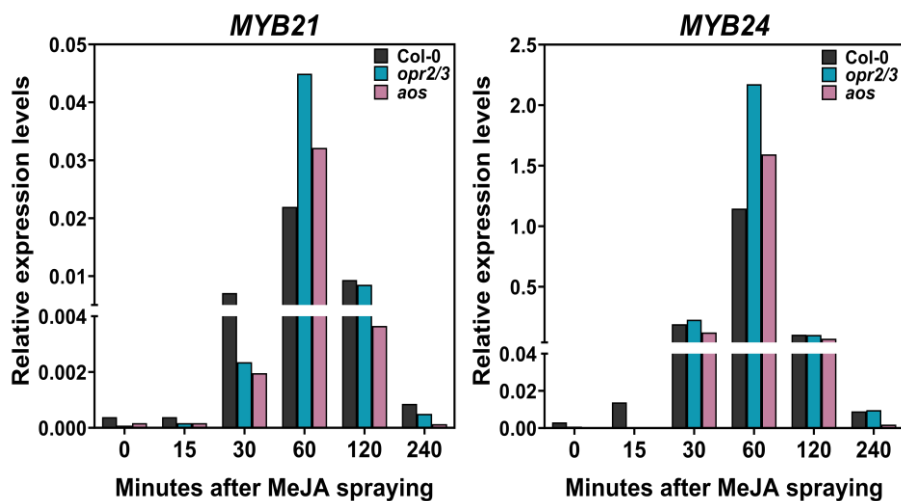


**Fig. S25** *MYB21* and *MYB24* are MeJA-responsive in leaves.

4-week-old rosette leaf was sprayed with 50  $\mu$ M MeJA and harvested at 0, 15, 30-, 60-, 120- and 240-minutes following spraying with 0 being non-sprayed control. Bars are from one biological replicate.

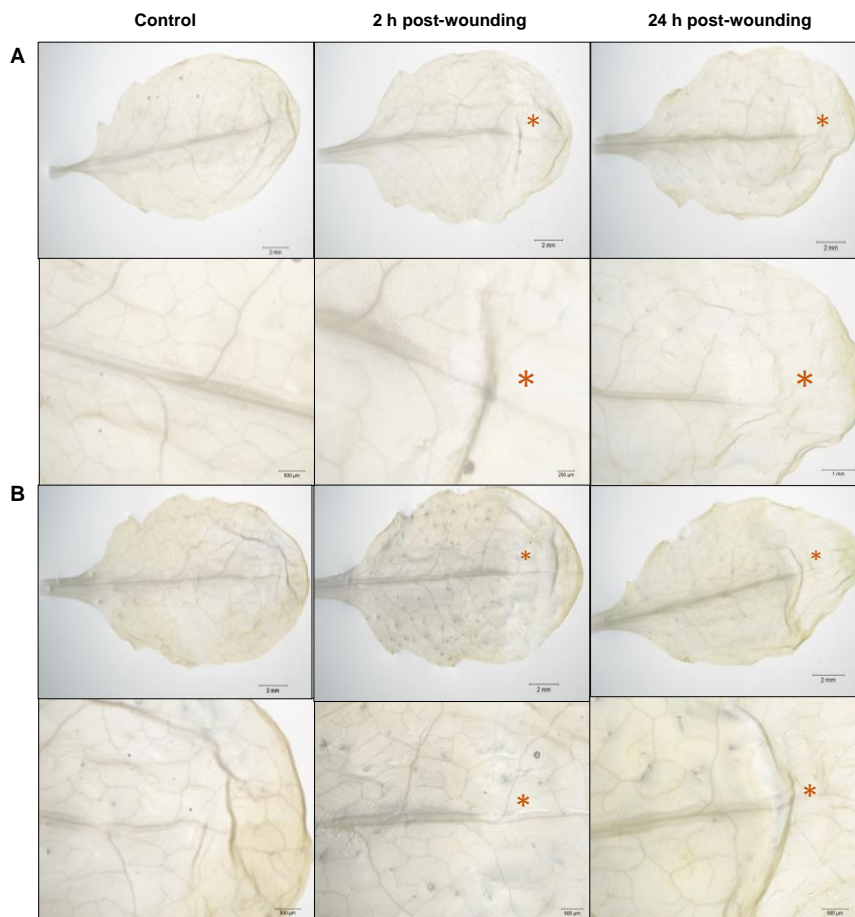


**Fig. S26** GUS reporter assay shows no expression with 2 kb *MYB21* and *MYB24* promoters.

*MYB21(2kb)pro::GUS* (A) and *MYB24(2kb)pro::GUS* (B) show no expression in leaf tissue neither at basal levels nor upon wounding. Leaves were wounded with forceps (orange asterisks) and tissue fixation was performed at 2 h and 24 h post-wounding with control leaves kept unwounded. X-Gluc (5-bromo-4-chloro-3-indolyl- $\beta$ -D-glucuronide) was used for histochemical staining to monitor GUS activity.



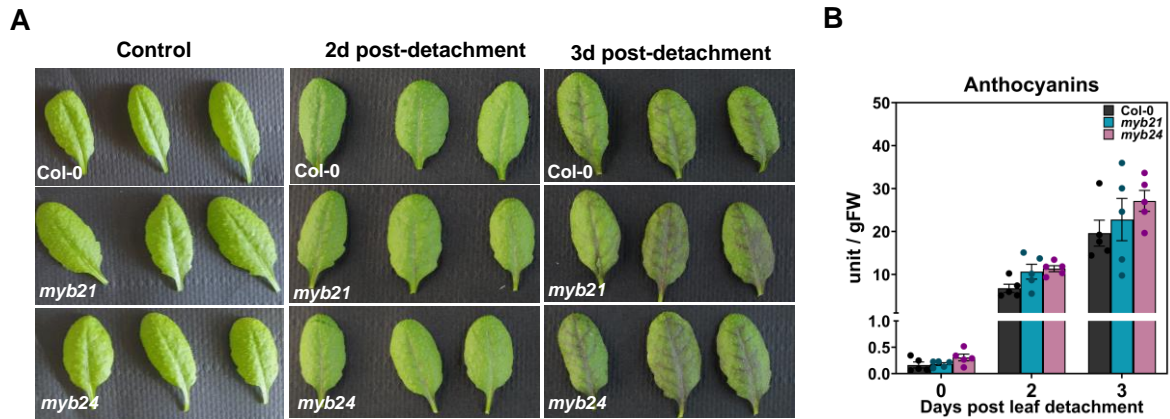


**Fig. S27 Anthocyanins accumulation in the 6th leaf following its detachment from the rosette.**

Plants from Col-0, *myb21* and *myb24* were grown on soil for 4 weeks; then leaf number six was detached from the rosette and anthocyanin content was measured at day 2 and 3 after leaf detachment with controls analyzed directly after detachment.

**A:** Photos of leaf number six detached from the rosette at day 0-, 2- and 3- after leaf detachment, showing accumulation of anthocyanins in the leaf veins.

**B:** Quantification of anthocyanins accumulation in leaf number six. Bar plots represent means of five biological replicates (single dots;  $\pm$ SEM). Differences among genotypes (within time points) were determined by One-way ANOVA followed by Tukey HSD and did not reveal significant differences.

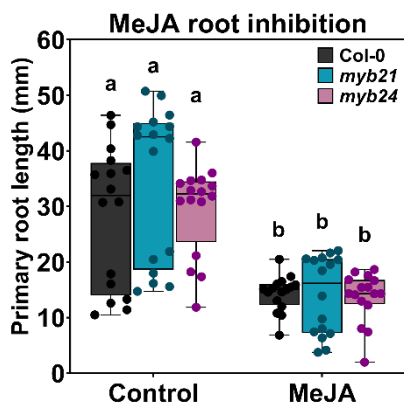


**Fig. S28 MeJA-mediated root growth inhibition.**

Two-week-old seedlings from Col-0, and the *myb21* and *myb24* mutants were grown on MS medium for three days then transferred to a new MS medium either with 50  $\mu$ M MeJA or without (control). Box plots represent data from 16 replicates per genotype (single dots) with standard deviations and means depicted in solid lines. Different letters denote statistically significant differences among genotypes as determined by Two-way ANOVA followed by Tukey HSD ( $p < 0.05$ )

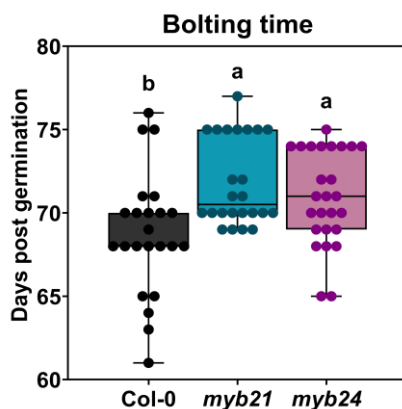


**Fig. S29 *myb21* and *myb24* reach bolting time later than Col-0.**

Plants from Col-0 and the *myb21* and *myb24* mutants were grown on soil under short-day-conditions. Plants with a stem of 1 cm height were considered as in bolting stage. The box plots are from 24-30 individual per genotype (single dots) with standard deviations and means depicted in solid lines. Different letters denote statistically significant differences among genotypes as determined by One-way ANOVA followed by Tukey HSD ( $p < 0.05$ ).

**Table S5 Arabidopsis mutant and transgenic lines and their corresponding genotyping primers**

| Arabidopsis line                              | Seed stock donor                            | Primer name            | 5' - 3' sequence                 | Amplicon (bp) |
|---|---|------------------------|----------------------------------|---------------|
| <i>aos/dde2-2</i>                             |   | prMEK26                | CGAACATGTAGAGCAGCAACAG           | 1893          |
|   |   | prMEK27                | GCCAGAGTCTCCAATAGATCTC           |               |
| <i>opr2opr3</i><br>SK24765                    | Dr. Annick Stintzi<br>(Hohenheim Uni.)      | prMEK208               | AATCCGTGTAGCCAACAACCTG           | 1134          |
|   |   | prMEK209               | CAGCCACATTCAAAGAAAAGG            |               |
| <i>opr2opr3</i><br>SALK_116381                | Dr. Annick Stintzi<br>(Hohenheim Uni.)      | prMEK210               | GTGGGTTATTGCTGATCATCC            | 1028          |
|   |   | prMEK211               | AGCTGTTGATTCAAGGGAAGG            |               |
| <i>str1</i><br>SALK_143476<br>C               | NASC stock<br>ID: N686919                   | prMEK137               | TCTTTCAAGCTCCATCAATGG            | 1084          |
|   |   | prMEK138               | TCATGGTTCCAGTACTGGGAC            |               |
| <i>dtx37</i><br>SALK_151525<br>C              | NASC stock<br>ID: N683058                   | prMEK314               | GAGAGTTTCGTGTACCGCAAG            | 1246          |
|   |   | prMEK315               | TGTTGCGTACGTAAACATTGG            |               |
| <i>dtx37</i><br>GABI_497E04                   | NASC stock<br>ID: N447668                   | prMEK232               | TCTGCTCGAAGCTTTCTCAAC            | 1020          |
|   |   | prMEK233               | AGAAACGGCATACTTGCAC              |               |
| <i>pec1.3</i><br>SALK_013399                  | NASC stock<br>ID: N513399                   | prMEK236               | CTAGGACTTGATATGTGCC              | 1059          |
|   |   | prMEK237               | AGGACAGGAGATACAGAGCCG            |               |
| <i>myb21-5</i>                                | Prof. Jason W.<br>Reed (UNC,<br>California) | prMEK268               | CAACTCACCCACATCTTTCTCTC          | 1052          |
|   |   | prMEK269               | CCTTGTACTTTGGGCCATATTT           |               |
| <i>myb24-5</i>                                | Prof. Jason W.<br>Reed (UNC,<br>California) | prMEK266               | ATACCCACCAATATGTTTGGC            | 1156          |
|   |   | prMEK267               | TGGTGAAGGTGTTTGGAACTC            |               |
| <i>PD1</i><br><i>PD2</i>                      | Prof. H-H Kunz<br>(LMU, Munich)             | Genotyped by the donor |                                  |               |
| <i>MYB21p-</i><br><i>GUSPLUS</i>              | Dr. Ivan F. Acosta<br>(MIPZ, Köln)          | Genotyped by the donor |                                  |               |
| <i>MYB24p-</i><br><i>GUSPLUS</i>              | Dr. Ivan F. Acosta<br>(MIPZ, Köln)          | Genotyped by the donor |                                  |               |
| <b>Left border primer for T-DNA insertion</b> |   |                        |                                  |               |
| LBb1.3 (for SALK lines)                       |   | prMEK122               | ATTTTGCCGATTTCCGGAAC             | NA            |
| 8474 (for GABI-Kat lines)                     |   | prMEK182               | ATAATAACGCTGCGGACATCTA<br>CATTTT | NA            |

**Table S6 Arabidopsis mutant and transgenic lines and their corresponding genotyping primers.**

| Primer name            | 5' - 3' sequence         | Gene name    | Gene ID   | Amplicon (bp) |
|------------------------|--------------------------|--------------|-----------|---------------|
| <b>qRT-PCR primers</b> |                          |              |           |               |
| prMEK318               | AGACAAGGTTCACTCAATCCGTG  | <i>PP2A3</i> | AT1G13320 | 75            |
| prMEK319               | CATTCAGGACCAAACCTTCAGC   |              |           |               |
| prMEK14                | ACGCTCGTGACGCCAAAGT      | <i>LOX2</i>  | AT3G45140 | 91            |
| prMEK15                | TCCTCAGCCAACCCCTTTTG     |              |           |               |
| prMEK10                | TGGTGGCGAGGTTGTTTGTGATTG | <i>AOS</i>   | AT5G42650 | 92            |
| prMEK11                | ATTAACGGAGCTTCTTAACGGCGA |              |           |               |
| OPR1 vor*.             | ATCCAGGAGCATTAGGGC       | <i>OPR1</i>  | AT1G76680 | 140           |
| OPR1 rück*.            | CGCTTTCCTCATCGGCAT       |              |           |               |
| prMEK22                | AATCGCGGTTTTCAGCCAAG     | <i>OPR2</i>  | AT1G76690 | 81            |

|               |                          |                |           |     |
|---------------|--------------------------|----------------|-----------|-----|
| prMEK23       | GCCATTAGCACGCATTTGAG     |                |           |     |
| prMEK12       | TGGTTGGCATGCTCAATAAG     |                |           |     |
| prMEK13       | GCCTTCCAGACTCTGTTTGC     | <i>OPR3</i>    | AT2G06050 | 108 |
| prMEK456      | TTTGGCGTTGTCTTGTCTGTG    |                |           |     |
| prMEK457      | TGTTTCATGCTAGGTCCCATCG   | <i>FAD-OXR</i> | AT4G20860 | 97  |
| prMEK458      | AGCAACAACAGCAGGATTCG     |                |           |     |
| prMEK459      | AGGTCACGTAGAAGCTCATCG    | <i>DREB2A</i>  | AT5G05410 | 115 |
| ZAT10 vor*.   | AGGCTCTTACATCACCAAGATTAG |                |           |     |
| ZAT10 rück*.  | TACTTGTAGCTCAACTTCTCCA   | <i>ZAT10</i>   | AT1G27730 | 237 |
| prMEK3        | AATTAGATCGACACAGCCCAAG   |                |           |     |
| prMEK4        | CCGAGACCGAACATTAAGCTGA   | <i>AOC2</i>    | AT3G25770 | 101 |
| prMEK438      | TCGTTCTGTTCTTCCCGAAC     |                |           |     |
| prMEK439      | GCGGTCAGTAGCAGTTTTCC     | <i>NATA1</i>   | AT2G39030 | 118 |
| prMEK440      | GAGTGTAAGGCGACGAAAGC     |                |           |     |
| prMEK441      | CATAACAACCGCCATAAACC     | <i>CLH1</i>    | AT1G19670 | 105 |
| prMEK20       | ATCAACTTGGCGAGCAAAGG     |                |           |     |
| prMEK21       | TGCGATAGTAGCGATGTTGC     | <i>JAZ1</i>    | AT1G19180 | 81  |
| JAZ10 vor*.   | AACCAACAACGCTCCTAAGC     |                |           |     |
| JAZ10 rück*.  | TATCTCGGAAACTACGACGG     | <i>JAZ10</i>   | AT5G13220 | 99  |
| prMEK462      | TACCCATCTTGAGGCTAACGC    |                |           |     |
| prMEK463      | ATCCGAACCGTCTGAACTTCTC   | <i>JAZ7</i>    | AT2G34600 | 91  |
| prMEK470      | TTTTTCTGCCGAGTGTTGGG     |                |           |     |
| prMEK471      | ACCCTTCTCCTTCAGGTAACG    | <i>JAZ2</i>    | AT1G74950 | 91  |
| prMEK460      | TCCCGATCTTAACGAGCCAAC    |                |           |     |
| prMEK461      | TTGCAATGCGTCCACAACC      | <i>JAZ6</i>    | AT1G72450 | 86  |
| prMEK446      | TGTTACCCATCTTCAGGCAAGA   |                |           |     |
| prMEK447      | ATCCGACCCGTTTGAGGATG     | <i>JAZ8</i>    | AT1G30135 | 82  |
| prMEK472      | AGAGAATGGGGGAAGTCAAAGG   |                |           |     |
| prMEK473      | AACATTGGCCGCAGAACTG      | <i>JAZ9</i>    | AT1G70700 | 120 |
| prMEK78       | ATAGAGATGGCGAGCAAGGATC   |                |           |     |
| prMEK79       | TCCTAACGGTGATTCCAGTCTC   | <i>JAZ13</i>   | AT3G22275 | 75  |
| GRX480 vor*.  | TGATTGTGATTGGACGGAGA     |                |           |     |
| GRX480 rück*. | TAAACCGCCGTAACTTCAC      | <i>GRX480</i>  | AT1G28480 | 181 |
| prMEK450      | TCAACACGCCGCTCTAAACT     |                |           |     |
| prMEK451      | GGATTAACCGCCGCATCAAC     | <i>LOX3</i>    | AT1G17420 | 83  |
| prMEK464      | ACCTTGCGATGTGCCTTATC     |                |           |     |
| prMEK465      | AATCATCCGCACCCAAAACC     | <i>SDI1</i>    | AT5G48850 | 96  |
| prMEK468      | ATCGAAATCCGCTGTTGCAG     |                |           |     |
| prMEK469      | TCCAAGGCTCTTTACGGTTCTC   | <i>APR1</i>    | AT4G04610 | 107 |
| prMEK466      | AGAGGCGATAACCAATGCTG     |                |           |     |
| prMEK467      | AAACGGGGAAAGCCTGAAAC     | <i>APS3</i>    | AT4G14680 | 106 |
| prMEK474      | TCCATGAGAAACCGTCCTAGAG   |                |           |     |
| prMEK475      | AATAGGAGGAGGAGGAAGAAGG   | <i>ERF094</i>  | AT1G06160 | 85  |
| prMEK183      | GGTTCCTTCTATACCGCCTAAC   |                |           |     |
| prMEK184      | CCCATCGTCTTCTTGATTCC     | <i>STR1</i>    | AT5G54170 | 97  |

|                       |                          |                 |           |      |
|-----------------------|--------------------------|-----------------|-----------|------|
| prMEK195              | GTCACTCCAAGTGCCTACATATC  |                 |           |      |
| prMEK196              | GACCGTAACCAAGACGATACAC   | <i>DTX37</i>    | AT1G61890 | 88   |
| prMEK322              | ACTACAACAGCCACAACGTC     |                 |           |      |
| prMEK323              | TGTTGTGGCGGATCTTGAAG     | <i>YFP</i>      |           | 81   |
| prMEK193              | GGCGTGGAGATGTTGTGAATA    |                 |           |      |
| prMEK194              | CCACTCCTCTTCTGTCCTCTAA   | <i>PEC1</i>     | AT5G02940 | 108  |
| prMEK74               | AGACGAATTTCTGATGTACGC    |                 |           |      |
| prMEK75               | TGCCTGTCTTCAGCAAGTTC     | <i>MYB21</i>    | AT3G27810 | 75   |
| prMEK76               | GACAGGAGATACAGAGCCGC     |                 |           |      |
| prMEK77               | GTGCCCTTCCCTCACTTTT      | <i>MYB24</i>    | AT5G40350 | 91   |
| <b>RT-PCR primers</b> |                          |                 |           |      |
| prMEK32               | AGACGAATTTCTGATGTACGC    |                 |           |      |
| prMEK33               | TGCCTGTCTTCAGCAAGTTC     | <i>PP2A3</i>    | AT1G13320 | 126  |
| prMEK276              | GACAGGAGATACAGAGCCGC     |                 |           |      |
| prMEK277              | GTGCCCTTCCCTCACTTTT      | <i>PEC1</i>     | AT5G02940 | 587  |
| prMEK292              | GAGATGTCGTCGGACTTGGG     |                 |           |      |
| prMEK245              | AGCTAAAACTGACAGAAAGTTGGT | <i>DTX37</i>    | AT1G61890 | 1105 |
| prMEK281              | TGGATGGGCATGAAAACCAA     |                 |           |      |
| prMEK282              | AGAAGAACGGGAAGTTGCGT     | <i>STR1</i>     | AT5G54170 | 632  |
| <b>PCR primers</b>    |                          |                 |           |      |
| prMEK61               | TACAAAGGCGGCAACAAACG     | <i>CaMV 35S</i> | NA        | NA   |
| prMEK62               | CCATCGGGCAACAAAACG       | <i>OPR3</i>     | NA        | NA   |
| prMEK63               | TTGTACTCCAGCTTGTGCC      | <i>YFP</i>      | NA        | NA   |
| prMEK70               | GGGTACAATCAGTAAATTGAACGG | <i>tOcs</i>     | NA        | NA   |

Primer pairs marked with an asterisk are from (Arnold et al., 2016).

**Table S7 List of cloning primers**

| Primer name              | 5'-3' sequence  | DNA template and codon alteration             |
|--------------------------|---|---|
| <b>OPR3-OPR2 cloning</b> |   |   |
| prMEK44                  | TTGAAGACAA <u>aggt</u> acggcggcacaaggaactc                | <i>AtOPR3 CDS</i> (4-205 bp), C205G           |
| prMEK45                  | TTGAAGACAA <u>ac</u> ccatggtgccttcggagatgag               |   |
| prMEK46                  | TTGAAGACAA <u>gt</u> gtctccggatccgcaggg                   | <i>AtOPR3 CDS</i> (205-1109 bp), C205G-G1109C |
| prMEK47                  | TTGAAGACAA <u>tg</u> cgattatatttcaactctcatcaatcttga       |   |
| prMEK48                  | TTGAAGACAA <u>cg</u> caagacgtttacactcaagatccagttg         | <i>AtOPR3 CDS</i> (1109-1164 bp), G1109C      |
| prMEK49                  | TTGAAGACAA <u>cga</u> accacaaaggagccaagaaaggataatccgtg    |   |
| prMEK50                  | TTGAAGACAA <u>ttc</u> ggtgagcaagggcgaggagc                | <i>YFP CDS</i> (4-729 bp)- <i>HDEL</i>        |
| prMEK71                  | TTGAAGACAA <u>aag</u> cttatagctcgtcatgctgtacagctcgtccatgc |   |
| prMEK52                  | TTGAAGACAA <u>aat</u> gacggcggcacaaggaactc                | <i>AtOPR3 CDS</i> (1-205bp), C205G            |
| prMEK53                  | TTGAAGACAA <u>ttc</u> ggtgagcaagggcgaggagc                |   |
| prMEK54                  | TTGAAGACAA <u>aag</u> cgaggcgggactgtacagctcgtccatgcc      | <i>YFP CDS</i> (4-729 bp)- <i>SRL</i>         |
| prMEK55                  | TTGAAGACAA <u>aggt</u> gtgagcaagggcgaggagc                |   |
| prMEK56                  | TTGAAGACAA <u>cga</u> actgtacagctcgtccatgcc               | <i>YFP CDS</i> (4-726 bp)                     |
| prMEK57                  | TTGAAGACAA <u>ttc</u> gacggcggcacaaggaactc                | <i>AtOPR3 CDS</i> (4-205bp), C205G            |

|                                      |   |  |
|--------------------------------------|---|--|
| prMEK60                              | TTGAAGACAAaagctagctcgtcatgcctcaaaaggagccaagaaag<br>gataatccgtg                    | <i>AtOPR3 CDS</i> (1109-1164 bp)- <i>HDEL</i> , G1109C |
| prMEK73                              | TTGAAGACAAaagcttagagggcggaaaaaggagccaagaaagg                                      | <i>AtOPR3 CDS</i> (1109-1167 bp), G1109C               |
| prMEK203                             | TTGAAGACAAaatgggtgagcaagggcgaggag   | <i>YFP CDS</i> (1-726 bp)                              |
| prMEK204                             | TTGAAGACAAcgaagatctaataagccgcgtttgtacag   |  |
| prMEK205                             | TTGAAGACAAaagcttaaaaaggagccaagaaaggataatccgtg                                     | <i>AtOPR3 CDS</i> (4-1164 bp)<br>G1109C                |
| prMEK206                             | TTGAAGACAAatcggtgagcaagggcgaggag  | <i>YFP</i> (4-729 bp)                                  |
| prMEK207                             | TTGAAGACAAaagcttatctaataagccgcgtttgtacagc   |  |
| prMEK264                             | TTGAAGACAAaagcttaatacaagagtaagtctctcaagcggtagc<br>tgaagtctaataagccgcgtttgtacagc   | <i>AtOPR3 CDS</i> (4-1164 bp)-<br><i>NES</i>           |
| prMEK265                             | TTGAAGACAAaagcttaatacaagagtaagtctctcaagcggtagc<br>tgaagaaaaggagccaagaaaggataatccg | <i>YFP CDS</i> (4-729 bp)                              |
| prMEK326                             | TTGAAGACAAaatggattcacagctagtctgtctc   | <i>AtRecATP CDS</i> (1-153 bp)                         |
| prMEK327                             | TTGAAGACAAacctctgtagacggtaaccggagaatagag  |  |
| prMEK357                             | TTGAAGACAAaatgtatcgttccgttctaacctcg   | <i>AtCPN60 CDS</i> (1-93 bp)                           |
| prMEK358                             | TTGAAGACAAacctctatagttcctgctccagctcattc   |  |
| prMEK382                             | TTGAAGACAAaggagcttacaacatcatgcttaccttttataaaatc<br>taatg                          | <i>AtOPR3</i> promoter(1-92 bp), C92G                  |
| prMEK383                             | TTGAAGACAAatcaagacaagtaaacctccacaacattc   |  |
| prMEK384                             | TTGAAGACAAatgaagtagttaggattattatcctagaattgtgc                                     | <i>AtOPR3</i> promoter(92-1332 bp), G92C-T1332A        |
| prMEK385                             | TTGAAGACAAgtagacactttgaccaagtaaaattgtattgtcaattc                                  |  |
| prMEK386                             | TTGAAGACAAactacggaggtgtcccttc   | <i>AtOPR3</i> promoter(1332-1723 bp), T1332A-C1723G    |
| prMEK387                             | TTGAAGACAAatccttccattaacaggtcagaataaagg   |  |
| prMEK388                             | TTGAAGACAAgagaactatgactttatacattgaaatgtgtcaac                                     | <i>AtOPR3</i> promoter(1723-2299 bp), C1723G           |
| prMEK389                             | TTGAAGACAAcattgtctccgccgatctgg  |  |
| prMEK399                             | TTGAAGACAAaatggaaatggtaaaccgcagaagca  | <i>AtOPR2 CDS</i> (1-1122 bp)                          |
| prMEK400                             | TTGAAGACAAcgaaccagctgttgattcaaggaagggtg   |  |
| <b>Putative transporters cloning</b> |   |  |
| prMEK370                             | TTGAAGACAAaatgaagaagagtatcgaaactccgttattg   | <i>AtDTX9 CDS</i> (1-841 bp), T841A                    |
| prMEK371                             | TTGAAGACAAgtagaccagacagcaaatgacacct   |  |
| prMEK372                             | TTGAAGACAAactactaccaactcaaagctcg  | <i>AtDTX9 CDS</i> (841-1447 bp), T841A                 |
| prMEK373                             | TTGAAGACAAcgaaccattaagcaatgagtcgtctccaaacttc                                      |  |
| prMEK374                             | TTGAAGACAAaatgggagagagagacgacg  | <i>AtDTX28 CDS</i> (1-1474 bp)                         |
| prMEK375                             | TTGAAGACAAcgaacccttctgtcgtgtgatacagacc  |  |
| prMEK376                             | TTGAAGACAAaatgggttcggaagcgacc   | <i>AtDTX36 CDS</i> (1-312 bp), C312G                   |
| prMEK377                             | TTGAAGACAAatcagaccaagagtgaacatattgaaaccgct  |  |
| prMEK378                             | TTGAAGACAAactgatgcttggaaatgggaagtgcag   | <i>AtDTX36 CDS</i> (312-693 bp), C312G-A693T           |
| prMEK379                             | TTGAAGACAAgtccaagtaagcccaaccaaac  |  |
| prMEK380                             | TTGAAGACAAaggactctccgttgtcatagtc  | <i>AtDTX36 CDS</i> (693-1513 bp), A693T                |
| prMEK381                             | TTGAAGACAAcgaaccttgcttaagaagcggagatgtgtc  |  |
| prMEK362                             | TTGAAGACAAaatgaattcagaatcgtagaaaaattcacc  | <i>AtDTX37 CDS</i> (1-969 bp), C969G                   |
| prMEK363                             | TTGAAGACAAacaccatgaatgagattgcagaaattgac   |  |
| prMEK364                             | TTGAAGACAAagtgtccgttgattcaacgcagc   | <i>AtDTX37 CDS</i> (969-1504 bp), C969G                |
| prMEK365                             | TTGAAGACAAcgaaccttgcttcaaaagcggctcacg   |  |
| prMEK366                             | TTGAAGACAAaatggcttggcttgagagataatattag  | <i>AtSTR1 CDS</i> (1-921 bp), T921C                    |
| prMEK367                             | TTGAAGACAAatctctgtggtggaatagaagtacttc   |  |



|                     |   |                                       |
|---------------------|---|---------------------------------------|
| prMEK368            | TTGAAGACAAgatatggaatacctagagaaatcgc                                       | <i>AtSTR1</i> CDS(921-1347 bp), T921C |
| prMEK369            | TTGAAGACAACgaaacctgaagaagtagtctgactctcac                                  |                                       |
| <b>BiFC cloning</b> |   |                                       |
| prMEK404            | TTGAAGACATaatggacaagcagaagaacggcatc                                       | <i>cYFP CDS(465-720 bp)-MYC</i>       |
| prMEK405            | TTGAAGACAAaagctcagccggccaggctcctcctctgagataagctctgttccattggcctacttccacctc |                                       |
| prMEK410            | TTGAAGACATaatgtatccttatgatgttctgattatgctagtagtgtagcaagggcgaggag           | <i>HA-nYFP CDS(1-465 bp)</i>          |
| prMEK411            | TTGAAGACATaagctcagttctgacttccacctccag                                     |                                       |
| prMEK407            | TTGAAGACATaagctcaaagttcatcatggccggccaggctcctcctctg                        | <i>cYFP CDS(465-720 bp)-MYC-HDEL</i>  |
| prMEK412            | TTGAAGACATaagctcaaagttcatcatggttctgacttccacctccag                         | <i>HA-nYFP CDS(1-465)bp-HDEL</i>      |
| prMEK426            | TTGAAGACAAaagctcagaggcgggagccggccaggctcctcctctgagataagc                   | <i>cYFP CDS(465-720 bp)-MYC-SRL</i>   |
| prMEK427            | TTGAAGACAAaagctcagaggcgggatggttctgacttccacctccag                          | <i>HA-nYFP CDS(1-465 bp)-SRL</i>      |

Upper-case letters represent *Bpil* restriction sites and dummies added for Golden Gate cloning. Lower case letters depict bases annealing to the template. Underlined letters are overhangs added to the template for Golden Gate modules assembly. Letters highlighted in grey are targeting sequences added to the template. Bases in bold represent bases that were changed for silent point mutations.

cttacaacatcatgcttacctcttttataaaatctaatgttcttacaacatcatgcttacctcttttataaaatctaatgttccagaagaacc  
agacattaagaatggtgtggagggttactgtctcgaagtagttaggattattatcctagaattgtgcatgttttgttgacaaaaattcgtgaccatcct  
ttgaatacatggtcattgattacatcctcagcgtgacaaatccaaattcacaataaatcatataagcaatacagcttttcgattacatcttaaacca  
ccttagtgagggtctataactaaaatggtgaattatataaactaaacaacaatgttttctaaaaatggtatgccaaaaatggttacgaaaaat  
agactcaaaaatacaaatgtcattggcgaaaaataatgacaattaatgaatatacaataatagataaaaagcaaaaatgaaataaatttcaat  
gttccatttagttaaagatagtgatcttgaagatcataacgtatttagattatgtacctgattataaagtggcttataaatcacctaccattttaccagt  
aacgatctaactacacacaataatcatctttactcttataagatttaaccatatttttagatctcataagaatcaatgcaatttcataaaaacat  
caaaaataattctataaattaaaattttctcaagataatatttaattttattataaatctcttaattagccatctttctacatttatcaaaagatattagcta  
tctgttctcataggcaatagataaaaaaaaaaacttttccaagtagggggcacaanaagagttccctgggactgggctgagaataatgaagt  
ggctgggaaatgattagtttaaggatggctgatgaattctcaatattctgttaggggaacaaaatatactaggaaggatgcaagtccagtttggtcta  
aacattgtacgaacccaaaacaatcaataaagtaactcagggtcacaatggtcgataatattctaaagttcagttctagaggatgagcaa  
aaggatttgatgaggagatgactagaggtaacagacaagagttcactgaagggtgaatttcagatattttaaatcacgtttggagtaacaaa  
aaacaaatgtgagaaggagctcaattagctccaactgaatctagtttattaggatactttggaaactccaattcaatcttaagatgtaggattg  
atgaattcatggaatcggcagatccatctatgaatttagtgggtttcttaggaattgacaatacaatttactgtgcaaaagtgtcttcggg  
aggtgtccctttcttttactcggaaattggaagtttaatttggaataaaaaaatatccttcaagaaggataaagtgcaggcatttgaacagat  
aattatcagagtaagtttgatggtcagtcctgaagaatgactcgtttctcaatttttagaagatcttgaaatgctatgtgtctcctttcttgct  
ttcttatttcatgtttatgaataactaaggcaactatttagcacaatattctaaacttttttctgaagttatttttaaacctttccctcctaattgg  
acaaccaatcatggaattagttttactgaaatgttttaactcactatttcacctttattctgacctgtaattggaagacaactatgactttatacattga  
aatgttgcaacctgttatataatgtaacatagctaatactacatcaatgtacgtaagcgaatgcaatcatattcgatccgttaatttcattta  
ggaaatcaggctcattgccaatccactaagaacaatctctgatagatccaaataataaaaataataatgaagcaaaaatagaacgaaat  
ctcacgcggaccaaactttgaactttattataaaacaatcagcagctgaaagtaatggtcgggtcgggtccaagatgccaagaactcctccggtc  
catcatcaactaacctttttggatataaaatttagcaaatccattccacgaccacacaacaacaacatccactcgaattttctatttccga  
atacaaaaaccggtaaactcatcaaaactaagttactttgtagttgtgttttctctttatgtaataagaagatccaactaactactactcaat  
atattgtattgacctgtatttctcagatctgacttttacttctccttctccagatcggcggagac¶

**Fig. S30 OPR3 promoter sequence (2299 bp)**

Promoter sequence includes the 5'UTR region marked in bold. *Bpil* restriction sites are marked in purple. Putative transcription factors (TF) binding sites predicted by PlantPlan database are marked in grey. Underlined regions are TF binding sites identified by (Li *et al.*, 2013).

**Table S8 List of constructs used for Arabidopsis stable transformation.**

| <b>Construct</b>                          | <b>Plasmid name</b> | <b>Given name</b>      |
|---|---------------------|------------------------|
| <i>35Sp::SIP-OPR3ΔSRL-YFP-HDEL::tOcs</i>  | pAGH1185            | ER-OPR3                |
| <i>35Sp::SIP-YFP-OPR3ΔSRL-HDEL::tOcs</i>  | pAGH1187            | ER-OPR3                |
| <i>35Sp::OPR3ΔSRL-YFP-SRL::tOcs</i>       | pAGH1186            | Px-OPR3                |
| <i>35Sp:: YFP-OPR3::tOcs</i>              | pAGH1188            | Px-OPR3                |
| <i>35Sp::NLS(SV40)-OPR3ΔSRL-YFP::tOcs</i> | pAGH1228            | NI-OPR3                |
| <i>35Sp::NLS(SV40)-YFP-OPR3ΔSRL::tOcs</i> | pAGH1230            | NI-OPR3                |
| <i>35Sp::OPR3ΔSRL-YFP-NES(HIV1)::tOcs</i> | pAGH1260            | Cy-OPR3                |
| <i>35Sp::YFP-OPR3ΔSRL-NES(HIV1)::tOcs</i> | pAGH1261            | Cy-OPR3                |
| <i>35Sp::TP(RecA)-OPR3ΔSRL-YFP::tOcs</i>  | pAGH1299            | Cp-OPR3                |
| <i>35Sp::TP(RecA)-YFP-OPR3ΔSRL::tOcs</i>  | pAGH1343            | Cp-OPR3                |
| <i>35Sp::TP(HSP60)-OPR3ΔSRL-YFP::tOcs</i> | pAGH1336            | Mt-OPR3                |
| <i>35Sp::TP(HSP60)-YFP-OPR3ΔSRL::tOcs</i> | pAGH1337            | Mt-OPR3                |
| <i>pICH75055 (empty backbone)</i>         | pAGH1189            | EV                     |
| <i>35Sp:: OPR2-YFP::tOcs</i>              | pAGH1489            | <i>35Sp:: OPR2-YFP</i> |
| <i>OPR3p::OPR2-YFP::tOcs</i>              | pAGH1483            | <i>OPR3p::OPR2-YFP</i> |

**Table S9 List of constructs used for *N. benthamiana* transient assays.**

| <b>Construct</b>                              | <b>Plasmid name</b> | <b>Given name</b>      |
|---|---------------------|------------------------|
| <i>35Sp::SIP-OPR3ΔSRL-YFP-HDEL::tOcs</i>      | pAGH1057            | ER-OPR3                |
| <i>35Sp::SIP-YFP-OPR3ΔSRL-HDEL::tOcs</i>      | pAGH1059            | ER-OPR3                |
| <i>35Sp::OPR3ΔSRL-YFP-SRL::tOcs</i>           | pAGH1058            | Px-OPR3                |
| <i>35Sp:: YFP-OPR3::tOcs</i>                  | pAGH1060            | Px-OPR3                |
| <i>35Sp::NLS(SV40)-OPR3ΔSRL-YFP::tOcs</i>     | pAGH1224            | NI-OPR3                |
| <i>35Sp::NLS(SV40)-YFP-OPR3ΔSRL::tOcs</i>     | pAGH1226            | NI-OPR3                |
| <i>35Sp::OPR3ΔSRL-YFP-NES(HIV1)::tOcs</i>     | pAGH1259            | Cy-OPR3                |
| <i>35Sp::YFP-OPR3ΔSRL-NES(HIV1)::tOcs</i>     | pAGH1258            | Cy-OPR3                |
| <i>35Sp::TP(RecA)-OPR3ΔSRL-YFP::tOcs</i>      | pAGH1297            | Cp-OPR3                |
| <i>35Sp::TP(RecA)-YFP-OPR3ΔSRL::tOcs</i>      | pAGH1341            | Cp-OPR3                |
| <i>35Sp::TP(HSP60)-OPR3ΔSRL-YFP::tOcs</i>     | pAGH1334            | Mt-OPR3                |
| <i>35Sp::TP(HSP60)-YFP-OPR3ΔSRL::tOcs</i>     | pAGH1335            | Mt-OPR3                |
| <i>35Sp::OPR3ΔSRL-YFP::tOcs</i>               | pAGH1225            | <i>OPR3ΔSRL-YFP</i>    |
| <i>35Sp::YFP-OPR3ΔSRL::tOcs</i>               | pAGH1227            | <i>YFP-OPR3ΔSRL</i>    |
| <i>35Sp::OPR2-YFP::tOcs</i>                   | pAGH1492            | <i>35Sp:: OPR2-YFP</i> |
| <i>OPR3p::OPR2-YFP::tOcs</i>                  | pAGH1482            | <i>OPR3p::OPR2-YFP</i> |
| <i>35Sp::DTX37-linker-GFP::tOcs</i>           | pAGH1408            | DTX37-GFP              |
| <i>35Sp::STR1-linker-GFP::tOcs</i>            | pAGH1409            | STR1-GFP               |
| <i>35Sp::DTX36-linker-GFP::tOcs</i>           | pAGH1431            | DTX36-GFP              |
| <i>35Sp::DTX9-linker-GFP::tOcs</i>            | pAGH1427            | DTX9-GFP               |
| <i>35Sp::DTX28-linker-GFP::tOcs</i>           | pAGH1428            | DTX28-GFP              |
| <i>35Sp::CHUP1CDS(75 bp)-mTurquoise::tOcs</i> | pAGH1540            | CHUP1-mTurquoise       |

## Acknowledgments

I would like to express my gratitude to **Prof. Dr. Bettina Hause** for her guidance and mentorship throughout my PhD thesis. I am particularly thankful for her positivity and her invaluable help in developing my scientific skills and establishing my own ideas.

I am also thankful to the members of my thesis committee, **Prof. Dr. Ingo Heilmann** and **Dr. Martin Schattat** for their constructive feedback and valuable suggestions, which greatly enriched the quality of this work. I extend my gratitude to the committee for evaluating my PhD work.

Next, I would like to thank **Dr. Sylvestre Marillonnet** for the help in Golden Gate cloning and especially for the collection of Golden Gate modules made available. I also thank **Dr. Khabat Vahabi** for his assistance in the RNAseq procedure and more importantly in giving me nice tools to analyse the resulting data effectively. I want also to thank **Prof. Dr. Hans-Henning Kunz** for the exciting collaboration we were able to establish around PEC1 function and jasmonate. I am also thankful to **Dr. Ivan F. Acosta** for kindly providing the *MYB21* and *MYB24* GUS reporter lines. And I thank **Dr. Tom Schreiber** for his help in the cloning design of the BiFC.

I also want to express my appreciation to **Hagen Stellmach** for performing the phytohormone measurements and assistance in the co-localization in protoplasts. With that I expand my appreciation to all other lab members, Esther, Mandy, Ranjit and Sayanthan. My deepest appreciation goes to the students with whom I had the occasion to collaborate and who helped expand my work, Olivia Putri Herdani, Fiona Smith, Amel Braham and Victoria Parafianczuk. I am grateful not only for the professional interactions but also the genuine human connections.

Additionally, I am thankful to the **Research Training Group 2498** at MLU Halle-Wittenberg for the insightful discussions and valuable contributions to this research throughout the RTG seminar series and retreats. Similarly, I would like to express my gratitude towards the **Cell and Metabolic Biology** department at IPB-Halle, for the pleasant working atmosphere in addition the contributions to the work through the discussions during my presentations.

I am undoubtedly grateful to my parents and my brother for their unending encouragement. My deepest gratitude goes to my sister Fatma for her unconditional support and friendship. And I won't miss expressing my gratitude to my deceased grandmother Chadlia as I reach this stage, just as she anticipated.

I am also thankful for the new friendships I formed during my PhD journey and the older ones that lasted. I deeply thank Mariem, Adel, Khaoula and Hama for being there for me. I am thankful to Ramona and Alfredo for the genuine friendship and for being supportive and caring.

I would like to express my heartfelt gratitude to the nice encounters I have made throughout my Ph.D. journey at IPB and within the RTG mainly Alejandro, Heena, Sarlita, Kathleen, Dario, Robert, Yaming, Jay, and Stephan.

## Curriculum vitae

### Personal information

---

Name Khansa Mekkaoui

### Education

---

07/2019 – now      Doctorate  
 PhD thesis: “From plastids to peroxisomes: Function of the JA precursor OPDA in *Arabidopsis thaliana*”.  
 Advisor: Prof. Dr. Bettina Hause  
 Leibniz Institute of Plant biochemistry, Halle/Saale and RTG2498 MLU Halle-Wittenberg, Halle/Saale

10/2015 – 08/2018      M.Sc. in Horticultural genetics and biotechnology.  
 Thesis: “Characterization of tomato P4H3 function during fruit growth and investigation of proline metabolism pathway in salt-stressed tomato”.  
 Advisor: Dr. Panagiotis Kalaitzis  
 Mediterranean Agronomic Institute of Chania (MAICh), Greece.

09/2007 – 06/2012      National Degree of Agricultural Engineering in plant production  
 B.Sc. project: “Study of the effect of Peptone fertilization on Tunisian olive cultivars under water stress”.  
 Higher Agronomic School of Mograne, and Higher Institute of Preparatory Studies in Biology and Geology (ISEPBG), Tunisia.

09/2003 – 06/2007      IBN Rachik High School, Ezzahra, Tunisia  
 High school diploma “Baccalauréat” in Experimental Sciences.

### Research experience

---

12/2017 – 05/2019      Research assistant: “Identification and characterization of olive poly-4 hydroxylases and arabinogalactan proteins in response to salinity”.  
 Laboratory of Horticultural Genetics and Biotechnology MAICh

12/2018 – 01/2019      Research assistant: “Characterization of LUGNANO olive germplasm collection using standard SSR markers”  
 National Research Council of Italy (CNR), Perugia, Italy.

02/2012 – 06/2012      Internship: Study of the olive Chemlali cultivar grown under moderate and severe water stress.  
 Advisors: Dr Larbi Lajmi, Dr Maaouia Kamel  
 Olive Tree Institute – Tunis, Tunisia

07/2011 – 08/2011      Internship: Economic and ecological valuation of a halophyte  
 Advisors: Dr Tahar Ghnaya, Dr Maaouia Kamel.  
 Biotechnology Center of Borj Cédria – Borj Cedria, Tunisia



## Conferences participation

---

Jasmonate meeting, Halle/Saale, Germany, 29 Aug to 01 Sep 2023

International Conference of the German Society for Plant Sciences – “Botanik-Tagung”, Bonn, Germany, 28 Aug to 01 Sep 2022; Winner of Best Poster Award

## Publications

Azariadis A, Vouligeas F, Salame E, Kouhen M, Rizou M, Blazakis K, Sotiriou P, Ezzat L, **Mekkaoui K**, Monzer A, Krokida A, Adamakis I. D, Dandachi F, Salha B, Kostelenos G, Figgou E, Giannoutsou E, and Kalaitzis P. (2023). Response of Prolyl 4 Hydroxylases, Arabinogalactan Proteins and Homogalacturonans in Four Olive Cultivars under Long-Term Salinity Stress in Relation to Physiological and Morphological Changes. **Cells**. 12(11):1466. <https://doi.org/10.3390/cells12111466>

Ruberti C, Feitosa-Araujo E, Xu Z., Wagner S, Grenzi M, Darwish E, Lichtenauer S, Fuchs P, Parmagnani A. S, Balcerowicz D, Schoenaers S, de la Torre C, **Mekkaoui K**, Nunes-Nesi A, Wirtz M, Vissenberg K, Van Aken O, Hause B, Costa A, Schwarzländer M. (2022). MCU proteins dominate in vivo mitochondrial Ca<sup>2+</sup> uptake in Arabidopsis roots. **The Plant Cell**, koac242. <https://doi.org/10.1093/plcell/koac242>

Perrakis A, Denic D, Blazakis K, Giannoutsou E, Kaloudas D, Bitá C, Rizou M, Krokida A, Kouhen M, Lazaridou A, **Mekkaoui K**, Belaidi S, El Zein Z, Khalil M, Ezzat L, Youssef N, Kosma M, González A, Monzer A, Papantoniou D, Tello A, Bouzayen M, Adamakis I, Driouich A, Billiaderis C, Kalogerakis N, Kalaitzis P. (2021). A tomato prolyl-4-hydroxylase causes relocation of abscission zone and alters abscission kinetics. **BioRxiv**. <https://doi.org/10.1101/2021.04.20.440677>

Perrakis A, Bitá E.C, Arhondakis S, Krokida A, **Mekkaoui K**, Denic D, Blazakis K.N, Kaloudas D and Kalaitzis P. (2019). Suppression of a prolyl 4 hydroxylase results in delayed abscission of overripe tomato fruits. **Front. Plant Sci**. <https://doi.org/10.3389/fpls.2019.00348>

## Erklärung

Hiermit erkläre ich, dass ich die vorliegende wissenschaftliche Arbeit selbständig und ohne fremde Hilfe angefertigt habe. Ich erkläre, dass ich keine anderen als die von mir angegebenen Quellen und Hilfsmittel benutzt habe und die den Werken wörtlich und inhaltlich entnommenen Stellen als solche kenntlich gemacht habe. Ich versichere weiterhin, dass ich mich erstmals mit dieser Arbeit um die Erlangung des Doktorgrades bewerbe. Diese Arbeit wurde an keiner anderen Fakultät oder Universität zur Begutachtung eingereicht. Die eingereichte schriftliche Fassung der Arbeit entspricht der auf dem elektronischen Speichermedium.

Khansa Mekkaoui

Halle/Saale, 29/09/2023